Estimation of Radio Frequency Impairments and Channels for Multi-Carrier 5G and Beyond 5G Systems

Thesis submitted in accordance with the requirements of
the University of Liverpool for the degree of Doctor in Philosophy by

Yujie Liu

Department of Electrical Engineering and Electronics
School of Electrical Engineering, Electronics and Computer Science

June 2020

Abstract

Multi-carrier techniques play an important role in the fifth generation (5G) and beyond 5G (B5G) wireless communication systems, as they can support high data rate communications and exhibit high resilience to frequency selective fading. However, the presence of radio frequency (RF) impairments, such as carrier frequency offset (CFO), in-phase/quadrature-phase (IQ) imbalance, hinder the effectiveness of multi-carrier techniques. Thus, the estimation of RF impairments and channel are very essential. In this thesis, RF impairments(s) and channel(s), and their estimation together are considered for various multi-carrier 5G and B5G systems. This thesis consists of four main contributions as follows.

First, a joint multi-time of arrival (TOA) and multi-CFO estimation scheme is proposed for multi-user orthogonal frequency division multiplexing (OFDM) systems, where TOA is a key component of channel. With a carefully designed pilot, U TOAs and U CFOs of U users are separated jointly, dividing a complex $2U$-dimensional estimation problem into $2U$ low-complexity one-dimensional estimation problems. Two CFO estimation approaches, including a low-complexity closed-form solution and a high-accuracy null-subcarrier assisted approach, are proposed to estimate the integer and fractional parts of each CFO as a whole. Each TOA estimate is robust against CFO by means of the features of the inter-carrier interference (ICI) matrix. Cramér-Rao lower bounds (CRLBs) of multi-TOA and mutli-CFO estimation are derived for multi-user OFDM systems. Extensive simulation results confirm the effectiveness of the proposed scheme.

Second, an iterative semi-blind (ISB) receiver structure is proposed for short-frame

full-duplex (FD) OFDM systems with CFO. An equivalent system model with CFO included implicitly is first derived. A subspace-based blind channel estimation is proposed for the initial stage, followed by a single pilot assisted CFO estimation and channel ambiguities elimination. Then, channel and CFO are refined iteratively. The integer and fractional parts of CFO in the full range are extracted as a whole and in closed-form at each iteration. The proposed ISB receiver, with halved training overhead, demonstrates superior performances than the existing methods. CRLBs are derived to verify the effectiveness of the proposed receiver structure. It also demonstrates fast convergence speed.

Third, a robust semi-blind CFO and channel estimation scheme is proposed for generalised frequency division multiplexing (GFDM) systems. Based on an equivalent system model with CFO included implicitly, initial blind channel estimation is performed by subspace. Then, full-range CFO and channel ambiguity are estimated consecutively utilising a small number of nulls and pilots in a single subsymbol, respectively. Both CFO and channel estimates demonstrate high robustness against ICI and inter-symbol interference (ISI) caused by the nonorthogonal filters of GFDM. Simulation results verify that the bit error rate (BER) performance of the proposed scheme approaches the ideal case with perfect CFO and channel estimations.

Last but not least, a semi-blind joint estimation scheme of multiple channels, multiple CFOs and IQ imbalance is proposed for generalised frequency division multiple access (GFDMA) systems, with no constraints on carrier assignment scheme, modulation type, cyclic prefix length and symmetry of IQ imbalance. By means of subspace approach, CFOs and channels of U users are first separated into U groups. For each individual group, the CFO is estimated by minimising the smallest eigenvalue, whose corresponding eigenvector is utilised to determine channel. Then, IQ imbalance parameters and channel ambiguities are estimated jointly by very few pilots. Simulation results show that the proposed scheme significantly outperforms the existing methods, while at much lower training overhead. It also achieves a close performance to the derived CRLB.

To summarise, this thesis focuses on developing the estimation schemes of RF impairments and channels for 5G and B5G systems, by considering both OFDM and GFDM based multi-carrier techniques, half-duplex and full-duplex modes, single-user and multi-user systems. The developed estimation schemes are either pilot-aided with low complexity or semi-blind by subspace with high spectrum efficiency. This research work is an essential reference for academics and professionals involved in this topic.

Keywords— OFDM, GFDM, GFDMA, full-duplex communications, short-frame transmission, URLLC, 5G, B5G, CFO, IQ imbalance, channel estimation, semi-blind, subspace.

Acknowledgements

I have learned a lot and indeed enjoyed while working on this thesis. There are countless people without whose helping hands this thesis would not have come to fruition. Their contributions are sincerely appreciated and gratefully acknowledged.

Foremost, I am deeply indebted to my supervisors, Prof. Eng Gee Lim, Dr. Xu (Judy) Zhu, and Prof. Yi Huang, for their endless help and support on my Ph.D. study and research. I am really fortunate to be able to work under their supervision. I would specially thank Dr. Xu (Judy) Zhu for her immense expertise, kind patience, continuous encouragement, invaluable comments and suggestions.

I would like to express my sincere gratitude to Xi'an Jiaotong-Liverpool University and University of Liverpool for providing me the golden opportunity to embark on this Ph.D. project as well as the financial support during my Ph.D. study.

Special thanks must be given to my talented and warm-hearted colleagues and friends, particularly to Dr. Zhongxiang Wei, Dr. Xing Luo, Dr. Yufei Jiang, Dr. Bing Han, Dr. Jingchen Wang, Ms. Zhenzhen Jiang, Dr. Haochuan Jiang, Dr. Li Yu, Dr. Xiaotong Xu, Mr. Ruotong Wang, Mr. Boda Liu, Mr. Yuanchen Wang, Mr. Rui Pei, Mr. Shufei Zhang, Dr. Samer Jammal and Ms. Yaqiong Liu. It is a great honour for me to work and befriend with them.

In addition, I owe my deepest gratitude toward my family. I would have no chance to pursue my dreams in my life without their great support, patience and love. This thesis is dedicated to them.

Finally, I am grateful for other people who help me in various ways in the past.

Contents

List of Figures

List of Tables

List of Acronyms

1G	First generation
2G	Second generation
3G	Third generation
3GPP	Third generation partnership project
4G	Fourth generation
5G	Fifth generation
AC	Analogue cancellation
B5G	Beyond fifth generation
BER	Bit error rate
BLAST	Bell-Labs layered space-time architecture
BS	Base station
CAS	Carrier assignment scheme
CDMA	Code division multiple access
CFO	Carrier frequency offset
CFR	Channel frequency response

CIR	Channel impulse response
CP	Cyclic prefix
CPI	Cyclic prefix insertion
CPR	Cyclic prefix removal
CRLB	Cramér-Rao lower bound
CSS	Chirp spread spectrum
DC	Digital cancellation
DFT-s-OFDM	Discrete Fourier transform spread orthogonal frequency division multiplexing
ELPC	Extremely low-power communications
eMBB	Enhanced mobile broadband
ESPRIT	Estimation of signal parameters via rotational invariance technique
eURLLC	Extremely ultra-reliable low-latency communications
EVD	Eigenvalue decomposition
FB	Forward-backward
FBMC	Filter bank multi-carrier
fCFO	Fractional carrier frequency offset
FD	Full-duplex
FDM	Frequency division multiplexing
FDMA	Frequency division multiple access
FeMBB	Further enhanced mobile broadband

FER	Frame error rate
FFT	Fast Fourier transform
FIM	Fisher information matrix
GFDM	Generalised frequency division multiplexing
GFDMA	Generalised frequency division multiple access
HD	Half-duplex
HSPA	High speed packet access
iCFO	Integer carrier frequency offset
ICI	Inter-carrier interference
IFFT	Inverse fast Fourier transform
IoT	Internet of things
IQ	In-phase/quadrature-phase
ISB	Iterative semi-blind
ISI	Inter-symbol interference
JCCIQE	Joint multi-carrier frequency offset, multi-channel and in-phase/quadrature-phase imbalance estimation
JMTMCE	Joint multi-time of arrival and multi-carrier frequency offset estimation
LDHMC	Long-distance and high-mobility communications
LMMSE	Linear minimum mean square error
LO	Local oscillator

LoS	Line-of-Sight
LS	Least-square
LTE	Long-term evolution
LTE-A	Long-term evolution advanced
MIMO	Multi-input multi-output
MISO	Multi-input single-output
ML	Maximum likelihood
mMTC	Massive machine-type communications
MS	Mobile station
MSE	Mean square error
MUSIC	Multiple signal classification
N/A	Not available
NLoS	Non-line-of-sight
NOMA	Non-orthogonal multiple access
NS	Null-subcarrier
OFDM	Orthogonal frequency division multiplexing
OFDMA	Orthogonal frequency division multiple access
PAPR	Peak-to-average-power-ratio
PC	Passive cancellation
PM	Parametric-model
PN	Pseudo noise

P/S	Parallel-to-serial
PSK	Phase shift keying
QAM	Quadrature amplitude modulation
QPSK	Quadrature phase shift keying
RAN	Radio access network
RF	Radio-frequency
RMSE	Root mean square error
RSCCE	Robust semi-blind channel and carrier frequency offset estimation
R-TOA	Robust-time of arrival
SB	Semi-blind
SC-FDE	Single-carrier frequency domain equalisation
SC-FDMA	Single-carrier frequency division multiple access
SI	Self-interference
SIMO	Single-input multi-output
SINR	Signal-to-interference-and-noise-ratio
SIR	Signal-to-interference-ratio
SISO	Single-input single-output
SNR	Signal-to-noise-ratio
S/P	Serial-to-parallel
TDMA	Time division multiple access
TOA	Time of arrival

TTI Transmission time interval

umMTC Ultra-massive machine-type communications

URLLC Ultra-reliable low-latency communications

UW Unique-word

V2X Vehicle to everything

ZF Zero-forcing

ZP Zero padding

List of Symbols

Notations

$(\cdot)^*$	Complex conjugate
$(\cdot)^T$	Transpose
$(\cdot)^H$	Complex conjugate transpose
$(\cdot)^\dagger$	Pseudo inverse
$\mathrm{diag}\{\cdot\}$	A diagonal matrix with vector on its diagonal, or a vector obtained from the diagonal of a matrix
$\mathbf{I}_K$	A $K \times K$ identity matrix
$\mathbf{1}_{M\times N}$	An $M \times N$ all-one matrix
$\mathbf{0}_{\boldsymbol{M}\times\boldsymbol{N}}$	An $M \times N$ all-zero matrix
$\otimes$	Kronecker product
$\odot$	Hadamard product
$\mathrm{vec}\{\mathbf{A}\}$	Vector-version of matrix $\mathbf{A}$
$\mathbb{E}\{\cdot\}$	Expectation operator
$\mathbf{A}(a:b:c, d:e:f)$	Submatrix of $\mathbf{A}$ with rows from a to c with step size b and columns from d to f with step size e
$\mathrm{Re}\{a\}$	Real part of a
$\mathrm{Im}\{a\}$	Imaginary part of a

$[\mathbf{A};\mathbf{B}]$	$\mathbf{A}$ and $\mathbf{B}$ are concatenated by rows
$[\mathbf{A},\mathbf{B}]$	$\mathbf{A}$ and $\mathbf{B}$ are concatenated by columns
$\\|\cdot\\|_{\mathrm{F}}^2$	Forbenius norm
$\mathrm{circshift}(\mathbf{A},K,\mathrm{dim})$	Function to shift the elements in array $\mathbf{A}$ by K positions along dimension dim
$\mathrm{toeplitz}(a,b)$	Create a Toeplitz matrix with a and b as its first column and first row, respectively
$\jmath$	Basic imaginary unit
$\det\{\cdot\}$	Determinant
$\lfloor\cdot\rfloor$	Round to the next lower integer
$\angle a$	Angle of a
Parameters	
K	Number of subcarriers per OFDM/OFDMA symbol or GFDM/GFDMA subsymbol
M	Number of subsymbols per GFDM/GFDMA symbol
U	Number of users
N_{t}	Number of transmit antennas
N_{r}	Number of receive antennas
L	Channel length
L_{p}	Number of resolvable channel paths
L_{cp}	CP length
L_{zp}	ZP length
N_{s}	Number of symbols in a frame
ϕ	CFO
ϕ_{I}	Integer CFO
ϕ_{F}	Fractional CFO
τ_l	Time delay of l-th path

α, β	IQ imbalance parameters
θ	Phase mismatch between I and Q branches
υ	Amplitude mismatch between I and Q branches
$\mathbf{x}$	Time-domain transmitted signal
$\mathbf{y}$	Time-domain received signal
$\bar{\mathbf{y}}$	Frequency-domain received signal
$\boldsymbol{\hbar}$	Channel impulse response
$\bar{\mathbf{h}}$	Channel frequency response

Chapter 1

Introduction

1.1 Background and Motivation

Wireless communications have been considered as one of the most remarkable technological innovations in modern society [16]. It plays a dominant role in our daily life, and revolutionises the way we live, communicate, study, make business, etc. It has experienced explosive growth over the past decades. Since 1980, four generations of wireless communications have been deployed, which are capable of enhancing data rate approximately 10^5 times from 24 Kb/s in the first generation (1G) network to 200 Mb/s in the fourth generation (4G) network [16]. The fifth generation (5G) network is under commercialising and deploying, and is foreseen to accomplish by 2020 [17]. To deal with the limitations and challenges in the existing networks, an intense discussion on the visions for next generation network, referred to as beyond 5G (B5G), is being carried out in both academia and industry [18–21]. In addition to achieving considerably high date rate, 5G and B5G networks are also expected to fulfil the stringent requirements in system reliability and latency, *i.e.*, ultra-reliable low-latency communications (URLLC) in 5G and extremely URLLC (eURLLC) in B5G [20].

Orthogonal frequency division multiplexing (OFDM) and generalised frequency division multiplexing (GFDM) have been regarded as two promising multi-carrier techniques for 5G and B5G networks [2,22]. OFDM enjoys a multitude of advantages, such as high robustness against frequency selective fading, high spectrum efficiency as well as low-complexity implementation at receiver thanks to one-tap equalisation [5,23–25]. GFDM, as a generalised form of OFDM, inherits the advantages of OFDM, but also offers high flexibility, thanks to its special two-dimensional structure in both time and frequency domains [2, 26–28]. Nevertheless, both of them are heavily sensitive to radio frequency (RF) impairments, for instance, carrier frequency offset (CFO), in-phase/quadrature-phase (IQ) imbalance. Error floors are likely to arise in the presence of RF impairments, which deteriorate system performance significantly.

Channel estimation is essential for signal detection and resource allocation in wireless communications systems. Time of arrival (TOA), as a key component of channel, is defined as the propagation delay of the first arriving path [6, 29, 30]. TOA plays an important role in localisation, synchronisation and channel estimation for wireless communications systems. However, it is of big challenge to jointly estimate RF impairment(s) and channel(s). Specifically, the individual estimations of RF impairment(s) and channel(s) not only are likely to interfere with each other, but also suffer high training overhead due to the demand of separate pilots for RF impairment(s) and channel(s).

Full-duplex (FD) communications can double the transmission rate and reduce the end-to-end latency, by allowing simultaneous transmission and reception over the same frequency slots [23, 31, 32]. It has been considered as a compelling technology to drive URLLC and eURLLC for 5G and B5G, and gained overwhelming interests in recent years [33]. However, FD communications introduce a strong self-interference (SI) from its transmitter to its own receiver. It is of great significance to cancel SI to an acceptable level. Besides, the presence of RF impairment(s) hinders the effectiveness of FD communications in terms of spectrum efficiency and network latency. SI cancellation and RF impairment(s) mitigation are two serious issues in FD communications.

Short-frame transmission is another fascinating technology for URLLC and eURLLC, which reduces network latency enormously by diminishing the transmission time interval (TTI) duration [4, 34, 35]. Generally, there are two ways to shorten the frame length, by means of reducing either the symbol duration (increasing the subcarrier spacing) or the number of symbols per TTI [33]. Pilot shortage is one of the biggest problem in short-frame transmission. A large number of pilots utilised for RF impairment(s) and channel(s) estimation are anticipated to enhance system reliability, which however occupy resources for data transmission, giving rise to low spectrum efficiency. On the other hand, a small number of pilots are more likely to increase the error probability, resulting in low reliability. With limited pilot and data symbols, how to design a high-reliability receiver is demanding in short-frame communication systems.

1.2 Objectives

Motivated by the aforementioned challenges, this thesis aims to investigate the joint estimation problem of RF impairments and channels for four kinds of multi-carrier 5G and B5G systems in the following.

- The first considered systems are multi-user OFDM systems in the presence of multiple CFOs. The objective is to develop a pilot assisted joint multi-TOA and multi-CFO estimation scheme for it, where multiple TOAs and multiple CFOs should be estimated separately, without suffering any error propagation from the estimation of another. The pilot of each user should be carefully designed to decompose the complex multi-dimensional estimation problem into a number of low-complexity one-dimensional estimation problems.

- The second considered systems are short-frame FD systems with CFO. The objective is to propose a semi-blind based estimation approach of channels and CFO to enable URLLC, *i.e.,* achieving low latency while maintaining high reliability. The proposed semi-blind estimation scheme should require a very short frame with tens of received symbols to calculate the second-order statistics of the received signal, and a much short pilot to estimate CFO and eliminate channel ambiguities jointly. For the sake of high reliability, the detected data symbols are expected to be utilised as virtual pilots to further refine both channel and CFO estimations.

- The third considered systems are single-user GFDM systems. The objective is to develop a robust estimation scheme of channel and CFO for it, while with high spectral efficiency. Both channel and CFO estimation should be robust against ICI and inter-symbol interference (ISI) caused by GFDM nonorthogonal filters. Only a small number of nulls and pilots are needed to estimate CFO and eliminate channel ambiguity, respectively.

- The fourth considered systems are GFDMA systems in the presence of multiple CFOs and IQ imbalance. The objective is to propose a joint semi-blind estimation scheme of multiple channels, multiple CFOs and IQ imbalance. First, multiple CFOs and multiple channels should be separated by user. Then, for each user, the CFO is supposed to be extracted by minimising the smallest eigenvalue whose corresponding eigenvector is utilised to estimate the channel in a blind manner. Finally, the IQ imbalance parameters should be estimated jointly with channel ambiguities by very few pilots. The proposed scheme should be feasible for a wider range of receive antennas number and has no constraints on carrier assignment scheme, modulation type, cyclic prefix length and symmetry of IQ imbalance.

1.3 Thesis Organisation

The rest of this thesis is organised as follows.

- **Chapter 2** demonstrates the fundamentals of wireless communications, including an evolution of wireless communications, an introduction to multi-carrier techniques as well as a number of emerging techniques, which lay the foundations for the remainder of the thesis.

- **Chapter 3** gives an overview of RF channel and impairments. A number of existing approaches for channel estimation and RF impairments estimation are presented.

- **Chapter 4** investigates joint multi-TOA and multi-CFO estimation problem for multi-user OFDM systems, by means of a carefully designed pilot.

- **Chapter 5** proposes an iterative semi-blind receiver structure with CFO and channels estimation to enable URLLC in short-frame FD OFDM systems with CFO, assisted by a subspace approach.
- **Chapter 6** proposes a robust semi-blind estimation scheme of channel and CFO for single-user GFDM systems.
- **Chapter 7** investigates the joint semi-blind estimation scheme of multiple channels, multiple CFOs and IQ imbalance for GFDMA systems with generalised CAS.
- **Chapter 8** draws conclusions and discusses future work.

1.4 Publication List

A number of publications, which can contribute to the work presented in this thesis, are listed in the following.

Journal Papers

1. **Y. Liu**, X. Zhu, E. G. Lim, Y. Jiang, and Y. Huang, "Fast iterative semi-blind receiver for URLLC in short-frame full-duplex systems with CFO," *IEEE Journal on Selected Areas in Communications*, vol. 37, pp. 839–853, Apr. 2019.
2. **Y. Liu**, X. Zhu, E. G. Lim, Y. Jiang, Y. Huang, W. Xu, and H. Lin, "High-robustness and low-complexity joint estimation of TOAs and CFOs for multiuser SIMO OFDM systems," *IEEE Transactions on Vehicular Technology*, vol. 67, pp. 7739–7743, Aug. 2018
3. **Y. Liu**, X. Zhu, E. G. Lim, Y. Jiang, and Y. Huang, "Semi-blind GFDMA with generalized carrier assignment in the presence of CFOs and IQ imbalance," submitted to *IEEE Transactions on Wireless Communications,* (under review).

4. X. Wan, X. Zhu, Y. Jiang, **Y. Liu**, and J. Zhao, "An interference alignment and ICA based semi-blind dual-user downlink NOMA system for high-reliability low-latency IoT," *IEEE Internet of Things*, (early access).

Conference Papers

1. X. Huang, X. Zhu, Y. Jiang, and **Y. Liu**, "Efficient enhanced K-means clustering for semi-blind channel estimation of cell-free massive MIMO," in *Proc. IEEE ICC 2020*, pp. 1–6, Dublin, Ireland, Jun. 2020.

2. Y. Wang, X. Zhu, E. G. Lim, Z. Wei, **Y. Liu**, and Y. Jiang, "Compressive sensing based user activity detection and channel estimation in uplink NOMA systems," in *Proc. IEEE WCNC 2020*, pp. 1–6, Seoul, South Korea, Apr. 2020.

3. **Y. Liu**, X. Zhu, E. G. Lim, Y. Jiang, and Y. Huang, "Semi-blind joint multi-CFO and multi-channel estimation for GFDMA with arbitrary carrier assignment," in *Proc. IEEE Globecom 2019*, pp. 1–6, Waikoloa, Hawaii, USA, Dec. 2019.

4. J. Cao, X. Zhu, Y. Jiang, **Y. Liu**, and F. Zheng, "Joint block length and pilot length optimization for URLLC in the finite block length regime," in *Proc. IEEE Globecom 2019*, pp. 1–6, Waikoloa, Hawaii, USA, Dec. 2019.

5. **Y. Liu**, X. Zhu, E. G. Lim, Y. Jiang, and Y. Huang, "Robust semi-blind estimation of channel and CFO for GFDM systems," in *Proc. IEEE ICC 2019*, pp. 1–7, Shanghai, China, May 2019.

6. H. Lin, X. Zhu, Y. Jiang, **Y. Liu**, Y. Zhuang, and L. Gao, "PA-efficiency-aware hybrid PAPR reduction for F-OFDM systems with ICA based blind equalization," in *Proc. IEEE WCNC 2019*, pp. 1–6, Marrakech, Morocco, Apr. 2019.

7. H. Duan, Y. Jiang, X. Zhu, Z. Wei, **Y. Liu**, and L. Gao, "Treating self-interference as source: An ICA assisted full-duplex relay system," in *Proc. IEEE WCNC 2019*, pp. 1–6, Marrakech, Morocco, Apr. 2019.

8. **Y. Liu**, X. Zhu, E. G. Lim, Y. Jiang, and Y. Huang, "Iterative semi-blind CFO estimation, SI cancelation and signal detection for full-duplex systems," in *Proc. IEEE Globecom 2018*, pp. 1–7,Abu Dhabi, UAE, Dec. 2018.

9. **Y. Liu**, X. Zhu, E. G. Lim, Y. Jiang, and Y. Huang, "High-accuracy joint multi-CFO and multi-TOA estimation for multiuser SIMO OFDM systems," in *Proc. IEEE ICC 2018*, pp. 1–6, Kansas City, MO, USA, May 2018.

Chapter 2

Fundamentals of Wireless Communications

This chapter begins with an introduction of the evolution of wireless communications. Then, multi-carrier techniques, including OFDM and GFDM, are presented, followed by the description of a number of emerging technologies, such as URLLC techniques, FD communications and multi-antenna communications.

2.1 Evolution of Wireless Communications

Wireless communications have been regarded as one of the most significant technological innovations in modern society, which is revolutionising almost every aspect of our daily life [16]. It changes the way we communicate, interact, shop and make business, and boosts the development of engineering, media and entertainment industry. It has experienced exponential growth over the past decades. To date, four generations of wireless communications have been implemented, while 5G network is still under commercialisation and deployment [16]. Since 5G network is reaching its limits and far from supporting the future applications in next decade, the visions for B5G, are being discussed intensively in the academia and industry [18–21]. The six generations of wireless communications are compared in Table 2.1, in terms of time period, key technologies and applications. Fig. 2.1 makes a comparison of eight capabilities of 4G, 5G and B5G networks, including peak data rate, user-experienced data rate, spectrum efficiency, mobility, latency, connectivity density, network energy efficiency and area traffic capacity.

Since approximately 1980, each new generation usually emerges every decade. 1G cellular network was deployed in 1981, which was a basic frequency division multiple access (FDMA) assisted analogue system and intended for voice communications [16]. 1G network has a number of shortcomings, including low quality, low security, restricted subscribers, limited to voice service only with the experienced date rate of 2.4 Kb/s, and low compatibility due to lack of an unified international standard [36]. The second generation (2G) network utilising time division multiple access (TDMA) was adopted in 1992, which was the first time to introduce digital system [16]. The experienced data rate of 2G network was increased up to 64 Kb/s [16, 36]. In addition to voice calls, 2G network also supported short messages service. Thanks to code division multiple access (CDMA), the third generation (3G) network was introduced in 2001, with the experienced data rate significantly increased up to 2 Mb/s. A number of new services were offered by 3G, for instance, multimedia messages, video conferencing and mobile TV [16, 36]. The fourth generation (4G) network is an enhanced network of 3G and deployed in 2011. The key technologies of 4G network are OFDM and multi-input multi-output (MIMO) [20], with the experienced data rate enhanced approximately 100-fold compared to that of 3G network. 4G network provides low latency of 10 ms and high mobility of 350 km/h [20]. Thanks to 4G technologies, high-definition videos, mobile Internet and mobile pay became a reality.

The deployment of 5G network is expected to be accomplished by 2020 [17]. Since 5G era, communication services will revolutionise from human-centric to both human-centric and thing-centric. 5G is anticipated to support three usage scenarios, namely enhanced mobile broadband (eMBB), massive machine-type communications (mMTC) and URLLC [17, 36]. eMBB aims to support high peak data rates, increasingly seamless user experience, while mMTC requires to provide wireless connectivity for massive

Table 2.1: Comparison of 1G, 2G, 3G, 4G, 5G and B5G.

Generation	Time Period	Key Technologies	Applications
1G	1980s	• Analogue cellular • FDMA	• Voice calls
2G	1990s	• Digital cellular • TDMA	• Voice calls • Short messages
3G	2000s	• CDMA	• Multimedia messages • Video conferencing • Mobile TV
4G	2010s	• OFDM • MIMO	• High-definition video • Mobile Internet • Mobile pay
5G	2020s	• Short-frame transmission • Full-duplex communications • Network slicing • Massive MIMO • Fog computing • Software defined network	• Virtual-reality video • Ultra-high-definition video • Vehicle to everything • Internet of things • Smart city
B5G	2030s	• Advanced waveforms • Artificial intelligence • Machine learning • Super-massive MIMO • Terahertz communications • Large intelligent surface • Quantum communications	• Holographic society • Tactile Internet • Fully-automated driving • Industrial Internet • Internet of Bio-Nano-Things • Deep-sea sightseeing

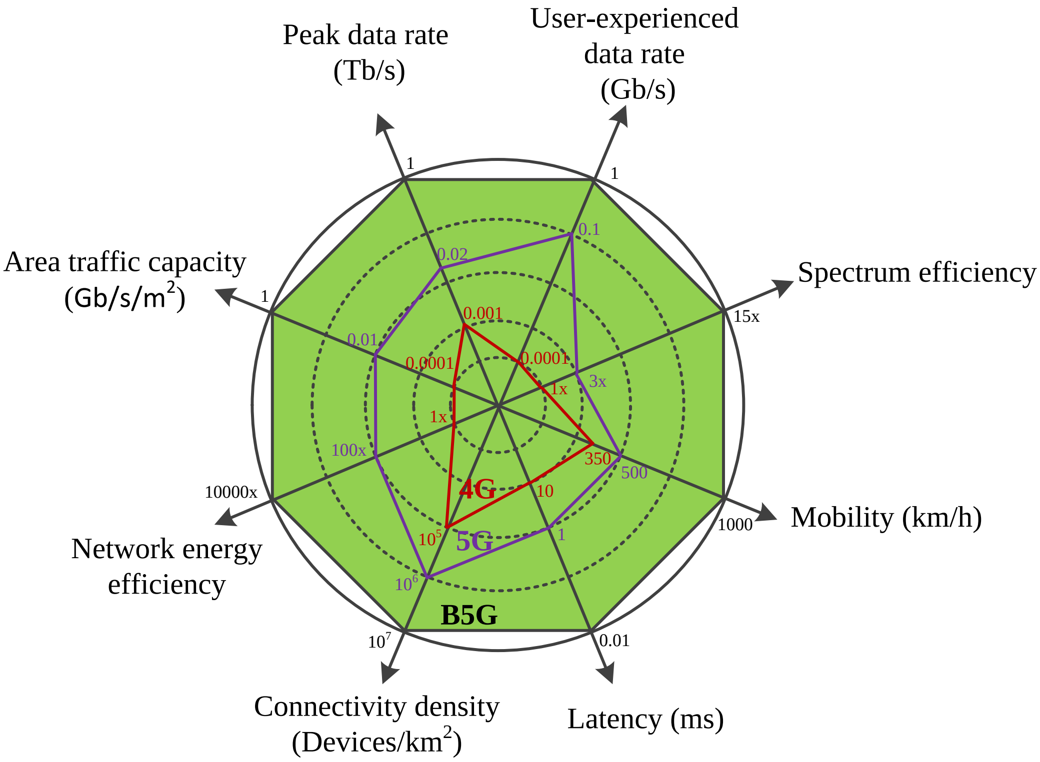

Figure 2.1: Comparison of capabilities of 4G, 5G and B5G networks.

number of Internet of things (IoT) devices. URLLC has stringent requirements on reliability and latency. The demanded experienced data rate and mobility in 5G network should reach 0.1 Gb/s and 500 km/h [20]. It requires an end-to-end latency of within 1 ms [20]. The number of connected devices in one square kilometres should be close to 10^6 in 5G, which is about ten-fold of that in 4G network [20]. The compelling technologies for 5G network are short-frame transmission, full-duplex communications, massive MIMO [37, 38], network slicing, fog computing, and so forth. 5G is an enabler for virtual-reality/augmented-reality videos, ultra-high-definition videos, vehicle to everything (V2X), IoT and smart city.

While 5G network has introduced a multitude of technological innovations, it is confronted with a number of new challenges and stringent performance requirements. It motivates researchers in the research community and industry to look at B5G, which is the mission for next decade. B5G network will revolutionise wireless communications from connected things to connected intelligence with extreme requirements on data rate, energy efficiency, latency, connectivity, mobility, etc. B5G network will support connection for everything, wireless coverage in full dimensions as well as an integration of numerous functions including sensing, communication, computing, caching, control, navigation and imaging [20]. The supporting typical scenarios for B5G were discussed in [20], including further enhanced mobile broadband (FeMBB), ultra-massive machine-type communications (umMTC), extremely ultra-reliable and low-latency communications (eURLLC), long-distance and high-mobility communications (LDHMC), and extremely low-power communications (ELPC). B5G network is foreseen to meet the experienced data rate of 1 Gb/s and end-to-end latency of 10-100 μs [20]. It should provide communications and network services for high-mobility end users with speed of 1000 km/h [20], while the connected devices in one square kilometres should attain 10^7. The promising technologies in B5G network are advanced waveforms [39], artificial intelligence, machine learning [40], Terahertz communications [41, 42] and large intelligent surface [17–20, 43]. Its leading applications are holographic society, Tactile Internet, fully-automated driving, industrial Internet, Internet of Bio-Nano-things, deep-sea sightseeing, etc. [20].

2.2 Multi-Carrier Techniques

Multi-carrier techniques are proposed to support high data rate communications and overcome frequency selective fading effect. In the following, two multi-carrier techniques, namely OFDM and GFDM, are introduced.

2.2.1 OFDM

OFDM is a powerful multi-carrier technique to combat frequency selective fading channel, by converting it into a number of frequency flat fading channels [5, 23–25]. It also enjoys low complexity at receiver thanks to its simplified one-tap equaliser as well as

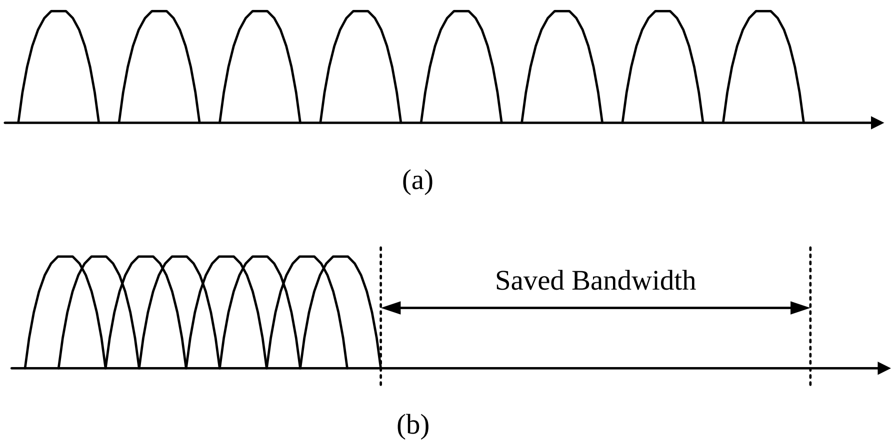

Figure 2.2: Frequency spectrums of a) FDM and b) OFDM [1].

high spectrum efficiency due to orthogonal multi-carrier modulation [44–47]. OFDM is a special case of frequency division multiplexing (FDM). Fig. 2.2 depicts the frequency spectrums of FDM and OFDM, respectively. It can be observed that guard intervals should be required for FDM to avoid interference, while OFDM allows the overlapping of subbands without suffering interference and thus greatly saves the bandwidth [1, 48]. OFDM has been adopted in numerous wireless standards, such as, IEEE 802.11, IEEE 802.16, Long-term Evolution (LTE) and LTE-Advanced (LTE-A) [49–51]. As specified in the third generation partnership project (3GPP) Release 15, OFDM with cyclic prefix (CP) has been standardised as both the uplink and downlink waveform for 5G network [22].

A guard interval between two consecutive OFDM symbols is required to deal with the ISI caused by frequency selective fading channel. There are two ways to insert the OFDM guard interval. One is CP where the last samples of the OFDM symbol is copied and added into its front. Another is zero padding (ZP), which pads the guard interval with zeros. Guard interval with CP is the focus of this thesis.

Fig. 2.3 depicts the simplified block diagram of OFDM implementation with inverse fast Fourier transform (IFFT) and fast Fourier transform (FFT). Define $d[0], d[1], \cdots, d[K-1]$ as the symbol stream after a quadrature amplitude modulation (QAM)/phase shift

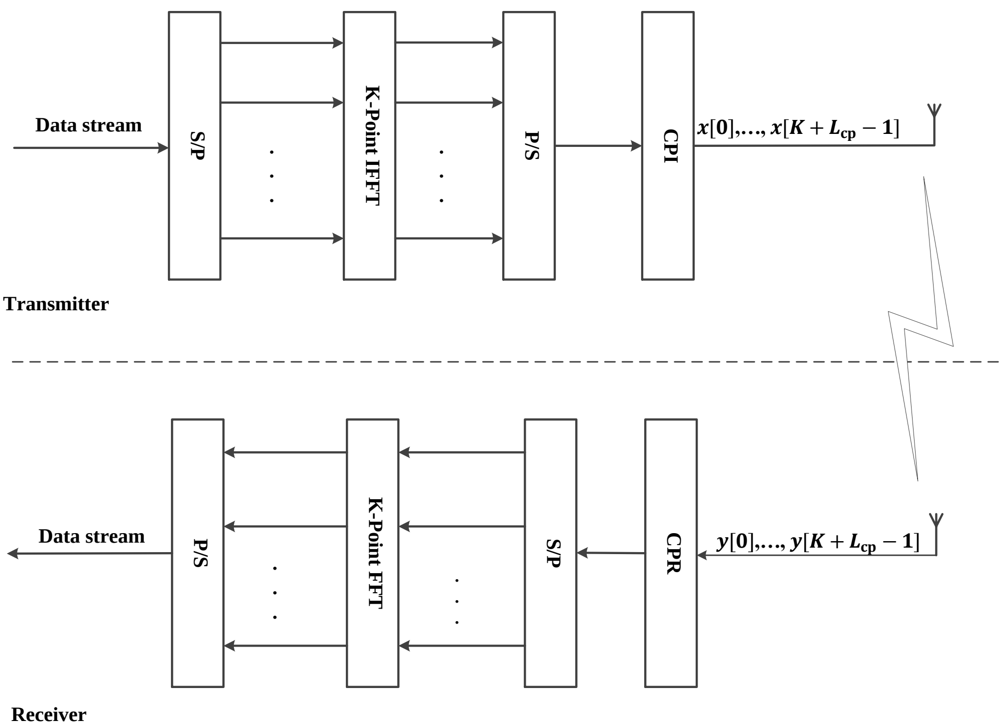

Figure 2.3: Simplified block diagram of OFDM implementation with IFFT/FFT (S/P: serial-to-parallel conversion, P/S: parallel-to-serial conversion, CPI: CP insertion, and CPR: CP removal).

keying (PSK) modulator, where K is the number of subcarriers in an OFDM symbol. After implementing serial to parallel conversion and K-point IFFT, the OFDM symbol vector containing $\epsilon[0], \epsilon[1], \cdots, \epsilon[K-1]$ is acquired, and $\epsilon[k]$ $(k = 0, 1, \cdots, K-1)$ is given by

$$\epsilon[k] = \frac{1}{\sqrt{K}} \sum\nolimits_{v=0}^{K-1} d[v] e^{j2\pi vk/K}. \tag{2.1}$$

The sequence $\epsilon[0], \epsilon[1], \cdots, \epsilon[K-1]$ is then converted in series, and the CP with length L_{cp} is added to the beginning of OFDM symbol, yielding $\mathbf{x} = [x[0], \cdots, x[L_{\text{cp}} - 1], x[L_{\text{cp}}], \cdots, x[G-1]]^T = [\epsilon[K - L_{\text{cp}}], \cdots, \epsilon[K-1], \epsilon[0], \cdots, \epsilon[K-1]]^T$, where $G = K + L_{\text{cp}}$.

After transmitted through channel and corrupted by additive noise, the received signal is obtained as

$$y[g] = \sum\nolimits_{l=0}^{L-1} \hbar[l]x[g-l] + w[g], \quad g = 0, 1, \cdots, G-1, \tag{2.2}$$

where $\hbar[0], \hbar[1], \cdots, \hbar[L-1]$ are channel impulse response (CIR) of length L, and $w[g]$ is the additive white Gaussian noise with zero mean and variance of σ^2. Then, the first L_{cp} samples from $y[0]$ to $y[L_{\mathrm{cp}}-1]$ corresponding to CP are removed, and the remaining samples are implemented with FFT, resulting in the frequency-domain OFDM symbol consisting of the sequence $\bar{y}[0], \bar{y}[1], \cdots, \bar{y}[K-1]$ of length K, where

$$\bar{y}[k] = \bar{h}[k]d[k] + \bar{w}[k], \quad k = 0, 1, \cdots, K-1, \tag{2.3}$$

where $\bar{h}[0], \bar{h}[1], \cdots, \bar{h}[K-1]$ are channel frequency response (CFR) of length K, and $\bar{w}[k]$ is corresponding noise in frequency domain. It is noteworthy that ISI within OFDM symbol due to frequency selective fading is eliminated with the removal of CP, as long as $L_{\mathrm{cp}} \geq L-1$.

According to (2.3), the transmitted signal can be easily recovered by $\hat{d}[k] = \bar{y}[k]/\bar{h}[k]$, if CFR has been acquired. It is known as one-tap equaliser, and contributes to low-complexity implementation at receiver. The matrix representation of OFDM in frequency domain is given by

$$\underbrace{\begin{bmatrix} \bar{y}[0] \\ \bar{y}[1] \\ \vdots \\ \bar{y}[K-1] \end{bmatrix}}_{\bar{\mathbf{y}}} = \underbrace{\begin{bmatrix} \bar{h}[0] & 0 & \cdots & 0 \\ 0 & \bar{h}[1] & \cdots & 0 \\ \vdots & \vdots & \ddots & \vdots \\ 0 & 0 & \cdots & \bar{h}[K-1] \end{bmatrix}}_{\bar{\mathbf{H}}} \underbrace{\begin{bmatrix} d[0] \\ d[1] \\ \vdots \\ d[K-1] \end{bmatrix}}_{\mathbf{d}} + \underbrace{\begin{bmatrix} \bar{w}[0] \\ \bar{w}[1] \\ \vdots \\ \bar{w}[K-1] \end{bmatrix}}_{\bar{\mathbf{w}}}. \tag{2.4}$$

Similarly, the time-domain received OFDM symbol is given in matrix form by

$$\mathbf{y} = \mathbf{H}\boldsymbol{\epsilon} + \mathbf{w}, \tag{2.5}$$

where $\mathbf{y} = [y[0], y[1], \cdots, y[K-1]]^T$, $\boldsymbol{\epsilon} = [\epsilon[0], \epsilon[1], \cdots, \epsilon[K-1]]^T$, $\mathbf{w} = [w[0], w[1], \cdots, w[K-1]]^T$, and

$$\mathbf{H} = \begin{bmatrix} \hbar[0] & 0 & \cdots & 0 & \hbar[L-1] & \cdots & \hbar[1]] \\ \hbar[1] & \hbar[0] & \ddots & \ddots & 0 & \ddots & \vdots \\ \vdots & \hbar[1] & \ddots & \ddots & \ddots & \ddots & \hbar[L-1] \\ \hbar[L-1] & \vdots & \ddots & \ddots & \ddots & \ddots & 0 \\ 0 & \hbar[L-1] & \ddots & \ddots & \ddots & \ddots & \vdots \\ \vdots & \ddots & \ddots & \ddots & \ddots & \ddots & \vdots \\ 0 & \cdots & 0 & \hbar[L-1] & \cdots & \hbar[1] & \hbar[0]] \end{bmatrix}. \quad (2.6)$$

Albeit OFDM brings numerous advantages, *e.g.*, high robustness against frequency selective fading, high spectrum efficiency and low-complexity equaliser design, it has several critical drawbacks as follows. First, OFDM is highly sensitive to RF impairments, such as CFOs, IQ imbalance, phase noise, etc [52]. They are likely to incur error floors and deteriorate BER performances considerably [1, 52]. Second, compared to single-carrier systems, OFDM systems suffer higher peak-to-average-power-ratio (PAPR), which lowers the signal-to-quantisation noise ratio of analogue-to-digital converter and digital-to-analogue converter, giving rise to low efficiency of power amplifier [1, 45, 52]. To overcome the high PAPR of OFDM, single-carrier FDMA (SC-FDMA) also known as DFT-spread-OFDM (DFT-s-OFDM) is adopted as the waveform for LTE uplink, and also as a complement waveform for 5G uplink.

OFDMA

Orthogonal frequency division multiple access (OFDMA) has been commercialised by Digital Video Broadcasting - Return Channel Terrestrial and wireless local area networks IEEE 802.11 standards [53], which originates from OFDM and frequency division multiple access (FDMA). In OFDMA systems, multiple users can share an OFDM symbol by allocating different subcarriers to each individual user [54]. OFDMA inherits the advantages of OFDM, such as high robustness against frequency selective fading, high spectrum efficiency and low-complexity equaliser design.

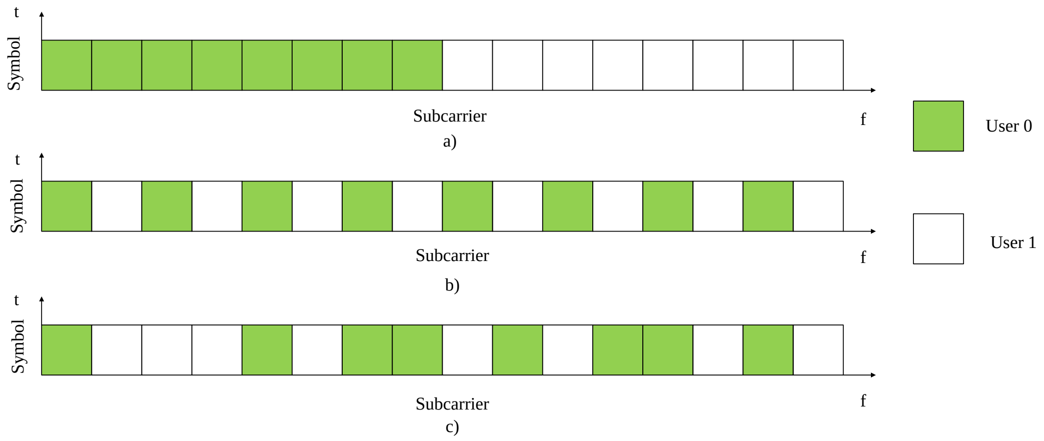

Figure 2.4: Examples of CAS of OFDMA: a) subband CAS, b) interleaved CAS and c) generalised CAS, with $U = 2$ users and $K = 16$ subcarriers.

Users in OFDMA systems can select their own subcarriers according to channel conditions. Typically, there are three carrier assignment schemes (CASs) for OFDM, including subband CAS, interleaved CAS and generalised CAS. With $U = 2$ users and $K = 16$ subcarriers, Fig. 2.4 depicts three examples of CAS for OFDMA:

- Subband CAS: A number of contiguous subcarriers are arranged for each user;
- Interleaved CAS: A number of subcarriers with an equidistant spacing are arranged for each user;
- Generalised CAS: A number of arbitrary subcarriers are arranged for each user exclusively.

Subband CAS is likely to suffer deep fade due to frequency selective fading [55]. Even if interleaved CAS is capable of addressing the issue in subband CAS, it is more attractive to work on generalised CAS where each user could occupy the best subcarriers with highest SNRs [55]. Similar to OFDM, OFDMA is also susceptible to RF impairments, *e.g.*, CFOs, IQ imbalance, and so forth.

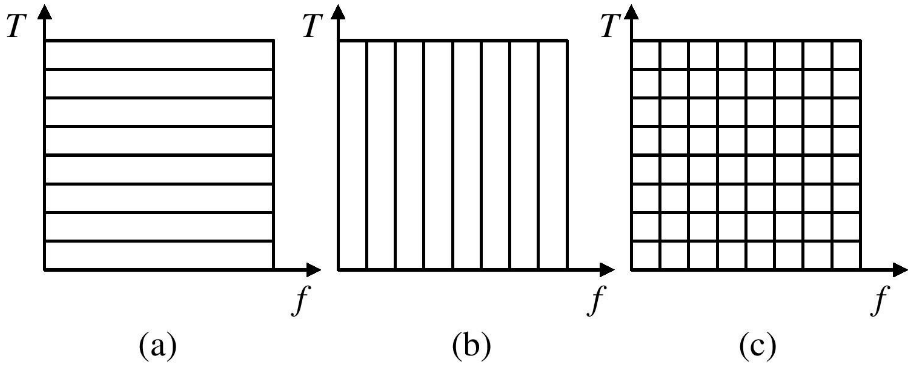

Figure 2.5: Symbol structures of a) SC-FDE, b) OFDM and c) GFDM [2].

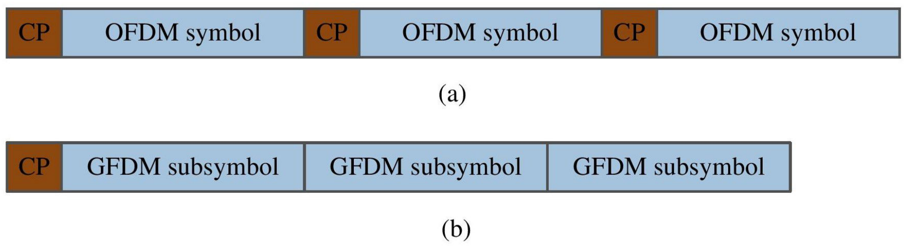

Figure 2.6: CP insertion for a) OFDM and b) GFDM [3].

2.2.2 GFDM

5G and B5G networks are expected to support massive number of connections with strict requirements in latency, throughput, data rate, mobility, etc., which motivates the shift of multi-carrier waveform design from orthogonality to nonorthogonality [26]. A number of attractive waveforms have been proposed for 5G and B5G networks, such as GFDM, universal filtered OFDM, filter bank multi-carrier (FBMC). B5G network needs to handle a wide range of services which may have diverse requirements in latency, throughput, data rate and mobility [27]. GFDM was first proposed in 2009 [56], and has been considered as a promising waveform for B5G networks thanks to its high flexibility opposed against other waveforms [2, 26–28].

Fig. 2.5 compares the symbol structures of a) single-carrier frequency domain equalisation (SC-FDE), b) OFDM and c) GFDM. It is noteworthy that GFDM has a two-dimensional structure in both time and frequency domains, which makes it more flexible

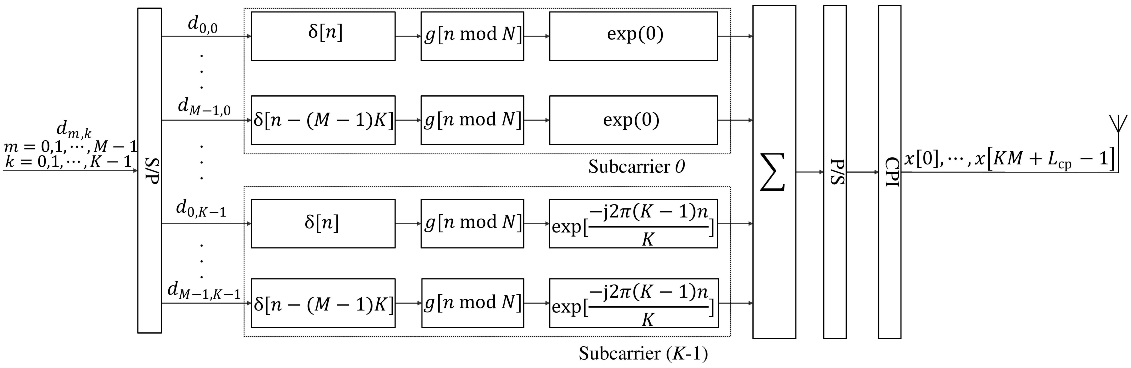

Figure 2.7: Block diagram of GFDM modulator.

than OFDM and SC-FDE, and thus able to fulfil various requirements in 5G and B5G networks. GFDM can easily turn out to be SC-FDE and OFDM, if the number of subcarriers per GFDM subsymbol K and the number of subsymbols per GFDM symbol M are respectively reduced to one. In addition to high flexibility, GFDM also offers high spectrum efficiency compared to OFDM [27], since only a single CP is added per GFDM symbol instead of per GFDM subsymbol, as depicted in Fig. 2.6 [3]. GFDM also exhibits lower PAPR and out-of-band emission than OFDM [28]. Low PAPR enables to reduce the hardware cost and power consumption, which is significant for ELPC scenario in B5G network. However, GFDM has several technical limitations and challenges. First, GFDM, as a nonorthogonal multi-carrier waveform, suffers severe ICI and intersymbol interference (ISI). It makes its receive design more complicated than that in OFDM systems, leading to high computational complexity. Second, similar to OFDM, GFDM is vulnerable to RF impairments, such as CFO, IQ imbalance, phase noise, etc. [28].

Fig. 2.7 depicts the block diagram of GFDM modulator [2]. Considering a GFDM symbol with M subsymbols each with K subcarriers, define $N = MK$ and $d_{m,k}$ as the transmitted data on the k-th ($k = 0, 1, \cdots, K-1$) subcarrier of the m-th ($m = 0, 1, \cdots, M-1$) subsymbol. Each $d_{m,k}$ is transmitted with the corresponding pulse shape [2]

$$g_{m,k}[n] = g[(n - mK) \bmod N] \cdot \exp(-j2\pi kn/K), \tag{2.7}$$

where n ($n = 0, \cdots, N-1$) is the sampling index. Each $g_{m,k}[n]$ is a time and frequency shifted version of a prototype filter $g[n]$, where the modulo operation performs a circularly shifted version of $g_{0,k}(n)$ and the complex exponential makes $g_{m,k}(n)$ a frequency shifted version of $g_{m,0}(n)$. After pulse shaping, the transmitted symbol $\epsilon[n]$ is given by

$$\epsilon[n] = \sum\nolimits_{k=0}^{K-1} \sum\nolimits_{m=0}^{M-1} g_{m,k}[n] d_{m,k}. \tag{2.8}$$

Denote $\boldsymbol{\epsilon} = [\epsilon[0], \epsilon[1], \cdots, \epsilon[N-1]]^T$ as the transmit symbol vector, which can be expressed as

$$\boldsymbol{\epsilon} = \mathbf{Ad}, \tag{2.9}$$

where $\mathbf{A} = [\mathbf{g}_{0,0}, \cdots, \mathbf{g}_{0,K-1}, \cdots, \mathbf{g}_{M-1,0}, \cdots, \mathbf{g}_{M-1,K-1}]$ is an $N \times N$ pulse shaping filter matrix with $\mathbf{g}_{m,k} = [g_{m,k}[0], \cdots, g_{m,k}[N-1]]^T$. A single CP with length L_{cp} is prepended to the GFDM symbol $\mathbf{x}$, obtaining $\mathbf{x} = [x[0], \cdots, x[L_{\mathrm{cp}}-1], x[L_{\mathrm{cp}}], \cdots, x[G-1]]^T = [\epsilon[N-L_{\mathrm{cp}}], \cdots, \epsilon[N-1], \epsilon[0], \cdots, \epsilon[N-1]]^T$, with $G = N + L_{\mathrm{cp}}$. After passing through channel and corrupted by noise, the received GFDM symbol in time domain is written as

$$y[g] = \sum\nolimits_{l=0}^{L-1} \hbar[l] x[g-l] + w[g], \quad g = 0, 1, \cdots, G-1, \tag{2.10}$$

where $\hbar[0], \hbar[1], \cdots, \hbar[L-1]$ are CIR and $w[n]$ is additive white Gaussian noise. After removing CP, define $\mathbf{y} = [y[L_{\mathrm{cp}}], y[L_{\mathrm{cp}}+1], \cdots, y[G-1]]^T$, which is given by

$$\mathbf{y} = \mathbf{HAd} + \mathbf{w}, \tag{2.11}$$

where $\mathbf{H}$ is circulant channel matrix in (2.6) and $\mathbf{w} = [w[0], w[1], \cdots, w[N-1]]^T$ is noise vector.

The ICI and ISI caused by the nonorthogonal filter matrix $\mathbf{A}$ complicates the GFDM receiver design, which is one of the major issues to be addressed for the adoption of

GFDM in B5G network. For instance, confronted with the scarce RF spectrum, it is much challenging to use few pilots to achieve high-accuracy estimation of RF impairments and channels for GFDM, while mitigating its ICI and ISI. It would be considerable to apply the blind/semi-blind algorithms to GFDM, which have been regarded as an effective solution to achieve high spectral efficiency in OFDM systems [53]. On the other hand, it is crucial to simplify the GFDM implementation. Recently, a simplified GFDM modem structure has been developed with a significant complexity reduction. Besides, a number of computationally efficient equaliser has been proposed for GFDM in the literature, such as ML detector [57], simplified ZF detector [58] and minimum mean square error (MMSE) detector [59–61]. All the aforementioned work makes GFDM more competitive and attractive in B5G network.

GFDMA

GFDMA, as a combination of GFDM and FDMA, has become a promising multi-user technique for B5G network [62–64]. Unlike single-user GFDM systems where all subcarriers are occupied by a single user for signal transmission, GFDMA allows multiple users to send data at the same time using exclusive subcarriers. Similar to OFDMA, GFDMA also allows users to choose the best subcarriers according to channel conditions. There are three CASs in GFDMA systems as well, including subband CAS, interleaved CAS and generalised CAS.

Fig. 2.8 illustrates three examples of CAS of GFDMA with $U = 2$ users, $M = 2$ subsymbols and $K = 16$ subcarriers: a) subband CAS where each user consists of 8 contiguous subcarriers; b) interleaved CAS where 8 subcarriers with equidistant spacing are arranged for each user; and c) generalised CAS where each user allows to occupy arbitrary 8 exclusive subcarriers. Fig. 2.8 also shows the existence of ICI and ISI in GFDMA systems, which are not present in OFDMA systems. GFDMA enjoys several advantages inherited from GFDM, such as high flexibility and high spectrum efficiency. However, GFDMA also inherits the drawbacks of GFDM, including ICI, ISI, high computational complexity, high sensitivity to RF impairments, and so forth.

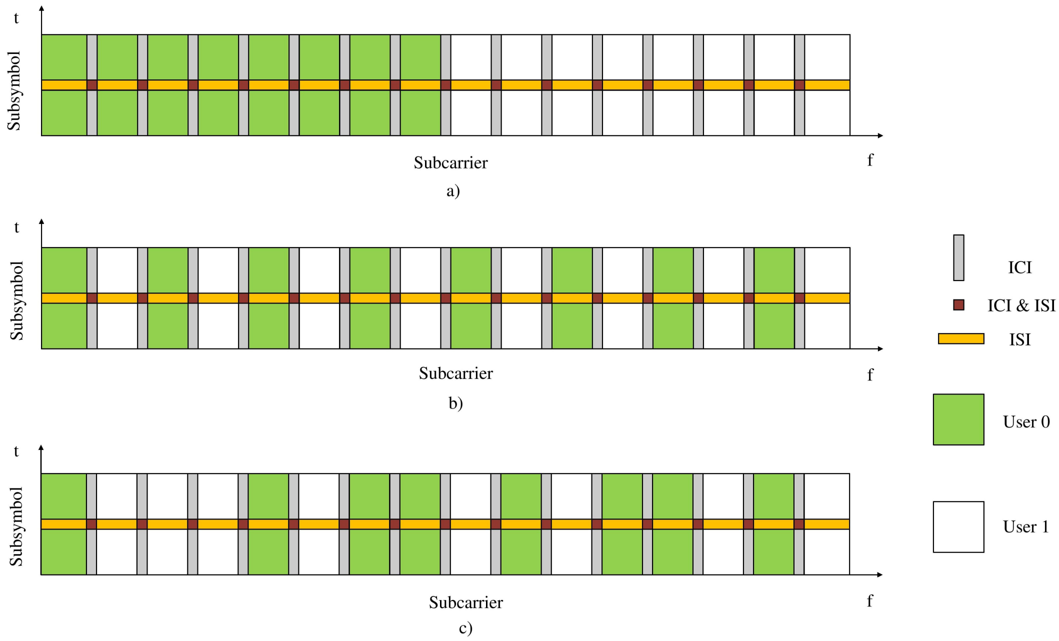

Figure 2.8: Examples of CAS of GFDMA: a) subband CAS, b) interleaved CAS and c) generalised CAS, with $U = 2$ users, $M = 2$ subsymbols and $K = 16$ subcarriers.

2.3 Emerging Techniques

A number of new technologies have recently emerged, which includes URLLC techniques, FD communications, multi-antenna communications and so forth. An introduction of such emerging techniques is given in this section.

2.3.1 URLLC Techniques

URLLC is an essential usage scenario for 5G network, with strict requirements on latency (less than 1 ms) and reliability (99.999%) [33]. URLLC is a key technology for numerous emerging applications, such as Tactile Internet, factory automation, virtual reality, intelligent transport systems [33, 65–68]. However, URLLC design has a great challenge: how to reduce the end-to-end latency while achieving similar reliability, which has attracted much attention from researchers. There are several surveys in the literature, which provided helpful insights of URLLC design. It is claimed in [33] that reliability can be enhanced through frequency and space diversity, robust channel cod-

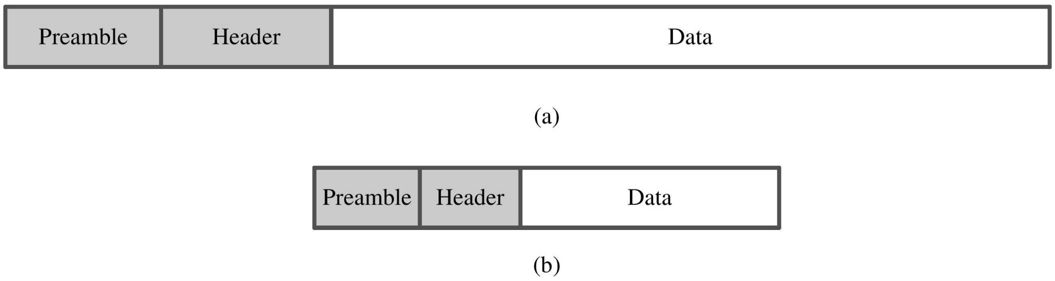

Figure 2.9: Example of a a) long-frame structure and b) short-frame structure [4].

ing schemes (Turbo codes, low density parity check codes (LDPC), polar codes) [69], multi-connectivity, retransmission, etc. A comprehensive survey of latency reduction solutions was provided in [65] from three aspects: 1) radio access network (RAN), 2) core network and 3) caching. From the perspective of RAN, latency can be minimised by shortening the TTI duration (short-frame transmission) [4, 34, 35], advanced multi-carrier techniques (*e.g.*, GFDM [70] , FBMC [71], universal filtered multi-carrier [71], nonorthogonal multiple access (NOMA) [72,73]), grant-free radio access [74], FD [75,76], etc. Most existing work on URLLC focused on short-frame transmission, through reducing either the symbol duration (increasing the subcarrier spacing) or the number of symbols per TTI [33].

Fig. 2.9 illustrates an example of a long-frame structure adopted in current wireless networks and a short-frame structure for 5G and B5G networks. Short-frame transmission has two serious problems as follows. On one hand, classical information-theoretic performance metrics relevant for long frames, *i.e.*, ergodic capacity and outage capacity, are no longer applicable for short frames, since the law of large number cannot be applied [4]. To tackle this, new performance metrics were introduced for short frames in [4], namely maximum coding rate at finite frame length and finite frame error probability. On the other hand, the length of pilot is a challenging issue in short-frame transmission [4, 34, 77, 78]. Pilot transmission is important for a reliable receiver design, such as obtaining a good synchronisation and channel estimation, which requires a large number of pilots. However, a large number of pilots are likely to reduce the useful data

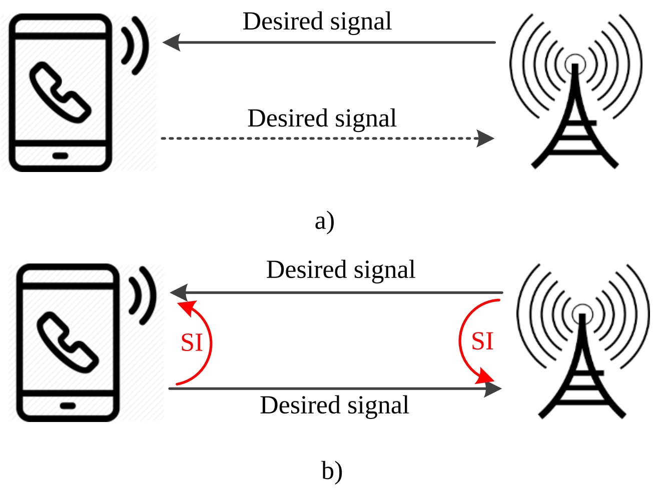

Figure 2.10: a) HD communications and b) FD communications.

rate fraction in short-frame transmission, resulting in low spectrum efficiency.

2.3.2 FD Communications

The traditional wireless communication systems usually work in half-duplex (HD) mode where a transceiver transmits and receivers information in disjoint time-slots or frequency-slots referred to as time-division duplex or frequency-division duplex, respectively, or in distinct orthogonal spectrum-spreading codes, so that SI from its transmission to its own reception can be avoided [32]. To meet the demand for high spectrum efficiency in 5G and B5G networks, FD communications have recently gained significant attention in academia and industry, where simultaneous transmission and reception are allowed over the same frequency slots [23, 31, 32]. Fig. 2.10 illustrates the transmission and reception schemes for HD and FD communication systems, respectively. In the following chapters, HD communications are investigated, unless otherwise specified.

As summarised in [31], FD communications offer a handful of advantages:

- The ergodic capacity can be doubled thanks to full utilisation of both time and frequency resources;

- The feedback delay can be reduced substantially, since the feedback signalling such as control information and channel state information can be received during data signal transmission and thus the air interface latency can be shortened;

- The end-to-end delay can be reduced especially for FD assisted relay systems, as the relay terminal allows the simultaneous reception of data from a source terminal and transmission of data to a destination terminal;

- The network security can be enhanced, since the eavesdropper is likely to receive a mixture of the desired signal and SI, which is hard for the eavesdropper to decode the desired signal due to the presence of SI.

Despite numerous merits, FD communications have a serious issue - strong SI. Due to the short distance between the transmit antennas and receive antennas at a terminal, the SI is likely to have stronger power than the desired signal. How to suppress SI to a reasonable and acceptable level is being extensively investigated. There are mainly three techniques to cancel SI, namely passive cancellation (PC), analogue cancellation (AC) and digital cancellation (DC) [79]. PC is the first stage of SI cancellation, which is achieved by antenna placement, directional antenna, antenna shielding, and so on [80, 81]. In the second stage, SI is further mitigated in the analogue domain before the low-noise amplifier and analogue-to-digital converter to avoid overloading or saturation [80, 82]. DC is the last stage of SI cancellation, which estimates the SI channel, creates a replica of the received SI and then cancels it from the received signal in the digital domain [80].

As mentioned previously, the acquiring of SI channel is an important step to recover the SI signal and then cancel it. The received mixed signal in the presence of both desired and SI signals can be given by [83]

$$\begin{aligned} y[k] = {} & \sum\nolimits_{l=0}^{L-1} \hbar_{\mathrm{S}}[l] x_{\mathrm{S}}[k-l] \\ & + \sqrt{\frac{1}{\rho}} \sum\nolimits_{l=0}^{L-1} \hbar_{\mathrm{I}}[]l] x_{\mathrm{I}}[k-l] + w[k], \quad k = 0, 1, \cdots, K-1, \end{aligned} \tag{2.12}$$

where x_{S} and x_{I} denote the desired signal and SI, respectively, $\hbar_{\mathrm{S}}[0], \hbar_{\mathrm{S}}[1], \cdots, \hbar_{\mathrm{S}}[L-1]$

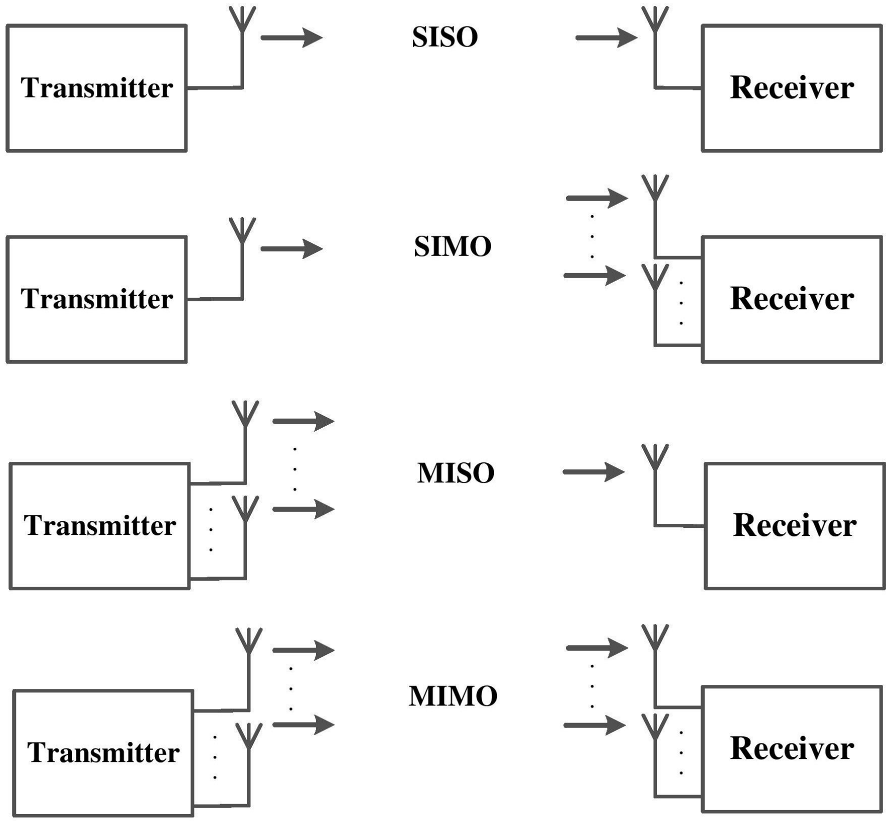

Figure 2.11: SISO, SIMO, MISO and MIMO

and $\hbar_{\mathrm{I}}[0], \hbar_{\mathrm{I}}[1], \cdots, \hbar_{\mathrm{I}}[L-1]$ are the desired CIR and SI CIR, ρ is the input desired signal to SI and noise ratio, denoted as SINR, and $w[k]$ is the additive noise. Specifically, in DC, the SI channel $\hbar_{\mathrm{I}}(l)$ $(l = 0, 1, \cdots, L-1)$ is estimated firstly, then the received SI signal is recovered since the transmitted SI signal is known, and finally it is cancelled from the received signal.

2.3.3 Multi-Antenna Communications

Multi-antenna communications, with multiple antennas at transmitter and/or receiver, are able to significantly improve the throughput and reliability of wireless communication systems [5, 39, 84–86]. It has gained overwhelming attention from both academia and industry in the past decades. According to the numbers of transmit antennas and receive antennas, wireless communications fall into four classes, including single-input single-ouput (SISO), single-input multi-output (SIMO), multi-input single-output (MISO) and MIMO, as depicted in Fig. 2.11. Multi-antenna communications have been extensively adopted in numerous wireless communication systems and commercial standards [13, 87], including WiFi, WiMax, LTE and LTE-A. Table 2.2 shows the antenna configurations for the respective commercial standards, where $N_\mathrm{t} \times N_\mathrm{r}$ denote that N_t and N_r antennas are equipped at transmitter and receiver, respectively. For instance, 8 antennas are equipped at both transmitter and receiver for LTE-A and IEEE 802.11ac communication systems. Four key benefits can be provided by multi-antenna communications, including spatial diversity gain, spatial multiplexing gain, array gain and interference suppression [13, 54].

Table 2.2: Commercial wireless standards that use multi-antenna technology [13].

Wireless standard	Antenna configurations
IEEE 802.11n (WiFi)	4×4
IEEE 802.16e (WiMAX)	4×4
HSPA$^+$ (Enhanced HSPA)	2×2
LTE (3.9G)	4×4
LTE-Advanced (4G)	8×8
IEEE 802.11ac	8×8

Spatial diversity gain

Due to wireless channel fading, the strength of the received signal fades/fluctuates with time, giving rise to poor BER. Diversity techniques are thus introduced to overcome the detrimental effects of wireless channel fading, where multiple copies of the same signal are transmitted through independent fading channels. There are mainly three types of diversity, including time diversity, frequency diversity and spatial diversity [88]. Time diversity and frequency diversity refer to transmitting the same signal at different time slots and frequency slots, respectively. With regard to spatial diversity, the same signal is transmitted through different physical paths between transmitter and receiver. Spatial diversity order is typically considered as a performance metric to evaluate the amount of spatial diversity. It is defined as the number of independent copies of transmitted signal that can be exploited for combining at receiver. In particular, a MIMO system equipped with N_t transmit antennas and N_r receive antennas is capable of offering $N_\mathrm{t}N_\mathrm{r}$ independent signal copies, yielding a spatial diversity order of $N_\mathrm{t}N_\mathrm{r}$. In general, the larger the spatial diversity order, the higher reliability of wireless communication system. Space-time coding is an effective and well-known approach to enhance spatial diversity, such as space-time trellis codes and space-time block codes [54].

Spatial multiplexing gain

The most remarkable advantage of multi-antenna communications is spatial multiplexing gain. Instead of spatial diversity which transmits multiple copies of the same signal, spatial multiplexing refers to transmitting multiple independent signals at the same time over the same bandwidth [54, 85]. By exploiting channel fading (*e.g.*, rich scatters over the air), the individual transmitted signal can be recovered. The maximum number of independent signals that can be supported through spatial multiplexing is the minimum of the number of transmit antennas N_t and the number of receive antennas N_r, *i.e.*, $\min\{N_\mathrm{r}, N_\mathrm{r}\}$. The spatial multiplexing can considerably increase the system throughput and data rate. A widely known spatial multiplexing scheme is Bell-Labs Layered Space-Time Architecture (BLAST) [89].

Array gain

In addition to providing small bit error rates and high data rates, multi-antenna communications are also able to enhance SNR at receiver by combining the received multiple signal copies coherently [54]. Such SNR enhancement is referred to as array gain. Combining techniques fall into three classes, including selective combining, equal gain combining and maximal ratio combining [54]. Selective combing compares the copies at each sample time and selects the largest value for the output of combiner, while equal gain combining aims to add all the received copies together. Regarding maximal ratio combining, all copies are first scaled with respect to SNR of each copy, and then add them together. Generally, the average SNR enhancement in a SIMO system is proportionate to the number of receive antennas.

Interference Suppression

Table 2.3: Benefits of multi-antenna communications.

Benefits	Purpose	Technique
Spatial diversity gain	Improve reliability (Decrease BER)	Space-time coding • Space-time trellis codes • Space-time block codes
Spatial multiplexing gain	Improve throughput (Increase data rate)	BLAST
Array gain	Improve SNR	Combining techniques • Selective combining • Equal gain combining • Maximal ratio combining
Interference suppression	Improve SINR	Beamforming

Interference may arise when multiple antennas transmit information using shared time and frequency resources. For the sake of interference suppression, multi-antenna communications introduce a spatial dimension that enables an increased separation between the desired signal and the interfering signal [13, 54]. Beamforming is a popular and intriguing technique, where the beam patterns of transmit and receive antennas can be steered in the desired directions only, thus suppressing the interference and increasing SINR.

Table 2.3 summarises the benefits of multi-antenna communications. Nevertheless, those benefits do not come for free. Multi-antenna communications are confronted with several challenges as follows [89]. First, the use of multiple transmitter/receiver chains gives rise to increased hardware costs and power consumption. Multi-antenna communications are also more susceptible to the impairments in practical links than single-antenna communications. Massive MIMO by means of a large number of antennas (100 or more) at base station (BS) gains lots of popularity in last few years, and has been regarded as a promising technique in 5G to support the ever-growing teletraffic [90–92]. However, it has a serious issue of pilot contamination.

Chapter 3

Overview of RF Channel and Impairments

A good understanding of RF channel and impairments is significant for any wireless communication systems. Wireless channel refers to everything that signals experience when they travel through transmit antennas to receive antennas. In addition, owing to the use of low-cost and low-power analogue components, such as filters, mixers and amplifiers, non-ideal factors inevitably arise in the transmitter and receiver, including CFO, IQ imbalance, and so forth [93,94]. Such non-ideal factors are likely to deteriorate the system performance, and thereby it is of great importance to investigate them.

This chapter starts with an introduction of channel model, including radio propagation mechanisms, large-scale fading and small-scale fading. Then, training based channel estimation approaches and decision-directed channel estimation method in the literature are presented. After that, an overview of CFO and IQ imbalance as well as their estimation approaches are demonstrated, respectively.

3.1 Channel Model

3.1.1 Radio Propagation Mechanisms

A signal transmitted into a wireless medium can arrive at receiver through either direct propagation path or indirect propagation path [13]. Direct propagation path is also known as line-of-sight (LoS) path, where the signal reaches at receiver directly [5]. Oppositely, non-LoS (NLoS) refers to that the signal arrives at receiver through reflection, diffraction or scattering [5]. LoS path typically has the shortest time delay and the strongest signal strength among all the received paths. Fig. 3.1 depicts the radio propagation mechanisms consisting of LoS path, NLoS paths with reflection, diffraction or scattering [5]. The reflection, diffraction and scattering are described as follows [5]:

- **Reflection:** when a signal bounces off a smooth object whose dimension is considerably large in comparison to the signal wavelength, such as the ground and buildings;

- **Diffraction:** when a signal propagates through sharp edges, such as street corners;

- **Scattering:** when a signal travels through multiple objects whose dimensions are smaller than or comparable to the signal wavelength, such as rain drops.

The aforementioned propagation mechanisms including LoS path, reflection, diffraction and scattering are combined and can be classified into large-scale fading and small-scale fading. Large-scale fading includes path loss and shadowing, which cause signal power attenuation by means of distance and large objects (*e.g.*, buildings and hills), respectively [95]. Small-scale fading, also known as multi-path fading, is caused by the constructive and destructive combining of multiple signal paths between transmitter and receiver. As its name suggests, the signal power fluctuates rapidly within a small region [95]. Fig. 3.2 illustrates the received signal power as a function of distance for path loss, shadowing and small-scale fading [5].

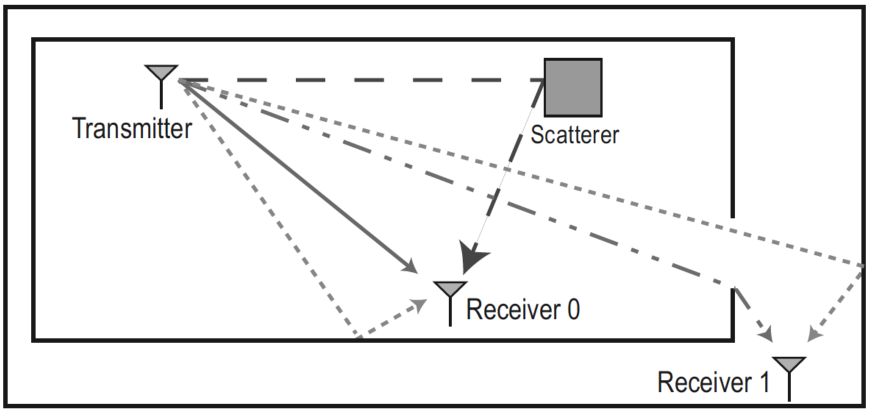

Figure 3.1: Radio propagation mechanisms - solid line: LoS path; dotted lines: reflection; dashed lines: scattering and dash-dot lines: diffraction [5].

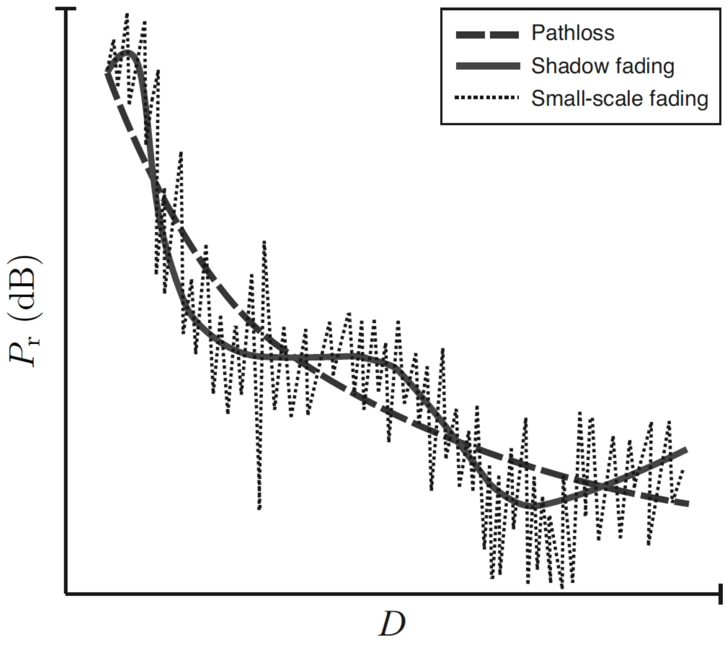

Figure 3.2: Received signal power as a function of distance for path loss, shadowing and small-scale fading [5].

3.1.2 Large-Scale Fading

Large-scale fading falls into two classes: path loss and shadowing. Path loss refers to the degree of signal power attenuation with the increase of the distance between transmitter and receiver [54]. A simplified log-distance path loss model is expressed as [54]

$$\mathrm{PL} = 10n\log_{10}\left(\frac{d}{d_{\mathrm{rf}}}\right) + \mathrm{PL}_{\mathrm{rf}}, \tag{3.1}$$

where n is the path loss exponent, d is the distance between transmitter and receiver, and $\mathrm{PL}_{\mathrm{rf}}$ is the path loss value in free space for the reference distance d_{rf}. However, the receivers with the same distance from the transmitter may suffer different signal attenuation due to the distinct surrounding environments. This effect or fading is called shadowing, which blocks the signal energy to some extent by means of several neighbouring objects, such as tall buildings and hills [54].

3.1.3 Small-Scale Fading

Two channel parameters are introduced first to facilitate a better understanding of small-scale fading, namely delay spread and Doppler spread. Delay spread is defined as a range of propagation delays of multiple versions of the transmitted signal along different paths [54]. Delay spread is typically utilised to evaluate the extent of small-scale fading. Doppler spread is a measure of frequency spreading of the received signal owing to relative motions between transmitter, scatters and receiver [54]. It is noteworthy that the inverse of delay spread is coherence bandwidth, whereas the inverse of Doppler spread is coherence time [54]. As a result, small-scaling fading channel falls into four classes as follows [13, 54, 96, 97]:

- **Frequency flat fading:** if the signal bandwidth is smaller than coherence bandwidth or the symbol period is larger than or comparable to delay spread;
- **Frequency selective fading:** if the signal bandwidth is larger than or equal to coherence bandwidth or the symbol period is smaller than delay spread;

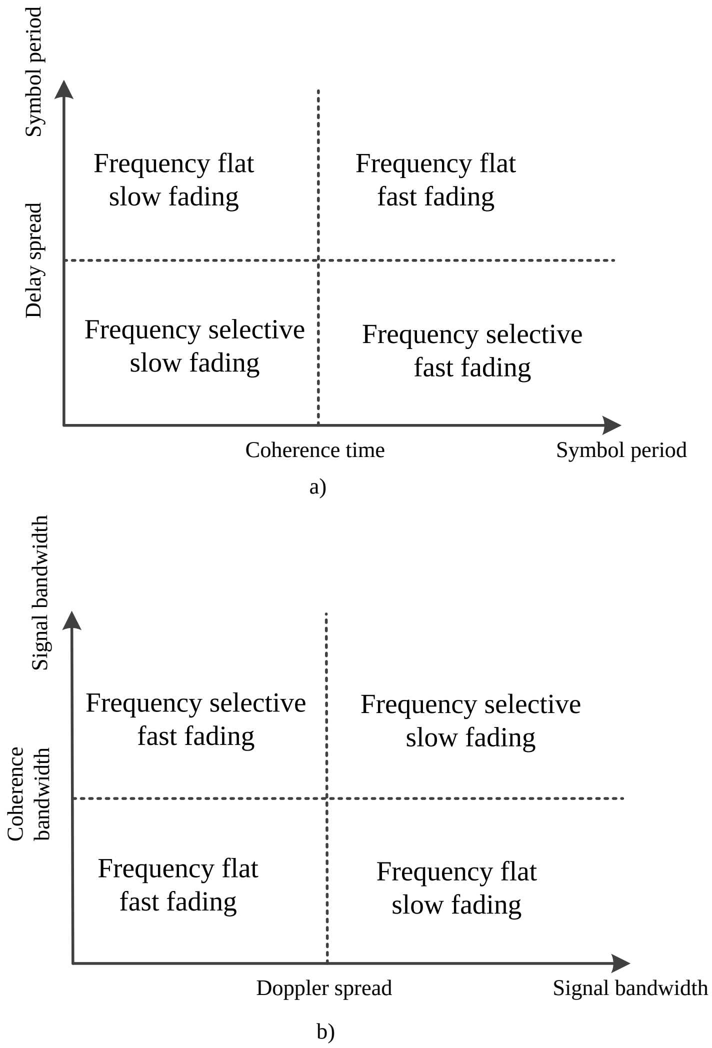

Figure 3.3: Four classes of small-scaling fading channel with respect to: a) symbol period and b) signal bandwidth, including flat slow fading, flat fast fading, frequency selective slow fading, and frequency selective fast fading.

- **Slow fading:** if symbol period is smaller than coherence time or the signal bandwidth is larger than or comparable to Doppler spread;

- **Fast fading:** if symbol period is larger than or equal to coherence time or the signal bandwidth is smaller than Doppler spread.

Fig. 3.3 summarises four classes of small-scaling fading channel with respect to symbol period and signal bandwidth, respectively. Frequency selective fading channel is the focus of this thesis.

Frequency selective fading channel

Frequency selective fading channel is also known as multi-path channel. Assume that there are L_{p} resolvable propagation paths. Define μ_l and τ_l as the complex path gain and path delay of the l-th ($l = 0, 1, \cdots, L_{\mathrm{p}} - 1$) path between transmitter and receiver, respectively. The time delay of the first arriving path τ_0, either being LoS or NLoS, represents the TOA [29, 98], and requires to be estimated for the desired application. For example, the estimated TOA can be used by the relevant localisation techniques in [98], either in LoS or NLoS scenarios, to determine the position of the target terminal.

The discrete CIR at the k-th ($k = 0, \cdots, K - 1$) sampling point is defined as

$$\hbar[k] = \sum\nolimits_{l=0}^{L_{\mathrm{p}}-1} \mu_l \delta(k/f_{\mathrm{s}} - \tau_l), \tag{3.2}$$

where f_{s} is the sampling rate. Denote $\boldsymbol{\hbar} = [\hbar[0], \hbar[1], \cdots, \hbar[K-1]]^T$ as the CIR vector. Its corresponding CFR vector is obtained as $\bar{\mathbf{h}} = [\bar{h}[0], \bar{h}[1], \cdots, \bar{h}[K-1]]^T$, with $\bar{h}[k]$ given by [99]

$$\bar{h}[k] = \sum\nolimits_{l=0}^{L_{\mathrm{p}}-1} \mu_l e^{-j2\pi k \tau_l f_{\mathrm{s}}/K}. \tag{3.3}$$

3.2 Channel Estimation

Channel estimation is a major task in wireless communications systems. The acquisition of channel state information is crucial for signal detection and resource allocation. Training based channel estimation approaches and decision-directed channel estimation approach are reviewed in the following.

3.2.1 Training Based Channel Estimation

Generally, training based channel estimation approaches fall into two classes: non-parametric model and parametric-model (PM). Non-parametric model based approach includes least-square (LS), linear minimum mean square error (LMMSE), semi-blind subspace-based channel estimator, etc. PM based approach approach aims to estimate channel parameters which characterise either CIR or CFR.

It is noteworthy that the training based approaches can be assisted by either preamble or pilot. Regarding the preamble aided approaches, all subcarriers of an OFDM symbol should be utilised for training. In contrast, regarding the pilot aided approaches, some subcarriers of an OFDM symbol are used for training while the rest subcarriers can be for data transmission. Hence, preamble can be regarded as a special case of pilot. For consistence, pilot is utilised throughout this thesis.

LS Based Channel Estimation

LS algorithm is very simple and has been widely applied for channel estimation [1]. Given a number of pilots, channel is estimated to minimise the squared error between the actual received signal and the estimated received signal. In the following, LS based channel estimators in both frequency domain and time domain are demonstrated for OFDM systems, respectively.

Frequency Domain

According to Subsection 2.2.1, the received OFDM signal vector in frequency domain is given by

$$\bar{\mathbf{y}} = \bar{\mathbf{H}}\mathbf{d} + \bar{\mathbf{w}}, \tag{3.4}$$

where $\bar{\mathbf{H}}$ is diagonal CFR matrix, $\mathbf{d}$ is frequency-domain pilot vector and $\bar{\mathbf{w}}$ is noise vector. (3.4) is equivalent to

$$\bar{\mathbf{y}} = \mathbf{D}\bar{\mathbf{h}} + \bar{\mathbf{w}}, \tag{3.5}$$

where $\mathbf{D} = \text{diag}\{\mathbf{d}\}$ is diagonal pilot matrix in frequency domain and $\bar{\mathbf{h}}$ is CFR vector. Hence, CFR vector $\bar{\mathbf{h}}$ can be estimated by

$$\hat{\bar{\mathbf{h}}}_{\text{LS}} = \arg \min_{\bar{\mathbf{h}}} \| \bar{\mathbf{y}} - \mathbf{D}\bar{\mathbf{h}} \|_{\text{F}}^2 . \tag{3.6}$$

The LS CFR estimate is finally written as

$$\hat{\hat{\mathbf{h}}}_{\mathrm{LS}} = (\mathbf{D}^H\mathbf{D})^{-1}\mathbf{D}^H\bar{\mathbf{y}}. \tag{3.7}$$

Since $\mathbf{D}$ is a diagonal matrix, LS CFR estimate can be further given by

$$\hat{\hat{\mathbf{h}}}_{\mathrm{LS}} = \mathbf{D}^{-1}\bar{\mathbf{y}}. \tag{3.8}$$

The LS CFR estimate can be written for each subcarrier as

$$\hat{\hat{h}}_{\mathrm{LS}}[k] = \frac{\bar{y}[k]}{d[k]}, \quad k = 0, 1, \cdots, K-1. \tag{3.9}$$

Time Domain

According to Subsection 2.2.1, the received OFDM signal in time domain is expressed as

$$\mathbf{y} = \mathbf{H}\boldsymbol{\epsilon} + \mathbf{w}, \tag{3.10}$$

where $\mathbf{H}$ is the circulant channel matrix and $\boldsymbol{\epsilon}$ is time-domain pilot vector. (3.10) is equivalent to

$$\mathbf{y} = \boldsymbol{\Xi}\boldsymbol{\hbar} + \mathbf{w}, \tag{3.11}$$

where $\boldsymbol{\hbar} = [\hbar_0, \hbar_1, \cdots, \hbar_{L-1}]^T$ is CIR vector of length L, and $\boldsymbol{\Xi}$ is time-domain circulant pilot matrix defined as

$$\boldsymbol{\Xi} = \begin{bmatrix} \epsilon[0] & \epsilon[K-1] & \cdots & \epsilon[K-L+1] \\ \epsilon[1] & \epsilon[0] & \ddots & \vdots \\ \vdots & \vdots & \ddots & \epsilon[K-1] \\ \vdots & \vdots & \ddots & \epsilon[0] \\ \vdots & \vdots & \ddots & \vdots \\ \epsilon[K-1] & \epsilon[K-2] & \cdots & \epsilon[K-L] \end{bmatrix}. \tag{3.12}$$

Given a pilot matrix $\mathbf{\Xi}$, CIR can be estimated by

$$\hat{\boldsymbol{\hbar}}_{\mathrm{LS}} = \arg\min_{\boldsymbol{\hbar}} \parallel \mathbf{y} - \mathbf{\Xi}\boldsymbol{\hbar} \parallel_{\mathrm{F}}^{2}. \tag{3.13}$$

Hence, the CIR LS estimate is given by

$$\hat{\boldsymbol{\hbar}}_{\mathrm{LS}} = (\mathbf{\Xi}^{H}\mathbf{\Xi})^{-1}\mathbf{\Xi}^{H}\mathbf{y}. \tag{3.14}$$

LS based channel estimator has been widely used in OFDM systems thanks to its low complexity. It has also been applied to GFDM systems, which however suffers high training overhead and an error floor due to ICI and ISI caused by the nonorthogonal filters of GFDM [9]. An LS based SI channel estimator was proposed in [100] for FD OFDM systems, which however treats the desired signal as additive noise, resulting in poor performance. A two-stage LS cancellation scheme was presented in [101] for FD OFDM, which iterates between SI cancellation and signal detection. However, its performance requires a good initial estimate of the desired channel.

LMMSE Based Channel Estimation

It is noteworthy that LS channel estimate may suffer noise enhancement due to the term $(\mathbf{D}^{H}\mathbf{D})^{-1}\mathbf{D}^{H}\bar{\mathbf{w}}$ or $(\mathbf{\Xi}^{H}\mathbf{\Xi})^{-1}\mathbf{\Xi}^{H}\mathbf{w}$. To suppress the noise enhancement in LS based channel estimator, LMMSE based channel estimator is proposed, which aims to minimise the mean square error between the true channel and the channel estimate [49]. Taking the LS CFR estimate as an example, the LMMSE based CFR estimate is given by

$$\hat{\bar{\mathbf{h}}}_{\mathrm{LMMSE}} = \arg\min_{\hat{\bar{\mathbf{h}}}_{\mathrm{LS}}} \parallel \bar{\mathbf{h}} - \hat{\bar{\mathbf{h}}}_{\mathrm{LS}} \parallel_{\mathrm{F}}^{2}. \tag{3.15}$$

Thus, the CFR estimate by means of LMMSE is

$$\hat{\bar{\mathbf{h}}}_{\mathrm{LMMSE}} = \mathbf{R}_{\bar{\mathbf{h}}\bar{\mathbf{h}}}(\mathbf{R}_{\bar{\mathbf{h}}\bar{\mathbf{h}}} + \sigma^{2}\mathbf{I}_{K})^{-1}\hat{\bar{\mathbf{h}}}_{\mathrm{LS}}, \tag{3.16}$$

where $\mathbf{R}_{\bar{\mathbf{h}}\bar{\mathbf{h}}} = \mathbb{E}\{\bar{\mathbf{h}}\bar{\mathbf{h}}\}$ is the auto-correlation matrix of CFR vector $\bar{\mathbf{h}}$, σ^2 is noise variance, and $\mathbf{I}_K$ is a $K \times K$ identity matrix.

PM Based Channel Estimation

PM based channel estimation aims to estimate channel parameters which characterise the channel response, such as the number of paths, path delays, and path gains [49]. PM based approach can enhance channel estimation greatly by exploiting spatial correlation and temporal correlation [99, 102]. The pilot overhead can be reduced greatly as well, since the number of required pilots can be shortened from K to $2L_{\mathrm{p}}$, where K and L_{p} are respectively the number of subcarriers per OFDM symbol and the number of resolvable channel paths [99].

Denote $\hat{\bar{\mathbf{h}}}_i = [\hat{\bar{h}}_i[0], \hat{\bar{h}}_i[1], \cdots, \hat{\bar{h}}_i[K-1]]^T$ as the CFR estimate by either LS or LMMSE in the i-th OFDM symbol. Define L_{p}, $\mu_{l,i}$ and $\tau_{l,i}$ as the number of resolvable propagation paths, the complex path gain and path delay of the l-th ($l = 0, 1, \cdots, L_{\mathrm{p}}-1$) path corresponding to the i-th symbol. It is assumed that channel path delays change slowly and remain constant for a frame of N_{s} OFDM symbols, *i.e.*, $\tau_l = \tau_{l,i}$ for $i = 0, 1, \cdots, N_{\mathrm{s}} - 1$. f_{s} is defined as the sampling rate. $\hat{\bar{\mathbf{h}}}_i$ can be expressed as

$$\hat{\bar{\mathbf{h}}}_i = \boldsymbol{\nu}\boldsymbol{\mu}_i + \bar{\mathbf{w}}_i, \tag{3.17}$$

where $\boldsymbol{\nu} = [\boldsymbol{\nu}_0, \boldsymbol{\nu}_1, \cdots, \boldsymbol{\nu}_{L_{\mathrm{p}}-1}]$ with $\boldsymbol{\nu}_l = [1, e^{-\jmath 2\pi\tau_l f_{\mathrm{s}}/K}, \cdots, e^{-\jmath 2\pi(K-1)\tau_l f_{\mathrm{s}}/K}]^T$, $\boldsymbol{\mu}_i = [\mu_{0,i}, \mu_{1,i}, \cdots, \mu_{L_{\mathrm{p}}-1,i}]^T$, and $\bar{\mathbf{w}}_i$ is noise vector.

The major task of PM based approach is to estimate path delays. The number of resolvable channel paths can be determined by minimum description length and Akaike information criterion [49]. After time delays are obtained, channel gains can be easily determined by LS approach [102]. In the following, estimation of signal parameters via rotational invariance technique (ESPRIT) algorithm is presented for estimation of time delays.

ESPRIT

ESPRIT and multiple signal classification (MUSIC) are well-known signal processing techniques [29]. They can be applied to a wide variety of problems including accurate detection and estimation of sinusoids in noise, such as direction of arrival, phase, frequency, time delay, etc. MUSIC algorithm requires an exhaustive search and is computationally inefficient [29]. In contrast, ESPRIT algorithm has a simple implementation with a closed-form solution, and gains lots of popularity from both the research community and industry [6, 99, 102, 103]. ESPRIT exploits an underlying rotational invariance among signal subspaces, and it operates as follows:

Step 1. Calculate the auto-correlation matrix of CFR vector

$$\mathbf{R}_{\bar{\mathbf{h}}\bar{\mathbf{h}}} = \frac{1}{N_\mathrm{s}} \sum_{i=0}^{N_\mathrm{s}-1} \hat{\bar{\mathbf{h}}}_i \hat{\bar{\mathbf{h}}}_i^H. \tag{3.18}$$

Step 2. Implement eigenvalue decomposition (EVD) on the channel auto-correlation matrix $\mathbf{R}_{\bar{\mathbf{h}}\bar{\mathbf{h}}}$ to obtain the eigenvectors corresponding to the signal subspace denoted as $\mathbf{u}$.

Step 3. Define $\mathbf{u}_1$ and $\mathbf{u}_2$ as $(K-1) \times L_\mathrm{p}$ matrices, which respectively correspond to the first $(K-1)$ rows and last $(K-1)$ rows of $\mathbf{u}$. Note that $\mathbf{u}_1$ and $\mathbf{u}_2$ have a relationship as

$$\mathbf{u}_2 = \mathbf{u}_1 \mathbf{v}, \tag{3.19}$$

where $\mathbf{v}$ is of size $L_\mathrm{p} \times L_\mathrm{p}$, whose diagonal element is given by $\mathrm{diag}\{\mathbf{v}\} = [e^{-\jmath 2\pi\tau_0 f_\mathrm{s}/K}, e^{-\jmath 2\pi\tau_1 f_\mathrm{s}/K}, \cdots, e^{-\jmath 2\pi\tau_{L_\mathrm{p}-1} f_\mathrm{s}/K}]$. The estimate of $\mathbf{v}$ is determined as

$$\hat{\mathbf{v}} = (\mathbf{u}_1^H \mathbf{u}_1)^{-1} \mathbf{u}_1^H \mathbf{u}_2. \tag{3.20}$$

Step 4. The time delays are extracted from the diagonal elements of $\hat{\mathbf{v}}$ by

$$\hat{\tau}_l = \frac{K \angle\{\hat{\mathbf{v}}(l,l)\}}{2\pi f_\mathrm{s}}, \quad l = 0, 1, \cdots, L_\mathrm{p} - 1. \tag{3.21}$$

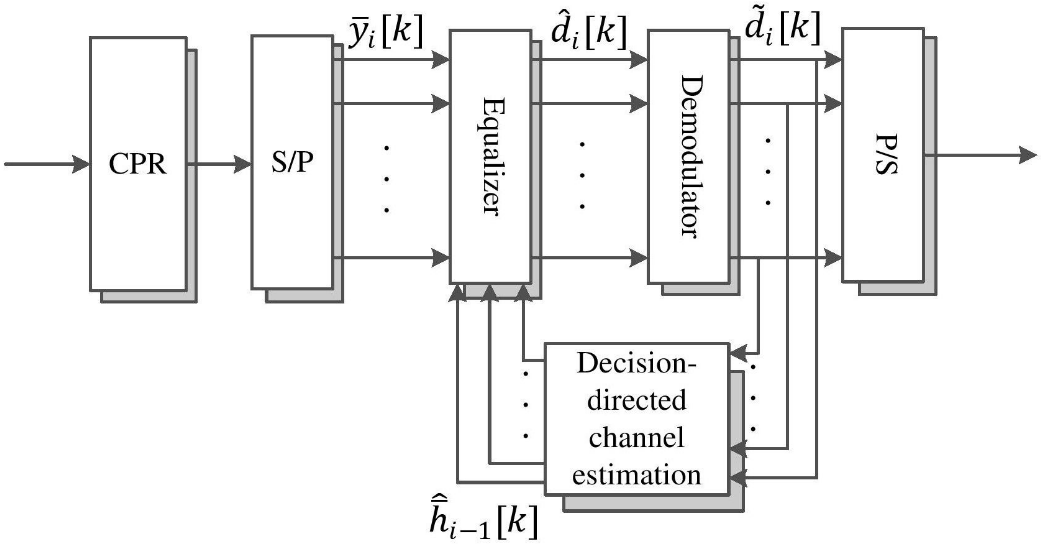

Figure 3.4: Block diagram for an OFDM receiver with decision-directed channel estimation [1].

The time delay of the first arriving path ($l = 0$) is referred to as TOA, which can be exploited for localisation.

3.2.2 Decision-Directed Channel Estimation

Once initial channel estimate is obtained by either LS or LMMSE approach with pilots, channel estimate can be updated and refined with decision-directed channel estimator [1]. In the following, how to exploit the detected signal feedback to track channel while utilising the new channel estimate to detect signal successively is demonstrated.

Fig. 3.4 shows the block diagram for an OFDM receiver with decision-directed channel estimation. Define $\hat{\bar{h}}_{i-1}[k]$ as the channel estimate by using the $(i-1)$-th OFDM symbol. The i-th OFDM symbol can be determined as

$$\hat{d}_i[k] = \frac{\bar{y}_i[k]}{\hat{\bar{h}}_{i-1}[k]}. \tag{3.22}$$

Let $\tilde{d}_i[k]$ denote the hard-decision value for the signal estimate $\hat{d}_i[k]$. Then, an updated

CFR estimate can be given by

$$\hat{\tilde{h}}_i[k] = \frac{\bar{y}_i[k]}{\tilde{d}_i[k]}. \tag{3.23}$$

As the second step needs the symbol decision made in the first step, this approach is known as decision-directed channel estimation approach. It can track the possibly time-varying channel or enhance channel estimation iteratively. With regard to iterative channel estimation, the index i in (3.22) and (3.23) should denote the i-th iteration, instead of the i-th OFDM symbol.

Decision-directed channel estimator was exploited to suppress SI in digital domain for FD OFDM systems in [101] and [104]. By means of decision-directed channel estimator, Lee *et al* regarded the detected symbols as virtual pilots to overcome the pilot shortage in short-frame communications for URLLC in [34]. The major issue of decision-directed channel estimation is error propagation, where any error in the detected symbol may propagate to the subsequent channel estimation. The performance deterioration due to error propagation can be mitigated to some extent by averaging over the channel estimates between adjacent subcarriers or successive OFDM symbols [1].

3.3 CFO and Its Estimation

In this section, CFO is first introduced, followed by a review of CFO estimation approaches.

3.3.1 CFO

In general, there are two ways to give rise to CFO. On one hand, CFO is incurred by the unavoidable frequency mismatch between local oscillators (LOs) at transmitter and receiver, which are utilised to respectively convert the baseband transmitted signal up to the passband at transmitter and the received passband signal down to the baseband at receiver [1, 53]. On the other hand, CFO is caused by Doppler frequency shift due to the relative motion between the transmitter and receiver [1, 53]. Both two types of CFO result in a serious performance degradation [105].

Define f_{t} and f_{r} as the carrier frequencies at transmitter and receiver, respectively. The normalised CFO ϕ is given by the ratio of the carrier frequency difference between transmitter and receiver to subcarrier spacing Δf [45], *i.e.*,

$$\phi = \frac{f_{\mathrm{r}} - f_{\mathrm{t}}}{\Delta f}, \tag{3.24}$$

where $\phi = \phi_{\mathrm{I}} + \phi_{\mathrm{F}}$, with $\phi_{\mathrm{I}} = \lfloor \phi \rfloor$ and ϕ_{F} as the integer part and fractional part of ϕ, respectively. The fractional CFO (fCFO) ϕ_{F} has a range of $[-0.5, 0.5)$, which is likely to destroy the orthogonality among subcarriers in OFDM systems and thus result in ICI [1, 53, 94, 106]. ICI becomes severe as fCFO increases. Besides, fCFO worsens ICI and ISI caused by the nonorthogonal prototype filters in GFDM/GFDMA systems. In contrast, the integer CFO (iCFO) does not lead to ICI, but induces a cyclic shift of ϕ_{I} in the received frequency-domain signal. After corrupted by CFO, the received OFDM signal in time domain can be given by

$$y[k] = e^{\frac{\jmath 2\pi \phi k}{K}} \sum\nolimits_{l=0}^{L-1} \hbar[l] x[k-l] + w[k], \quad k = 0, 1, \cdots, K-1. \tag{3.25}$$

3.3.2 CFO Estimation

A number of CFO estimation approaches for wireless communication systems are reviewed in the following, including Moose's CFO estimator [107], maximum likelihood (ML) CFO estimator [7], CP aided blind CFO estimator [108], blind closed-form CFO estimator [8], semi-blind subspace-based joint channels and CFOs estimator [12], and rank-reduction criterion based CFO estimator [14]. Tables 3.1 and 3.2 summarise and compare the aforementioned six CFO estimators.

Moose's CFO Estimator

Assuming that channel maintains constant for two consecutive identical OFDM symbols, the corresponding two received OFDM symbols in the presence of CFOs and absence

Table 3.1: Comparison among CFO estimation approaches (Q: Parameter for training sequence design in [7], M: Number of subsymbols per GFDM/GFDMA symbol, K: Number of subcarriers per OFDM symbol or GFDM/GFDMA subsymbol).

CFO estimation algorithm	Users	Antennas	Estimation range	Complexity	Training overhead
Moose's CFO estimator [107]	Single	SISO	$[-0.5, 0.5)$	Low	High
ML CFO estimator [7]	Single	MIMO	$[-\frac{Q}{2}, \frac{Q}{2})$	High	High
CP aided blind CFO estimator [108]	Single	SISO	$[-\frac{0.5}{M}, \frac{0.5}{M})$	Low	Low
Blind closed-form CFO estimator [8]	Single	SIMO	$[-0.5, 0.5)$	Low	Low
Semi-blind subspace-based joint channels and CFOs estimator [12]	Multiple	MIMO	$[-\frac{K}{2}, \frac{K}{2})$	Medium	Low
Rank-reduction criterion based CFO estimator [14]	Multiple	SIMO	$[-0.5, 0.5)$	High	Low

Table 3.2: Comparison among CFO estimation approaches (continued).

CFO estimation	Required number of symbols	Other comments
Moose's CFO estimator [107]	≥ 2	• Closed-form solution • Performance degradation due to null subcarriers
ML CFO estimator [7]	≥ 1	• Exhaustive search • Suffering error propagation from iCFO estimation to fCFO estimation
CP aided blind CFO estimator [108]	≥ 1	• Closed-form solution • Sensitive to frequency selective channel
Blind closed-form CFO estimator [8]	≥ 2	• Closed-form solution • Requiring null subcarriers
Semi-blind subspace-based joint channels and CFOs estimator [12]	≥ 100	• Closed-form solution • Not applicable to CP-based systems
Rank-reduction criterion based CFO estimator [14]	≥ 1	• Exhaustive search • Requiring massive receive antennas

of noise have a constant phase shift relationship as follows [107]:

$$y_2[k] = y_1[k]e^{j2\pi\phi}, \quad k = 0, 1, \cdots, K-1, \tag{3.26}$$

where $y_1[k]$ and $y_2[k]$ are respectively the first and second OFDM symbol corresponding to k-th sample. As a result, CFO can be estimated by

$$\hat{\phi} = \frac{1}{2\pi}\tan^{-1}\{\frac{\sum_{k=0}^{K-1}\mathrm{Im}\{y_1^*[k]y_2[k]\}}{\sum_{k=0}^{K-1}\mathrm{Re}\{y_1^*[k]y_2[k]\}}\}. \tag{3.27}$$

Moose's CFO estimator is very simple and provides a closed-form solution. However, it has a number of drawbacks as follows:

- It demands at least two symbols for training, giving rise to low spectrum efficiency;
- Its performance is vulnerable to channel variation, which may degrade greatly if channel varies from symbol to symbol;

- The presence of null subcarriers is likely to degrade the system performance;
- It is feasible for fCFO estimation only, and has an estimation range of $[-0.5, 0.5)$;
- Moose's estimator was extended to GFDM systems in [3] and [11], which however is susceptible to the intrinsic ICI and ISI in GFDM systems and forms an error floor at medium and high SNRs.

ML CFO Estimator

By carefully designing the training sequence, both iCFO estimation and fCFO estimation were investigated for MIMO OFDM systems in [7]. iCFO was first estimated by ML approach, whereas fCFO was then determined through the roots of the real polynomial. iCFO estimation is mainly described in the following. Define $Q = K/P$ with P being the length of training sequence. Define $\mathbf{\Theta}_q = [\mathbf{e}_1, \mathbf{e}_2, \cdots, \mathbf{e}_{q+(P-1)Q}]$ $(0 \leq q < Q)$, where $\mathbf{e}_q$ denotes the q-th column vector of an identity matrix $\mathbf{I}_K$. Denote $\mathbf{F}$ as an $K \times K$ FFT matrix. Define N_t and N_r as the number of antennas at transmitter and receiver, respectively. The ML estimate of iCFO is given by

$$\hat{\phi}_\mathrm{I} = \arg \max_{-Q/2<\phi_\mathrm{I}\leq Q/2} \parallel \{\mathbf{I}_{N_\mathrm{r}} \otimes [\bar{\mathbf{F}}\mathbf{E}_K(-\phi_\mathrm{I})]\}\mathbf{y} \parallel_\mathrm{F}^2, \tag{3.28}$$

where $\mathbf{I}_{N_\mathrm{r}}$ is an $N_\mathrm{r} \times N_\mathrm{r}$ identity matrix, $\bar{\mathbf{F}} = [\mathbf{\Theta}_0, \mathbf{\Theta}_1, \cdots, \mathbf{\Theta}_{N_\mathrm{t}-1}]^T\mathbf{F}$, $\mathbf{E}_K(-\phi_\mathrm{I}) = \mathrm{diag}\{[1, e^{\jmath 2\pi\phi_\mathrm{I}/K}, \cdots, e^{\jmath 2\pi\phi_\mathrm{I}(K-1)/K}]^T\}$ is a diagonal iCFO matrix and $\mathbf{y}$ is the received training sequence. The ML CFO estimator has several limitations as follows:

- All transmit and receiver antennas share a common CFO;
- iCFO estimation range is limited by $[-Q/2, Q/2)$;
- It requires a mass of computations due to an exhaustive search;
- Due to two-step estimation, it suffers an error propagation from iCFO estimation to fCFO estimation.

By adopting ML approach, CFO was blindly estimated for GFDM systems in [109], which however has a limited CFO estimation range of $[-0.5/M, 0.5/M)$, where M is the number of subsymbols per GFDM symbol.

CP Aided Blind CFO Estimator

As described in Subsection 3.3.1, a CFO of ϕ leads to a phase rotation of $2\pi k\phi/K$ in the received OFDM symbol. In the ideal case, there is a phase difference of $2\pi K\phi/K = 2\pi\phi$ between CP and the corresponding rear part of an OFDM symbol, *i.e.*,

$$y[k+K] = y[k]e^{j2\pi\phi}, \quad k = 0, 1, \cdots, L_{\mathrm{cp}} - 1. \tag{3.29}$$

Hence, by means of CP, CFO can be estimated blindly in closed form by

$$\hat{\phi} = \frac{1}{2\pi}\tan^{-1}\left\{\frac{\sum_{k=0}^{L_{\mathrm{cp}}-1} \mathrm{Im}\{y[k+K]y^*[k]\}}{\sum_{k=0}^{L_{\mathrm{cp}}-1} \mathrm{Re}\{y[k+K]y^*[k]\}}\right\}. \tag{3.30}$$

CP based approach has two attractive merits: high spectrum efficiency without requiring any training symbols and low computational complexity thanks to the closed-form solution [1]. Nonetheless, CP based approach is confronted with the following challenges and limitations:

- It is vulnerable to frequency selective channel, and suffers an error floor at medium and high SNRs. This performance degradation may be mitigated by utilising more symbols in CP or increasing the CP length, which however is spectrally inefficient [53];

- Similar to Moose's CFO estimator, CP based blind CFO estimator also works for fCFO, with an estimation range of $[-0.5, 0.5)$ for OFDM and $[-0.5/M, 0.5/M)$ for GFDM [3], respectively.

Blind Closed-Form CFO Estimator

A blind closed-form CFO estimator was proposed by means of multiple receive antennas for OFDM systems in [8], where a cost function was well designed and could be expressed as a cosine function. The CFO estimate is obtained by solving the minimisation problem

$$\hat{\phi} = \arg \min_{\tilde{\phi}} C\{\tilde{\phi}\}, \tag{3.31}$$

where $\tilde{\phi}$ is the CFO trial value and $C\{\tilde{\phi}\}$ is the cost function defined as

$$C\{\tilde{\phi}\} = \sum_{n_{\mathrm{r}}=0}^{N_{\mathrm{r}}-2} \sum_{n'_{\mathrm{r}}=n_{\mathrm{r}}+1}^{N_{\mathrm{r}}-1} \sum_{i=0}^{N_{\mathrm{s}}-2} \sum_{i'=i+1}^{N_{\mathrm{s}}-1} \sum_{k=0}^{K-1} \| \epsilon^{k}_{n_{\mathrm{r}},i}\{\tilde{\phi}\}\epsilon^{k}_{n'_{\mathrm{r}},i'}\{\tilde{\phi}\} - \epsilon^{k}_{n'_{\mathrm{r}},i}\{\tilde{\phi}\}\epsilon^{k}_{n_{\mathrm{r}},i'}\{\tilde{\phi}\} \|^2_{\mathrm{F}}, \tag{3.32}$$

with $\epsilon^{k}_{n_{\mathrm{r}},i}\{\tilde{\phi}\}$ ($\epsilon^{k}_{n'_{\mathrm{r}},i'}\{\tilde{\phi}\}$) being the compensated received symbol on the k-th subcarrier in the i-th (i'-th) symbol at the n_{r}-th (n'_{r}-th) receive antenna.

An exhaustive search is demanded to solve (3.31) directly, which however requires a large number of computations. It was shown in [8] that (3.31) was exactly a cosine function. As a result, CFO could be obtained with a closed-form solution by

$$\hat{\phi} = \frac{1}{2\pi}\angle\left(\frac{C\{0.5\} - C\{0\}}{2} + \jmath\left(\frac{C\{0.5\} + C\{0\}}{2} - C\{0.25\}\right)\right). \tag{3.33}$$

The blind closed-form CFO estimator is attractive due to high spectrum efficiency and low complexity. However, it is also limited to fCFO estimation. Additionally, null subcarriers are required to enhance estimation accuracy, when fCFO approaches 0.5 or -0.5.

Semi-Blind Subspace-Based Joint Channels and CFOs Estimator

A semi-blind approach assisted by subspace was proposed to jointly estimate channels and CFOs for multi-user SIMO ZP-OFDM systems in [12]. An equivalent system model was derived first by incorporating CFOs into the corresponding transmitted signals and channels. Then, the CFO-included channels were estimated blindly with an ambiguity matrix by means of subspace approach. Periodical and consecutive pilots were carefully designed to allow joint estimation of CFOs and channel ambiguity matrix.

Define $\hbar_{u,n_\mathrm{r}}[0], \hbar_{u,n_\mathrm{r}}[1], \cdots, \hbar_{u,n_\mathrm{r}}[L-1]$ as CIR between user u and n_r-th receive antenna, $x_u[g]$ as time-domain transmitted signal of user u, and L_zp as ZP length. CFO is incorporated into channel and transmitted signal, respectively, yielding the corresponding CFO-included channel and CFO-included signal defined as $h_{u,n_\mathrm{r}}[l] = e^{\jmath 2\pi\phi l/K}\hbar_{u,n_\mathrm{r}}[l]$ and $s_u[g] = e^{\jmath 2\pi\phi g/K}x_u[g]$. Thereby, the equivalent system model with CFO included implicitly for U-user SIMO ZP-OFDM systems was expressed as

$$y_{i,n_\mathrm{r}}[g] = \sum\nolimits_{u=0}^{U-1}\sum\nolimits_{l=0}^{L-1} h_{u,n_\mathrm{r}}[l]s_{u,i}[g-l] + w_i[g], \quad g = 0, 1, \cdots, G, \tag{3.34}$$

where $y_{i,n_\mathrm{r}}[g]$ is the g-th sample of i-th ($i = 0, 1, \cdots, N_\mathrm{s}-1$) received OFDM symbol at the n_r-th receive antenna, and $G = K + L_\mathrm{zp}$. Define

$$\mathbf{h}(l) = \begin{bmatrix} h_{0,0}[l] & h_{1,0}[l] & \cdots & h_{U-1,0}[l] \\ h_{0,1}[l] & h_{1,1}[l] & \cdots & h_{U-1,1}[l] \\ \vdots & \vdots & \ddots & \vdots \\ h_{0,N_\mathrm{r}-1}[l] & h_{1,N_\mathrm{r}-1}[l] & \cdots & h_{U-1,N_\mathrm{r}-1}[l] \end{bmatrix}. \tag{3.35}$$

The received signal samples from all the received antenna were collected into a vector, obtaining $\mathbf{y}_i = [y_{i,0}[0], y_{i,0}[1], \cdots, y_{i,0}[G-1], \cdots, y_{i,N_\mathrm{r}-1}[0], y_{i,N_\mathrm{r}-1}[1], \cdots, y_{i,N_\mathrm{r}-1}[G-1]]^T$. $\mathbf{y}_i$ could be given by

$$\mathbf{y}_i = \mathbf{H}\mathbf{s}_i + \mathbf{w}_i, \tag{3.36}$$

where $\mathbf{s}_i = [s_{0,i}[0], s_{1,i}[0], \cdots, s_{U-1,i}[0], \cdots, s_{0,i}[G-1], s_{1,i}[G-1], \cdots, s_{U-1,i}[G-1]]^T$,

$\mathbf{w}_i$ is noise vector, and

$$\mathbf{H} = \begin{bmatrix} \mathbf{h}(0) & & & \\ \vdots & \mathbf{h}(0) & & \\ \mathbf{h}(L-1) & \vdots & \ddots & \\ & \mathbf{h}(L-1) & \ddots & \\ & & \ddots & \mathbf{h}(0) \\ & & \ddots & \vdots \\ & & & \mathbf{h}(L-1) \end{bmatrix}. \tag{3.37}$$

Then, the key steps of joint estimation of channels and CFOs are demonstrated in the following:

Step 1. Compute the auto-correlation matrix of the received signal $\mathbf{y}_i$, *i.e.*,

$$\mathbf{R}_{\text{yy}} = \frac{1}{N_{\text{s}}} \sum\nolimits_{i=0}^{N_{\text{s}}-1} \mathbf{y}_i \mathbf{y}_i^H, \tag{3.38}$$

where N_{s} is the number of OFDM symbols used for calculating the second-order statistics of the received signal.

Step 2. $Q = GN_{\text{r}} - UK$ eigenvectors corresponding to Q smallest eigenvalues of $\mathbf{R}_{\text{yy}}$ are obtained. The q-th ($q = 0, 1, \cdots, Q-1$) eigenvector is denoted as $\boldsymbol{\gamma}_q = [\boldsymbol{\gamma}_q^T(0), \boldsymbol{\gamma}_q^T(1), \cdots, \boldsymbol{\gamma}_q^T(G-1)]^T$, where $\boldsymbol{\gamma}_q(g)$ is a vector of length N_{r}.

Step 3. Formulate matrix $\boldsymbol{\iota}$ from $\boldsymbol{\gamma}_q$, where

$$\boldsymbol{\iota} = \sum\nolimits_{q=0}^{Q-1} \boldsymbol{\iota}_q, \tag{3.39}$$

and

$$\boldsymbol{\iota}_q = \begin{bmatrix} \boldsymbol{\gamma}_q(L-1) & \boldsymbol{\gamma}_q(L-2) & \cdots & \boldsymbol{\gamma}_q(0) \\ \boldsymbol{\gamma}_q(L) & \boldsymbol{\gamma}_q(L-1) & \cdots & \boldsymbol{\gamma}_q(1) \\ \vdots & \vdots & \ddots & \vdots \\ \boldsymbol{\gamma}_q(G-1) & \boldsymbol{\gamma}_q(G-2) & \cdots & \boldsymbol{\gamma}_q(K-1) \end{bmatrix}. \tag{3.40}$$

Step 4. Perform EVD on $\boldsymbol{\iota}$ and U eigenvectors corresponding to U smallest eigenvalues are obtained as $\mathbf{G}$. The CFO-included channel $\mathbf{h}(l)$ is obtained by selecting the lN_r to $((l+1)N_\mathrm{r}-1)$ rows of $\mathbf{G}$. Denote the CFO-included channel estimate as $\hat{\mathbf{h}}_0(l)$. Note that there is an ambiguity matrix between the true CFO-included channel $\mathbf{h}(l)$ and the CFO-included channel estimate $\hat{\mathbf{h}}_0(l)$, *i.e.*, $\mathbf{h}(l) = \hat{\mathbf{h}}_0(l)\mathbf{c}$, where $\mathbf{c}$ is the channel ambiguity matrix.

Step 5. By designing a periodical pilot pattern and a consecutive pilot pattern as illustrated in Tables 3.3 and 3.4, respectively, CFOs and channel ambiguity matrix could be easily obtained by either two-step estimator or best linear unbiased estimator in [12].

Table 3.3: Example of periodical pilot pattern, with $K = 16$ and $U = 4$ [12].

User	Pilot symbol in time domain															
1	1	0	0	0	1	0	0	0	1	0	0	0	1	0	0	0
2	0	1	0	0	0	1	0	0	0	1	0	0	0	1	0	0
3	0	0	1	0	0	0	1	0	0	0	0	1	0	0	1	0
4	0	0	0	1	0	0	0	1	0	0	0	1	0	0	0	1

Table 3.4: Example of consecutive pilot pattern, with $K = 16$ and $U = 4$ [12].

User	Pilot symbol in time domain															
1	1	1	1	1	0	0	0	0	0	0	0	0	0	0	0	0
2	0	0	0	0	1	1	1	1	0	0	0	0	0	0	0	0
3	0	0	0	0	0	0	0	0	1	1	1	1	0	0	0	0
4	0	0	0	0	0	0	0	0	0	0	0	0	1	1	1	1

The proposed semi-blind joint channels and CFOs estimator in [12] is spectrally efficient, thanks to the semi-blind implementation. However, CFO estimation based on the periodical pilot pattern has a limited estimation range of $[-K/2U, K/2U)$. Besides that, the proposed semi-blind approach requires a large number of received symbols (typically $N_\mathrm{s} > 100$) to compute the second order statistics of the received signal, which is not applicable to short-frame transmission with tens of symbols per frame. In addition, it was developed for ZP-OFDM systems, and could not be directly extended to the widely applied CP-OFDM systems. In [110], a subspace-based algorithm was proposed to jointly estimate the coefficients of both SI and desired channels as well as RF impairments. Nevertheless, it also requires a mass of data symbols to achieve a good second-order statistics of received signal.

Rank-Reduction Criterion Based CFO Estimator

A rank-reduction criterion based blind multi-CFO estimator was proposed for OFDMA systems with a large number of receive antennas in [14]. By means of null subcarriers and massive receive antennas, the blind multi-CFO estimator could estimate each CFO separately, avoiding the necessity of multi-dimensional search.

CFO compensation with a trial value of $\tilde{\phi}$ was performed on the received frequency-domain signal $\bar{\mathbf{y}}_{i,n_\mathrm{r}}$, with $i = 0, 1, \cdots, N_\mathrm{s} - 1$ and $n_\mathrm{r} = 0, 1, \cdots, N_\mathrm{r} - 1$, obtaining $\check{\mathbf{y}}_{i,n_\mathrm{r}}\{\tilde{\phi}\}$ of length K. Define $\check{\mathbf{Y}}_i\{\tilde{\phi}\} = [\check{\mathbf{y}}_{i,0}\{\tilde{\phi}\}, \check{\mathbf{y}}_{i,1}\{\tilde{\phi}\}, \cdots, \check{\mathbf{y}}_{i,N_\mathrm{r}-1}\{\tilde{\phi}\}]^T$ and $\mathbf{T}_u$ as the null-subcarrier assignment matrix for user u. Their multiplication yields

$$\mathbf{\Gamma}_{i,u}\{\tilde{\phi}\} = \check{\mathbf{Y}}_i\{\tilde{\phi}\}\mathbf{T}_u. \tag{3.41}$$

Then, the auto-correlation matrix of $\mathbf{\Gamma}_{i,u}\{\tilde{\phi}\}$ is computed by

$$\mathbf{R}_u\{\tilde{\phi}\} = \sum\nolimits_{i=0}^{N_\mathrm{s}-1} \mathbf{\Gamma}_{i,u}\{\tilde{\phi}\}(\mathbf{\Gamma}_{i,u}\{\tilde{\phi}\})^H. \tag{3.42}$$

It was demonstrated in [14] that CFO of user u could be acquired by calculating the rank of $\mathbf{R}_u\{\tilde{\phi}\}$, *i.e.*,

$$\begin{aligned} &\mathrm{Rank} = (U-1)L, \quad \text{if } \tilde{\phi} = \phi_u; \\ &\mathrm{Rank} = UL, \quad \text{if } \tilde{\phi} \neq \phi_u. \end{aligned} \tag{3.43}$$

where L is channel length. Thus, the CFO of user u could be estimated by solving the following minimisation problem

$$\hat{\phi}_u = \arg \min_{\tilde{\phi}} \sum\nolimits_{k=0}^{N_\mathrm{r}-(U-1)L} \gamma_{u,k}\{\tilde{\phi}\}, \tag{3.44}$$

where $\gamma_{u,k}\{\tilde{\phi}\}$ is the k-th smallest eigenvalue of $\mathbf{R}_u\{\tilde{\phi}\}$. Hence, the CFOs of U users could be determined separately by (3.44), decomposing a complex U-dimensional estimation problem into U one-dimensional estimation problems. However, the rank-reduction criterion based CFO estimator has several limitations. First, it needs a large number of receive antennas which is proportional to the number of users U as well as channel length L, *i.e.*, $N_\mathrm{r} \geq UL$. Second, each CFO was estimated by an exhaustive search, resulting in high computational complexity. Last but not least, it works for fCFO that is less than one subcarrier spacing.

3.4 IQ Imbalance and Its Estimation

The basics of IQ imbalance and its estimation are described in this section.

3.4.1 IQ Imbalance

IQ imbalance is typically induced when low-cost direct-conversion receivers are equipped. It is likely to incur an additional image interference, lead to biased signal estimates and result in poor system performance [24, 25, 54, 93, 94, 106, 111]. IQ imbalance arises at both transmitter and receiver. The focus of this thesis is on IQ imbalance at receiver. According to frequency dependence, IQ imbalance falls into two classes: frequency independent and frequency dependent. Frequency independent IQ imbalance results from the gain and phase mismatches between the local oscillator signals utilised for down- and up- conversion of I and Q branches, and maintains constant over the whole signal frequency band [93]. Frequency dependent IQ is caused by filter response mismatch of the low-pass filters, and is frequency selective. Frequency independent IQ imbalance is the focus of this thesis. According to the symmetry, IQ imbalance can be modelled in two ways either symmetric or asymmetric. In the symmetric model, the branches of I and Q experience half of the phase and amplitude errors, whose IQ imbalance parameters α and β are defined as [112]

$$\alpha = \cos(\theta/2) + \jmath\upsilon\sin(\theta/2), \tag{3.45}$$

and

$$\beta = \upsilon\cos(\theta/2) - \jmath\sin(\theta/2), \tag{3.46}$$

where θ and υ are the phase and amplitude mismatches between the I and Q branches, respectively. In the asymmetric model, the I branch is modelled to be perfect while the imbalances are modelled in the Q branch, whose IQ imbalance parameters are [15, 112]

$$\alpha = (1 + \upsilon e^{-\jmath\theta})/2, \tag{3.47}$$

and

$$\beta = (1 - \upsilon e^{j\theta})/2. \tag{3.48}$$

Note that asymmetric IQ imbalance has a property of $\alpha + \beta^* = 1$ [15, 112]. It is much easier to work with asymmetric model, as it needs to estimate only one IQ imbalance parameter either α or β and another one can be easily acquired by means of its property. This is why many researches are working on asymmetric IQ imbalance. Symmetric and asymmetric IQ imbalance models can be equivalent through several manipulations, which however is arduous [112].

After being corrupted by IQ imbalance at receiver, the received signal is given by

$$\begin{aligned}\tilde{y}[k] &= \alpha y[k] + \beta y^*[k] \\ &= \alpha \sum\nolimits_{l=0}^{L-1} \hbar[l]x[k-l] + \beta \sum\nolimits_{l=0}^{L-1} \hbar^*[l]x^*[k-l] + \alpha w[k] + \beta w^*[k], \\ &\quad k = 0, 1, \cdots, K-1,\end{aligned} \tag{3.49}$$

where α and β are obtained through either symmetric model in (3.45) and (3.46) or asymmetric model (3.47) and (3.48). It is noteworthy that IQ imbalance gives rise to an additional image signal y^*. If IQ imbalance is left uncompensated, the system performance will be degraded substantially.

3.4.2 IQ Imbalance Estimation

By means of a specific training sequence, a computationally efficient IQ imbalance estimator was proposed for GFDM systems without any prior knowledge of channel in [15]. Assuming a whole GFDM symbol was exploited for training, its first half part should be designed to be a known sequence, whereas its last half part should be zero. An example of the time-domain training sequence is

$$\mathbf{x} = [x[0], x[1], \cdots, x[N/2-1], 0, 0, \cdots, 0]^T. \tag{3.50}$$

Define $\tilde{\mathbf{y}} = \alpha\bar{\mathbf{y}} + \beta\bar{\mathbf{y}}^*$ as the received frequency-domain training sequence corrupted by an asymmetric IQ imbalance at receiver, where α and β are the asymmetric IQ imbalance parameters with $\alpha + \beta = 1$, and $\bar{\mathbf{y}}$ is the received frequency-domain training sequence. Thanks to the training sequence design,

$$\underbrace{\begin{bmatrix} \tilde{\mathbf{y}}(2) \\ \tilde{\mathbf{y}}(3) \\ \vdots \\ \tilde{\mathbf{y}}(N/2) \end{bmatrix}}_{\tilde{\mathbf{Y}}} = \underbrace{\begin{bmatrix} \tilde{\mathbf{y}}(2)+\tilde{\mathbf{y}}^*(2) & 0 & \cdots & 0 \\ 0 & \tilde{\mathbf{y}}(3)+\tilde{\mathbf{y}}^*(3) & \cdots & 0 \\ \vdots & \vdots & \ddots & \vdots \\ 0 & 0 & \cdots & \tilde{\mathbf{y}}(N/2)+\tilde{\mathbf{y}}^*(N/2) \end{bmatrix}}_{\mathbf{G}} \underbrace{\begin{bmatrix} \alpha \\ \alpha \\ \vdots \\ \alpha \end{bmatrix}}_{\boldsymbol{\alpha}} + \mathbf{w} \tag{3.51}$$

is obtained, where $\mathbf{w}$ is noise vector. Thus, IQ imbalance vector $\boldsymbol{\alpha}$ could be acquired by

$$\hat{\boldsymbol{\alpha}} = (\mathbf{G}^H\mathbf{G})^{-1}\mathbf{G}^H\tilde{\mathbf{Y}}. \tag{3.52}$$

IQ imbalance parameter α could then be estimated through $\hat{\alpha} = \sum_{n=0}^{N/2-2} \hat{\boldsymbol{\alpha}}(n)$. The estimate of β is easily obtained by utilising the relationship between α and β. Although the IQ imbalance estimator is computationally efficient with closed-form solutions, it has several drawbacks. On one hand, it suffers high training overhead due to the use of a whole GFDM symbol for training. On the other hand, it is based on an asymmetric

IQ imbalance, and could not be directly extended to symmetric IQ imbalance.

Chapter 4

Joint Estimation of TOAs and CFOs for Multi-User OFDM Systems

In this chapter, a joint multi-TOA and multi-CFO estimation scheme is proposed for multi-user OFDM systems. With a carefully designed pilot, multiple TOAs and multiple CFOs of U users are separated jointly, dividing a complex $2U$-dimensional estimation problem into $2U$ low-complexity one-dimensional estimation problems. Two CFO estimation approaches, including a low-complexity closed-form solution and a high-accuracy null-subcarrier assisted accurate estimation approach, are proposed, where the integer and fractional parts of each CFO are estimated as a whole rather separately. Each TOA is estimated regardless of CFO by exploring the features of the ICI matrix of CFO. The CRLBs of multi-TOA and mutli-CFO estimation are derived for the first time for multi-user OFDM systems. Simulation results show that the proposed TOA and CFO estimators provide higher estimation accuracy than the ESPRIT based TOA estimator [6] in Subsection 3.2.1, and the existing ML CFO estimator [7] and the blind closed-form CFO estimator [8] in Subsection 3.3.2. The proposed scheme also achieves performances close to the CRLBs especially at high SNRs.

4.1 Introduction

TOA, defined as the propagation delay of the first arriving path, plays an important role in localisation, synchronisation and channel estimation of mobile networks, wireless sensor networks, etc. [6, 29, 30]. A number of TOA estimators have been proposed for OFDM in the literature, such as ESPRIT [6] and MUSIC [29] as mentioned in Subsection 3.2.1, and matrix pencil in [30]. However, none of them proposed a scheme to combat CFO. When the received signals are perturbed by CFO, the aforementioned TOA estimators will be biased. In [113], a TOA estimator robust against CFO was proposed for IEEE 802.15.4a Chirp Spread Spectrum (CSS) signals. However, it is invalid for OFDM systems. Meanwhile, all aforementioned TOA estimators consider a single user only. To the best of the author's knowledge, the research of robust multi-TOA estimator against CFOs in OFDM systems is still an open problem.

Furthermore, the existing methods usually estimate CFO in two steps. The first step is to estimate the integer/fractional part of CFO whereas the second step is to estimate the rest fractional/integer part [8,29,114,115]. Nevertheless, they perform poorly if the residual fCFO or iCFO exists. Thus, it is crucial to develop a one-step CFO estimator so that iCFO and fCFO can be estimated as a whole rather than separately.

Moreover, the existing studies in OFDM systems usually estimated either TOAs [6, 29, 30] or CFOs [7, 8, 114, 115], but not both together. A joint TOA and CFO estimation algorithm has been proposed for IEEE 802.15.4a CSS signals [116]. However, it has considered a single user only and is not applicable for OFDM systems. The joint estimation of TOAs and CFOs in multi-user OFDM systems is still an open issue. It is not straightforward to apply the aforementioned TOA and CFO estimators to multi-user OFDM systems as they will interfere with each other. Thus, they need to be performed sequentially. For example, multiple CFOs should be estimated first at BS and compensated at individual users via feedback. Only after CFOs compensation, can multiple TOAs be estimated. This requires separate training processes for CFOs and TOAs estimation, which is complex and spectrally inefficient.

In this chapter, a joint multi-TOA and multi-CFO estimation (JMTMCE) scheme is proposed for multi-user OFDM systems. The estimation is performed in two steps: 1) TOAs and CFOs are separated into U groups corresponding to U users, by performing correlation between the received and transmitted pilots; 2) the TOA and CFO of each user are separated and estimated. This work is different in the following aspects.

- To the best of the author's knowledge, this is the first attempt to consider both TOAs and CFOs and their estimation together, for multi-user OFDM systems, without requiring separate training processes as by existing methods [6–8, 29, 30, 99,114,115,117,118]. Simulation results show that the proposed JMTMCE scheme outperforms the existing methods [6–8] in terms of both TOA and CFO estimation accuracy. CRLBs of TOA and CFO estimation for multi-user OFDM systems are derived for the first time, which verify the effectiveness of the proposed scheme.
- Through a careful pilot design, multiple TOAs and CFOs of U users are separated, dividing a complex $2U$-dimensional CFO and TOA estimation problem into $2U$ low-complexity one-dimensional problems. Each TOA and CFO are estimated independent of each other, while the existing methods [6–8, 29, 30, 99, 114, 115, 117, 118] separate U CFOs and U TOAs sequentially, resulting in error propagations from CFO estimates to TOA estimates, and the previous TOA estimators [6, 29, 30, 99, 118] require a CFO estimation and compensation procedure in advance.
- Two CFO estimation approaches, including a computationally efficient closed-form solution and a NS assisted accurate estimation approach, are proposed, where the integer and fractional parts of each CFO are estimated as a whole, whereas the existing CFO estimator approaches [7, 8, 114, 115, 117] estimate iCFO and fCFO separately through two sequential algorithms, giving rise to error propagations. The proposed closed-form CFO estimator is very computationally efficient, with a complexity reduction of 7-fold over the methods in [6–8].

The rest of this chapter is organised as follows. System model and pilot design are described in Sections 4.2 and 4.3, respectively. The proposed JMTMCE scheme is

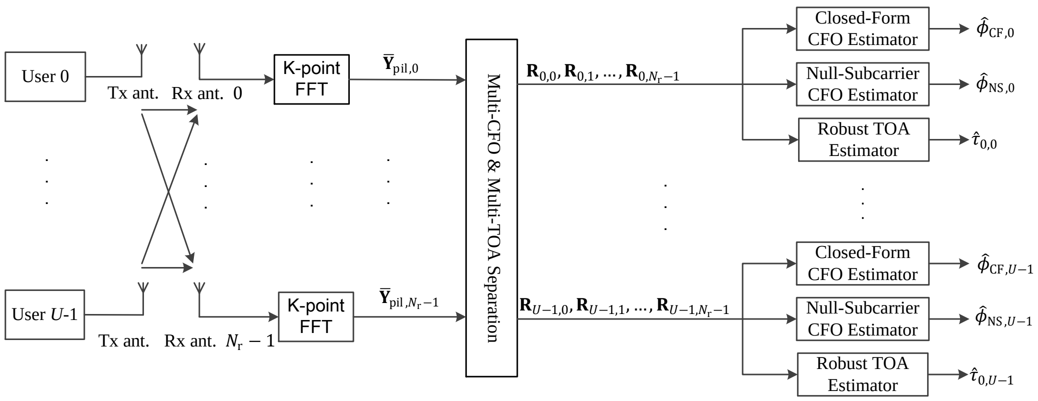

Figure 4.1: Block diagram of the proposed JMTMCE scheme for a U-user SIMO OFDM system.

presented in Section 4.4. CRLB analysis and complexity analysis are given in Section 4.5. Simulation results are presented in Section 4.6. Section 4.7 draws conclusion.

4.2 System Model

An uplink U-user SIMO OFDM system is considered, as depicted in Fig. 4.1. Each user and the BS are equipped with a single transmit antenna and N_{r} receive antennas, respectively. A data frame consists of N_{s} OFDM symbols with K subcarriers each. Define $\mathbf{d}_{u,i} = [d_{u,i}[0], d_{u,i}[1], \cdots, d_{u,i}[K-1]]^T$ as the data vector of user u ($u = 0, 1, \cdots, U-1$) and i-th ($i = 0, 1, \cdots, N_{\mathrm{s}}-1$) OFDM symbol, with $d_{u,i}[k]$ denoting the data on subcarrier k ($k = 0, 1, \cdots, K-1$). Before transmission, each OFDM symbol $\mathbf{d}_{u,i}$ is processed by IFFT, and then a CP of length L_{cp} is pre-pended.

The channel is assumed to remain constant for a frame's duration. Define L_{p}, $\mu_{l,u,n_{\mathrm{r}}}$ and $\tau_{l,u,n_{\mathrm{r}}}$ as the number of resolvable propagation paths, the complex path gain and path delay of the l-th ($l = 0, 1, \cdots, L_{\mathrm{p}}-1$) path between user u and the n_{r}-th ($n_{\mathrm{r}} = 0, 1, \cdots, N_{\mathrm{r}}-1$) receive antenna of the BS respectively. Since the scale of the transmit or receive antenna array is very small compared to the large signal transmission distance, the channels of different transmit-receive antenna pairs share very similar scatters [102]. Meanwhile, the path delay differences among the similar scatters are much smaller than the system sampling interval [102]. Hence, common time delays can be assumed for different transmit-receive antenna pairs [102], *i.e.*, $\tau_{l,u} = \tau_{l,u,n_\mathrm{r}}$ for $n_\mathrm{r} = 0, 1 \cdots, N_\mathrm{r} - 1$. The time delay of the first arriving path $\tau_{0,u}$, either being LoS or NLoS, represents the TOA [29, 98], and requires to be estimated for the desired application. The discrete CIR at the k-th ($k = 0, \cdots, K-1$) sampling point is given by

$$\hbar_{u,n_\mathrm{r}}[k] = \sum\nolimits_{l=0}^{L_\mathrm{P}-1} \mu_{l,u,n_\mathrm{r}} \delta(k/f_\mathrm{s} - \tau_{l,u}). \tag{4.1}$$

Denote $\boldsymbol{\hbar}_{u,n_\mathrm{r}} = [\hbar_{u,n_\mathrm{r}}[0], \hbar_{u,n_\mathrm{r}}[1], \cdots, \hbar_{u,n_\mathrm{r}}[K-1]]^T$ as the CIR vector. Its corresponding CFR vector is obtained as $\bar{\mathbf{h}}_{u,n_\mathrm{r}} = [\bar{h}_{u,n_\mathrm{r}}[0], \bar{h}_{u,n_\mathrm{r}}[1], \cdots, \bar{h}_{u,n_\mathrm{r}}[K-1]]^T$ with $\bar{h}_{u,n_\mathrm{r}}[k]$ defined as [99]

$$\bar{h}_{u,n_\mathrm{r}}[k] = \sum\nolimits_{l=0}^{L_\mathrm{P}-1} \mu_{l,u,n_\mathrm{r}} e^{-\jmath 2\pi k \tau_{l,u} f_\mathrm{s}/K}. \tag{4.2}$$

Define ϕ_u ($\phi_u = \phi_{\mathrm{I},u} + \phi_{\mathrm{F},u}$) as the CFO between user u and the BS with $\phi_{\mathrm{I},u}$ and $\phi_{\mathrm{F},u}$ being the iCFO and fCFO, assuming all antennas at the BS share one local oscillator [8]. After removing the CP, the received data on subcarrier k in OFDM symbol i is obtained as $\bar{y}_{i,n_\mathrm{r}}[k]$. Define $\mathbf{F}$ as $K \times K$ FFT matrix with $\mathbf{F}(a,b) = 1/\sqrt{K} e^{-\jmath 2\pi ab/K}$, ($a, b = 0, 1, \cdots, K-1$), and $\mathbf{E}_{\mathrm{K},u} = \mathrm{diag}\{\mathbf{e}_{\mathrm{K},u}\}$ as the diagonal CFO matrix with $\mathbf{e}_{\mathrm{K},u} = [1, e^{\jmath 2\pi \phi_u/K}, \cdots, e^{\jmath 2\pi (K-1)\phi_u/K}]^T$ being the CFO vector. The received signal at the n_r-th receive antenna in the frequency domain can be written as

$$\bar{\mathbf{Y}}_{n_\mathrm{r}} = \sum\nolimits_{u=0}^{U-1} \bar{\mathbf{E}}_{\mathrm{K},u} \bar{\mathbf{H}}_{u,n_\mathrm{r}} \mathbf{d}_u + \bar{\mathbf{W}}_{n_\mathrm{r}}, \tag{4.3}$$

where $\bar{\mathbf{Y}}_{n_\mathrm{r}} = [\bar{\mathbf{y}}_{0,n_\mathrm{r}}, \bar{\mathbf{y}}_{1,n_\mathrm{r}}, \cdots, \bar{\mathbf{y}}_{N_\mathrm{s}-1,n_\mathrm{r}}]$ with $\bar{\mathbf{y}}_{i,n_\mathrm{r}} = [\bar{y}_{i,n_\mathrm{r}}[0], \bar{y}_{i,n_\mathrm{r}}[1], \cdots, \bar{y}_{i,n_\mathrm{r}}[K-1]]^T$; $\bar{\mathbf{E}}_{\mathrm{K},u} = \mathbf{F}\mathbf{E}_{\mathrm{K},u}\mathbf{F}^H$ is the ICI matrix of user u; $\bar{\mathbf{H}}_{u,n_\mathrm{r}} = \mathrm{diag}\{\bar{\mathbf{h}}_{u,n_\mathrm{r}}\}$ is the diagonal CFR matrix; $\mathbf{d}_u = [\mathbf{d}_{u,0}, \mathbf{d}_{u,1}, \cdots, \mathbf{d}_{u,N_\mathrm{s}-1}]$; $\bar{\mathbf{W}}_{n_\mathrm{r}}$ is the additive white Gaussian noise matrix with zero mean and variance of σ^2.

4.3 Pilot Design

The pilots are designed for joint estimation of multiple TOAs and CFOs. A pilot of P_{pil} OFDM symbols $\mathbf{d}_{\text{pil},u} = [\mathbf{d}_{u,0}, \mathbf{d}_{u,1}, \cdots, \mathbf{d}_{u,P_{\text{pil}}-1}]$ is designed for each user from two aspects. First, the pilots of different users should be orthogonal to each other, allowing the joint separation of multiple TOAs and multiple CFOs in Subsection 4.4.1. Second, for each user, the training symbols on the occupied subcarriers should be orthogonal to enable the independent estimation of TOA and CFO in Subsections 4.4.2 and 4.4.3.

A Hadamard matrix $\mathbf{M}$ of size $P_{\text{pil}} \times P_{\text{pil}}$ can be applied to achieve these, in which any two different rows are orthogonal to each other [115]. Hence, every occupied subcarrier of each user should be assigned an unique row of $\mathbf{M}$. For each user, K_{o} ($K_{\text{o}} < K$) subcarriers are used for the joint estimation. Define $T = \frac{K}{K_{\text{o}}}$ as the subcarrier spacing. Each user uses an unique initial subcarrier index, *e.g.*, j_u ($j_u = 0, 1, \cdots, T-1$) for user u. The subcarrier index of the k_{o}-th ($k_{\text{o}} = 0, 1, \cdots, K_{\text{o}} - 1$) pilot tone for the u-th user is $J_u^{k_{\text{o}}} = j_u + k_{\text{o}} T$. Denote $\mathbf{J}_u = [J_u^0, J_u^1, \cdots, J_u^{K_{\text{o}}-1}]^T$. Then K_{o} different rows of $\mathbf{M}$ ($P_{\text{pil}} \geq K_{\text{o}} U$) are randomly chosen and placed on those subcarriers with index $\mathbf{J}_u$. In contrast, the remaining $(K - K_{\text{o}})$ subcarriers are allocated with nulls. Define $\mathbf{R}_{u,v}^{\mathbf{dd}} = \frac{1}{P_{\text{pil}}} \mathbf{d}_{\text{pil},u} \mathbf{d}_{\text{pil},v}^H$ as the pilot correlation matrix averaged over P_{pil} symbols between the u-th and the v-th ($v = 0, 1, \cdots, U-1$) users. With this pilot structure, the correlation matrix $\mathbf{R}_{u,v}^{\mathbf{dd}}$ becomes

$$\mathbf{R}_{u,v}^{\mathbf{dd}} = \begin{cases} \mathbf{I}_{K_{\text{o}}} \otimes \boldsymbol{\zeta}_u, & u = v; \\ \mathbf{0}_{K \times K}, & u \neq v. \end{cases} \tag{4.4}$$

where $\boldsymbol{\zeta}_u$ is a $T \times T$ single-entry matrix with $\boldsymbol{\zeta}_u(j_u, j_u) = 1$.

Note that (4.4) can also be achieved by an identity matrix, whose off-diagonal entries however are zeros and thus more susceptible to the noise than the Hadamard matrix. Hence, the Hadamard matrix is utilised to design the pilot in this Chapter. It is noteworthy that an orthogonal training sequence with the help of a Hadamard matrix was also designed in [115]. However, it allows only the estimation of multiple CFOs not the joint estimation of multiple TOAs and multiple CFOs. As P_{pil} is lower bounded by $K_{\text{o}}U$, the choice of K_{o} is essential. The minimum value of K_{o} for joint TOA and CFO estimation is $2L_{\text{p}}$, as suggested in [99].

4.4 Joint Multi-TOA and Multi-CFO Estimation

By performing correlation between the received and transmitted pilots, the TOAs and CFOs of U users are first separated jointly by user, dividing a $2U$-dimensional joint multi-TOA and multi-CFO estimation problem into U 2-dimensional joint TOA and CFO estimation problems. Then, for each of U users, the 2-dimensional estimation problem can be divided into two 1-dimensional problems to allow independent estimations of TOA and CFO. The integer and fractional parts of each CFO are estimated in an integral by two CFO estimators. The proposed JMTMCE scheme is illustrated in Fig. 4.1.

4.4.1 Joint Multi-TOA Separation and Multi-CFO Separation

As the pilot design is orthogonal in the user domain, the pilot of each user is used as a projection matrix, to separate U TOAs and U CFOs jointly. Let $\bar{\mathbf{Y}}_{\text{pil},n_{\text{r}}} = [\bar{\mathbf{y}}_{0,n_{\text{r}}}, \bar{\mathbf{y}}_{1,n_{\text{r}}} \cdots, \bar{\mathbf{y}}_{P_{\text{pil}}-1,n_{\text{r}}}]$ denote the received pilot matrix at the n_{r}-th receive antenna. Define $\mathbf{R}_{u,n_{\text{r}}} = \frac{1}{P_{\text{pil}}}\bar{\mathbf{Y}}_{\text{pil},n_{\text{r}}}\mathbf{d}_{\text{pil},u}^{H}$ as the correlation matrix between the received mixture of pilots from U users at the n_{r}-th receive antenna and the transmit pilot of user u averaged over P_{pil} symbols. By using (4.3) and (4.4), $\mathbf{R}_{u,n_{\text{r}}}$ can be written as

$$\mathbf{R}_{u,n_{\text{r}}} = \bar{\mathbf{E}}_{\text{K},u}\boldsymbol{\Gamma}_{u,n_{\text{r}}} + \bar{\mathbf{W}}_{\text{S},u,n_{\text{r}}}, \tag{4.5}$$

where $\boldsymbol{\Gamma}_{u,n_{\text{r}}} = \bar{\mathbf{H}}_{u,n_{\text{r}}}(\mathbf{I}_{K_{\text{o}}} \otimes \boldsymbol{\zeta}_u)$ and $\bar{\mathbf{W}}_{\text{S},u,n_{\text{r}}} = \frac{1}{P}\bar{\mathbf{W}}_{\text{pil},n_{\text{r}}}\mathbf{d}_{\text{pil},u}^{H}$ is the noise matrix averaged over P_{pil} symbols.

Hence, U $\mathbf{R}_{u,n_{\text{r}}}$ matrices at the n_{r}-th receive antenna have been separated with no interference from other users. Since the TOA and CFO of user u are embedded in $\mathbf{R}_{u,n_{\text{r}}}$, U TOAs and U CFOs have been separated jointly by user.

4.4.2 Multi-TOA Estimation

A robust TOA (R-TOA) estimator is proposed, where the TOA can be recovered from $\mathbf{R}_{u,n_\mathrm{r}}$ directly, without requiring any explicit procedures for CFO estimation and compensation in advance. The core idea is to obtain a CFO-independent channel correlation matrix from $\mathbf{R}_{u,0}, \mathbf{R}_{u,1}, \cdots, \mathbf{R}_{u,N_\mathrm{r}-1}$ firstly, and then to apply it with the ESPRIT algorithm to extract the TOA. The extraction of the CFO-independent channel correlation matrix can be summarised in three steps.

Step 1: K CFO-dependent channel correlation matrices are calculated from the diagonal vectors of $\mathbf{R}_{u,n_\mathrm{r}}$ and the shift versions of $\mathbf{R}_{u,n_\mathrm{r}}$ respectively.

Let $\mathbf{f}^k_{u,n_\mathrm{r}} = \mathrm{diag}\{\mathbf{R}^k_{u,n_\mathrm{r}}(j_u\colon T\colon K, j_u\colon T\colon K)\}$ denote the truncated diagonal vector of $\mathbf{R}^k_{u,n_\mathrm{r}}$, where $\mathbf{R}^k_{u,n_\mathrm{r}}$ indicates that $\mathbf{R}_{u,n_\mathrm{r}}$ is up-shifted by k rows ($k = 0, 1, \cdots, K-1$). $k = 0$ means there is no shift. Define $[\bar{e}^0_u, \bar{e}^1_u, \cdots, \bar{e}^{K-1}_u]^T$ as the first column vector of $\bar{\mathbf{E}}_{\mathrm{K},u}$. Then, the k-th CFO-dependent channel correlation matrix $\mathbf{R}^{\mathbf{ff},k}_{u,n_\mathrm{r}}$ is computed by $\mathbf{R}^{\mathbf{ff},k}_{u,n_\mathrm{r}} = \mathbf{f}^k_{u,n_\mathrm{r}}(\mathbf{f}^k_{u,n_\mathrm{r}})^H$. Due to the Toeplitz property of $\bar{\mathbf{E}}_{\mathrm{K},u}$ and the diagonal feature of $\mathbf{\Gamma}_{u,n_\mathrm{r}}$, $\mathbf{R}^{\mathbf{ff},k}_{u,n_\mathrm{r}}$ can be expressed as

$$\mathbf{R}^{\mathbf{ff},k}_{u,n_\mathrm{r}} = |\bar{e}^k_u|^2 \bar{\mathbf{h}}_{\mathrm{t},u,n_\mathrm{r}} \bar{\mathbf{h}}^H_{\mathrm{t},u,n_\mathrm{r}} + \bar{\mathbf{W}}^k_{\mathrm{T},u,n_\mathrm{r}}, \tag{4.6}$$

where $\bar{\mathbf{h}}_{\mathrm{t},u,n_\mathrm{r}} = \bar{\mathbf{h}}_{u,n_\mathrm{r}}(j_u\colon T\colon K, 1)$ is the truncated CFR vector and $\bar{\mathbf{W}}^k_{\mathrm{T},u,n_\mathrm{r}}$ is the noise correlation matrix. Since $|\bar{e}^k_u|^2$ varies with the CFO, $\mathbf{R}^{\mathbf{ff},k}_{u,n_\mathrm{r}}$ is susceptible to CFO.

Step 2: To achieve TOA estimation independently of CFO, all of K CFO-dependent channel correlation matrices are summed. Denote $\mathbf{R}^{\mathbf{ff}}_{u,n_\mathrm{r}} = \sum_{k=0}^{K-1} \mathbf{R}^{\mathbf{ff},k}_{u,n_\mathrm{r}}$ as the summed correlation matrix. By considering $\bar{\mathbf{E}}^H_{\mathrm{K},u}\bar{\mathbf{E}}_{\mathrm{K},u} = \mathbf{F}\mathbf{E}^H_{\mathrm{K},u}\mathbf{F}^H\mathbf{F}\mathbf{E}_{\mathrm{K},u}\mathbf{F}^H = \mathbf{I}_K$, $\sum_{k=0}^{K-1}|\bar{e}^k_u|^2 = 1$ can be obtained, which is a constant. Thus, $\mathbf{R}^{\mathbf{ff}}_{u,n_\mathrm{r}}$ can be given by

$$\mathbf{R}^{\mathbf{ff}}_{u,n_\mathrm{r}} = \bar{\mathbf{h}}_{\mathrm{t},u,n_\mathrm{r}} \bar{\mathbf{h}}^H_{\mathrm{t},u,n_\mathrm{r}} + \bar{\mathbf{W}}_{\mathrm{T},u,n_\mathrm{r}}, \tag{4.7}$$

where $\bar{\mathbf{W}}_{\mathrm{T},u,n_\mathrm{r}} = \sum_{k=0}^{K-1} \bar{\mathbf{W}}^k_{\mathrm{T},u,n_\mathrm{r}}$. Hence, the impact of CFO has been mitigated and $\mathbf{R}^{\mathbf{ff}}_{u,n_\mathrm{r}}$ is independent of CFO.

Step 3: Thanks to the assumption of equal delays among antennas, N_r receive antennas can provide space diversity to enhance TOA estimation. The spatial averaged CFO-independent channel correlation matrix $\mathbf{R}_u^{\mathbf{ff}}$ is calculated by

$$\mathbf{R}_u^{\mathbf{ff}} = \frac{1}{N_\mathrm{r}} \sum\nolimits_{n_\mathrm{r}=0}^{N_\mathrm{r}-1} \mathbf{R}_{u,n_\mathrm{r}}^{\mathbf{ff}}. \tag{4.8}$$

Then, it is improved by the forward-backward (FB) averaging technique, obtaining

$$\mathbf{R}_{\mathrm{FB},u}^{\mathbf{ff}} = \frac{1}{2}(\mathbf{R}_u^{\mathbf{ff}} + \mathbf{O}(\mathbf{R}_u^{\mathbf{ff}})^*\mathbf{O}), \tag{4.9}$$

where $\mathbf{O}$ is the $K_\mathrm{o} \times K_\mathrm{o}$ matrix whose components are zero except for ones on the anti-diagonal.

Last, $\mathbf{R}_{\mathrm{FB},u}^{\mathbf{ff}}$ is applied to Step 2 of ESPRIT algorithm described in Subsection 3.2.1 to obtain the TOA estimate of user u as $\hat{\tau}_{0,u}$.

4.4.3 Multi-CFO Estimation

U CFOs of U users are separated by the separation of U $\mathbf{R}_{u,n_\mathrm{r}}$ matrices, and can be estimated independently at the BS. A closed-from CFO estimator and a NS based CFO estimator are proposed for each CFO, both of which are independent of TOA.

Closed-Form CFO Estimator

A closed-form CFO estimator is proposed, where CFO is extracted independently of TOA and its integer and fractional parts are estimated as a whole. The core idea of CFO estimation is similar to that of TOA estimation. Specifically, a TOA-independent correlation matrix of CFO vector is computed firstly, which is then applied with ESPRIT algorithm to extract the unknown CFO. The computation of TOA-independent correlation matrix of CFO vector involves four steps.

Step 1: A channel-perturbed CFO matrix $\breve{\mathbf{R}}_{u,n_\mathrm{r}}$ is calculated by performing IFFT on

$\mathbf{R}_{u,n_\mathrm{r}}$, *i.e.*, $\breve{\mathbf{R}}_{u,n_\mathrm{r}} = \mathbf{F}^H\mathbf{R}_{u,n_\mathrm{r}}\mathbf{F}$. Substituting (4.5) into it, $\breve{\mathbf{R}}_{u,n_\mathrm{r}}$ can be given by

$$\breve{\mathbf{R}}_{u,n_\mathrm{r}} = \mathbf{E}_{\mathrm{K},u}\mathbf{T}_{u,n_\mathrm{r}} + \bar{\mathbf{W}}_{\mathrm{C},u,n_\mathrm{r}}, \tag{4.10}$$

where $\mathbf{T}_{u,n_\mathrm{r}} = \mathbf{F}^H\mathbf{\Gamma}_{u,n_\mathrm{r}}\mathbf{F}$ is a kind of channel circulant matrix with its first column vector being $\breve{\boldsymbol{\hbar}}_{u,n_\mathrm{r}} = [\breve{\hbar}^0_{u,n_\mathrm{r}}, \breve{\hbar}^1_{u,n_\mathrm{r}}, \cdots, \breve{\hbar}^{K-1}_{u,n_\mathrm{r}}]^T$ and $\bar{\mathbf{W}}_{\mathrm{C},u,n_\mathrm{r}} = \mathbf{F}^H\bar{\mathbf{W}}_{\mathrm{S},u,n_\mathrm{r}}\mathbf{F}$ is the noise matrix.

Step 2: K TOA-dependent correlation matrices of CFO vector are extracted from the diagonal vectors of the original and shifted versions of $\breve{\mathbf{R}}_{u,n_\mathrm{r}}$. Denote $\breve{\mathbf{r}}^k_{u,n_\mathrm{r}} = \mathrm{diag}\{\breve{\mathbf{R}}^k_{u,n_\mathrm{r}}(j_u\colon T\colon K, j_u\colon T\colon K)\}$ as the truncated diagonal vector of $\breve{\mathbf{R}}^k_{u,n_\mathrm{r}}$, where $\breve{\mathbf{R}}^k_{u,n_\mathrm{r}}$ means that $\breve{\mathbf{R}}_{u,n_\mathrm{r}}$ is right-shifted by k columns ($k = 0, 1, \cdots, K-1$). Then, the k-th TOA-dependent correlation matrix of the CFO vector $\mathbf{R}^{\mathbf{ee},k}_{u,n_\mathrm{r}}$ is computed by $\mathbf{R}^{\mathbf{rr},k}_{u,n_\mathrm{r}} = \breve{\mathbf{r}}^k_{u,n_\mathrm{r}}(\breve{\mathbf{r}}^k_{u,n_\mathrm{r}})^H$. Due to the diagonal feature of $\mathbf{E}_{\mathrm{K},u}$ and the circulant property of $\mathbf{T}_{u,n_\mathrm{r}}$, $\mathbf{R}^{\mathbf{rr},k}_{u,n_\mathrm{r}}$ can be represented as

$$\mathbf{R}^{\mathbf{rr},k}_{u,n_\mathrm{r}} = |\breve{\hbar}^k_{u,n_\mathrm{r}}|^2\mathbf{e}_{\mathrm{t},u}\mathbf{e}^H_{\mathrm{t},u} + \bar{\mathbf{W}}^k_{\mathrm{Ct},u,n_\mathrm{r}}, \tag{4.11}$$

where $\mathbf{e}_{\mathrm{t},u} = \mathbf{e}_{\mathrm{K},u}(j_u\colon T\colon K, 1)$ and $\bar{\mathbf{W}}^k_{\mathrm{Ct},u,n_\mathrm{r}}$ is the corresponding noise correlation matrix. $|\breve{\hbar}^k_{u,n_\mathrm{r}}|^2$ is the channel power of the k-th sampling point, whose value changes with TOA.

Step 3: To enable the independence of CFO estimation of TOA, K TOA-dependent correlation matrices in (4.11) are added up. Denote $\mathbf{R}^{\mathbf{rr}}_{u,n_\mathrm{r}} = \sum_{k=0}^{K-1}\mathbf{R}^{\mathbf{rr},k}_{u,n_\mathrm{r}}$ as the summed correlation matrix, which can be written as

$$\mathbf{R}^{\mathbf{rr}}_{u,n_\mathrm{r}} = \| \breve{\boldsymbol{\hbar}}_{u,n_\mathrm{r}} \|^2_\mathrm{F}\ \mathbf{e}_{\mathrm{t},u}\mathbf{e}^H_{\mathrm{t},u} + \bar{\mathbf{W}}_{\mathrm{Ct},u,n_\mathrm{r}}, \tag{4.12}$$

with $\| \breve{\boldsymbol{\hbar}}_{u,n_\mathrm{r}} \|^2_\mathrm{F} = \sum_{k=0}^{K-1}|\breve{\hbar}^k_{u,n_\mathrm{r}}|^2$ and $\bar{\mathbf{W}}_{\mathrm{Ct},u,n_\mathrm{r}} = \sum_{k=0}^{K-1}\bar{\mathbf{W}}^k_{\mathrm{Ct},u,n_\mathrm{r}}$. Since $\| \breve{\boldsymbol{\hbar}}_{u,n_\mathrm{r}} \|^2_\mathrm{F}$ is the summed channel power and insusceptible to TOA, the impact of TOA has been mitigated.

Step 4: The TOA-independent correlation matrix is similarly enhanced by the spatial and FB averaging techniques, obtaining

$$\mathbf{R}^{\mathbf{rr}}_{\mathrm{FB},u} = \frac{1}{2}(\mathbf{R}^{\mathbf{rr}}_{u} + \mathbf{O}(\mathbf{R}^{\mathbf{rr}}_{u})^{*}\mathbf{O}), \tag{4.13}$$

with $\mathbf{R}^{\mathbf{rr}}_{u} = \frac{1}{N_{\mathrm{r}}}\sum_{n_{\mathrm{r}}=0}^{N_{\mathrm{r}}-1}\mathbf{R}^{\mathbf{rr}}_{u,n_{\mathrm{r}}}$.

The CFO of user u is obtained as $\hat{\phi}_{\mathrm{CF},u}$, by introducing $\mathbf{R}^{\mathbf{rr}}_{\mathrm{FB},u}$ to the ESPRIT algorithm. Let $\mathbf{u}_u$ denote the signal eigenvector corresponding to the largest eigenvalue of $\mathbf{R}^{\mathbf{rr}}_{\mathrm{FB},u}$. $\mathbf{u}_{1,u}$ and $\mathbf{u}_{2,u}$ are defined as the first and last $(K_{\mathrm{o}} - 1)$ elements of $\mathbf{u}_u$ respectively. $\hat{v}_u = (\mathbf{u}^{H}_{1,u}\mathbf{u}_{1,u})^{-1}\mathbf{u}^{H}_{1,u}\mathbf{u}_{2,u}$ can be obtained, and the iCFO and fCFO of user u are computed as a whole with

$$\hat{\phi}_{\mathrm{CF},u} = \frac{K\angle\hat{v}_u}{2T\pi}. \tag{4.14}$$

NS Based CFO Estimator

A more accurate NS based CFO estimator, referred to as NS-CFO, is derived by employing the orthogonality of FFT matrix as well as the orthogonality among the occupied subcarriers of the designed pilot, which are independent of TOA. It involves two steps.

Step 1: CFO is estimated initially by utilising the orthogonality between the truncated FFT matrices corresponding to the respective null subcarriers and the occupied subcarriers in the designed pilot.

Step 1.1: IFFT is performed on $\mathbf{R}_{u,n_{\mathrm{r}}}$, yielding $\bar{\mathbf{R}}_{u,n_{\mathrm{r}}} = \mathbf{F}^{H}\mathbf{R}_{u,n_{\mathrm{r}}}$. Due to null subcarriers, the truncated matrix of $\bar{\mathbf{R}}_{u,n_{\mathrm{r}}}$ is defined as $\bar{\mathbf{R}}_{\mathrm{t},u,n_{\mathrm{r}}} = \bar{\mathbf{R}}_{u,n_{\mathrm{r}}}(:\,, j_u\colon T\colon K)$, which can be re-expressed as

$$\bar{\mathbf{R}}_{\mathrm{t},u,n_{\mathrm{r}}} = \mathbf{E}_{\mathrm{K},u}\mathbf{F}_{K_{\mathrm{o}}}\mathbf{\Gamma}_{\mathrm{t},u,n_{\mathrm{r}}} + \bar{\mathbf{W}}_{\mathrm{N},u,n_{\mathrm{r}}}, \tag{4.15}$$

with $\mathbf{\Gamma}_{\mathrm{t},u,n_{\mathrm{r}}} = \mathrm{diag}\{\mathbf{\Gamma}_{u,n_{\mathrm{r}}}(j_u\colon T\colon K, j_u\colon T\colon K)\}$, $\mathbf{F}_{K_{\mathrm{o}}} = \mathbf{F}^{H}(:\,, j_u\colon T\colon K)$ and $\bar{\mathbf{W}}_{\mathrm{N},u,n_{\mathrm{r}}}$ being noise matrix.

Step 1.2: In the absence of CFO ($\phi_u = 0$), $(\mathbf{F}^{\perp}_{K_{\mathrm{o}}})^{H}\bar{\mathbf{R}}_{\mathrm{t},u,n_{\mathrm{r}}} = \mathbf{0}_{(K-K_{\mathrm{o}})\times K_{\mathrm{o}}}$ where $\mathbf{F}^{\perp}_{K_{\mathrm{o}}}$ is the complementary part of $\mathbf{F}_{K_{\mathrm{o}}}$, thanks to the orthogonality between the truncated

FFT matrices corresponding to the $(K-K_{\mathrm{o}})$ subcarriers and occupied K_{o} subcarriers in the designed pilot. However, this is not true for $\phi_u \neq 0$. Given a possible CFO search range of $[e_1, e_2]$ and a trial value of ϕ_u, *i.e.*, $\tilde{\phi}_u$, a compensated $\bar{\mathbf{R}}_{\mathrm{t},u,n_{\mathrm{r}}}$ is obtained as $\tilde{\mathbf{R}}_{u,n_{\mathrm{r}}}(\tilde{\phi}_u) = \mathbf{E}^H_{\mathrm{K},u}(\tilde{\phi}_u)\bar{\mathbf{R}}_{\mathrm{t},u,n_{\mathrm{r}}}$. A good trial value $\tilde{\phi}_u$ will make all the elements of $\mathbf{P}_1(\tilde{\phi}_u) = (\mathbf{F}^{\perp}_{K_{\mathrm{o}}})^H\tilde{\mathbf{R}}_{u,n_{\mathrm{r}}}(\tilde{\phi}_u)$ as zero. Thus, the CFO of user u is estimated by

$$\hat{\phi}_{\mathrm{NS},u} = \arg \min_{\tilde{\phi}_u \in [e_1, e_2]} \frac{1}{N_{\mathrm{r}}} \sum_{n_{\mathrm{r}}=0}^{N_{\mathrm{r}}-1} \parallel \mathbf{P}_1(\tilde{\phi}_u) \parallel^2_{\mathrm{F}} . \tag{4.16}$$

Step 2: The initial CFO estimate in (4.16) is further enhanced by exploiting the orthogonality between the occupied Q subcarriers in the designed pilot. CFO compensation is performed on $\mathbf{R}_{u,n_{\mathrm{r}}}$, obtaining $\check{\mathbf{R}}_{u,n_{\mathrm{r}}} = \bar{\mathbf{E}}^H_{\mathrm{K},u}(\tilde{\phi}_u)\mathbf{R}_{u,n_{\mathrm{r}}}$ and its truncated version is given by $\check{\mathbf{R}}_{\mathrm{t},u,n_{\mathrm{r}}} = \check{\mathbf{R}}_{u,n_{\mathrm{r}}}(:, j_u : T : K)$. Thanks to the orthogonality between the occupied K_{o} subcarriers in the designed pilot, the off-diagonal elements of $\check{\mathbf{R}}_{\mathrm{t},u,n_{\mathrm{r}}}$ should all be zero if with an accurate CFO compensation. Hence, CFO is enhanced by

$$\hat{\phi}_{\mathrm{NS},u} = \arg \min_{\tilde{\phi}_u \in \hat{\boldsymbol{\phi}}_u} \frac{1}{N_{\mathrm{r}}} \sum_{n_{\mathrm{r}}=0}^{N_{\mathrm{r}}-1} \parallel \mathbf{P}_2(\tilde{\phi}_u) \parallel^2_{\mathrm{F}}, \tag{4.17}$$

where $\mathbf{P}_2(\tilde{\phi}_u) = \check{\mathbf{R}}_{\mathrm{t},u,n_{\mathrm{r}}} \odot (\mathbf{1}_{K\times K_{\mathrm{o}}} - \mathbf{R}^{\mathbf{dd}}_{\mathrm{t},uu})$, $\mathbf{R}^{\mathbf{dd}}_{\mathrm{t},u,u} = \mathbf{R}^{\mathbf{dd}}_{u,u}(:, j_u : T : K)$ and $\hat{\boldsymbol{\phi}}_u$ is denoted as the CFO estimate set, *i.e.*, $\hat{\boldsymbol{\phi}}_u = [\hat{\phi}_{u,0}, \hat{\phi}_{u,1}, \cdots, \hat{\phi}_{u,w-1}]$ corresponding to w minimum values of $\parallel \mathbf{P}_1(\tilde{\phi}_u) \parallel^2_{\mathrm{F}}$. In this chapter $w = 4$ is used.

It is noteworthy that the proposed JMTMCE scheme is more suitable for long-range systems due to the assumption of equal time delays among different antennas. This assumption does not hold in short-range scenario, since the links between different transmit-receive antenna pairs are more likely to encounter different scatters. This can be solved by simply utilising time diversity rather than space diversity for long-range case. Instead of utilising N_{r} receive antennas, each user transmits N_{r} pilots, and the spatial averaged correlation matrices in Steps 3 and 4 of Subsections 4.4.2 and 4.4.3 are replaced by the temporal averaged correlation matrices. The other parts of the proposed ESPRIT based TOA and CFO estimation scheme remain the same.

4.5 Performance and Complexity Analysis

In this section, the CRLB for pilot assisted joint multi-TOA and multi-CFO estimation in multi-user SIMO OFDM systems is derived, which provides an analytical benchmark for the proposed JMTMCE scheme. Then, the computational complexity of the proposed JMTMCE scheme is investigated.

4.5.1 CRLBs Analysis

The CRLBs on the MSEs of TOA estimation and CFO estimation are derived with the proposed pilot $\mathbf{d}_{\mathrm{pil},u}$. Generally, CRLB is usually determined by taking a derivative of the received signal vector with respect to the unknown variables vector. Thus, the received pilot is written as a column vector, obtaining $\bar{\mathbf{Y}} = [\mathrm{vec}\{\bar{\mathbf{Y}}_0\}^T, \mathrm{vec}\{\bar{\mathbf{Y}}_1\}^T, \cdots, \mathrm{vec}\{\bar{\mathbf{Y}}_{N_\mathrm{r}-1}\}^T]^T$. Define $\mathbf{D}_{\mathrm{pil},u} = [\mathrm{diag}\{\mathbf{d}_{0,u}\}, \mathrm{diag}\{\mathbf{d}_{1,u}\}, \cdots, \mathrm{diag}\{\mathbf{d}_{P_\mathrm{pil}-1,u}\}]^T$ of size $KP_\mathrm{pil} \times K$, and $\boldsymbol{\nu}_{l,u} = [1, e^{-\jmath 2\pi \tau_{l,u} f_\mathrm{s}/K}, \cdots, e^{-\jmath 2\pi (K-1)\tau_{l,u} f_\mathrm{s}/K}]^T$ of length K. The CFR vector $\bar{\mathbf{h}}_{u,n_\mathrm{r}}$ in Section 4.2 can be expressed as

$$\bar{\mathbf{h}}_{u,n_\mathrm{r}} = \boldsymbol{\nu}_u \boldsymbol{\mu}_{u,n_\mathrm{r}}, \tag{4.18}$$

where $\boldsymbol{\nu}_u = [\boldsymbol{\nu}_{0,u}, \boldsymbol{\nu}_{1,u}, \cdots, \boldsymbol{\nu}_{L_\mathrm{p}-1,u}]$ and $\boldsymbol{\mu}_{u,n_\mathrm{r}} = [\mu_{0,u,n_\mathrm{r}}, \mu_{1,u,n_\mathrm{r}}, \cdots, \mu_{L_\mathrm{p}-1,u,n_\mathrm{r}}]^T$. $\bar{\mathbf{Y}}$ can be written as

$$\bar{\mathbf{Y}} = (\mathbf{I}_{N_\mathrm{r}} \otimes \mathbf{Z})\bar{\mathbf{h}} + \mathbf{W}, \tag{4.19}$$

where $\mathbf{Z} = [\mathbf{z}_0, \mathbf{z}_1, \cdots, \mathbf{z}_{U-1}]$, $\mathbf{z}_u = (\mathbf{I}_{P_\mathrm{pil}} \otimes \bar{\mathbf{E}}_{\mathrm{K},u})\mathbf{D}_{\mathrm{pil},u}$, $\bar{\mathbf{h}} = [\bar{\mathbf{h}}_0^T, \bar{\mathbf{h}}_1^T, \cdots, \bar{\mathbf{h}}_{U-1}^T]^T$, $\bar{\mathbf{h}}_u = [\bar{\mathbf{h}}_{u,0}^T, \bar{\mathbf{h}}_{u,1}^T, \cdots, \bar{\mathbf{h}}_{u,N_\mathrm{r}-1}^T]^T = (\mathbf{I}_{N_\mathrm{r}} \otimes \boldsymbol{\nu}_u)\boldsymbol{\mu}_u$, $\boldsymbol{\mu}_u = [\boldsymbol{\mu}_{u,0}^T, \boldsymbol{\mu}_{u,1}^T, \cdots, \boldsymbol{\mu}_{u,N_\mathrm{r}-1}^T]^T$, and $\bar{\mathbf{W}} = [\mathrm{vec}\{\bar{\mathbf{W}}_0\}^T, \mathrm{vec}\{\bar{\mathbf{W}}_1\}^T, \cdots, \mathrm{vec}\{\bar{\mathbf{W}}_{N_\mathrm{r}-1}\}^T]^T$ is the noise matrix.

Denote $\mathbf{U} = (\mathbf{I}_{N_\mathrm{r}} \otimes \mathbf{Z})\bar{\mathbf{h}}$ as the received noise-free signal vector, and $\mathbf{Z}_u = \mathbf{I}_{N_\mathrm{r}} \otimes \mathbf{z}_u$. The unknown variables vector is defined as $\boldsymbol{\theta} = [\boldsymbol{\phi}, \boldsymbol{\tau}, \mathrm{Re}\{\boldsymbol{\mu}\}, \mathrm{Im}\{\boldsymbol{\mu}\}]$ with $\boldsymbol{\phi} = [\phi_0, \phi_1, \cdots, \phi_{U-1}]$, $\boldsymbol{\tau} = [\boldsymbol{\tau}_0, \boldsymbol{\tau}_1, \cdots, \boldsymbol{\tau}_{U-1}]$, $\boldsymbol{\mu} = [\boldsymbol{\mu}_0, \boldsymbol{\mu}_1, \cdots, \boldsymbol{\mu}_{U-1}]$. The Fisher information matrix (FIM) is given by

$$\mathbf{\Pi} = \frac{2}{\sigma^2}\mathrm{Re}[\frac{\partial \mathbf{U}^H}{\partial \boldsymbol{\theta}}\frac{\partial \mathbf{U}}{\partial \boldsymbol{\theta}^T}]. \tag{4.20}$$

Through some manipulations,

$$\mathbf{\Pi} = \frac{2}{\sigma^2}\mathrm{Re}\begin{bmatrix} \mathbf{Q}_\tau^H\mathbf{Q}_\tau & -\mathbf{Q}_\tau^H\mathbf{Q}_\phi & -\jmath\mathbf{Q}_\tau^H\mathbf{Q}_\mu & \mathbf{Q}_\tau^H\mathbf{Q}_\mu \\ -\mathbf{Q}_\phi^H\mathbf{Q}_\tau & \mathbf{Q}_\phi^H\mathbf{Q}_\phi & \jmath\mathbf{Q}_\phi^H\mathbf{Q}_\mu & -\mathbf{Q}_\phi^H\mathbf{Q}_\mu \\ \jmath\mathbf{Q}_\mu^H\mathbf{Q}_\tau & -\jmath\mathbf{Q}_\mu^H\mathbf{Q}_\phi & \mathbf{Q}_\mu^H\mathbf{Q}_\mu & \jmath\mathbf{Q}_\mu^H\mathbf{Q}_\mu \\ \mathbf{Q}_\mu^H\mathbf{Q}_\tau & -\mathbf{Q}_\mu^H\mathbf{Q}_\phi & -\jmath\mathbf{Q}_\mu^H\mathbf{Q}_\mu & \mathbf{Q}_\mu^H\mathbf{Q}_\mu \end{bmatrix} \tag{4.21}$$

is obtained, where $\mathbf{Q}_\tau = [\mathbf{Q}_{\tau,0}, \mathbf{Q}_{\tau,1}, \cdots, \mathbf{Q}_{\tau,K-1}]$ with $\mathbf{Q}_{\tau,u} = \frac{2\pi}{K}\{\mathbf{I}_{N_\mathrm{r}} \otimes [(\mathbf{I}_{P_\mathrm{pil}} \otimes \mathbf{F}\mathbf{E}_{\mathrm{K},u}\mathbf{L}\mathbf{F}^H)\mathbf{D}_{\mathrm{pil},u}]\}\bar{\mathbf{h}}_u$, $\mathbf{L} = \mathrm{diag}\{\mathbf{l}\}$, $\mathbf{l} = [0, 1, \cdots, K-1]^T$, $\mathbf{Q}_\phi = [\mathbf{Q}_{\phi,0}, \mathbf{Q}_{\phi,1}, \cdots, \mathbf{Q}_{\phi,K-1}]$, $\mathbf{Q}_{\phi,u} = \frac{2\pi f_\mathrm{s}}{K}\mathbf{Z}_u(\mathbf{I}_{N_\mathrm{r}}\otimes\mathbf{K}\boldsymbol{\nu}_u)\bar{\boldsymbol{\mu}}_u$, $\tilde{\boldsymbol{\mu}}_u = [\mathrm{diag}\{\boldsymbol{\mu}_{u,0}\}, \mathrm{diag}\{\boldsymbol{\mu}_{u,1}\}, \cdots, \mathrm{diag}\{\boldsymbol{\mu}_{u,N_\mathrm{r}-1}\}]^T$, $\mathbf{Q}_\mu = [\mathbf{Q}_{\mu,0}, \mathbf{Q}_{\mu,1}, \cdots, \mathbf{Q}_{\mu,U-1}]$ with $\mathbf{Q}_{\mu,u} = \mathbf{Z}_u(\mathbf{I}_{N_\mathrm{r}} \otimes \boldsymbol{\nu}_u)$.

The CRLB of $\boldsymbol{\theta}$ is given by the inverse of FIM $\mathbf{\Pi}$, *e.g.*, $\boldsymbol{\chi} = \mathbf{\Pi}^{-1}$. Therefore, the CRLBs of CFO and TOA are given by

$$\mathrm{CRLB}_{\mathrm{CFO}} = \frac{1}{U}\sum\nolimits_{u=0}^{U-1}\boldsymbol{\chi}(u,u), \tag{4.22}$$

and

$$\mathrm{CRLB}_{\mathrm{TOA}} = \frac{1}{U}\sum\nolimits_{u=0}^{U-1}\boldsymbol{\chi}(f(u),f(u)), \tag{4.23}$$

where $f(u) = U + uL_\mathrm{p}$.

4.5.2 Complexity Analysis

In Table 4.1, the computational complexity of multi-TOA and multi-CFO estimation for the proposed JMTMCE scheme and the existing approaches are presented, in terms of the number of complex additions and multiplications. The proposed TOA and CFO estimators contribute to two JMTMCE schemes. JMTMCE-1 includes the closed-form CFO estimator and the R-TOA estimator, whereas JMTMCE-2 consists of the NS-

CFO estimator and the R-TOA estimator. The existing ML CFO estimator [7] and the blind closed-form CFO estimator [8] in Subsection 3.3.2, and the ESPRIT based TOA estimatior [6] in Subsection 3.2.1 are selected for comparison in terms of iCFO estimation, fCFO estimation and TOA estimation, referred to as g1: iCFO [7]+fCFO [8]+ESPRIT [6]. It is worth noting that the proposed JMTMCE1 and JMTMCE2 schemes could estimate iCFO and fCFO together whereas the existing methods [7, 8] need two separate algorithms for iCFO and fCFO estimation. Since the NS-CFO estimator is based on a direct search, JMTMCE-2 suffers high complexity, however contributes to high estimation accuracy, as will be shown in Fig. 4.5. With $K = 64, U = 2, K_\mathrm{o} = 4, N_\mathrm{r} = 4, Q_1 = 8, P_1 = 8, e_{12} = 6, P_2 = 2, P_3 = 2$ and $\delta = 0.01$, the numerical complexity of the proposed schemes and the existing methods [6–8] can be computed. It is found the proposed JMTMCE-1 scheme is very computationally efficient, with complexity reduction of around 7-fold than the existing methods [6–8].

Table 4.1: Analytical computational complexity (K: Number of subcarriers in an OFDM symbol, U: Number of users, K_o: Number of occupied subcarriers for pilot design, N_r: Number of receive antennas, $e_{12} = e_2 - e_1$: CFO search range of NS-CFO estimator, δ: CFO search step size of NS-CFO estimator, P_1 and Q_1: Correspond to P and Q in [7], P_2 and P_3: Number of symbols of [8] and [6], sep.: separation, est.: estimation.)

<table>
<tr><th>Item</th><th>JMTMCE-1</th><th>JMTMCE-2</th><th>g1: iCFO [7]+fCFO [8] +ESPRIT [6]</th></tr>
<tr><td>Multi-CFO multi-TOA sep.</td><td colspan="2">$2K^2UK_\mathrm{o}N_\mathrm{r}$</td><td>$K_\mathrm{o}^2U^2N_\mathrm{r}$</td></tr>
<tr><td>Multi-iCFO est.</td><td rowspan="2">$U(4K^2K_\mathrm{o} + 5K_\mathrm{o}^3$
$+2K_\mathrm{o}^2KN_\mathrm{r})$</td><td rowspan="2">$UN_\mathrm{r}e_{12}(2K-1)$
$(2KK_\mathrm{o} - K_\mathrm{o}^2)/\delta$</td><td>$UQ_1(4K^2P_1 + 5N_\mathrm{r}^2KP_1)$</td></tr>
<tr><td>Multi-fCFO est.</td><td>$\frac{3}{4}UN_\mathrm{r}^3P_2^3K\log_2 K$</td></tr>
<tr><td>Multi-TOA est.</td><td colspan="2">$U(9K_\mathrm{o}^3 + 2K_\mathrm{o}^2KN_\mathrm{r})$</td><td>$2K_\mathrm{o}^2N_\mathrm{r}P_3U + 5K_\mathrm{o}^3U$</td></tr>
</table>

4.6 Simulation Results

4.6.1 Simulation Setup

A simulation study is carried out to demonstrate the performance of the proposed multi-TOA and multi-CFO estimation scheme, with $U = 2$ users. System parameters are set as follows. Each OFDM symbol contains $K = 64$ subcarriers. The modulation scheme is quadrature phase shift keying (QPSK). The CP length is $L_{\mathrm{cp}} = 16$. The two-ray channel model [118] is applied. The sampling rate f_{s} is 200 MHz. Note that the MSE value of TOA estimate is extremely small, whose order of magnitude would be as low as -20. Hence, similarly to [30] and [113], the root MSE (RMSE) is adopted in this chapter to evaluate the performance of the proposed scheme in terms of CFO estimation and TOA estimation. Note that RMSE curves and the corresponding MSE curves follow the same trend, and only differ in values. The RMSE of CFO for the proposed closed-form CFO estimator is defined as

$$\mathrm{RMSE}_{\mathrm{CFO}}^{\mathrm{CF}} = \sqrt{\frac{1}{U}\sum\nolimits_{u=0}^{U-1}\mathbb{E}\{(\hat{\phi}_{\mathrm{CF},u} - \phi_u)^2\}}, \tag{4.24}$$

while that for the proposed NS-CFO estimator is

$$\mathrm{RMSE}_{\mathrm{CFO}}^{\mathrm{NS}} = \sqrt{\frac{1}{U}\sum\nolimits_{u=0}^{U-1}\mathbb{E}\{(\hat{\phi}_{\mathrm{NS},u} - \phi_u)^2\}}. \tag{4.25}$$

The RMSE of TOA is

$$\mathrm{RMSE}_{\mathrm{TOA}} = \sqrt{\frac{1}{U}\sum\nolimits_{u=0}^{U-1}\mathbb{E}\{(\hat{\tau}_{0,u} - \tau_{0,u})^2\}}. \tag{4.26}$$

The lower bounds of RMSEs of CFO and TOA are obtained from the square root of $\mathrm{CRLB}_{\mathrm{CFO}}$ (4.22) and $\mathrm{CRLB}_{\mathrm{TOA}}$ (4.23), respectively. The CFO of each user is randomly generated between -3 and 3. For fairness, the same number of symbols are used for the proposed JMTMCE-1 scheme, JMTMCE-2 scheme, the existing ESPRIT [6] and g1: iCFO [7]+fCFO [8]+ESPRIT [6] based approaches.

4.6.2 RMSE of TOA Estimation

Fig. 4.2 demonstrates the RMSE of TOA estimation as a function of two CFOs for the proposed R-TOA estimator and the existing ESPRIT estimator [6] at SNR=25 dB. The range of two CFOs is from -3 to 3. The RMSE of TOA estimation of the

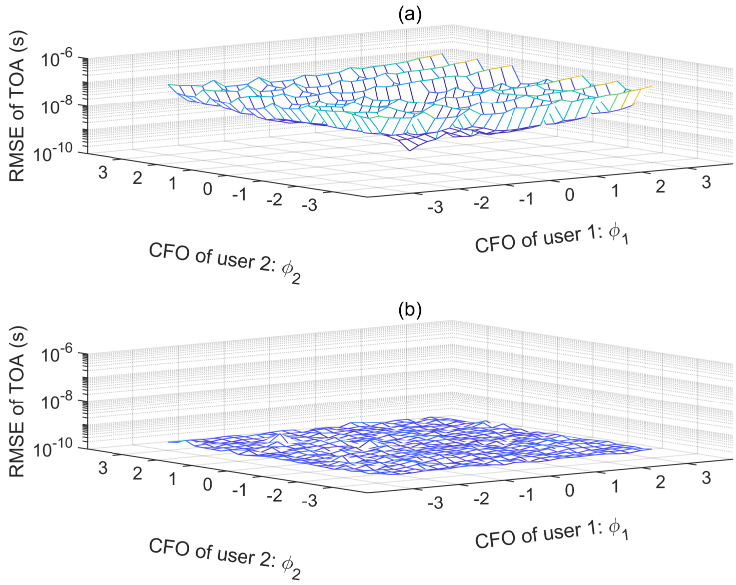

Figure 4.2: RMSE of TOA estimation as a function of two CFOs for: a) the existing ESPRIT estimator [6]; b) the proposed R-TOA estimator.

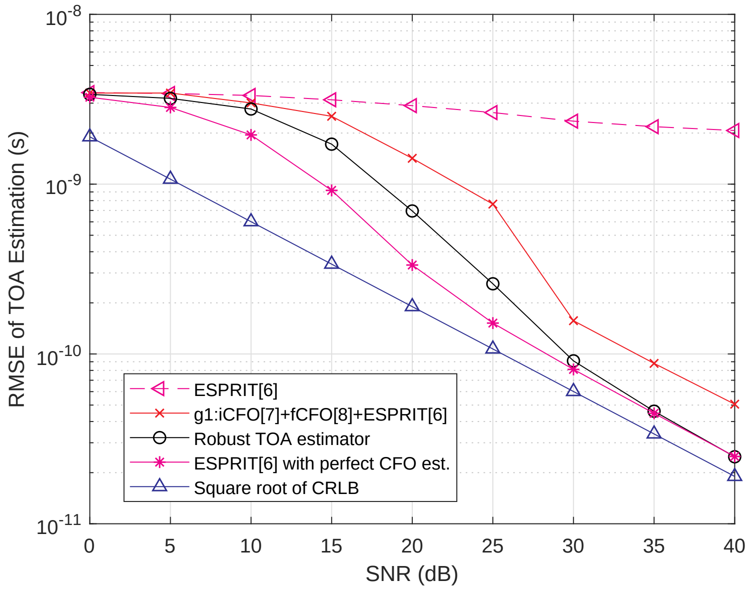

Figure 4.3: RMSE of TOA estimation of the proposed R-TOA estimator and the existing approaches [6–8].

ESPRIT estimator [6] increases with CFOs until a large error floor is formed. However, the proposed R-TOA estimator shows almost the same RMSE performances for various CFOs. It is because the existing ESPRIT estimator [6] is susceptible to CFO and needs the procedure of CFO estimation and compensation in advance, while the proposed R-TOA estimator is independent of the CFO by deriving a CFO-independent channel correlation matrix as demonstrated in Subsection 4.4.2.

Fig. 4.3 shows the RMSE of TOA estimation of the proposed R-TOA estimator with $K_{\mathrm{o}} = 4$ and $N_{\mathrm{r}} = 4$, in comparison to the existing approaches [6–8] and the derived CRLB in Subsection 4.5.1. First, the proposed R-TOA estimator demonstrates a much better performance than g1: iCFO [7]+fCFO [8]+ESPRIT [6] and ESPRIT [6]. At RMSE of TOA with 10^{-10}, the proposed R-TOA estimator achieves an SNR of 5 dB over g1: iCFO [7]+fCFO [8]+ESPRIT [6]. The ESPRIT estimator [6] has the worst performance, forming an error floor due to the presence of CFOs. Moreover, the proposed R-TOA estimator achieves a TOA RMSE performance close to the ESPRIT [6] with perfect CFO estimation and compensation and also to CRLB especially at high SNRs.

In Fig. 4.4, the impacts of the number of receive antennas N_{r} and number of occupied subcarriers in the designed pilot K_{o} on the RMSE of TOA estimation are presented, with SNR=25 dB. First, regarding the proposed R-TOA estimator, the increase of N_{r} and K_{o} can lower the RMSE of TOA estimation significantly. Meanwhile, the proposed R-TOA estimator has a performance much closer to CRLB as N_{r} increases. Nevertheless, the ESPRIT estimator [6] always performs poorly, regardless of the values of N_{r} and K_{o}.

4.6.3 RMSE of CFO Estimation

Figs. 4.5 shows the respective RMSE of CFO estimation of the proposed closed-form CFO estimator and NS-CFO estimator with $K_{\mathrm{o}} = 4$ and $N_{\mathrm{r}} = 4$, in comparison to the existing approaches [6–8]. First, the proposed two CFO estimators significantly outperform the existing approaches [7,8]. For instance, at RMSE of CFO with 2×10^{-2}, the proposed closed-form CFO and NS-CFO estimators achieve an SNR of 5 dB and

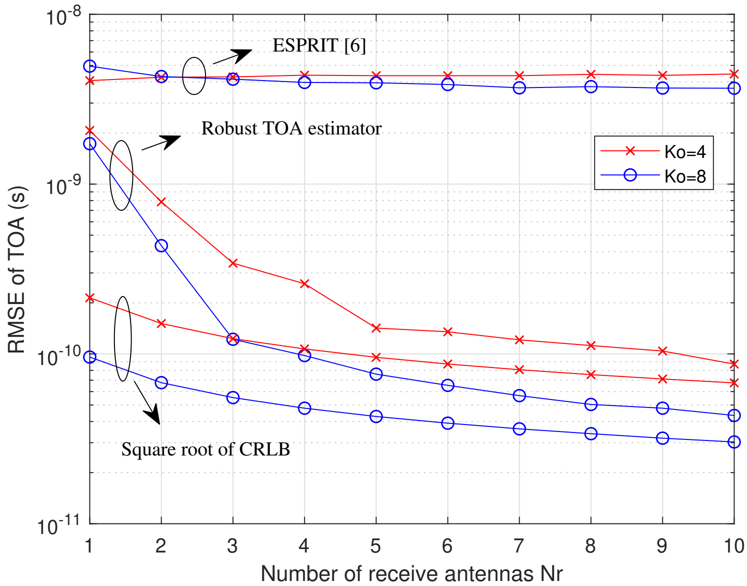

Figure 4.4: Impact of the number of receive antennas N_r and number of occupied subcarriers in the designed pilot K_o on the RMSE of TOA estimation at SNR= 25 dB.

12.5 dB, respectively, over the existing approaches [6–8]. Besides, the proposed NS-CFO estimator has the best performance, whose performance approaches the CRLB from SNR=20 dB to SNR=40 dB.

Fig. 4.6 demonstrates the RMSE of CFO estimation of the proposed closed-form CFO and NS-CFO estimators with $K_\mathrm{o} = 4$ and $K_\mathrm{o} = 8$, respectively, where $N_\mathrm{r} = 4$ receive antennas are used. The NS-CFO estimator always outperforms the closed-form CFO estimator, despite of the value of N_r. The RMSE of both two estimators are lowered with the increase of K_o, especially for the closed-form CFO estimator. For instance, the RMSE of CFO by closed-form CFO estimator is reduced by 5 times when K_o is increased from 4 to 8 at SNR=20 dB.

Fig. 4.7 shows the impacts of the number of receive antennas N_r on the RMSE of CFO estimation of the proposed closed-form CFO and NS-CFO estimators, in comparison to the existing approaches [6–8]. All approaches demonstrate a decreased RMSE of CFO estimation, as N_r increases. The proposed closed-form CFO and NS-CFO estimators all dramatically outperform the existing approaches [6–8] at all N_r. The proposed

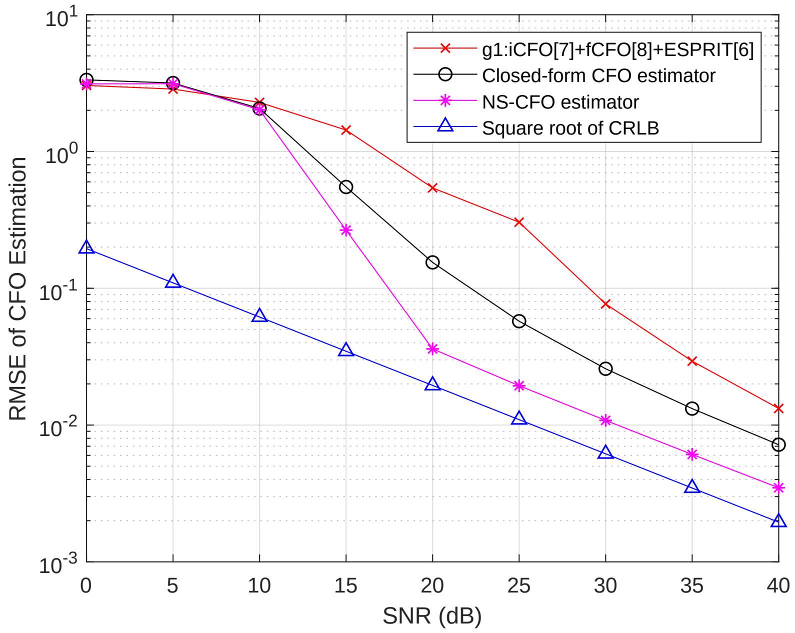

Figure 4.5: RMSE of CFO estimation of the proposed closed-form CFO estimator, NS-CFO estimator and the existing approaches [6–8].

NS-CFO estimator exhibits a higher CFO estimation accuracy than that of closed-form CFO, and has a close performance to that of CRLB.

4.7 Summary

A pilot assisted joint multi-TOA and multi-CFO estimation scheme has been proposed for multi-user OFDM systems, including a closed-form CFO estimator, an NS-CFO estimator and an R-TOA estimator. Table 4.2 compares the proposed JMTMCE scheme with the existing approaches [6–8]. Both two CFO estimators provide higher CFO estimation accuracy than the existing approaches [7,8]. Meanwhile, the NS-CFO estimator has an RMSE performance close to the CRLB from medium to high SNRs, while at the expense of high computational complexity. The proposed closed-form CFO estimator is very computationally efficient, with a complexity reduction of 7-fold over the approaches in [6–8]. The proposed R-TOA estimator demonstrates the RMSE performance close

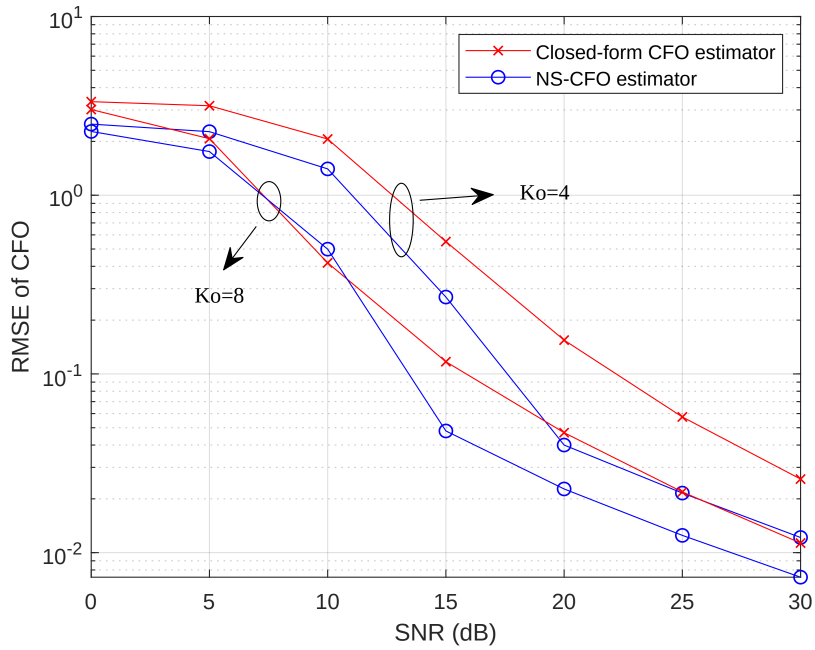

Figure 4.6: Impacts of the number of occupied subcarriers in the designed pilot K_o on the RMSE of CFO estimation, with $N_\mathrm{r} = 4$.

to the ideal case with perfect CFO compensation and the CRLB at high SNRs, without suffering an error propagation from CFO estimation in [6]. Also, their performances can be enhanced with the increase in the number of receive antennas and the number of occupied subcarriers in the designed pilot.

However, the proposed joint multi-TOA and multi-CFO estimation scheme suffers high training overhead, where the pilot length is linearly proportional to the number of users. As a result, it would be spectrally inefficient to extend this work directly to the scenario with a large number of users. Against this limitation, it would be interesting to make use of the beamforming technique [119] to group the large number of users into several groups first. After that, the pilot assisted scheme can be applied for each user group separately to jointly estimate their TOAs and CFOs. Besides, it would be a good attempt to express the cost function of the NS-CFO estimator as a cosine function so that each CFO can be obtained with a closed-form solution similarly to that in [8], for the sake of low computational complexity.

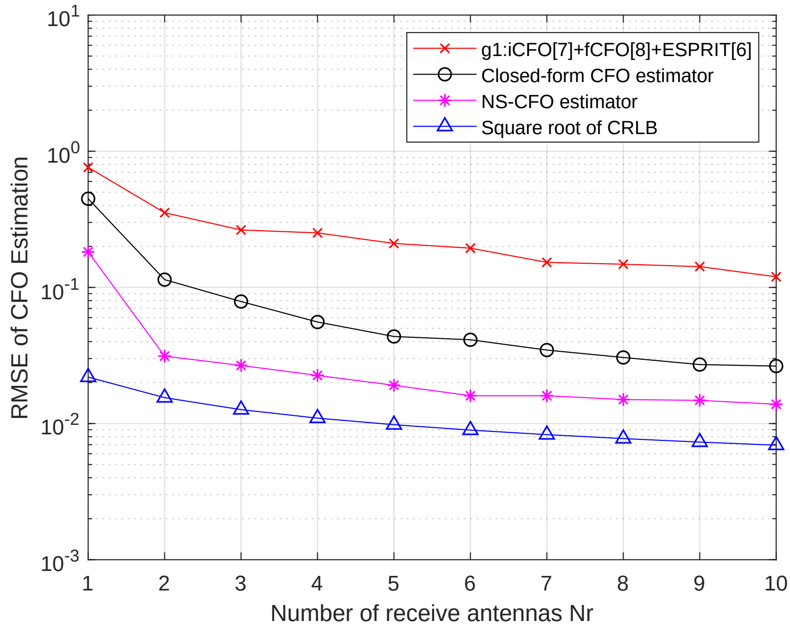

Figure 4.7: Impacts of the number of receive antennas N_{r} on the RMSE of CFO estimation, with $K_{\mathrm{o}} = 4$.

Table 4.2: Comparison of the proposed JMTMCE schemes and the existing approaches [6–8] (JMTMCE-1: R-TOA estimator+Closed-form CFO estimator, and JMTMCE-2: R-TOA estimator+NS-CFO estimator).

Item	JMTMCE-1	JMTMCE-2	ML CFO estimator [7]	Blind CFO estimator [8]	ESPRIT [6]
Users	Multiple	Multiple	Single	Single	Single
iCFO estimation	✓	✓	✓	✗	✗
fCFO estimation	✓	✓	✗	✓	✗
TOA estimation	✓	✓	✗	✗	✓
Accuracy	High	Very High	Medium	Medium	Low
Training overhead	High	High	High	Low	High
Complexity	Low	High	High	Low	Low

Chapter 5

Iterative Semi-Blind Estimation of Channels and CFO in Short-Frame FD OFDM Systems for URLLC

In Chapter 4, the joint estimation of multiple TOAs and multiple CFOs is proposed for multi-user OFDM systems. The system is operated in HD mode, and its estimation is assisted by a long pilot. In this chapter, an ISB receiver structure is proposed to enable URLLC in short-frame FD systems with CFO. To the best of the author's knowledge, this is the first work to propose an integral solution to channel estimation and CFO estimation for short-frame FD OFDM systems by utilising a single pilot. By deriving an equivalent system model with CFO included implicitly, a subspace-based blind channel estimation is proposed for the initial stage, followed by CFO estimation and channel ambiguities elimination. Then refinement of channel and CFO estimates is conducted iteratively. The integer and fractional parts of CFO in the full range are estimated as a whole and in closed-form at each iteration. The proposed ISB receiver significantly outperforms the previous methods in terms of FER, MSEs of channel estimation and CFO estimation and output SINR, while at a halved spectral overhead. CRLBs are derived to verify the effectiveness of the proposed ISB receiver structure. It also demonstrates fast convergence speed.

5.1 Introduction

URLLC, supporting the transmission of information with stringent requirements on reliability and latency, is a key technology for numerous emerging applications, such as tactile Internet, factory automation, virtual reality, intelligent transport systems, and so on [33, 65–68]. Most existing work on URLLC focused on short-frame transmission, through reducing either the symbol duration (increasing the subcarrier spacing) or the number of symbols per TTI [33].

Based on maximum coding rate at finite frame length and finite frame error probability, the performance of NOMA in short-frame communications was investigated in both [72] and [73] and it was concluded that NOMA has a much superior performance than orthogonal multiple access in terms of both latency and throughput. Also, a wireless-powered communication network at finite frame length regime was studied in [35] and [120], respectively. On the other hand, the length of pilot is a challenging issue in short-frame communications [4, 34, 77, 78]. The impact of pilot length on the performance of short-frame physical-layer network coding systems was studied and random coding bound was utilised to identify good pilot-length regimes [77]. The authors in [78] optimised the pilot overhead for short-frame communications and studied the relationship between the pilot overhead and the frame length and error probability. To overcome the reduced training overhead due to short frames, the detected data symbols were utilised to further enhance the reliability of short-frame communications in [34].

FD communication, which allows simultaneous transmission and reception at the same frequency, can double the transmission rate and reduce the end-to-end latency [65, 66, 121, 122]. However, much less work on short-frame communications has considered it. When introducing FD to short-frame communications, two research problems can be investigated: 1) how much throughput can FD achieve at finite frame length regime, in comparison to HD mode? and 2) with limited pilot and data symbols, how to design a high-reliability receiver for FD systems? Regarding the first problem, Gu *et al.* analysed and compared the performance of FD and HD relaying for URLLC and concluded that FD relaying is more preferable [75]. However, its superior performance is achieved only if SI resulting from FD transmission has been cancelled to a reasonable level. Hence, the second question to design a reliable receiver is very essential. To the best of the author's knowledge, it is still an open area in the literature.

One of the major challenges of FD implementation is the SI from its transmitter to its own receiver. Several DC methods have been proposed in the literature for long-frame OFDM systems. As mentioned in Subsection 3.2.1, an LS based SI channel estimator was proposed in [80], which however treats the desired signal as additive noise, degrading the system performance. A two-stage LS cancellation in [101] iterates between SI cancellation and signal detection, however requiring a good initial estimate of the desired channel. An iterative ML channel estimator was described for the estimation of both SI and desired channels in [104], by utilising the known SI, the pilots and unknown data symbols of the desired signal. Nevertheless, it has high training overhead, due to the consecutive pilot transmission for a long period. When applied to short-frame communications, it has a significant performance degradation. Koohian proposed a superimposed signalling technique to cancel SI and detect the desired signal without requiring the procedure of channel estimation [123]. However, its SI channel is assumed to be flat fading only, and thus it cannot be utilised if frequency selective channel fading exists. In [110], a subspace-based algorithm was proposed to jointly estimate the coefficients of both SI and desired channels and transceiver impairments. However, it requires lots of data symbols to achieve a good second-order statistics of received signal, which performs poorly if applied to short-frame communications.

Meanwhile, when considering system impairments, the existing work on FD systems with long frames usually considered IQ imbalances at transmitter and/or receiver [110,124,125], phase noises [104,125] and power amplifier nonlinearities [110,125], and only a few considered CFO. When CFO is present, the reliability of FD systems degrades greatly. CFO estimation and compensation are well-researched problems in

HD OFDM systems [7, 8, 12]. However, it is not straightforward to apply them to FD OFDM systems, since the compensation of CFO based on the desired signal would introduce CFO to the SI. Only a few works in the literature have investigated CFO in FD systems. CFO estimation was investigated in [126] for FD systems. Nevertheless, it requires long training sequences and its pilots of the desired signal and SI should be non-overlapping, *i.e.*, sent in different time slots, resulting in high training overhead and latency. Meanwhile, its integer and fractional parts of CFO are estimated separately, requiring two processes and suffering error propagation. A two-step frequency synchronisation structure was proposed in [127] that synchronises based on SI firstly and then the desired signal. However, the first synchronisation step treats the desired signal as noise, resulting in poor performance, and it considers fCFO only. Furthermore, both [126] and [127] did not consider the estimation of desired channel.

In this chapter, an ISB receiver structure with CFO and channel estimation and signal detection is proposed for URLLC in short-frame FD CP-OFDM systems. By deriving an equivalent system model with CFO included implicitly, a subspace-based blind channel estimation is proposed for the initial stage, followed by CFO estimation and channel ambiguities elimination assisted by a single pilot. Then refinement of channel and CFO estimates is conducted iteratively. This work is different in the following aspects.

- To the best of the author's knowledge, this is the first work to propose a high-reliability receiver structure for short-frame FD CP-OFDM systems in the presence of CFO. The proposed ISB receiver structure requires only a short frame to calculate the second-order statistics of the received signal, which is about tens of times less than the existing semi-blind methods [104, 110]. It significantly outperforms the methods in [7, 8, 104] and [110] in terms of FER, MSEs of channel estimation and CFO estimation and output SINR. CRLBs on the MSEs of channel estimation, CFO estimation and signal detection are derived for the first time for short-frame FD CP-OFDM systems, which verify the effectiveness of the proposed ISB receiver structure.

- This is the first work to provide an integral solution to channel estimation and CFO estimation for FD CP-OFDM systems by utilising a single pilot, considering their impact on each other, while in [80, 101, 104, 110, 123–126] and [127] only one of the issues was addressed assuming perfect estimation of the other and also two training processes were required to estimate CFO and channels separately. The joint semi-blind channels and CFOs estimator for ZP-OFDM [12] described in Subsection 3.3.2 is not applicable for widely-applied CP-OFDM systems. Also, the hard decisions of data symbols are exploited to refine both CFO and channel estimates iteratively, while in [34] and [104] only channel estimation was iterated assuming perfect CFO estimation and compensation.

- The proposed ISB receiver enables high spectrum efficiency with only a single pilot required for joint CFO estimation and channel ambiguities elimination. Its training overhead is much lower than that of [7, 8, 104] and [110]. A short pilot for both the desired signal and SI is carefully designed and superimposed to enable simultaneous transmission of them in FD training mode, while the pilots of joint channels and CFOs estimator for ZP-OFDM [12] are sent in different time slots (refer to Tables 3.3 and 3.4), resulting in reduced spectrum efficiency. The proposed ISB receiver also converges fast within 3 iterations, and is more computationally efficient than the iterative ML approach [104].

- The integer and fractional parts of CFO in the full range are estimated as a whole with a closed-form solution rather than separately as in [7, 8, 126] and [127], without suffering error propagation. The closed-form solution is independent of iCFO estimation range and does not require an advanced acquisition of iCFO range, unlike the ML iCFO estimator [7] demonstrated in Subsection 3.3.2. CFO compensation is performed on the desired signal estimates, avoiding the introduction of CFO to the SI by the methods in [126] and [127].

The rest of this chapter is organised as follows. Section 5.2 describes the short-frame FD CP-OFDM system and derives an equivalent system with CFO included

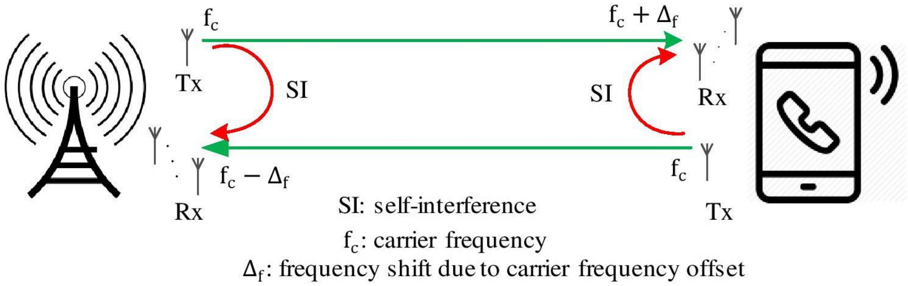

Figure 5.1: A bidirectional FD CP-OFDM system in the presence of CFO.

implicitly. The proposed ISB receiver structure is given in Sections 5.3 and 5.4. Section 5.3 illustrates the initial stage of the proposed ISB receiver structure while Section 5.4 demonstrates the iterative decision-directed stages. Performance analysis and simulation results are given in Sections 5.5 and 5.6. Section 5.7 draws conclusion.

5.2 System Model

5.2.1 Short-Frame FD CP-OFDM System

A bidirectional short-frame FD CP-OFDM system in the presence of CFO is considered, where the BS and mobile station (MS) operate in FD scheme, as illustrated in Fig. 5.1. The BS and MS are equipped with a single transmit antenna and $N_{\rm r}$ receive antennas. Due to the inherent symmetry, MS is chosen as the research object, as the same performance can be observed at BS. The signal transmitted from BS to MS is referred to as the desired signal while the signal transmitted from MS to MS is SI. The purpose of this chapter is to cancel the residual SI in the digital domain after passive and analogue cancellation.

Each short frame consists of $N_{\rm s}$ OFDM symbols with K subcarriers each. The transmit signal vectors corresponding to the i-th ($i = 0, 1, \cdots, N_{\rm s} - 1$) OFDM symbol for the desired signal and SI are given by $\mathbf{d}_{{\rm S},i} = [d_{{\rm S},i}[0], d_{{\rm S},i}[1], \cdots, d_{{\rm S},i}[K-1]]^T$ and $\mathbf{d}_{{\rm I},i} = [d_{{\rm I},i}[0], d_{{\rm I},i}[1], \cdots, d_{{\rm I},i}[K-1]]^T$, respectively, where $d_{{\rm S},i}[k]$ and $d_{{\rm I},i}[k]$ are the corresponding data on subcarrier k ($k = 0, 1, \cdots, K-1$). Each OFDM symbol $\mathbf{d}_{{\rm S},i}$ and $\mathbf{d}_{{\rm I},i}$ are processed by IFFT, and then a CP of length $L_{\rm cp}$ is pre-pended. The transmit signal vectors of the desired signal and SI in the time domain are denoted as $\mathbf{x}_{\mathrm{S},i} = [x_{\mathrm{S},i}[0], x_{\mathrm{S},i}[1], \cdots, x_{\mathrm{S},i}(G-1)]^T$ and $\mathbf{x}_{\mathrm{I},i} = [x_{\mathrm{I},i}[0], x_{\mathrm{I},i}[1], \cdots, x_{\mathrm{I},i}(G-1)]^T$, respectively, with $G = K + L_{\mathrm{cp}}$.

Define $\boldsymbol{\hbar}_{\mathrm{S},n_{\mathrm{r}}} = [\hbar_{\mathrm{S},n_{\mathrm{r}}}[0], \hbar_{\mathrm{S},n_{\mathrm{r}}}[1], \cdots, \hbar_{\mathrm{S},n_{\mathrm{r}}}[L-1]]^T$ and $\boldsymbol{\hbar}_{\mathrm{I},n_{\mathrm{r}}} = [\hbar_{\mathrm{I},n_{\mathrm{r}}}[0], \hbar_{\mathrm{I},n_{\mathrm{r}}}[1], \cdots, \hbar_{\mathrm{I},n_{\mathrm{r}}}[L-1]]^T$ as the respectively desired and SI CIR vectors for the n_{r}-th receive antenna, with L being the length of CIR. The channels are assumed to exhibit quasi-static block fading and the CIRs remain constant for a short frame's duration. Define $\phi = \phi_{\mathrm{I}} + \phi_{\mathrm{F}}$ as the CFO between the BS and MS, where ϕ_{I} and ϕ_{F} are the respective iCFO and fCFO. The SI does not experience CFO assuming all the transmit and receive antennas of MS share one local oscillator [126, 127]. The received signal in the i-th symbol at the n_{r}-th ($n_{\mathrm{r}} = 0, 1, \cdots, N_{\mathrm{r}} - 1$) receive antenna in the time domain can be written as

$$y_{i,n_{\mathrm{r}}}[g] = e^{\jmath 2\pi\phi g/K} \sum_{l=0}^{L-1} \hbar_{\mathrm{S},n_{\mathrm{r}}}[l] x_{\mathrm{S},i}[g-l] + \sqrt{\frac{1}{\rho}} \sum_{l=0}^{L-1} \hbar_{\mathrm{I},n_{\mathrm{r}}}[l] x_{\mathrm{I},i}[g-l] + w_{i,n_{\mathrm{r}}}[g], \quad (5.1)$$

where ρ is the average input desired signal-to-SI-ratio, denoted as SIR, before digital cancellation, and $w_{i,n_{\mathrm{r}}}[g]$ ($g = 0, 1, \cdots, G-1$) is the noise term.

5.2.2 Equivalent System with CFO Included Implicitly

According to (5.1), it can be observed that the received signal is corrupted by both CFO and SI, making the desired signal detection more challenging. The existing methods require two separate training processes for the respective CFO and channel estimation, suffering high training overhead and high latency [80, 101, 104, 110, 123–127]. In the following, an equivalent system model with CFO included implicitly is derived so that CFO and channel can be estimated jointly with a short pilot. By incorporating the CFO into the desired signal and channel, (5.1) is equivalent to

$$y_{i,n_{\mathrm{r}}}[g] = \sum_{l=0}^{L-1} h_{\mathrm{S},n_{\mathrm{r}}}[l] s_{\mathrm{S},i}[g-l] + \sqrt{\frac{1}{\rho}} \sum_{l=0}^{L-1} \hbar_{\mathrm{I},n_{\mathrm{r}}}[l] x_{\mathrm{I},i}[g]-l] + w_{i,n_{\mathrm{r}}}[g], \quad (5.2)$$

where $h_{\mathrm{S},n_\mathrm{r}}[l] = e^{\jmath 2\pi\phi l/K}\hbar_{\mathrm{S},n_\mathrm{r}}[l]$ and $s_{\mathrm{S},i}[g] = e^{\jmath 2\pi\phi g/K}x_{\mathrm{S},i}[g]$ are denoted as the respectively CFO-included channel and CFO-included desired signal in the equivalent system model. It is worth noticing that SI and its channel are not modified since it does not experience CFO.

Among the received signal samples in CP, $y_{i,n_\mathrm{r}}[L-1]$ to $y_{i,n_\mathrm{r}}[L_\mathrm{cp}-1]$ are free from ISI caused by frequency selective fading, and hence are utilised alongside signal samples $y_{i,n_\mathrm{r}}[L_\mathrm{cp}]$ to $y_{i,n_\mathrm{r}}[G-1]$ for estimation of CFO and channels. Collecting all these samples from N_r received antennas into a vector yields $\mathbf{y}_i = [y_{i,0}[L-1], y_{i,1}[L-1], \cdots, y_{i,N_\mathrm{r}-1}[L-1], \cdots, y_{i,0}[G-1], y_{i,1}[G-1), \cdots, y_{i,N_\mathrm{r}-1}[G-1]]^T$, which is formulated as

$$\mathbf{y}_i = \mathbf{H}\mathbf{s}_i + \mathbf{w}_i, \tag{5.3}$$

where $\mathbf{H} = [\mathbf{H}_\mathrm{S}, \mathbf{H}_\mathrm{I}]$, with $\mathbf{H}_\mathrm{S}$ of size $(G-L+1)N_\mathrm{r} \times G$ defined as

$$\mathbf{H}_\mathrm{S} = \begin{bmatrix} \mathbf{h}_\mathrm{S}(L-1) & \cdots & \mathbf{h}_\mathrm{S}(0) & \cdots & \cdots & \mathbf{0}_{N_\mathrm{r}\times 1} \\ \vdots & \ddots & \ddots & \ddots & \ddots & \vdots \\ \mathbf{0}_{N_\mathrm{r}\times 1} & \cdots & \cdots & \mathbf{h}_\mathrm{S}(L-1) & \cdots & \mathbf{h}_\mathrm{S}(0) \end{bmatrix}, \tag{5.4}$$

$\mathbf{h}_\mathrm{S}(l) = [h_{\mathrm{S},0}[l], h_{\mathrm{S},1}[l], \cdots, h_{\mathrm{S},N_\mathrm{r}-1}[l]]^T$, $\mathbf{H}_\mathrm{I}$ is defined as the same form to $\mathbf{H}_\mathrm{S}$ but with $\mathbf{h}_\mathrm{S}[l]$ replaced by $\mathbf{h}_\mathrm{I}[l] = \sqrt{\frac{1}{\rho}}[\hbar_{\mathrm{I},0}[l], \hbar_{\mathrm{I},1}[l], \cdots, \hbar_{\mathrm{I},N_\mathrm{r}-1}[l]]^T$; $\mathbf{s}_i = [\mathbf{s}_{\mathrm{S},i}^T, \mathbf{x}_{\mathrm{I},i}^T]^T$, with $\mathbf{s}_{\mathrm{S},i} = [s_{\mathrm{S},i}[0], s_{\mathrm{S},i}[1], \cdots, s_{\mathrm{S},i}(G-1)]^T$ and $\mathbf{x}_{\mathrm{I},i} = [x_{\mathrm{I},i}[0], x_{\mathrm{I},i}[1], \cdots, x_{[I],i}[G-1]]^T$; $\mathbf{w}_i = [w_{i,0}[L-1], w_{i,1}[L-1], \cdots, w_{i,N_\mathrm{r}-1}[L-1], \cdots, w_{i,0}[G-1], w_{i,1}[G-1), \cdots, w_{i,N_\mathrm{r}-1}[G-1]]^T$. It is easily found that the rank of $\mathbb{E}\{\mathbf{s}_i\mathbf{s}_i^H\}$ is $2K$ instead of $2G$ due to the redundancy from CP. Since $\mathbb{E}\{\mathbf{s}_i\mathbf{s}_i^H\}$ is rank deficient, (5.3) cannot be applied to the subspace-based blind channel estimation methods [128, 129].

To address this problem, $(L_\mathrm{cp}+1)$ subvectors of length $(K-L+1)N_\mathrm{r}$ from $\mathbf{y}_i$ are formed, and the t-th ($t = 0, 1, \cdots, L_\mathrm{cp}$) subvector is denoted as

$$\begin{aligned} \mathbf{y}_i^t =& [y_{i,0}(L-1+t), y_{i,1}(L-1+t), \cdots, y_{i,N_\mathrm{r}-1}(L-1+t), \\ & \cdots, y_{i,0}[K-1+t], y_{i,1}[K-1+t], \cdots, y_{i,N_\mathrm{r}-1}[K-1+t]]^T, \end{aligned} \tag{5.5}$$

which is written as

$$\mathbf{y}_i^t = \tilde{\mathbf{H}}\mathbf{s}_i^t + \mathbf{w}_i^t, \quad t = 0, 1, \cdots, L_{\text{cp}}, \tag{5.6}$$

where $\tilde{\mathbf{H}} = [\tilde{\mathbf{H}}_{\text{S}}, \tilde{\mathbf{H}}_{\text{I}}]$, with $\tilde{\mathbf{H}}_{\text{S}}$ and $\tilde{\mathbf{H}}_{\text{I}}$ following the similar form to $\mathbf{H}_{\text{S}}$ but with a reduced size of $(K-L+1)N_{\text{r}} \times K$ instead of $(G-L+1)N_{\text{r}} \times G$; $\mathbf{s}_i^t = [(\mathbf{s}_{\text{S},i}^t)^T, (\mathbf{x}_{\text{I},i}^t)^T]^T$ with $\mathbf{s}_{\text{S},i}^t = [s_{\text{S},i}[t], s_{\text{S},i}[t+1], \cdots, s_{\text{S},i}[K-1+t]]^T$ and $\mathbf{x}_{\text{I},i}^t = [x_{\text{I},i}[t], x_{\text{I},i}[t+1], \cdots, x_{\text{I},i}(K-1+t)]^T$; $\mathbf{w}_i^t = [w_{i,0}(L-1+t), w_{i,1}(L-1+t), \cdots, w_{i,N_{\text{r}}-1}(L-1+t), \cdots, w_{i,0}[K-1+t], w_{i,1}[K-1+t], \cdots, w_{i,N_{\text{r}}-1}[K-1+t]]^T$.

Since $\mathbb{E}\{\mathbf{s}_i^t(\mathbf{s}_i^t)^H\}$ is full rank with $2K$, (5.6) can be applied to the subspace-based blind channel estimation methods, as long as $\tilde{\mathbf{H}}$ is a tall matrix which can be achieved by setting $(K-L+1)N_{\text{r}} > 2K$. Meanwhile, thanks to the partition of the received signal into several subvectors, the second-order statistics of the received signal can be achieved by utilising a short frame with a small number of OFDM symbols. It is noteworthy that such an equivalent system model was derived for ZP-OFDM systems in [12], which however cannot be applied here for widely-used CP-OFDM systems and also requires a large number of symbols to achieve the second-order statistics of the received signal, as mentioned in Subsection 3.3.2.

Based on the equivalent system model derived, an ISB receiver structure is proposed for URLLC in short-frame FD CP-OFDM systems in the presence of CFO, which consists of two kinds of stages. On one hand, the CFO and channel estimation as well as signal detection are performed initially by the proposed subspace-based semi-blind method, referred to as the initial stage. On the other hand, the initial estimation and detection performance are enhanced significantly by performing iterations among them, where the previous hard decisions are utilised to overcome the pilot shortage due to the short frame structure, referred to as iterative decision-directed stages. The block diagram of the proposed ISB receiver structure is illustrated in Fig. 5.2.

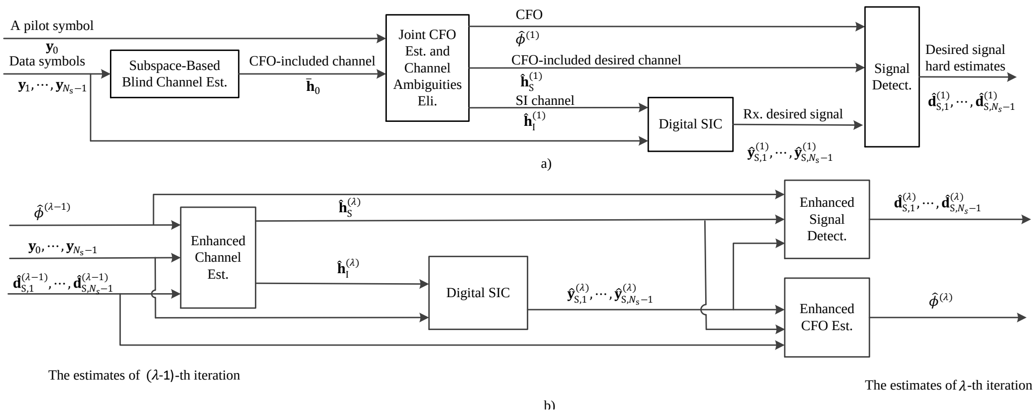

Figure 5.2: a) Initial stage and b) the λ-th ($\lambda \geq 2$) iterative decision-directed stage of the proposed ISB receiver structure (Est.: estimation, SIC: SI cancellation and Detect.: detection).

5.3 Initial Stage of the ISB Receiver Structure

First, a subspace-based blind method is proposed to estimate the CFO-included desired channel and SI channel with some ambiguities, which requires a very short frame to obtain the second-order statistics of the received signal. Second, a single pilot for the desired signal and SI is carefully designed and superimposed to enable simultaneous transmission of them to achieve FD training mode, and the corresponding channel ambiguities and CFO can be extracted jointly by PM channel estimation approach in Subsection 3.2.1. Third, based on the CFO-included desired and SI channel estimates, the received SI is generated and cancelled from the received signal, and then the desired signal can be easily detected.

5.3.1 Blind Channel Estimation

A subspace-based blind channel estimator is proposed to jointly estimate the CFO-included desired channel and SI channel, by utilising a short frame. It is assumed that 1) noise samples are uncorrelated and 2) noise and signal samples are uncorrelated. N_{r} receive antennas with $(K-L+1)N_{\mathrm{r}} > 2K$ are utilised. It is easily seen that the number of receive antennas should be larger than 2, *i.e.,* $N_{\mathrm{r}} > 2$. The proposed estimator is summarised in four steps below.

Step 1. $(N_{\rm s}-1)$ received data symbols within a short frame are used to compute the auto-correlation matrix of the received signal, obtaining

$$\mathbf{R}_{\mathbf{yy}} = \frac{1}{(N_{\rm s}-1)(L_{\rm cp}+1)} \sum\nolimits_{i=1}^{N_{\rm s}-1} \sum\nolimits_{t=0}^{L_{\rm cp}} \mathbf{y}_i^t (\mathbf{y}_i^t)^H. \tag{5.7}$$

It is worth noting that the number of signal samples per received symbol used to compute the auto-correlation matrix of the received signal has been increased, thanks to the partition of the received signal vector $\mathbf{y}_i$ into a number of subvectors $\mathbf{y}_i^t$ when deriving the equivalent system model. Thus, the required frame length $N_{\rm s}$ to achieve the second-order statistics of the received signal can be much shorter than the methods in [12, 110, 128] and [129].

Step 2. EVD is performed on the auto-correlation matrix $\mathbf{R}_{\mathbf{yy}}$. The signal subspace has a dimension of $2K$, while the noise subspace has Q $(Q = (K-L+1)N_{\rm r} - 2K)$ eigenvectors corresponding to Q smallest eigenvalues of the matrix $\mathbf{R}_{\rm yy}$. Denote the q-th eigenvector as $\boldsymbol{\gamma}_q = [\boldsymbol{\gamma}_q^T(0), \boldsymbol{\gamma}_q^T(1), \cdots, \boldsymbol{\gamma}_q^T(K-L)]^T$ $(q = 0, 1, \cdots, Q-1)$, where $\boldsymbol{\gamma}_q(\omega)$ $(\omega = 0, 1, \cdots, K-L)$ is a column vector of length $N_{\rm r}$. Due to the inherent orthogonality between the signal and noise subspaces, the columns of $\tilde{\mathbf{H}}$ are orthogonal to each vector $\boldsymbol{\gamma}_q$ $(q = 0, 1, \cdots, Q-1)$, *i.e.*,

$$\boldsymbol{\gamma}_q^H \tilde{\mathbf{H}} = \mathbf{0}_{1\times 2K}. \tag{5.8}$$

Therefore, $\boldsymbol{\gamma}_q$ spans the left null space of $\tilde{\mathbf{H}}$. Since $\tilde{\mathbf{H}}$ is formulated by the vectors $\mathbf{h}_{\rm S}(l)$ and $\mathbf{h}_{\rm I}(l)$, $(l = 0, 1, \cdots, L-1)$, channel estimation can be restricted to $\mathbf{h}_{\rm S}(l)$ and $\mathbf{h}_{\rm I}(l)$, instead of the whole matrix $\tilde{\mathbf{H}}$.

Step 3. Defining $\mathbf{h}(l) = [\mathbf{h}_{\rm S}(l), \mathbf{h}_{\rm I}(l)]$, it can be found (5.8) is equivalent to the following equations:

$$\begin{aligned}&\sum\nolimits_{l=L-1-k}^{L-1}\boldsymbol{\gamma}_q^H(l-L+1+k)\mathbf{h}(l)=\mathbf{0}_{1\times 2},\quad \text{for } k=0,1,\cdots,L-2;\\&\sum\nolimits_{l=0}^{L-1}\boldsymbol{\gamma}_q^H(k-L+1+l)\mathbf{h}(l)=\mathbf{0}_{1\times 2},\quad \text{for } k=L-1,L,\cdots,K-L;\\&\sum\nolimits_{l=0}^{K-1-k}\boldsymbol{\gamma}_q^H(k-L+1+l)\mathbf{h}(l)=\mathbf{0}_{1\times 2},\quad \text{for } k=K-L+1,\cdots,K-1.\end{aligned} \tag{5.9}$$

or in the following matrix form:

$$\boldsymbol{\iota}_q\mathbf{h}=\mathbf{0}_{K\times 2}, \tag{5.10}$$

and $\boldsymbol{\iota}_q$ of size $K\times N_{\mathrm{r}}L$ is given by

$$\boldsymbol{\iota}_q=\begin{bmatrix}\boldsymbol{\gamma}_q^H(K-L) & \mathbf{0}_{1\times N_{\mathrm{r}}} & \cdots & \mathbf{0}_{1\times N_{\mathrm{r}}}\\ \boldsymbol{\gamma}_q^H(K-L-1) & \boldsymbol{\gamma}_q^H(K-L) & \cdots & \mathbf{0}_{1\times N_{\mathrm{r}}}\\ \vdots & \vdots & \ddots & \vdots\\ \boldsymbol{\gamma}_q^H(K-2L+1) & \boldsymbol{\gamma}_q^H(K-2L+2) & \cdots & \boldsymbol{\gamma}_q^H(K-L)\\ \boldsymbol{\gamma}_q^H(K-2L) & \boldsymbol{\gamma}_q^H(K-2L+1) & \cdots & \boldsymbol{\gamma}_q^H(K-L-1)\\ \vdots & \vdots & \ddots & \vdots\\ \boldsymbol{\gamma}_q^H(0) & \boldsymbol{\gamma}_q^H(1) & \cdots & \boldsymbol{\gamma}_q^H(L-1)\\ \mathbf{0}_{1\times N_{\mathrm{r}}} & \boldsymbol{\gamma}_q^H(0) & \cdots & \boldsymbol{\gamma}_q^H(L-2)\\ \vdots & \vdots & \ddots & \vdots\\ \mathbf{0}_{1\times N_{\mathrm{r}}} & \mathbf{0}_{1\times N_{\mathrm{r}}} & \cdots & \boldsymbol{\gamma}_q^H(0)\end{bmatrix}, \tag{5.11}$$

where $\mathbf{h}=[\mathbf{h}^T(0),\mathbf{h}^T(1),\cdots,\mathbf{h}^T(L-1)]^T$ is of size $N_{\mathrm{r}}L\times 2$.

Step 4. All $\boldsymbol{\iota}_q$ matrices with $q=0,1,\cdots,Q-1$ are considered as follows

$$\boldsymbol{\iota}=[\boldsymbol{\iota}_0^T,\boldsymbol{\iota}_1^T,\cdots,\boldsymbol{\iota}_{Q-1}^T]^T, \tag{5.12}$$

and

$$\boldsymbol{\iota}\mathbf{h}=\mathbf{0}_{KQ\times 2} \tag{5.13}$$

can be obtained. Hence, $\mathbf{h}$ can be estimated by choosing the 2 right singular vectors of $\boldsymbol{\iota}$, denoted as $\hat{\mathbf{h}}_0$. However, there exist ambiguities between the real CFO-included channel $\mathbf{h}$ and the blindly estimated CFO-included channel $\hat{\mathbf{h}}_0$, *i.e.*,

$$\mathbf{h} = \hat{\mathbf{h}}_0 \mathbf{c}, \tag{5.14}$$

where $\mathbf{c}$ with a dimension of 2×2 is the complex channel ambiguity matrix. The first and second columns of $\hat{\mathbf{h}}_0$ are the respectively CFO-included desired channel and SI channel by the subspace-based blind channel estimation approach, denoted as $\hat{\mathbf{h}}_{\mathrm{S},0}$ and $\hat{\mathbf{h}}_{\mathrm{I},0}$, respectively. The proposed subspace-based blind channel estimation algorithm is depicted in Algorithm 1. In the following, a short pilot is carefully designed to enable the joint CFO estimation and channel ambiguities elimination.

Algorithm 1 Subspace-based blind channel estimation.

Input:
The received data symbol subvectors, $\mathbf{y}_i^t$, $i = 1, 2, \cdots, N_\mathrm{s} - 1$, $t = 0, 1, \cdots, L_\mathrm{cp}$;

Output:
CFO-included desired channel and SI channel estimates, $\hat{\mathbf{h}}_{\mathrm{S},0}$ and $\hat{\mathbf{h}}_{\mathrm{I},0}$;

1: Compute the auto-correlation matrix of the received signal by (5.7), obtaining $\mathbf{R}_{\mathbf{yy}}$;
2: Obtain Q eigenvectors, corresponding to the smallest Q eigenvalues of the matrix $\mathbf{R}_{\mathbf{yy}}$;
3: Form matrix $\boldsymbol{\iota}_q$ according to (5.11);
4: Obtain the CFO-included desired channel and SI channel estimates, by choosing 2 right singular vectors of $\boldsymbol{\iota}$;
5: **return** $\hat{\mathbf{h}}_{\mathrm{S},0}$, $\hat{\mathbf{h}}_{\mathrm{I},0}$.

5.3.2 Pilot Design

A short pilot of the desired signal and SI is well designed to enable the simultaneous transmission of them to achieve FD training mode so that the corresponding CFO and channel ambiguities can be extracted jointly by the PM channel estimation method in Subsection 3.2.1.

With the channel estimates by the proposed subspace-based blind method, (5.6) can be rewritten as

$$\mathbf{y}_i^t = \tilde{\mathbf{H}}_0 \mathbf{C}_{\mathrm{S}} \mathbf{s}_{\mathrm{S},i}^t + \tilde{\mathbf{H}}_0 \mathbf{C}_{\mathrm{I}} \mathbf{x}_{\mathrm{I},i}^t + \mathbf{w}_i^t, \tag{5.15}$$

where $\tilde{\mathbf{H}}_0$ is defined as the same form to $\tilde{\mathbf{H}}$ but with $\mathbf{h}$ replaced by $\hat{\mathbf{h}}_0$; $\mathbf{C}_{\mathrm{S}} = \mathbf{I}_K \otimes \mathbf{c}_{\mathrm{S}}$ and $\mathbf{C}_{\mathrm{I}} = \mathbf{I}_K \otimes \mathbf{c}_{\mathrm{I}}$ with $\mathbf{c}_{\mathrm{S}}$ and $\mathbf{c}_{\mathrm{I}}$ being the first and second columns of $\mathbf{c}$, respectively. The received signal $\mathbf{y}_i^t$ is multiplied with the pseudoinverse of $\tilde{\mathbf{H}}_0$, yielding

$$\mathbf{r}_i^t = \mathbf{C}_{\mathrm{S}} \mathbf{s}_{\mathrm{S},i}^t + \mathbf{C}_{\mathrm{I}} \mathbf{x}_{\mathrm{I},i}^t + \tilde{\mathbf{w}}_i^t, \tag{5.16}$$

where $\tilde{\mathbf{w}}_i^t = (\tilde{\mathbf{H}}_0^H \tilde{\mathbf{H}}_0)^{-1} \tilde{\mathbf{H}}_0^H \mathbf{w}_i^t$. Then, $\mathbf{r}_i^t$ is divided into K column vectors of length 2 as $\mathbf{r}_i^t = [(\mathbf{r}_i^t(0))^T, (\mathbf{r}_i^t(1))^T, \cdots, (\mathbf{r}_i^t(K-1))^T]^T$, and $\mathbf{r}_i^t(k)$ is given by

$$\mathbf{r}_i^t(k) = \mathbf{c}_{\mathrm{S}} e^{\jmath 2\pi\phi(k+t)/K} \mathbf{x}_{\mathrm{S},i}^t(k) + \mathbf{c}_{\mathrm{I}} \mathbf{x}_{\mathrm{I},i}^t(k) + \tilde{\mathbf{w}}_i^t(k), \tag{5.17}$$

where $\tilde{\mathbf{w}}_i^t(k)$ is a column vector of length 2 and $\tilde{\mathbf{w}}_i^t = [(\tilde{\mathbf{w}}_i^t(0))^T, (\tilde{\mathbf{w}}_i^t(1))^T, \cdots, (\tilde{\mathbf{w}}_i^t(K-1))^T]^T$.

According to (5.17), it can be observed that as long as $\mathbf{x}_{\mathrm{S},i}^t(0) = \cdots = \mathbf{x}_{\mathrm{S},i}^t(K-1) = \xi_1$ and $\mathbf{x}_{\mathrm{I},i}^t(0) = \cdots = \mathbf{x}_{\mathrm{I},i}^t(K-1) = \xi_2$, (5.17) can be rewritten as

$$\mathbf{r}_i^t(k) = \mathbf{c} e^{\jmath 2\pi\boldsymbol{\phi}(k+t)/K} + \tilde{\mathbf{w}}_i^t(k), \tag{5.18}$$

where $\boldsymbol{\phi} = [\phi, 0]^T$. For simplicity, ξ_1 and ξ_2 have been specified as 1 in (5.18). It can be noticed that (5.18) looks like the CFR model in (3.17). Therefore, PM channel estimation methods, *e.g.*, ESPRIT [49] and LS, can be exploited here to estimate CFO and channel ambiguities, respectively. By utilising all (L_{cp}+1) subvectors of the received pilot $\mathbf{y}_i$, it is easily obtained that the transmitted pilot ought to meet $x_{\mathrm{S},i}(g) = 1$ and $x_{\mathrm{I},i}(g) = 1$ for $g = 0, 1, \cdots, G-1$. In this chapter, it is assumed that the first OFDM symbol $i = 0$ is transmitted for training.

It is noteworthy that two pilot patterns have also been designed in [12] to jointly estimate the CFOs and channel ambiguities for ZP-OFDM systems, as demonstrated in Subsection 3.3.2. However, to avoid multi-user interference, the pilots of different users should be non-overlapping, resulting in reduced spectral efficiency. In contrast, the pilot design proposed in this chapter can be overlapping, which is indeed designed for FD systems. Meanwhile, the CFO and channel ambiguities can be extracted jointly by utilising a single pilot. Therefore, the FD training mode and low training overhead make it more applicable for URLLC.

5.3.3 Joint CFO Estimation and Channel Ambiguities Elimination

As discussed earlier, with the pilot design, the estimation problem of CFO and channel ambiguities relates to the PM channel estimation problem. Thus, the time delay estimator, *e.g.*, ESPRIT, for PM channel estimation, can be exploited here to extract the unknown CFO, while the path amplitude estimator, *e.g.*, LS, can be used to determine the channel ambiguities.

CFO Estimation

Utilising the ESPRIT algorithm, the CFO estimation is summarised in four steps below:
Step 1. Form the matrix $\mathbf{r}_{\text{pil}}^t = [\mathbf{r}_0^t(0), \cdots, \mathbf{r}_0^t(K-1)]^T$ with size $K \times 2$, given by

$$\mathbf{r}_{\text{pil}}^t = \mathbf{E}_{\text{SI}}^t \mathbf{c}^T + \tilde{\mathbf{w}}_{\text{pil}}^t, \tag{5.19}$$

where $\mathbf{E}_{\text{SI}}^t = [\mathbf{E}_{\text{K}}^t(\phi), \mathbf{1}_{K\times 1}]$ with $\mathbf{E}_{\text{K}}^t(\phi) = [e^{\jmath 2\pi\phi t/K}, \cdots, e^{\jmath 2\pi\phi(K-1+t)/K}]^T$, and $\tilde{\mathbf{w}}_{\text{pil}}^t = [\tilde{\mathbf{w}}_0^t(0), \cdots, \tilde{\mathbf{w}}_0^t(K-1)]^T$.
Step 2. Compute the auto-correlation matrix of $\mathbf{r}_{\text{pil}}^t$ considering all the received subvector samples of the pilot,

$$\mathbf{R}^{\mathbf{rr}} = \frac{1}{2(L_{\text{cp}}+1)} \sum\nolimits_{t=0}^{L_{\text{cp}}} \mathbf{r}_{\text{pil}}^t (\mathbf{r}_{\text{pil}}^t)^H. \tag{5.20}$$

Hence, the auto-correlation matrix has been averaged by $(L_{\text{cp}}+1)$, thanks to the partition of the received signal into a number of subvectors, which can enhance the CFO estimation. It is also worth noting the auto-correlation matrix has been averaged by 2, which results from the ambiguities incurred by the blind channel estimation. $\mathbf{R}^{\text{rr}}$ is further improved by FB averaging technique [49], obtaining

$$\mathbf{R}^{\mathbf{rr}}_{\mathrm{FB}} = \frac{1}{2}(\mathbf{R}^{\mathbf{rr}} + \mathbf{O}(\mathbf{R}^{\mathbf{rr}})^{*}\mathbf{O}), \tag{5.21}$$

where $\mathbf{O}$ is the $K \times K$ matrix whose components are zero except for ones on the anti-diagonal.

Step 3. 2 eigenvectors corresponding to 2 largest eigenvalues of $\mathbf{R}^{\mathbf{rr}}_{\mathrm{FB}}$ are found, denoted as $\mathbf{u}$ of size $K \times 2$. Due to the phase rotational invariance property, there exists the following relationship $\mathbf{u}_2 = \mathbf{u}_1 \mathrm{diag}\{e^{\jmath 2\pi\phi/K}\}$ where $\mathbf{u}_1$ and $\mathbf{u}_2$ of size $(K-1) \times 2$ are the first $(K-1)$ and last $(K-1)$ rows of $\mathbf{u}$, respectively.

Step 4. The CFO can be extracted by

$$\hat{\boldsymbol{\phi}}^{(1)} = \frac{\angle \hat{\mathbf{v}} K}{2\pi}, \tag{5.22}$$

where $\hat{\mathbf{v}}$ is the eigenvalues of $(\mathbf{u}_1^H \mathbf{u}_1)^{-1} \mathbf{u}_1^H \mathbf{u}_2$, and the superscript $^{(1)}$ denotes this is the initial estimation. It is worth noticing that $\hat{\boldsymbol{\phi}}^{(1)}$ consists of two CFOs. The one with the largest absolute value is the unknown CFO ϕ, *i.e.*, $\hat{\phi}^{(1)} = \max |\hat{\boldsymbol{\phi}}^{(1)}|$, since the CFO of SI is always 0. Note that CFO has been estimated in one step where the integer and fractional parts of CFO are estimated as a whole and with a closed-form solution, unlike the existing methods in [7, 8, 126] and [127].

Channel Ambiguities Elimination

The channel ambiguities can then be computed by the LS method, with the CFO estimate $\hat{\phi}^{(1)}$. It involves three steps.

Step 1. Form the matrix $\hat{\mathbf{E}}^{t}_{\mathrm{SI}} = [\mathbf{E}^{t}_{\mathrm{K}}(\hat{\phi}^{(1)}), \mathbf{1}_{K\times 1}]$.

Step 2. According to (5.19), the channel ambiguities are estimated by the LS method,

$$\hat{\mathbf{c}} = ((\hat{\mathbf{E}}_{\mathrm{SI}})^{\dagger} \mathbf{r}_{\mathrm{pil}})^{T}, \tag{5.23}$$

where $\hat{\mathbf{E}}_{\mathrm{SI}} = [(\hat{\mathbf{E}}_{\mathrm{SI}}^{0})^T, (\hat{\mathbf{E}}_{\mathrm{SI}}^{1})^T, \cdots, (\hat{\mathbf{E}}_{\mathrm{SI}}^{L_{\mathrm{cp}}})^T]$ and $\mathbf{r}_{\mathrm{pil}} = [(\mathbf{r}_{\mathrm{pil}}^{0})^T, (\mathbf{r}_{\mathrm{pil}}^{1})^T, \cdots, (\mathbf{r}_{\mathrm{pil}}^{L_{\mathrm{cp}}})^T]$. Thus, the desired and SI channel ambiguity vectors are obtained as $\hat{\mathbf{c}}_{\mathrm{S}}$ and $\hat{\mathbf{c}}_{\mathrm{I}}$ by choosing the first and second columns of $\hat{\mathbf{c}}$, respectively.

Step 3. The CFO-included desired and SI channel estimates are obtained as

$$\hat{\mathbf{h}}_{\mathrm{S}}^{(1)} = \hat{\mathbf{h}}_0 \hat{\mathbf{c}}_{\mathrm{S}}, \quad \hat{\mathbf{h}}_{\mathrm{I}}^{(1)} = \hat{\mathbf{h}}_0 \hat{\mathbf{c}}_{\mathrm{I}}. \tag{5.24}$$

Define $\hat{\mathbf{H}}_{\mathrm{S}}^{(1)}$ and $\hat{\mathbf{H}}_{\mathrm{I}}^{(1)}$ as the circulant desired and SI channel matrices, following the same form to $\mathbf{H}_{\mathrm{S}}$ and $\mathbf{H}_{\mathrm{I}}$ with replacing $\mathbf{h}_{\mathrm{s}}$ and $\boldsymbol{\hbar}_{\mathrm{I}}$ by $\hat{\mathbf{h}}_{\mathrm{S}}^{(1)}$ and $\hat{\mathbf{h}}_{\mathrm{I}}^{(1)}$, respectively.

Algorithm 2 Joint CFO estimation and channel ambiguities elimination.

Input:

The received pilot subvectors, $\mathbf{r}_0^t(k)$, with $k = 0, 1, \cdots, K-1$, $g = 0, 1, \cdots, L_{\mathrm{cp}}$;

The blind channel estimate, $\hat{\mathbf{h}}_0$;

Output:

CFO estimate, $\hat{\phi}^{(1)}$;

CFO-included desired and SI channel estimates, $\hat{\mathbf{h}}_{\mathrm{S}}^{(1)}$ and $\hat{\mathbf{h}}_{\mathrm{I}}^{(1)}$;

Form the matrix $\mathbf{r}_{\mathrm{pil}}^t$;
Compute the auto-correlation matrix of $\mathbf{r}_{\mathrm{pil}}^t$, obtaining $\mathbf{R}_{\mathrm{FB}}^{\mathbf{rr}}$ by (5.20) and (5.21);
Find 2 eigenvectors corresponding to 2 largest eigenvalues of $\mathbf{R}_{\mathrm{FB}}^{\mathbf{rr}}$, denoted as $\mathbf{u}$;
Estimate CFO by (5.22);
Form the matrix $\hat{\mathbf{E}}_{\mathrm{SI}}^t$;
Estimate channel ambiguities by (5.23);
Obtain the CFO-included desired channel and SI channel estimates through (5.24);
return $\hat{\phi}^{(1)}$, $\hat{\mathbf{h}}_{\mathrm{S}}^{(1)}$ and $\hat{\mathbf{h}}_{\mathrm{I}}^{(1)}$.

5.3.4 SI Cancellation and Signal Detection

With the SI channel estimate, the received SI can be generated and cancelled from the received signal, obtaining $\hat{\mathbf{y}}_{\mathrm{S},i}^{(1)} = \mathbf{y}_i - \hat{\mathbf{H}}_{\mathrm{I}}^{(1)} \mathbf{x}_{\mathrm{I},i}$. With the CFO estimate $\hat{\phi}^{(1)}$, the desired signal in the time domain is estimated by

$$\hat{\mathbf{x}}_{\mathrm{S},i}^{(1)} = \mathbf{E}_{\mathrm{G}}(\hat{\phi}^{(1)})(\hat{\mathbf{H}}_{\mathrm{S}}^{(1)})^{\dagger} \hat{\mathbf{y}}_{\mathrm{S},i}^{(1)}, \tag{5.25}$$

where $\mathbf{E}_{\mathrm{G}}(\hat{\phi}^{(1)})= \mathrm{diag}\{[1, e^{-\jmath 2\pi\hat{\phi}^{(1)}/K}, \cdots, e^{-\jmath 2\pi\hat{\phi}^{(1)}(G-1)/K}]\}$. Define $\boldsymbol{\epsilon}_i^{(1)}$ of size $K \times 1$ as the desired signal estimate in the time domain. $\boldsymbol{\epsilon}_i^{(1)}(k) = \hat{\mathbf{x}}_{\mathrm{S},i}^{(1)}(k + L_{\mathrm{cp}})$ for $k = 0, 1, \cdots, K - L_{\mathrm{cp}} - 1$. As the first L_{cp} elements of $\hat{\mathbf{x}}_{\mathrm{S},i}^{(1)}$ are the CP, the last L_{cp} elements of $\boldsymbol{\epsilon}_i^{(1)}$ can be refined by

$$\begin{aligned}\boldsymbol{\epsilon}_i^{(1)}(k) =& \frac{1}{2}(\hat{\mathbf{x}}_{\mathrm{S},i}^{(1)}(k + L_{\mathrm{cp}}) + \hat{\mathbf{x}}_{\mathrm{S},i}^{(1)}(k - K + L_{\mathrm{cp}})),\\ &\text{for } k = K - L_{\mathrm{cp}}, \cdots, K - 1.\end{aligned} \tag{5.26}$$

It is noteworthy that CFO compensation has been performed on the CFO-included desired signal estimate instead of the received signal, avoiding the introduction of CFO to SI by the existing methods [126, 127]. By performing FFT on $\boldsymbol{\epsilon}_i^{(1)}$, the frequency-domain desired signal is detected, and the hard estimate is obtained as $\hat{\mathbf{d}}_{\mathrm{S},i}^{(1)}$.

5.4 Iterative Decision-Directed Stages of the ISB Receiver Structure

To mitigate the impact of short training overhead due to the short frame, the hard decisions are utilised to enhance channel estimation, signal detection and CFO estimation iteratively. First, the enhanced CFO-included desired channel and SI channel estimates are determined by the previous desired signal estimates, the pilot and the known SI. Then, a more accurate SI cancellation is performed. Last, the desired signal estimate is refined, while an enhanced CFO estimate is obtained thanks to the inherent relationship between the previous desired signal estimate and the newly CFO-included desired signal estimate. The iterative channel estimation, signal detection and CFO estimation algorithm is shown in Algorithm 3.

5.4.1 Enhanced Channel Estimation, SI Cancellation and Signal Detection

It is easy to show that (5.3) is equivalent to

$$\mathbf{y}_i = \mathbf{S}_{\mathrm{S},i}\mathbf{h}_{\mathrm{S}} + \mathbf{X}_{\mathrm{I},i}\boldsymbol{\hbar}_{\mathrm{I}} + \mathbf{w}_i, \tag{5.27}$$

where

$$\mathbf{S}_{\mathrm{S},i} = \begin{bmatrix} \dot{\mathbf{s}}_{\mathrm{S},i}(L-1) & \dot{\mathbf{s}}_{\mathrm{S},i}(L-2) & \cdots & \dot{\mathbf{s}}_{\mathrm{S},i}(0) \\ \dot{\mathbf{s}}_{\mathrm{S},i}(L) & \dot{\mathbf{s}}_{\mathrm{S},i}(L-1) & \cdots & \dot{\mathbf{s}}_{\mathrm{S},i}(1) \\ \vdots & \vdots & \ddots & \vdots \\ \dot{\mathbf{s}}_{\mathrm{S},i}(G-1) & \dot{\mathbf{s}}_{\mathrm{S},i}(G-2) & \cdots & \dot{\mathbf{s}}_{\mathrm{S},i}(G-L) \end{bmatrix}, \tag{5.28}$$

with $\dot{\mathbf{s}}_{\mathrm{S},i}(g) = \mathbf{I}_{N_{\mathrm{r}}} \otimes s_{\mathrm{S},i}(g)$, and $\mathbf{S}_{\mathrm{I},i}$ follows the same form to $\mathbf{S}_{\mathrm{S},i}$, but with $s_{\mathrm{S},i}(g)$ replaced by $x_{\mathrm{I},i}(g)$.

The hard decision can be utilised to refine channel estimation iteratively. By performing IFFT on the previous desired signal hard estimate in the $(\lambda-1)$-th iteration $\hat{\mathbf{d}}_{\mathrm{S},i}^{(\lambda-1)}$, the time-domain desired signal with CP insertion is determined as $\hat{\mathbf{x}}_{\mathrm{S},i}^{(\lambda-1)}$, and the CFO-included signal is obtained as $\hat{\mathbf{s}}_{\mathrm{S},i}^{(\lambda-1)} = \mathbf{E}_{\mathrm{G}}(-\hat{\phi}^{(\lambda-1)})\hat{\mathbf{x}}_{\mathrm{S},i}^{(\lambda-1)}$. Note that the first symbol ($i=0$) is pilot and is always known at the receiver, thus $\hat{\mathbf{d}}_{\mathrm{S},0}^{(\lambda-1)} = \mathbf{d}_{\mathrm{S},0}$ regardless of the value of λ. Then, $\hat{\mathbf{S}}_{\mathrm{S},i}^{(\lambda-1)}$ can be easily obtained by replacing $s_{\mathrm{S},i}(g)$ in $\mathbf{S}_{\mathrm{S},i}$ by $\hat{s}_{\mathrm{S},i}^{(\lambda-1)}(g)$. Therefore, the CFO-included desired and SI channels can be enhanced by

$$[\hat{\mathbf{h}}_{\mathrm{S}}^{(\lambda)}; \hat{\mathbf{h}}_{\mathrm{I}}^{(\lambda)}] = (\hat{\mathbf{S}}^{(\lambda-1)})^{\dagger}\mathbf{y}_{\mathrm{all}}, \tag{5.29}$$

where $\hat{\mathbf{S}}^{(\lambda-1)} = [\hat{\mathbf{S}}_{\mathrm{S},0}^{(\lambda-1)}, \mathbf{X}_{\mathrm{I},0}; \cdots; \hat{\mathbf{S}}_{\mathrm{S},N_{\mathrm{s}}-1}^{(\lambda-1)}, \mathbf{X}_{\mathrm{I},N_{\mathrm{s}}-1}]$ and $\mathbf{y}_{\mathrm{all}} = [\mathbf{y}_0; \mathbf{y}_1; \cdots; \mathbf{y}_{N_{\mathrm{s}}-1}]$.

Similarly, the size-reduced circulant desired channel matrix is obtained as $\tilde{\mathbf{H}}_{\mathrm{S}}^{(\lambda)}$ following the form of $\tilde{\mathbf{H}}_{\mathrm{S}}$ with $\mathbf{h}_{\mathrm{S}}$ replaced by $\hat{\mathbf{h}}_{\mathrm{S}}^{(\lambda)}$, while the circulant desired and SI channel matrices $\hat{\mathbf{H}}_{\mathrm{S}}^{(\lambda)}$ and $\hat{\mathbf{H}}_{\mathrm{I}}^{(\lambda)}$ are determined following the form of $\mathbf{H}_{\mathrm{S}}$, with $\mathbf{h}_{\mathrm{S}}$ replaced by $\hat{\mathbf{h}}_{\mathrm{S}}^{(\lambda)}$ and $\hat{\mathbf{h}}_{\mathrm{I}}^{(\lambda)}$, respectively. Then, SI is cancelled from the received signal, obtaining $\hat{\mathbf{y}}_{\mathrm{S},i}^{(\lambda)} = \mathbf{y}_i - \hat{\mathbf{H}}_{\mathrm{I}}^{(\lambda)}\mathbf{x}_{\mathrm{I},i}$. With the new estimates $\hat{\mathbf{H}}_{\mathrm{S}}^{(\lambda)}$ and $\hat{\mathbf{y}}_{\mathrm{S},i}^{(\lambda)}$ and the previous

CFO estimate $\hat{\phi}^{(\lambda-1)}$, the new hard estimate of the desired signal can be obtained as $\hat{\mathbf{d}}_{\mathrm{S},i}^{(\lambda)}$ by utilising (5.25) and (5.26). It is noteworthy that the CFO included in the desired channel and signal should be the same in the derived equivalent system model. As the CFO-included desired channel estimate $\hat{\mathbf{H}}_{\mathrm{S}}^{(\lambda)}$ is obtained by the previous CFO estimate $\hat{\phi}^{(\lambda-1)}$, the hard estimate of the desired signal should be determined by performing CFO compensation with the previous CFO estimate.

5.4.2 Enhanced CFO Estimation

To enhance CFO estimation, the estimated received signal vector $\hat{\mathbf{y}}_{\mathrm{S},i}^{(\lambda)}$ is divided into $(L_{\mathrm{cp}}+1)$ subvectors, and the t-th $(t=0,1,\cdots,L_{\mathrm{cp}})$ subvector is defined as

$$\begin{aligned}\hat{\mathbf{y}}_{\mathrm{S},i}^{t,(\lambda)} &= [\hat{\mathbf{y}}_{\mathrm{S},i}^{(\lambda)}(tN_{\mathrm{r}}), \hat{\mathbf{y}}_{\mathrm{S},i}^{(\lambda)}(tN_{\mathrm{r}}+1), \cdots, \hat{\mathbf{y}}_{\mathrm{S},i}^{(\lambda)}(tN_{\mathrm{r}}+N_{\mathrm{r}}-1),\\ &\cdots, \hat{\mathbf{y}}_{\mathrm{S},i}^{(\lambda)}((t+K-L)N_{\mathrm{r}}), \hat{\mathbf{y}}_{\mathrm{S},i}^{(\lambda)}((t+K-L)N_{\mathrm{r}}+1),\\ &\cdots, \hat{\mathbf{y}}_{\mathrm{S},i}^{(\lambda)}((t+K-L)N_{\mathrm{r}}+N_{\mathrm{r}}-1)]. \end{aligned} \tag{5.30}$$

Similarly to (5.6), $\hat{\mathbf{y}}_{\mathrm{S},i}^{t,(\lambda)}$ is given by

$$\hat{\mathbf{y}}_{\mathrm{S},i}^{t,(\lambda)} = \tilde{\mathbf{H}}_{\mathrm{S}} \hat{\mathbf{s}}_{\mathrm{S},i}^{t} + \mathbf{w}_{\mathrm{c},i}^{t}, \tag{5.31}$$

where $\mathbf{w}_{\mathrm{c},i}^{t}$ is the noise term. With the new CFO-included desired channel estimate $\tilde{\mathbf{H}}_{\mathrm{S}}^{(\lambda)}$, the CFO-included desired signal is estimated by

$$\hat{\mathbf{s}}_{\mathrm{S},i}^{t,(\lambda)} = (\tilde{\mathbf{H}}_{\mathrm{S}}^{(\lambda)})^{\dagger} \hat{\mathbf{y}}_{\mathrm{S},i}^{t,(\lambda)}. \tag{5.32}$$

There exists an inherent relationship between the re-estimated CFO-included desired signal $\hat{\mathbf{s}}_{\mathrm{S},i}^{t,(\lambda)}$ and the previous desired signal estimate $\hat{\mathbf{x}}_{\mathrm{S},i}^{t,(\lambda-1)}$ in the ideal case, *i.e.*,

$$\hat{\mathbf{s}}_{\mathrm{S},i}^{t,(\lambda)} = \mathrm{diag}\{\mathbf{E}_{\mathrm{K}}^{t}(\phi)\} \hat{\mathbf{x}}_{\mathrm{S},i}^{t,(\lambda-1)}, \tag{5.33}$$

where $\hat{\mathbf{x}}_{\mathrm{S},i}^{t,(\lambda-1)} = [\hat{\mathbf{x}}_{\mathrm{S},i}^{(\lambda-1)}(t), \cdots, \hat{\mathbf{x}}_{\mathrm{S},i}^{(\lambda-1)}(t+K-1)]^T$. Therefore, utilising all the previous

Algorithm 3 Iterative channel estimation, signal detection and CFO estimation.

Input:

Frequency-domain desired signal estimate, $\hat{\mathbf{d}}_{\mathrm{S},i}^{(\lambda-1)}$, $i = 0, 1, \cdots, N_{\mathrm{s}} - 1$;
Frequency-domain SI signal, $\mathbf{d}_{\mathrm{I},i}$, $i = 0, 1, \cdots, N_{\mathrm{s}} - 1$;
CFO estimate, $\hat{\phi}^{(\lambda-1)}$;
Time-domain received signal, $\mathbf{y}_i$, $i = 0, 1, \cdots, N_{\mathrm{s}} - 1$;

Output:

CFO-included desired channel and SI channel estimates, $\hat{\mathbf{h}}_{\mathrm{S}}^{(\lambda)}$ and $\hat{\mathbf{h}}_{\mathrm{I}}^{(\lambda)}$;
Frequency-domain desired signal estimate, $\hat{\mathbf{d}}_{\mathrm{S},i}^{(\lambda)}$;
CFO estimate, $\hat{\phi}^{(\lambda)}$;

1: Refine the CFO-included desired channel and SI channel by (5.29);
2: Refine SI cancellation, obtaining the received desired signal $\hat{\mathbf{y}}_{\mathrm{S},i}^{(\lambda)}$;
3: Obtain the refined desired signal estimate, $\hat{\mathbf{d}}_{\mathrm{S},i}^{(\lambda)}$, by (5.25) and (5.26);
4: Form $(L_{\mathrm{cp}} + 1)$ subvectors from $\hat{\mathbf{y}}_{\mathrm{S},i}^{(\lambda)}$ by (5.30);
5: Determine the CFO-included desired signal estimate by (5.32);
6: Compute the CFO vector by (5.34);
7: Calculate the auto-correlation of the CFO vector through (5.35);
8: Obtain the refined CFO estimate, $\hat{\phi}^{(\lambda)}$, following the similar procedures of Steps 3 and 4 of Algorithm 2;
9: **return** $\hat{\mathbf{h}}_{\mathrm{S}}^{(\lambda)}$, $\hat{\mathbf{h}}_{\mathrm{I}}^{(\lambda)}$, $\hat{\mathbf{d}}_{\mathrm{S},i}^{(\lambda)}$ and $\hat{\phi}^{(\lambda)}$.

desired signal estimates ($i = 0, 1, \cdots, N_{\mathrm{S}} - 1$), the CFO can be further enhanced by the ESPRIT algorithm as follows.

Step 1. Compute the CFO vector $\hat{\mathbf{e}}_i^t = [\hat{e}_i^t(0), \hat{e}_i^t(1), \cdots, \hat{e}_i^t(K-1)]^T$ with

$$\hat{e}_i^t(k) = \hat{\mathbf{s}}_{\mathrm{S},i}^{t,(\lambda)}(k) / \hat{\mathbf{x}}_{\mathrm{S},i}^{t,(\lambda-1)}(k). \tag{5.34}$$

Step 2. Calculate the averaged auto-correlation matrix of the CFO vector by

$$\mathbf{R}^{\mathbf{ee}} = \frac{1}{N_{\mathrm{s}}(L_{\mathrm{cp+1}})} \sum_{i=0}^{N_{\mathrm{s}}-1} \sum_{t=0}^{L_{\mathrm{cp}}} \hat{\mathbf{e}}_i^t (\hat{\mathbf{e}}_i^t)^H. \tag{5.35}$$

It is further enhanced by the FB averaging technique, obtaining $\mathbf{R}_{\mathrm{FB}}^{\mathbf{ee}} = \frac{1}{2}(\mathbf{R}^{\mathbf{ee}} + \mathbf{O}(\mathbf{R}^{\mathbf{ee}})^* \mathbf{O})$.

Step 3. The remaining of the CFO estimation keeps the same to Steps 3 and 4 of the

CFO estimator in Subsection 5.3.3, but selecting one eigenvector corresponding to the largest eigenvalue only. Denote the new CFO estimate as $\hat{\phi}^{(\lambda)}$.

The rounded integer of $\hat{\phi}^{(\lambda)}$ is defined as the iCFO estimate $\hat{\phi}_{\mathrm{I}}^{(\lambda)}$, while the rest is the fCFO estimate $\hat{\phi}_{\mathrm{F}}^{\lambda}$. The CFO-free desired channel estimate is easily obtained as $\boldsymbol{\hbar}_{\mathrm{S}}^{(\lambda)} = \mathrm{diag}\{\mathbf{e}_{\mathrm{L}} \otimes \mathbf{1}_{N_{\mathrm{r}}\times 1}\}\hat{\mathbf{h}}_{\mathrm{S}}^{(\lambda)}$, where $\mathbf{e}_{\mathrm{L}} = [1, e^{-\jmath 2\pi\hat{\phi}^{(\lambda)}/K}, \cdots, e^{-\jmath 2\pi\hat{\phi}^{(\lambda)}(L-1)/K}]^T$. Note that the decision-directed CFO estimation can refine fCFO only. To avoid error propagation from the desired signal detection to CFO estimation, the rounded integer parts of $\hat{\phi}^{(\lambda)}$ and $\hat{\phi}^{(\lambda-1)}$ are compared. If they are equal, the CFO estimate in the λ-th iteration is $\hat{\phi}^{(\lambda)}$ and otherwise is $\hat{\phi}^{(\lambda-1)}$.

The above procedures, namely channel estimation, SI cancellation, signal detection and CFO estimation, are repeated until a satisfactory performance is obtained. Define I as the number of total iterations. Therefore, the hard decision of the desired signal has been utilised to overcome the problems resulting from the reduced training overhead due to short frames and can also enhance the system performance significantly.

5.5 Performance and Complexity Analysis

5.5.1 CRLBs Analysis

As stated in [130], the theoretical analysis of the iterative decision-directed channel estimation is hard to make, due to its complex processing. The performance analysis of the initial stage of the proposed ISB receiver is mainly investigated in the following and the corresponding CRLBs for channel estimation, CFO estimation and signal detection are derived to serve as an analytical benchmark.

CRLB is usually obtained by taking a derivative of the received signal vector with respect to the unknown variables vector [128]. To simplify the process of derivative, the received pilot and data samples in a short frame and from all the received antennas are collected as a column vector, *i.e.*, $\mathbf{y} = [y_{0,0}(L-1), \cdots, y_{0,0}(G-1), \cdots, y_{0,N_{\mathrm{r}}-1}(L-1), \cdots, y_{0,N_{\mathrm{r}}-1}(G-1), \cdots, y_{N_{\mathrm{s}}-1,0}(L-1), \cdots, y_{N_{\mathrm{s}}-1,0}(G-1), \cdots, y_{N_{\mathrm{s}}-1,N_{\mathrm{r}}-1}(L-1), \cdots, y_{N_{\mathrm{s}}-1,N_{\mathrm{r}}-1}(G-1)]^T$, where $y_{0,0}(L-1)$ to $y_{0,N_{\mathrm{r}}-1}(G-1)$ are the pilot symbol samples and the rest are the data symbol samples. According to (5.3), $\mathbf{y}$ can be expressed as

$$\mathbf{y} = (\mathbf{I}_{N_\mathrm{s}} \otimes ((\mathbf{I}_{N_\mathrm{r}} \otimes \mathbf{E}_{\text{G-L+1}})\check{\mathbf{H}}_\mathrm{S}\mathbf{F}_\mathrm{all}))\mathbf{d}_\mathrm{S} + \sqrt{\frac{1}{\rho}}(\mathbf{I}_{N_\mathrm{s}} \otimes (\check{\mathbf{H}}_\mathrm{I}\mathbf{F}_\mathrm{all}))\mathbf{d}_\mathrm{I} + \mathbf{w}, \tag{5.36}$$

where $\mathbf{E}_{\text{G-L+1}} = \mathrm{diag}\{[e^{\jmath 2\pi\phi(L-1)/K}, \cdots, e^{\jmath 2\pi\phi(G-1)/K}]\}$ and $\check{\mathbf{H}}_\mathrm{S} = [\check{\mathbf{H}}_{\mathrm{S},0}; \cdots; \check{\mathbf{H}}_{\mathrm{S},N_\mathrm{r}-1}]$ are respectively the CFO matrix and the circulant desired channel matrix, with $\check{\mathbf{H}}_{\mathrm{S},n_\mathrm{r}}$ of size $(G-L+1)\times G$ defined as

$$\check{\mathbf{H}}_{\mathrm{S},n_\mathrm{r}} = \begin{bmatrix} \hbar_{\mathrm{S},n_\mathrm{r}}(L-1) & \cdots & \hbar_{\mathrm{S},n_\mathrm{r}}(0) & \cdots & \cdots & 0 \\ \vdots & \ddots & \ddots & \ddots & \ddots & \vdots \\ 0 & \cdots & \cdots & \hbar_{\mathrm{S},n_\mathrm{r}}(L-1) & \cdots & \hbar_{\mathrm{S},n_\mathrm{r}}(0) \end{bmatrix}, \tag{5.37}$$

$\check{\mathbf{H}}_\mathrm{I} = [\check{\mathbf{H}}_{\mathrm{I},0}; \check{\mathbf{H}}_{\mathrm{I},1}; \cdots; \check{\mathbf{H}}_{\mathrm{I},N_\mathrm{r}-1}]$, with $\check{\mathbf{H}}_{\mathrm{I},n_\mathrm{r}}$ defined as a similar form to $\check{\mathbf{H}}_{\mathrm{S},n_\mathrm{r}}$ but replacing $\hbar_{\mathrm{S},n_\mathrm{r}}(l)$ by $\hbar_{\mathrm{I},n_\mathrm{r}}(l)$; $\mathbf{F}_\mathrm{all} = [\mathbf{F}(K-L_\mathrm{cp}\colon K-1, 0\colon K-1); \mathbf{F}]$ with $\mathbf{F}$ denoting the IFFT matrix of size $K \times K$; $\mathbf{d}_\mathrm{S} = [\mathbf{d}_{\mathrm{S},0}; \mathbf{d}_{\mathrm{S,D}}]$ with $\mathbf{d}_{\mathrm{S},0}$ denoting the pilot symbol vector of the desired signal in the frequency domain and $\mathbf{d}_{\mathrm{S,D}} = [\mathbf{d}_{\mathrm{S},1}; \mathbf{d}_{\mathrm{S},2}; \cdots; \mathbf{d}_{\mathrm{S},N_\mathrm{s}-1}]$ denoting the data symbol vector in the frequency domain; $\mathbf{d}_\mathrm{I} = [\mathbf{d}_{\mathrm{I},0}; \mathbf{d}_{\mathrm{I},1}; \cdots; \mathbf{d}_{\mathrm{I},N_\mathrm{s}-1}]$ is the SI symbol vector in the frequency domain and $\mathbf{w} = [w_{0,0}(L-1), \cdots, w_{0,0}(G-1), \cdots, w_{0,N_\mathrm{r}-1}(L-1), \cdots, w_{0,N_\mathrm{r}-1}(G-1), \cdots, w_{N_\mathrm{s}-1,0}(L-1), \cdots, w_{N_\mathrm{s}-1,0}(G-1), \cdots, w_{N_\mathrm{s}-1,N_\mathrm{r}-1}(L-1), \cdots, w_{N_\mathrm{s}-1,N_\mathrm{r}-1}(G-1)]^T$ is the noise vector.

Regarding the semi-blind estimation of CFO and channels in FD systems, the unknown variables are the CFO ϕ, the desired CIR vector denoted as $\boldsymbol{\hbar}_\mathrm{S} = [\boldsymbol{\hbar}_\mathrm{S}(0); \cdots; \boldsymbol{\hbar}_\mathrm{S}(L-1)]$, the SI CIR vector denoted as $\boldsymbol{\hbar}_\mathrm{I} = [\boldsymbol{\hbar}_\mathrm{I}(0); \cdots; \boldsymbol{\hbar}_\mathrm{I}(L-1)]$ and the vector of the desired data symbols $\mathbf{d}_{\mathrm{S,D}}$. Note that the real and imaginary parts of the unknown complex variables should be considered separately for derivatives [128]. Then, all of the unknown variables are collected in a column vector, *i.e.*, $\boldsymbol{\Theta} = [\phi, \mathrm{Re}\{\boldsymbol{\hbar}_\mathrm{S}^T\}, \mathrm{Im}\{\boldsymbol{\hbar}_\mathrm{S}^T\}, \mathrm{Re}\{\boldsymbol{\hbar}_\mathrm{I}^T\}, \mathrm{Im}\{\boldsymbol{\hbar}_\mathrm{I}^T\}, \mathrm{Re}\{\mathbf{d}_{\mathrm{S,D}}^T\}, \mathrm{Im}\{\mathbf{d}_{\mathrm{S,D}}^T\}]^T$. Denote $\mathbf{U} = (\mathbf{I}_{N_\mathrm{s}} \otimes ((\mathbf{I}_{N_\mathrm{r}} \otimes \mathbf{E}_{\text{G-L+1}})\check{\mathbf{H}}_\mathrm{S}\mathbf{F}_\mathrm{all}))\mathbf{d}_\mathrm{S} + \sqrt{\frac{1}{\rho}}(\mathbf{I}_{N_\mathrm{s}} \otimes (\check{\mathbf{H}}_\mathrm{I}\mathbf{F}_\mathrm{all}))\mathbf{d}_\mathrm{I}$. According to [131], the FIM can be given by

$$\boldsymbol{\Pi} = \frac{2}{\sigma^2}\mathrm{Re}[\frac{\partial \mathbf{U}^H}{\partial \boldsymbol{\theta}}\frac{\partial \mathbf{U}}{\partial \boldsymbol{\theta}^T}], \tag{5.38}$$

where σ^2 is the noise variance. Through some derivations, the following two equations are obtained

$$\frac{\partial \mathbf{U}^H}{\partial \boldsymbol{\theta}} = [-\jmath\mathbf{Q}_{\phi}^H; \mathbf{Q}_{\boldsymbol{\hbar}_S}^H; -\jmath\mathbf{Q}_{\boldsymbol{\hbar}_S}^H; \mathbf{Q}_{\boldsymbol{\hbar}_I}^H; -\jmath\mathbf{Q}_{\boldsymbol{\hbar}_I}^H; \mathbf{Q}_{\mathbf{D}_{\mathrm{S,D}}}^H; -\jmath\mathbf{Q}_{D_{\mathrm{S,D}}}^H], \tag{5.39}$$

and

$$\frac{\partial \mathbf{U}}{\partial \boldsymbol{\theta}^T} = [\jmath\mathbf{Q}_{\phi}, \mathbf{Q}_{\boldsymbol{\hbar}_S}, \jmath\mathbf{Q}_{\boldsymbol{\hbar}_S}, \mathbf{Q}_{\boldsymbol{\hbar}_I}, \jmath\mathbf{Q}_{\boldsymbol{\hbar}_I}, \mathbf{Q}_{\mathbf{D}_{\mathrm{S,D}}}, \jmath\mathbf{Q}_{\mathbf{D}_{\mathrm{S,D}}}], \tag{5.40}$$

where $\mathbf{Q}_{\phi} = \frac{2\pi}{K}(\mathbf{I}_{N_{\mathrm{s}}} \otimes ((\mathbf{I}_{N_{\mathrm{r}}} \otimes (\mathbf{L}\mathbf{E}_{\text{G-L+1}}))\check{\mathbf{H}}_{\mathrm{S}}\mathbf{F}_{\mathrm{all}}))\mathbf{d}_{\mathrm{S}}$ with $\mathbf{L} = \mathrm{diag}\{[L-1, \cdots, G-1]\}$; $\mathbf{Q}_{\boldsymbol{\hbar}_S} = [\mathbf{Q}_{\boldsymbol{\hbar}_S,0,0}, \cdots, \mathbf{Q}_{\boldsymbol{\hbar}_S,0,N_{\mathrm{r}}-1}, \cdots, \mathbf{Q}_{\boldsymbol{\hbar}_S,L-1,0} \cdots, \mathbf{Q}_{\boldsymbol{\hbar},L-1,N_{\mathrm{r}}-1}]$ with $\mathbf{A}_{l,n_{\mathrm{r}}} = (\mathbf{I}_{N_{\mathrm{s}}} \otimes ((\mathbf{I}_{N_{\mathrm{r}}} \otimes \mathbf{E}_{\text{G-L+1}})\mathrm{circshift}(\mathbf{q}_l, (G-L+1)n_{\mathrm{r}}, 1)\mathbf{F}_{\mathrm{all}})\mathbf{d}_{\mathrm{S}}$, $\mathbf{q}_l = \mathrm{circshift}(\mathbf{q}_{\boldsymbol{\hbar}_S}, -l, 2)$, $\mathbf{q} = [\mathbf{q}^1; \mathbf{q}^2]$, $\mathbf{q}^1$ and $\mathbf{q}^2$ are respectively given by $\mathbf{q}^1 = \mathrm{toeplitz}(\mathbf{0}_{(G-L+1)\times 1}, [\mathbf{0}_{1\times(L-1)}, 1, \mathbf{0}_{1\times(G-L)}])$ and $\mathbf{q}^2 = \mathbf{0}_{(G-L+1)(N_{\mathrm{r}}-1)\times G}$; $\mathbf{B}$ is defined in a similar form to $\mathbf{A}$ but with $\mathbf{A}_{l,n_{\mathrm{r}}}$ replaced by $\mathbf{B}_{l,n_{\mathrm{r}}} = (\mathbf{I}_{N_{\mathrm{s}}} \otimes (\mathrm{circshift}(\mathbf{q}_l, (G-L+1)n_{\mathrm{r}}, 1)\mathbf{F}_{\mathrm{all}})\mathbf{d}_{\mathrm{I}}$; $\mathbf{Q}_{\mathbf{D}_{\mathrm{S,D}}} = [\mathbf{Q}_{D_{\mathrm{S,D}},0,0}, \cdots, \mathbf{Q}_{D_{\mathrm{S,D}},K-1,0}, \cdots, \mathbf{Q}_{D_{\mathrm{S,D}},0,N_{\mathrm{s}}-2}, \cdots, \mathbf{Q}_{D_{\mathrm{S,D}},K-1,N_{\mathrm{s}}-2}]$ with $\mathbf{Q}_{\mathrm{S,D},k,i} = (\mathbf{I}_{N_{\mathrm{s}}} \otimes ((\mathbf{I}_{N_{\mathrm{r}}} \otimes \mathbf{E}_{\text{G-L+1}})\check{\mathbf{H}}_{\mathrm{S}}\mathbf{F}_{\mathrm{all}}))$ $\mathrm{circshift}(\mathbf{q}_{\boldsymbol{d}_{\mathrm{S,D}},k}, iK, 1)$, $\mathbf{q}_{\mathbf{d}_{\mathrm{S,D}},k} = \mathrm{circshift}(\mathbf{q}_{\mathbf{d}_{\mathrm{S,D}}}, k, 1)$ and $\mathbf{q}_{\mathbf{d}_{\mathrm{S,D}}} = [\mathbf{0}_{K\times 1}; 1; \mathbf{0}_{((N_{\mathrm{s}}-1)K-1)\times 1}]$. Based on (5.38), (5.39) and (5.40), the FIM can be easily determined and is denoted as $\boldsymbol{\Pi}$.

The CRLBs can be obtained using the diagonal elements of $\boldsymbol{\chi} = \boldsymbol{\Pi}^{-1}$ [128, 131]. The CRLBs for CFO estimation, channel estimation (including both desired and SI channels) and signal detection are respectively given by

$$\mathrm{CRLB}_{\mathrm{CFO}} = \boldsymbol{\chi}(0,0), \tag{5.41}$$

$$\mathrm{CRLB}_{\mathrm{channel}} = \frac{1}{2N_{\mathrm{r}}L}\sum\nolimits_{p=1}^{4N_{\mathrm{r}}L} \boldsymbol{\chi}(p,p), \tag{5.42}$$

and

$$\mathrm{CRLB}_{\mathrm{signal}} = \frac{1}{N(N_{\mathrm{s}}-1)}\sum\nolimits_{p=1+4N_{\mathrm{r}}L}^{2N(N_{\mathrm{s}}-1)+4N_{\mathrm{r}}L} \boldsymbol{\chi}(p,p). \tag{5.43}$$

Moreover, the output SINR can be related to the MSE of signal detection by $\mathrm{SINR}_{\mathrm{out}} = 1/\mathrm{MSE}_{\mathrm{signal}} - 1$ in [132]. Since $\mathrm{MSE}_{\mathrm{signal}} \geq \mathrm{CRLB}_{\mathrm{signal}}$, the output SINR is bounded by

$$\mathrm{SINR}_{\mathrm{out}} \leq \frac{1}{\mathrm{CRLB}_{\mathrm{signal}}} - 1. \tag{5.44}$$

5.5.2 Complexity Analysis

Table 5.1: Number of complex multiplications and additions (K: Number of subcarriers in an OFDM symbol, L_{cp}: CP length, N_{s}: Frame length, N_{r}: Number of receive antennas, L: Channel length, $G = K + L_{\mathrm{cp}}$ and Λ: Number of iterations, est.: estimation, cancel.: cancellation and detec.: detection).

<table>
<tr><th>Item</th><th>ISB receiver</th><th>iCFO-HD [7]
+fCFO-HD [8]
+ML [104]</th><th>iCFO-HD [7]
+fCFO-HD [8]
+Subspace [110]</th></tr>
<tr><td>Channel
est.</td><td>$(2(K-L+1)N_{\mathrm{r}}N_{\mathrm{s}}(L_{\mathrm{cp}}+1)$
$+(K-L+1)^2N_{\mathrm{r}}^2+N_{\mathrm{r}}^2L^2K$
$+(22K-8)(L_{\mathrm{cp}}+1)$
$+4K(L_{\mathrm{cp}}+1)+16K^2$
$+8K^3)(K-L+1)N_{\mathrm{r}}+$
$(16N_{\mathrm{r}}^3L^2+4N_{\mathrm{r}}^2LN_{\mathrm{s}})$
$(G-L+1)(\Lambda-1)$</td><td>$8N_{\mathrm{r}}^3L^2KN_{\mathrm{s}}+$
$4N_{\mathrm{r}}^2LKN_{\mathrm{s}}$
$+8\Lambda N_{\mathrm{r}}^2KLN_{\mathrm{s}}(1$
$+N_{\mathrm{r}}K+N_{\mathrm{r}}L)$</td><td>$2N_{\mathrm{r}}^2G^2N_{\mathrm{s}}+$
$N_{\mathrm{r}}^3G^3+$
$KN_{\mathrm{r}}^2L^2$
$(N_{\mathrm{r}}G-2K)+$
$68N_{\mathrm{s}}K+20K$</td></tr>
<tr><td>iCFO est.</td><td rowspan="2">$5K^3\Lambda+4K^2L_{\mathrm{cp}}+2K^2$
$+(2KN_{\mathrm{s}}+1)N(L_{\mathrm{cp}}+1)(\Gamma-1)$</td><td colspan="2">$4K^3+5K^2N_{\mathrm{r}}^2$</td></tr>
<tr><td>fCFO est.</td><td colspan="2">$6N_{\mathrm{r}}^3K\log_2K$</td></tr>
<tr><td>SI cancel.</td><td>$2(G-L+1)GN_{\mathrm{s}}N_{\mathrm{r}}\Lambda$</td><td colspan="2">$2(G-L+1)GN_{\mathrm{s}}N_{\mathrm{r}}$</td></tr>
<tr><td>Signal
detec.</td><td>$\Lambda(2GN_{\mathrm{r}}(G-L+1)(2G+N_{\mathrm{s}})$
$+G^3+N_{\mathrm{s}}K\log_2K)$</td><td colspan="2">$2GN_{\mathrm{r}}(G-L+1)(2G+N_{\mathrm{s}})$
$+G^3+N_{\mathrm{s}}K\log_2K$</td></tr>
</table>

The symbolic computational complexities of the proposed ISB receiver structure and the existing methods [7, 8, 104, 110] are demonstrated in Table 5.1, in terms of the number of complex additions and multiplications. Due to lack of integral solutions to CFO estimation and channel estimation for FD systems in the literature, the ML iCFO estimator [7] and blind closed-form fCFO estimator [8] described in Subsection 3.3.2 for HD systems, referred to as iCFO-HD and fCFO-HD, are exploited for comparison in terms of iCFO and fCFO estimation, whereas the iterative ML [104] and subspace [110] methods, which are respectively the variants of decision-directed channel estimator in Subsection 3.2.2 and semi-blind joint channels and CFOs estimator in Subsection 3.3.2, are chosen as references for channel estimation and SI cancellation. Their complexities are compared in four aspects, namely channel estimation, CFO estimation, SI cancellation and signal detection. Regarding the proposed ISB receiver structure, the complexity of each aspect depends on the number of iterations, owing to its decision-directed estimation, while the channel estimation in [104] is iterative and the methods in [7, 8, 110] are all non-iterative. Moreover, it can be seen that the proposed ISB receiver structure provides an integral solution to iCFO and fCFO estimation, while the existing methods [7, 8] require two separate processes for iCFO and fCFO estimation, respectively. The signal detection algorithm in the proposed ISB receiver is shared by the reference receivers.

Table 5.2: Normalised numerical complexity ($K = 32$, $L_{\text{cp}} = 8$, $N_{\text{s}} = 20$, $N_{\text{r}} = 4$, $L = 2$ and $G = 40$. est.: estimation, cancel.: cancellation, detect.: detection.)

<table>
<tr><th rowspan="2">Item</th><th colspan="2">ISB receiver</th><th colspan="2">iCFO-HD [7] +fCFO-HD [8] +ML [104]</th><th colspan="2">iCFO-HD [7] +fCFO-HD [8] +Subspace [110]</th></tr>
<tr><th>$\Lambda = 1$</th><th>$\Lambda = 3$</th><th>$\Lambda = 1$</th><th>$\Lambda = 3$</th><th>$\Lambda = 1$</th><th>$\Lambda = 3$</th></tr>
<tr><td>Channel estimation</td><td>161</td><td>169</td><td>369</td><td>1063</td><td colspan="2">124</td></tr>
<tr><td>iCFO estimation</td><td rowspan="2">3</td><td rowspan="2">20</td><td colspan="4">4</td></tr>
<tr><td>fCFO estimation</td><td colspan="4">1</td></tr>
<tr><td>SI cancellation</td><td>4</td><td>12</td><td colspan="4">4</td></tr>
<tr><td>Signal detection</td><td>23</td><td>68</td><td colspan="4">23</td></tr>
<tr><td>Total</td><td>191</td><td>269</td><td>400</td><td>1094</td><td colspan="2">155</td></tr>
</table>

Based on the symbolic complexity analysis, a numerical complexity analysis is provided in Table 5.2 using the parameter settings in Subsection 5.6.1, where all complexities are normalised to the lowest complexity of all items, which is the complexity of the fCFO-HD estimator in [8]. The following observations can be made from Table 5.2.

First, it can be seen that channel estimation dominates the overall complexity of all receivers. The ML [104] based channel estimation has the highest complexity. With a single iteration, the complexity of the proposed ISB receiver structure is approximately half of that of the ML method [104] and is also comparable to that of the subspace method [110]. As the number of iterations is increased to 3, the complexity of the proposed ISB receiver structure is around six-times less than that of the ML approach [104].

Second, the complexity of channel estimation in the proposed ISB receiver increases slower than that of the ML method [104] with the increase of the number of iterations, reflected by a complexity increase of 5% versus 200% as the number of iterations increases from 1 to 3. This is because regarding the proposed ISB receiver structure, the subspace-based blind channel estimation at the initial stage plays a dominant role in complexity, which requires a large number of computations for auto-correlation matrix, EVD, etc, while the complexity of the ML method in [104] is high to solve the ML function and proportional to the number of iterations.

5.6 Simulation Results

5.6.1 Simulation Setup

Monte Carlo simulations have been carried out to demonstrate the performance of the proposed ISB receiver structure for URLLC in a short-frame FD CP-OFDM system with CFO. As mentioned in Subsection 5.5.2, channel estimation methods based on ML [104] and subspace [110], and the CFO estimation methods of iCFO-HD [7] and fCFO-HD [8], are chosen for comparison. The signal detection algorithm in the proposed ISB receiver is shared by the reference receivers. The derived CRLBs in Subsection 5.5.1 are also used as benchmarks. Each frame contains $N_\mathrm{s} = 20$ OFDM symbols of $K = 32$ subcarriers, except for Fig. 5.6, where the frame length is a variable. The CP length is $L_\mathrm{cp} = 8$. QPSK modulation is assumed. A two-ray channel model of length $L = 2$ is used. The CFO is randomly generated, whose iCFO is in the range of $[-K/2, K/2)$ and fCFO is in the range of $[-0.5, 0.5)$, except for Fig. 5.8. The number of receive antennas is $N_\mathrm{r} = 4$, except for Fig. 5.9. The average SIR ρ before the digital SI cancellation is set to -20 dB. The first OFDM symbol within a frame is used as pilot for joint CFO estimation and channel ambiguities elimination. Up to 10000 channel realisations are used to meet the requirement of Monte Carlo simulations.

Other specific simulation setups in [7, 8, 104] and [110] are adopted. One symbol are used for iCFO estimation in iCFO-HD [7] and two symbols each with a null subcarrier are used for fCFO estimation in fCFO-HD [8]. As for channel estimation, 50% of a symbol is used by the subspace method [110] and 6.25% of each symbol by the ML method [104]. With a short frame length of $N_{\mathrm{s}} = 20$, the overall training overheads of the proposed ISB receiver, the receiver with [104]+ [7]+ [8] and the receiver with [110]+ [7]+ [8] are 5%, 11% and 8%, respectively.

The MSEs of channel and fCFO estimation for the λ-th iteration are respectively defined as

$$\mathrm{MSE}^{(\lambda)}_{\mathrm{Channel}} = \mathbb{E}\{\frac{1}{2N_{\mathrm{r}}L}[(\hat{\boldsymbol{\hbar}}^{(\lambda)}_{\mathrm{S}} - \boldsymbol{\hbar}_{\mathrm{S}})^2 + (\hat{\boldsymbol{\hbar}}^{(\lambda)}_{\mathrm{I}} - \boldsymbol{\hbar}_{\mathrm{I}})^2]\}, \tag{5.45}$$

and

$$\mathrm{MSE}^{(\lambda)}_{\mathrm{fCFO}} = \mathbb{E}\{(\hat{\phi}^{(\lambda)}_{\mathrm{F}} - \phi_{\mathrm{F}})^2\}. \tag{5.46}$$

The output SINR is defined as the ratio of the power of the desired signal estimate to the power of the residual SI and noise after SI cancelation, *i.e.*,

$$\mathrm{SINR}^{(\lambda)}_{\mathrm{output}} = \frac{\sum_{i=1}^{N_{\mathrm{s}}-1}\sum_{k=0}^{K-1}\hat{\mathbf{d}}^{(\lambda)}_{\mathrm{S},i}(k)}{\sum_{i=1}^{N_{\mathrm{s}}-1}\sum_{k=0}^{K-1}(\mathbf{d}_{\mathrm{S},i}(k) - \hat{\mathbf{d}}^{(\lambda)}_{\mathrm{S},i}(k))}. \tag{5.47}$$

5.6.2 Results and Discussion

Figs. 5.3, 5.4 and 5.5 demonstrate respectively the FER, output SINR and MSE of channel estimation performances of the proposed ISB receiver structure in comparison to the ML [104] and subspace [110] methods with $N_{\mathrm{s}} = 20$ symbols per frame and $N_{\mathrm{r}} = 4$ receive antennas. The proposed ISB receiver in the presence of CFO achieves much better FER performance than that of ML [104] and subspace [110] approaches with perfect CFO estimation, while the latter two demonstrates an error floor. This is because the ISB receiver can calculate the second-order statistics of the received signal with a short frame of data, while [104] and [110] are dependent on long data frames.

Similar trends to Fig. 5.3 can be observed in Fig. 5.4, where the output SINR by the proposed ISB receiver is much closer to the CRLB after iterations. In contrast, the output SINR by the ML approach [104] degrades slightly with the increase of SNR, because of the noise amplifications from iterations.

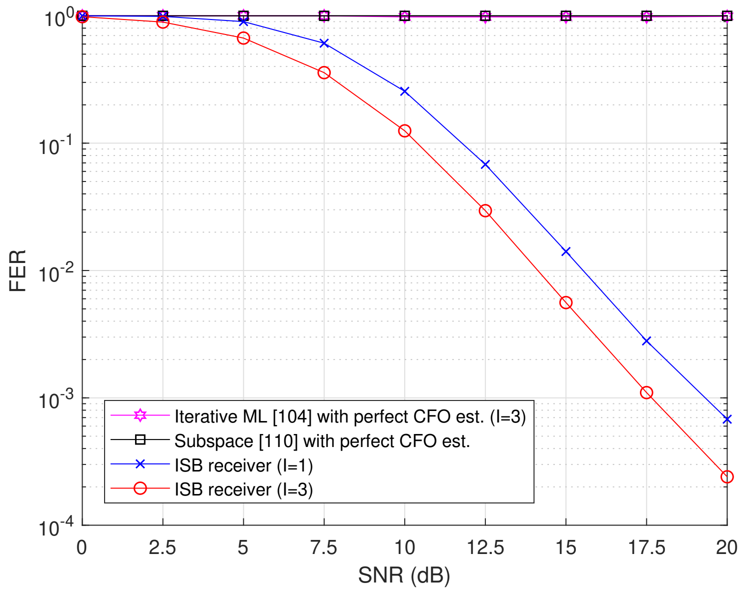

Figure 5.3: FER performance of the proposed ISB receiver structure, with $N_s = 20$ symbols per frame and $N_r = 4$ receive antennas (est.: estimation).

Fig. 5.5 demonstrates that at the MSE of channel estimation of 10^{-4}, the proposed ISB receiver with $\Lambda = 3$ iterations achieves an SNR gain of around 7 dB over its counterpart with one iteration. The CRLB is close to the numerical results of the ISB receiver, while ML [104] and subspace [110] demonstrate poor channel estimation accuracy across all SNRs.

Fig. 5.6 shows the impact of the frame length N_s on the MSE performance of channel estimation of the proposed ISB receiver and the existing ML [104] and subspace [110] methods at SNR=20 dB. It is easily observed that the proposed ISB receiver can achieve a good MSE performance while using a much shorter frame than the existing methods [104,110]. For example, the proposed ISB receiver with three iterations can achieve MSE of 10^{-3} with 10 symbols only, while more than 100 symbols are required for the existing methods [104, 110]. This is because the number of signal samples to compute the auto-correlation matrix of the received signal is increased by the proposed ISB receiver, as discussed in Subsection 5.3.1. Thus, it can achieve a similar performance while with a much fewer symbols. Furthermore, as the frame length increases, the training overhead

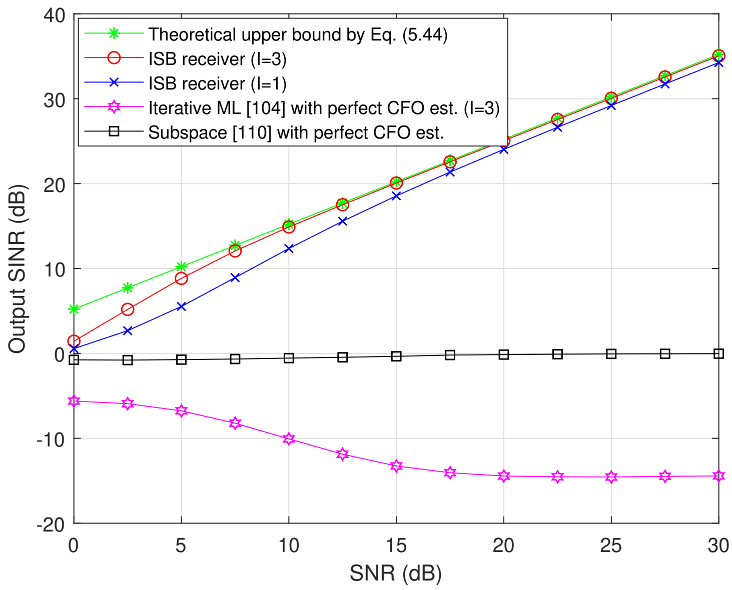

Figure 5.4: Output SINR of the proposed ISB receiver structure, with $N_{\mathrm{s}} = 20$ symbols per frame and $N_{\mathrm{r}} = 4$ receive antennas.

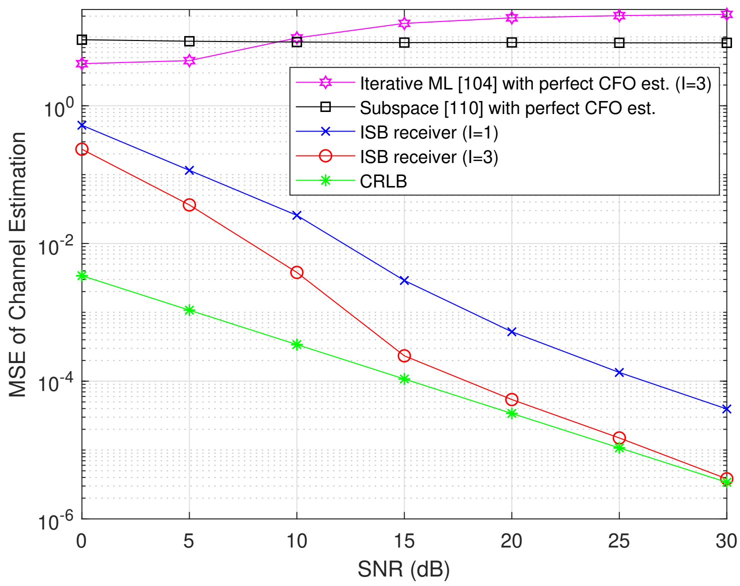

Figure 5.5: MSE of channel estimation of the proposed ISB receiver structure, with $N_{\mathrm{s}} = 20$ symbols per frame and $N_{\mathrm{r}} = 4$ receive antennas.

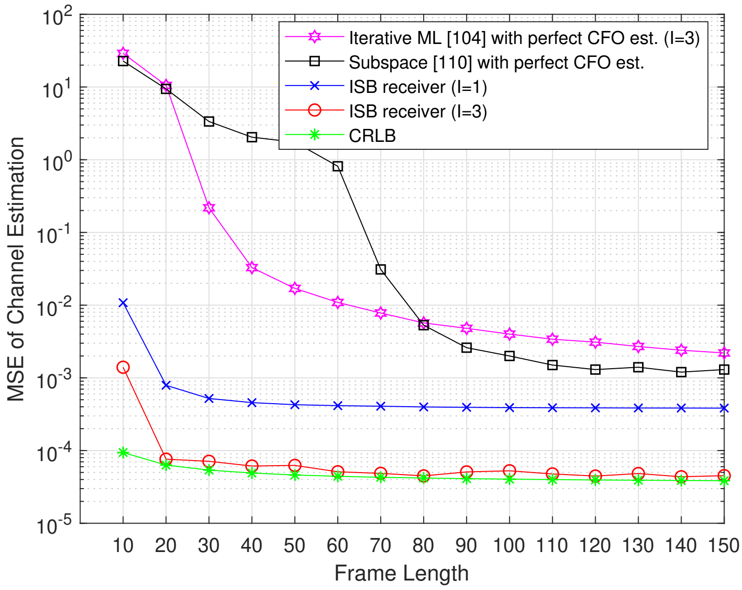

Figure 5.6: Impact of the frame length on the MSE of channel estimation of the proposed ISB receiver structure, with $N_{\mathrm{r}} = 4$ receive antennas and SNR=20 dB.

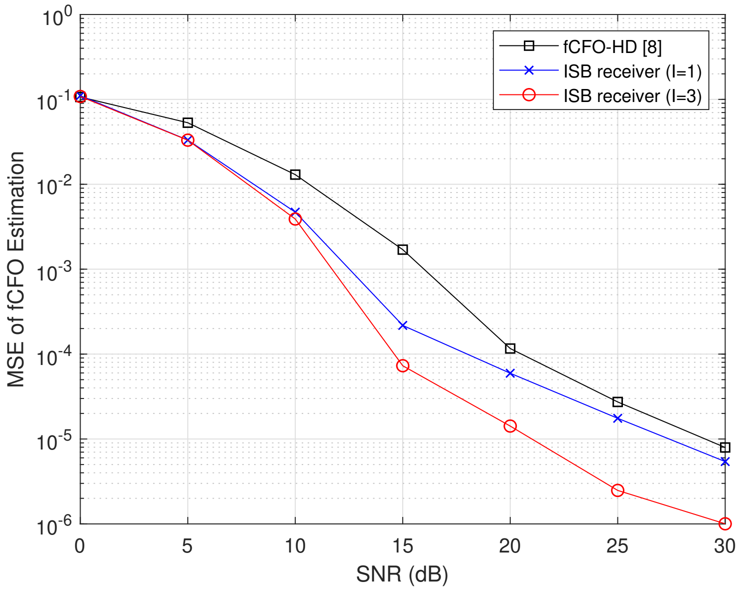

Figure 5.7: MSE of fCFO estimation of the proposed ISB receiver structure, with $N_{\mathrm{s}} = 20$ symbols per frame and $N_{\mathrm{r}} = 4$ receive antennas.

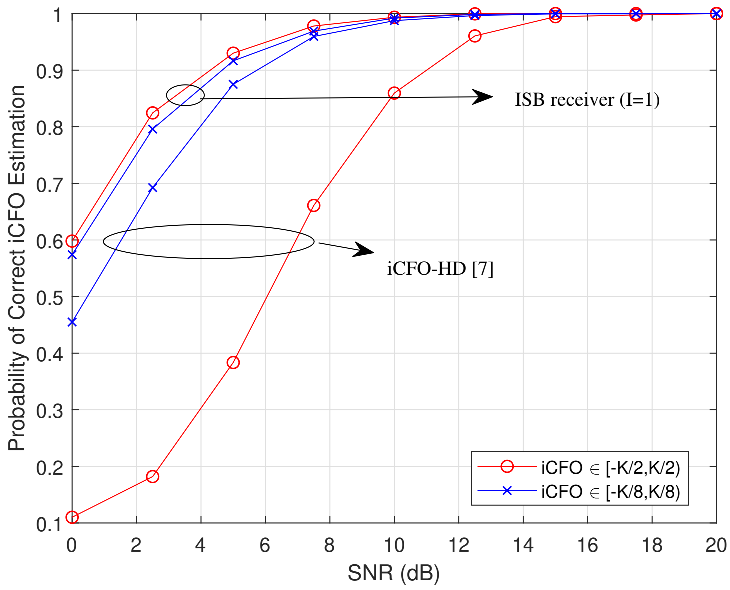

Figure 5.8: Impact of the iCFO estimation range on the probability of correct iCFO estimation of the proposed ISB receiver structure, with $N_\mathrm{s} = 20$ symbols per frame and $N_\mathrm{r} = 4$ receive antennas.

of the proposed ISB receiver decreases greatly. For example, at $N_\mathrm{s} = 150$, the training overhead of the proposed ISB receiver is reduced to 0.6% while that of the iterative ML method [104] is always 6.25%. Consequently, the proposed ISB receiver has advantages in both latency and spectral efficiency. Additionally, thanks to the decision-directed estimation in the proposed ISB receiver, the MSE of channel estimation is reduced by approximately ten-fold after three iterations and also approaches the derived CRLB. It is seen that the proposed ISB receiver achieves a convergence after $N_\mathrm{s} = 20$. This is why the frame length is specified as 20 for the proposed ISB receiver in other figures.

To better compare the proposed ISB receiver with the existing iCFO-HD [7] and fCFO-HD [8] estimators, the CFO estimation performance of the proposed ISB receiver is studied through two aspects: a) MSE of fCFO estimation and b) probability of correct iCFO estimation. Fig. 5.7 exhibits the MSE of fCFO estimation of the proposed ISB receiver, in comparison to the existing method [8]. It can be seen that the proposed ISB receiver with a single iteration is slightly better than fCFO-HD [8]. However, after three

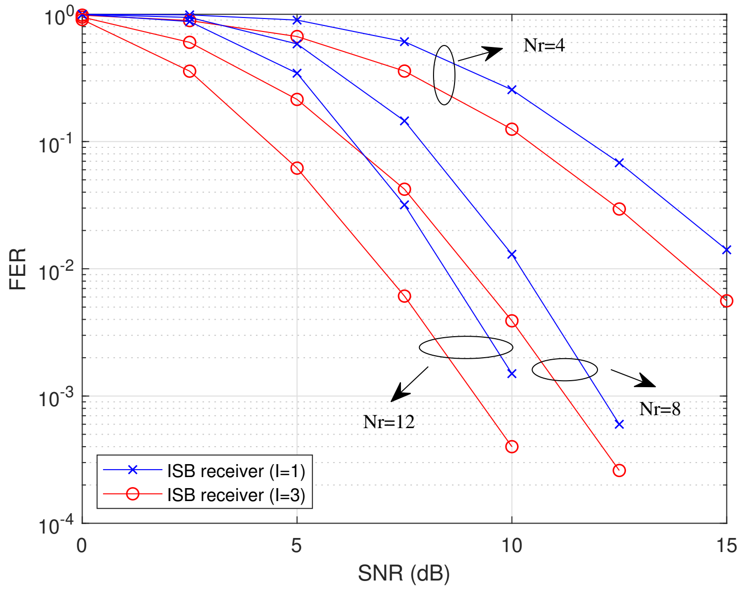

Figure 5.9: Impact of the number of receive antennas N_r on the FER performance of the proposed ISB receiver structure, with $N_s = 20$ symbols per frame.

iterations, the proposed ISB receiver demonstrates a much better performance than the existing fCFO-HD [8] especially at high SNRs. For instance, at $\text{MSE}_{\text{fCFO}} = 10^{-5}$, the proposed ISB receiver has an SNR gain of around 9 dB over the fCFO-HD [8] estimator.

The probability of correct iCFO estimation of the proposed ISB receiver and the existing iCFO-HD estimator [7] is studied in Fig. 5.8, with two iCFO estimation ranges $[-K/2, K/2)$ and $[-K/8, K/8)$. It is noteworthy that the existing iCFO estimator [7] allows a certain iCFO estimation range only which is determined by its algorithm parameter as discussed in Subsection 3.3.2. Also, the estimation range should be known in advance for the following iCFO search. In contrast, the proposed ISB receiver not only enables full-range iCFO estimation but also provides a closed-form solution without an advanced acquisition of iCFO estimation range. It is easily observed from Fig. 5.8 that the existing iCFO estimator [7] is susceptible to iCFO estimation range, while the proposed ISB receiver is almost independent of that. Specifically, the probability of correct iCFO estimation decreases greatly as the estimation range widens especially at low SNRs for the iCFO-HD estimator [7]. As mentioned in Subsection 5.4.2, decision-

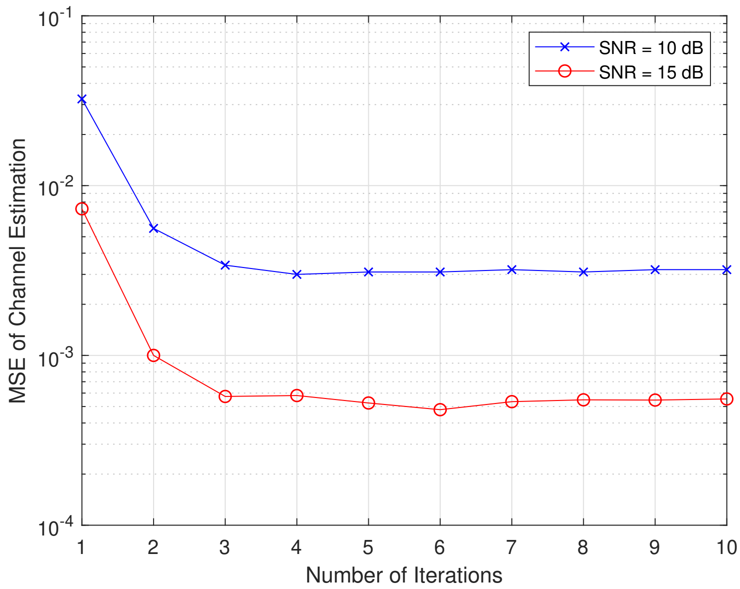

Figure 5.10: Impact of the number of iterations on the MSE of channel estimation of the proposed ISB receiver structure at SNR=10 dB and SNR=15 dB, with $N_\mathrm{s} = 20$ symbols per frame and $N_\mathrm{r} = 4$ receive antennas.

directed CFO estimation refines fCFO only, the probability of iCFO estimation tends not to vary with the number of iterations. Thus, the proposed ISB receiver with a single iteration is illustrated in Fig. 5.8.

Fig. 5.9 shows the impact of receive antennas on FER performance of the proposed ISB receiver, with $N_\mathrm{r} = 4$, $N_\mathrm{r} = 8$ and $N_\mathrm{r} = 12$, respectively. It can be concluded that the reliability of the proposed ISB receiver can be enhanced significantly by utilising more antennas at the receiver. Thus, space diversity is an effective technique for URLLC, as suggested in [33].

Fig. 5.10 demonstrates the MSE of channel estimation against the number of iterations of the proposed ISB receiver at SNR=10 dB and SNR=15 dB, respectively. It can be observed that the proposed receiver converges fast within 3 iterations. At SNR=15 dB, the initial MSE performance is improved around 10-fold after three iterations.

5.7 Summary

An ISB receiver structure with CFO and channel estimation and signal detection has been proposed for URLLC in short-frame FD CP-OFDM systems. Table 5.3 makes a comparison of the proposed ISB receiver structure with the existing approaches [7, 8, 104, 110]. Compared to the approaches in [7, 8, 104] and [110], the proposed ISB receiver achieves much better performance in short-frame case with tens of symbols at almost a halved training overhead, in terms of FER, MSEs of channel estimation and fCFO estimation, probability of correct iCFO estimation and output SINR. In addition, thanks to the decision-directed estimation, the CRLBs derived are close to the numerical results, while at the cost of medium complexity due to the iterative semi-blind estimation. The proposed receiver converges within 3 iterations, and is more computationally efficient than the iterative ML approach [104]. However, multiple receive antennas are demanded for the proposed ISB receiver to guarantee the blind channel estimation, making it infeasible for SISO systems. The re-modulation technique on the received signal in [128] would be a possible way to reduce the number of receive antennas for the proposed ISB receiver.

Table 5.3: Comparison of the proposed ISB receiver and the existing approaches.

Item	ISB Receiver	iCFO-HD [7]	fCFO-HD [8]	ML [104]	Subspace [110]
Duplex mode	FD	HD	HD	FD	FD
Decision-directed estimation	✓	✗	✗	✓	✗
iCFO estimation	✓	✓	✗	✗	✗
fCFO estimation	✓	✗	✓	✗	✗
Channel estimation	✓	✗	✗	✓	✓
Training overhead	Low	High	Low	High	Medium
Number of symbols for semi-blind estimation	Tens	N/A	N/A	Hundreds	Hundreds
Complexity	Medium	Medium	Low	High	Medium
Receive antennas	Multiple	Multiple	Multiple	Single/ Multiple	Multiple

Chapter 6

Robust Semi-Blind Estimation of Channel and CFO for Single-User GFDM Systems

Estimation of channel and CFO has been studied for OFDM systems in Chapters 4 and 5. In this chapter, a robust semi-blind estimation scheme of channel and CFO is proposed for single-user GFDM systems. This, to the best of the author's knowledge, is the first work to propose an integral solution to channel and full-range CFO for a wide range of GFDM systems. Based on the derived equivalent system model with CFO included implicitly, a subspace-based method is proposed to perform initial channel estimation blindly. Then, CFO estimation and channel ambiguity elimination are undertaken in series by utilising a small number of nulls and pilots in a single subsymbol. fCFO is first determined by means of rank-reduction criterion, whereas iCFO estimation is then solved by minimising the signal power on the null subcarriers in the designed subsymbol. Both channel and CFO estimations are more robust against ICI and ISI caused by the nonorthogonal filters of GFDM, compared to the existing LS based channel estimator and the variant of Moose's CFO estimator [107] described in Chapter 3. The proposed scheme achieves a BER performance close to the ideal case with perfect CFO and channel estimations especially at medium and high SNRs.

6.1 Introduction

GFDM, a generalised form of OFDM, has been considered as a potential waveform candidate for B5G wireless communications [2, 3, 9–11, 109, 133–139]. However, GFDM suffers from ICI and ISI caused by its nonorthogonal prototype filters, which makes its channel estimation and CFO estimation more challenging than those in OFDM, and the solutions for OFDM [7, 12, 128] cannot be applied directly.

Channel estimation for GFDM systems has been studied in [9, 133–136] assuming perfect CFO estimation. Scattered-pilot aided channel estimation was presented in [133], where the interference was pre-cancelled at the transmitter. However, its performance was vulnerable to frequency selective fading. LS channel estimation with a rectangular-pattern pilot was shown to outperform that with a block-pattern pilot in [9]. However, they required high training overhead and were biased due to ICI and ISI. By properly localising the pilots in time domain and utilising the pilots' information from CP, an LMMSE based parallel ICI and ISI cancellation method was proposed for channel estimation in GFDM [140], where two subsymbols are utilised as pilots and the CP length should be the same as the subsymbol length, giving rise to reduced spectral efficiency. The prototype filters in [134–136] were modified to enable the interference-free pilot aided channel estimation, which however worked only for specific GFDM systems.

GFDM is sensitive to CFO, including an iCFO and a fCFO [7, 137]. Most previous work on CFO estimation for GFDM systems have focused on fCFO only [3, 11, 109]. A pseudo noise (PN) based pilot with two identical subsymbols was utilised to estimate fCFO in [3] and [11], which is a variant of Moose's CFO estimator [107] in Subsection 3.3.2. However, it required high training overhead and was sensitive to ICI and ISI. As mentioned in Chapter 3, fCFO was blindly estimated for GFDM utilising CP and ML approach in [3] and [109]. However, their fCFO estimation range was limited. The work that has considered iCFO estimation was [138], however, it was applicable to a specific GFDM system only and its performance degraded substantially in the multi-path fading channel. A pilot containing two similar Zaduff-Chu sequences was utilised to achieve low-complexity full-range CFO estimation in [141], with just a specific frequency spreading GFDM transmitter structure in [50].

The aforementioned work [3, 9, 11, 109, 133–136, 138] dealt with either channel estimation or CFO estimation, without considering their effect on each other. In [139], both estimations were considered, which however focused on small-scale CFO and was applicable only for unique-word (UW) GFDM systems. Semi-blind joint estimation of channels and CFOs for ZP-OFDM systems were presented in [12] as demonstrated in Subsection 3.3.2, which however cannot be utilised for CP-GFDM systems.

In this chapter, a robust semi-blind channel and CFO estimation (RSCCE) scheme is proposed for single-user GFDM systems. Based on the derived equivalent system model with CFO included implicitly, a subspace-based method is proposed to perform initial channel estimation blindly, and then full-range CFO estimation and channel ambiguity elimination are undertaken in series by utilising a small number of nulls and pilots in a single subsymbol only. fCFO estimation is first performed by exploiting the rank-reduction criterion due to null subcarriers, while iCFO is estimated by minimising the power on the null subcarriers of the designed subsymbol. This work is different in the following aspects.

- This, to the best of the author's knowledge, is the first attempt to propose an integral solution to channel estimation and CFO estimation for GFDM, considering their effect on each other, while in [3, 9, 11, 109, 133–138] only one of the issues was addressed assuming perfect estimation of the other.

- The proposed RSCCE scheme is applicable to a wide range of GFDM systems and allows full-range CFO estimation, while the previous work either was applicable to specific GFDM systems such as interference-free GFDM in [134–136] and UW-GFDM in [139] or considered CFO estimation in a limited range only [3, 11, 109, 139].

- The proposed RSCCE scheme achieves a BER performance close to the ideal case with perfect channel and CFO estimations especially from medium to high SNRs. Both channel and CFO estimations are more robust against ICI and ISI caused by the nonorthogonal filters of GFDM than the existing methods [3,9,11], thanks to the subspace-based initial channel estimation and the ICI and ISI mitigation in subsequent CFO estimation and channel ambiguity elimination.

- The proposed semi-blind scheme utilises a small number of nulls and pilots in a single subsymbol to enable CFO estimation and channel ambiguity elimination respectively, with much lower training overhead than that required in [3, 9, 11]. Also, the proposed blind channel estimation algorithm achieves the second order statistics of the received signal with only a small number of received symbols, about tens of times less than that required in [12] and [128].

The rest of this chapter is organised as follows. Section 6.2 presents the system model. The proposed RSCCE scheme is described in Section 6.3. Complexity analysis and simulation results are given in Sections 6.4 and 6.5, respectively. Section 6.6 draws conclusion.

6.2 System Model

6.2.1 GFDM System with CFO

A SIMO GFDM system with a single user is considered where the receiver is equipped with N_r receive antennas. Each GFDM symbol is divided into M subsymbols each with K subcarriers and define $N = KM$. Let $\mathbf{d}_i = [d_{i,0,0}, \cdots, d_{i,0,K-1}, \cdots, d_{i,M-1,0}, \cdots, d_{i,M-1,K-1}]^T$ denote the data vector of the i-th GFDM symbol, where $d_{i,m,k}$ is the data transmitted on the k-th subcarrier in the m-th subsymbol of the i-th symbol. Then, each $d_{i,m,k}$ is transmitted with the corresponding pulse shape [2]

$$g_{m,k}[n] = g[(n - mK) \bmod N] \cdot \exp(-\jmath 2\pi kn/K), \tag{6.1}$$

where n $(n = 0, \cdots, N-1)$ is the sampling index. After pulse shaping, the transmit symbol $\epsilon_i[n]$ is given by

$$\epsilon_i[n] = \sum\nolimits_{k=0}^{K-1} \sum\nolimits_{m=0}^{M-1} g_{m,k}[n] d_{i,m,k}. \tag{6.2}$$

Denote $\boldsymbol{\epsilon}_i = [\epsilon_i[0], \cdots, \epsilon_i[N-1]]^T$ as the transmit data vector, which is expressed as

$$\boldsymbol{\epsilon}_i = \mathbf{A}\mathbf{d}_i, \tag{6.3}$$

where $\mathbf{A} = [\mathbf{g}_{0,0}, \cdots, \mathbf{g}_{0,K-1}, \cdots, \mathbf{g}_{M-1,0}, \cdots, \mathbf{g}_{M-1,K-1}]$ is an $N \times N$ pulse shaping filter matrix with $\mathbf{g}_{m,k} = [g_{m,k}[0], \cdots, g_{m,k}[N-1]]^T$. A single CP with length L_{cp} is prepended to the GFDM symbol $\mathbf{x}_i$, obtaining $\mathbf{x}_i = [x_i[0], \cdots, x_i[L_{\mathrm{cp}}-1], x_i[L_{\mathrm{cp}}], \cdots, x_i[G-1]]^T = [\epsilon_i[N-L_{\mathrm{cp}}], \cdots, \epsilon_i[N-1], \epsilon_i[0], \cdots, \epsilon_i[N-1]]^T$, with $G = N + L_{\mathrm{cp}}$.

The channel is assumed to exhibit quasi-static block fading and CIR remains constant for a frame of N_{s} GFDM symbols. Denote $\boldsymbol{\hbar}_{n_{\mathrm{r}}} = [\hbar_{n_{\mathrm{r}}}[0], \cdots, \hbar_{n_{\mathrm{r}}}[L-1]]^T$ as the CIR for the n_{r}-th receive antenna with L being the length of CIR. $\phi = \phi_{\mathrm{F}} + \phi_{\mathrm{I}}$ $(\phi \in [-K/2, K/2))$ is defined as the CFO between the transmitter and receiver, where ϕ_{F} and ϕ_{I} are respectively the fCFO and iCFO. The time-domain received signal in the i-th symbol at the n_{r}-th receive antenna is written as

$$y_{i,n_{\mathrm{r}}}[g] = e^{\jmath 2\pi\phi g/K} \sum\nolimits_{l=0}^{L-1} \hbar_{n_{\mathrm{r}}}[l]\epsilon_i[g-l] + w_{i,n_r}[g], \tag{6.4}$$

where $w_{i,n_r}[g]$ $(g = 0, \cdots, G-1)$ is the noise term.

6.2.2 Equivalent System Model with CFO Included Implicitly

To enable robust semi-blind estimation of channel and CFO, an equivalent system model similar to that in Chapter 5 is derived, which includes CFO in the transmitted signal and channel implicitly. By incorporating CFO into the transmitted signal and channel, (6.4) is equivalent to

$$y_{i,n_\mathrm{r}}[g] = \sum\nolimits_{l=0}^{L-1} h_{n_\mathrm{r}}[l] s_i[g-l] + w_{i,n_r}[g], \tag{6.5}$$

with $h_{n_\mathrm{r}}[l] = e^{\jmath 2\pi\phi l/K} \hbar_{n_\mathrm{r}}[l]$ and $s_i[g] = e^{\jmath 2\pi\phi g/K} x_i[g]$ denoted as the CFO-included channel and CFO-included transmitted signal. Similar to Chapter 5, $y_{i,n_\mathrm{r}}[L-1]$ to $y_{i,n_\mathrm{r}}[L_\mathrm{cp}-1]$ are free from ISI caused by multi-path fading, and thus are utilised alongside signal samples $y_{i,n_\mathrm{r}}[L_\mathrm{cp}]$ to $y_{i,n_\mathrm{r}}[G-1]$ for semi-blind estimation of CFO and channel. Collecting all these samples from N_r receive antennas into a vector, $\mathbf{y}_i = [y_{i,0}[L-1], \cdots, y_{i,N_\mathrm{r}-1}[L-1], \cdots, y_{i,0}[G-1], \cdots, y_{i,N_\mathrm{r}-1}[G-1]]^T$ is obtained and given by

$$\mathbf{y}_i = \mathbf{H}\mathbf{s}_i + \mathbf{w}_i, \tag{6.6}$$

where $\mathbf{H}$ of size $(G-L+1)N_\mathrm{r} \times G$ is defined as

$$\mathbf{H} = \begin{bmatrix} \mathbf{h}(L-1) & \cdots & \mathbf{h}(0) & \cdots & \cdots & \mathbf{0}_{N_\mathrm{r}\times 1} \\ \vdots & \ddots & \ddots & \ddots & \ddots & \vdots \\ \mathbf{0}_{N_\mathrm{r}\times 1} & \cdots & \cdots & \mathbf{h}(L-1) & \cdots & \mathbf{h}(0) \end{bmatrix}, \tag{6.7}$$

with $\mathbf{h}(l) = [h_0[l], \cdots, h_{N_\mathrm{r}-1}[l]]^T$, $\mathbf{s}_i = [s_i[0], s_i[1], \cdots, s_i[G-1]]^T$, and $\mathbf{w}_i = [w_{i,0}[L-1], \cdots, w_{i,N_\mathrm{r}-1}[L-1], \cdots, w_{i,0}[G-1], \cdots, w_{i,N_\mathrm{r}-1}[G-1]]^T$.

Since $\mathbb{E}\{\mathbf{s}_i\mathbf{s}_i^H\}$ is rank deficient whose rank is N instead of G due to the redundancy from CP, (6.6) cannot be applied to the subspace-based blind channel estimation approach. To address this problem, the consecutive $(N-L+1)N_\mathrm{r}$ samples from $\mathbf{y}_i$ are collected as a subvector, and it is easily found that $(L_\mathrm{cp}+1)$ such subvectors can be formed. The t-th ($t = 0, 1, \cdots, L_\mathrm{cp}$) subvector is denoted as $\mathbf{y}_i^t = [y_{i,0}[L-1+t], \cdots, y_{i,N_\mathrm{r}-1}[L-1+t], \cdots, y_{i,0}[N-1+t], \cdots, y_{i,N_\mathrm{r}-1}[N-1+t]]^T$, which is written as

$$\mathbf{y}_i^t = \tilde{\mathbf{H}}\mathbf{s}_i^t + \mathbf{w}_i^t, \quad t = 0, \cdots, L_\mathrm{cp}, \tag{6.8}$$

where $\tilde{\mathbf{H}}$ follows the similar form to $\mathbf{H}$ but with a reduced size of $(N-L+1)N_\mathrm{r} \times N$;

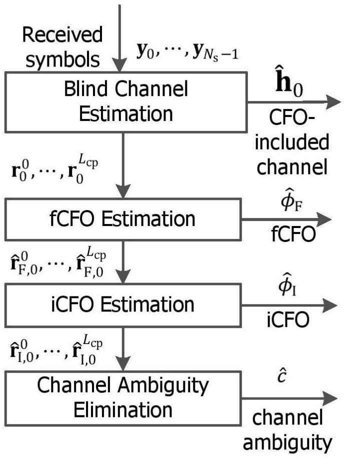

Figure 6.1: Flow chart of the proposed RSCCE scheme for GFDM systems.

$\mathbf{s}_i^t = [s_i[t], \cdots, s_i[N-1+t]]^T$; and $\mathbf{w}_i^t = [w_{i,0}[L-1+t], \cdots, w_{i,N_r-1}[L-1+t], \cdots, w_{i,0}[N-1+t], \cdots, w_{i,N_r-1}[N-1+t]]^T$.

6.3 Robust Semi-Blind Channel and CFO Estimation

Based on the derived equivalent system model in (6.8), an RSCCE scheme is proposed for GFDM systems in the presence of CFO, which mainly consists of three stages, as shown in Fig. 6.1: a) subspace-based blind channel estimation is performed in the presence of CFO; b) both fCFO and iCFO in the full range are estimated; c) channel ambiguity due to blind estimation in stage a) is eliminated. The processes at stages b) and c) are semi-blind, which respectively utilise a small number of nulls and a small number of pilots in a single subsymbol, as illustrated in Fig. 6.2.

6.3.1 Blind Channel Estimation

A subspace-based blind channel estimator similar to that in Chapter 5 is proposed to enable the robust estimation of the CFO-included channel in (6.8). It is assumed that 1) noise samples are uncorrelated and 2) noise and signal samples are uncorrelated. N_r receive antennas with $(N-L+1)N_r > N$ are utilised, which suggests $N_r > 1$. The proposed estimator is summarised in four steps below.

Step 1. $(N_\mathrm{s}-1)$ received symbols are used to compute the auto-correlation matrix of the received signal, obtaining

$$\mathbf{R}_{\mathbf{yy}} = \frac{1}{(N_\mathrm{s}-1)(L_\mathrm{cp}+1)} \sum\nolimits_{i=1}^{N_\mathrm{s}-1} \sum\nolimits_{t=0}^{L_\mathrm{cp}} \mathbf{y}_i^t (\mathbf{y}_i^t)^H. \tag{6.9}$$

Note that the number of signal samples per received symbol utilised to compute the auto-correlation matrix of the received signal has been increased, thanks to the partition of the received signal vector $\mathbf{y}_i$ into a number of subvectors $\mathbf{y}_i^t$ when deriving the equivalent system model. Thereby, the required number of received symbols to achieve the second order statistics of the received signal can be much smaller than the methods in OFDM [12, 128].

Step 2. EVD is performed on the auto-correlation matrix $\mathbf{R}_{\mathbf{yy}}$. The signal subspace has a dimension of N, regardless of the GFDM nonorthogonal filters. Consequently, the noise subspace has Q $(Q = (N-L+1)N_\mathrm{r} - N)$ eigenvectors corresponding to the smallest Q eigenvalues of the matrix $\mathbf{R}_{\mathbf{yy}}$. Denote the q-th eigenvector as $\boldsymbol{\gamma}_q = [\boldsymbol{\gamma}_q^T(0), \cdots, \boldsymbol{\gamma}_q^T(N-L)]^T$ $(q = 0, \cdots, Q-1)$, where $\boldsymbol{\gamma}_q(\omega)$ $(\omega = 0, 1, \cdots, N-L)$ is a column vector of size N_r. Due to the inherent orthogonality between the signal and noise subspaces, the columns of $\tilde{\mathbf{H}}$ are orthogonal to each vector $\boldsymbol{\gamma}_q$, *i.e.*,

$$\boldsymbol{\gamma}_q^H \tilde{\mathbf{H}} = \mathbf{0}_{1\times N}. \tag{6.10}$$

Therefore, $\boldsymbol{\gamma}_q$ spans the left null space of $\tilde{\mathbf{H}}$. As $\tilde{\mathbf{H}}$ is formulated by the matrices $\mathbf{h}(l)$, channel estimation is restricted to $\mathbf{h}(l)$, instead of the whole matrix $\tilde{\mathbf{H}}$.

Step 3. Similar to Chapter 5, $\boldsymbol{\iota}_q \mathbf{h} = \mathbf{0}_{N\times 1}$ can be obtained where $\boldsymbol{\iota}_q$ of size $N \times N_\mathrm{r}L$

is defined as

$$\boldsymbol{\iota}_q = \begin{bmatrix} \boldsymbol{\gamma}_q^H(N-L) & \mathbf{0}_{1\times N_\mathrm{r}} & \cdots & \mathbf{0}_{1\times N_\mathrm{r}} \\ \boldsymbol{\gamma}_q^H(N-L-1) & \boldsymbol{\gamma}_q^H(N-L) & \cdots & \mathbf{0}_{1\times N_\mathrm{r}} \\ \vdots & \vdots & \ddots & \vdots \\ \boldsymbol{\gamma}_q^H(N-2L+1) & \boldsymbol{\gamma}_q^H(N-2L+2) & \cdots & \boldsymbol{\gamma}_q^H(N-L) \\ \boldsymbol{\gamma}_q^H(N-2L) & \boldsymbol{\gamma}_q^H(N-2L+1) & \cdots & \boldsymbol{\gamma}_q^H(N-L-1) \\ \vdots & \vdots & \ddots & \vdots \\ \boldsymbol{\gamma}_q^H(0) & \boldsymbol{\gamma}_q^H(1) & \cdots & \boldsymbol{\gamma}_q^H(L-1) \\ \mathbf{0}_{1\times N_\mathrm{r}} & \boldsymbol{\gamma}_q^H(0) & \cdots & \boldsymbol{\gamma}_q^H(L-2) \\ \vdots & \vdots & \ddots & \vdots \\ \mathbf{0}_{1\times N_\mathrm{r}} & \mathbf{0}_{1\times N_\mathrm{r}} & \cdots & \boldsymbol{\gamma}_q(0) \end{bmatrix}, \tag{6.11}$$

where $\mathbf{h} = [\mathbf{h}^T(0), \cdots, \mathbf{h}^T(L-1)]^T$ is with size $N_\mathrm{r}L \times 1$.

Step 4. Considering all $\boldsymbol{\iota}_q$ matrices as follows $\boldsymbol{\iota} = [\boldsymbol{\iota}_0^T, \cdots, \boldsymbol{\iota}_{Q-1}^T]^T$,

$$\boldsymbol{\iota}\mathbf{h} = \mathbf{0}_{NQ\times 1} \tag{6.12}$$

is obtained. Hence, the CFO-included channel $\mathbf{h}$ can be estimated by choosing the right singular vectors of $\boldsymbol{\iota}$, denoted as $\hat{\mathbf{h}}_0$. However, there exists a complex scalar ambiguity c between the real CFO-included channel $\mathbf{h}$ and the blindly estimated CFO-included channel $\hat{\mathbf{h}}_0$, *i.e.*, $\mathbf{h} = \hat{\mathbf{h}}_0 c$.

It is noteworthy that the blind estimate of the CFO-included channel is robust against the ICI and ISI introduced by the nonorthogonal filters, as the proposed scheme is based on the inherent orthogonality between the signal and noise subspaces and their dimensions are not changed by the nonorthogonal filters. With the blind channel estimate, (6.8) can be rewritten as

$$\mathbf{y}_i^t = \tilde{\mathbf{H}}_0\mathbf{C}\mathbf{s}_i^t + \mathbf{w}_i^t, \tag{6.13}$$

Figure 6.2: Example of the first GFDM symbol structure: $P_{\text{pil,cfo}} = 2$ nulls and $P_{\text{pil,cha}} = 2$ pilots within the first subsymbol are utilised for CFO estimation and channel ambiguity elimination, respectively.

where $\tilde{\mathbf{H}}_0$ is defined as the same form to $\tilde{\mathbf{H}}$ but with $\mathbf{h}(l)$ replaced by $\hat{\mathbf{h}}_0(l)$ and $\mathbf{C} = \text{diag}\{[c, \cdots, c]\}$ is with size $N \times N$. By performing equalisation, the received signal $\mathbf{y}_i^t$ is multiplied with the pseudoinverse of $\tilde{\mathbf{H}}_0$, obtaining

$$\mathbf{r}_i^t = \mathbf{C}\mathbf{s}_i^t + \tilde{\mathbf{w}}_i^t, \tag{6.14}$$

where $\tilde{\mathbf{w}}_{i,t} = \tilde{\mathbf{H}}_0^{\dagger}\mathbf{w}_i^t$. (6.14) is easily rewritten as

$$\mathbf{r}_i^t = \mathbf{E}_{\text{N}}^t(\phi)\mathbf{A}^t\mathbf{C}\mathbf{d}_i + \bar{\mathbf{w}}_i^t, \tag{6.15}$$

where $\mathbf{A}^t = \mathbf{A}_{\text{cp}}(t\colon N-1+t, :\,)$ with $\mathbf{A}_{\text{cp}} = [\mathbf{A}^T(N - L_{\text{cp}} : N-1, 1 : N), \mathbf{A}^T]^T$ and $\mathbf{E}_{\text{N}}^t(\phi) = \text{diag}\{[e^{\jmath 2\pi\phi t/K}, \cdots, e^{\jmath 2\pi\phi(t+N-1)/K}]\}$. It is noteworthy that (6.15) looks like a GFDM system in the presence of flat-fading channel so that CFO estimation problem is much easier to solve, allowing the robust estimation of both fCFO and iCFO in the full range in the following.

6.3.2 First Subsymbol Design

Based on (6.15), CFO estimation and channel ambiguity elimination can be achieved by designing a single subsymbol of the first received symbol with a small number of nulls and pilots. Assuming its first subsymbol is utilised for training, $P_{\text{pil,cfo}}$ and $P_{\text{pil,cha}}$ ($P_{\text{pil,cfo}} + P_{\text{pil,cha}} \leq K$) subcarriers within it are transmitted as nulls and pilots to enable

CFO estimation and channel ambiguity elimination, respectively. Note that in theory the values of $P_{\text{pil,cfo}}$ and $P_{\text{pil,cha}}$ can be as small as 1. Denote $\mathbb{P}_{\text{pil,cfo}}$ and $\mathbb{P}_{\text{pil,cha}}$ as the respective subcarrier index set for CFO estimation and channel ambiguity elimination. Fig. 6.2 provides a general example for the first symbol design with $P_{\text{pil,cfo}} = 2$ and $P_{\text{pil,cha}} = 2$.

6.3.3 CFO Estimation

After performing equalisation with the blind channel estimate, both fCFO and iCFO in the full range can be easily estimated by utilising the designed first subsymbol with a small number of nulls. By eliminating interference through zero-forcing (ZF) algorithm, both fCFO and iCFO estimations are resilient against the ICI and ISI introduced by the GFDM nonorthogonal filters.

fCFO Estimation

fCFO estimation is based on the rank-reduction criterion. In the absence of fCFO ($\phi_{\text{F}} = 0$), the rank of $\text{diag}\{(\mathbf{A}^t)^{\dagger}\mathbf{r}_0^t\}$ should be $(N - P_{\text{pil,cfo}})$, due to the null subcarriers. This property is true even in the presence of iCFO, since iCFO is likely to induce the cyclic shift and would not change its rank. However, if fCFO exists ($\phi_{\text{F}} \neq 0$), this property is destroyed and the rank becomes N due to the fCFO-induced ICI.

Given a largest fCFO search range $[-0.5, 0.5)$, fCFO is compensated with a fCFO trial value of $\tilde{\phi}_{\text{F}}$ on $\mathbf{r}_0^t$, yielding $\boldsymbol{\kappa}_{\text{F}}^t(\tilde{\phi}_{\text{F}}) = \mathbf{E}_{\text{N}}^t(-\tilde{\phi}_{\text{F}})\mathbf{r}_0^t$. Therefore, with a good fCFO trial, the rank of $\tilde{\boldsymbol{\kappa}}_{\text{F}}^t(\tilde{\phi}_{\text{F}}) = \text{diag}\{(\mathbf{A}^t)^{\dagger}\boldsymbol{\kappa}_{\text{F}}^t(\tilde{\phi}_{\text{F}})\}$ should be $(N - P_{\text{pil,cfo}})$. fCFO is determined as follows.

Step 1. Compute the auto-correlation matrix of $\tilde{\boldsymbol{\kappa}}_{\text{F}}^t(\tilde{\phi}_{\text{F}})$, yielding

$$\mathbf{R}^{\boldsymbol{\kappa}\boldsymbol{\kappa}}(\tilde{\phi}_{\text{F}}) = \frac{1}{L_{\text{cp}} + 1} \sum_{t=0}^{L_{\text{cp}}} \tilde{\boldsymbol{\kappa}}_{\text{F}}^t(\tilde{\phi}_{\text{F}})(\tilde{\boldsymbol{\kappa}}_{\text{F}}^t(\tilde{\phi}_{\text{F}}))^H. \tag{6.16}$$

Step 2. Perform EVD on $\mathbf{R}^{\boldsymbol{\kappa}\boldsymbol{\kappa}}(\tilde{\phi}_{\text{F}})$, and the eigenvalue vector in an ascending order is determined as $\boldsymbol{\eta}^{\tilde{\phi}_{\mathrm{F}}}$.

Step 3. fCFO is estimated by

$$\hat{\phi}_{\mathrm{F}} = \arg \min_{\tilde{\phi}_{\mathrm{F}} \in [-0.5, 0.5)} \parallel \boldsymbol{\eta}^{\tilde{\phi}_{\mathrm{F}}}(1 : P_{\mathrm{pil,cfo}}) \parallel_{\mathrm{F}}^{2} . \tag{6.17}$$

fCFO compensation is then performed, yielding $\hat{\mathbf{r}}_{\mathrm{F},0}^{t} = \mathbf{E}_{\mathrm{N}}^{t}(-\hat{\phi}_{\mathrm{F}})\mathbf{r}_{0}^{t}$. Note that ZF algorithm has been performed on the received signal (*i.e.*, $(\mathbf{A}^{t})^{\dagger}\mathbf{r}_{0}^{t}$), allowing the elimination of ICI and ISI from the nonorthogonal filter, assuming the filter matrix $\mathbf{A}$ is well-conditioned and its inverse exists [2]. Similarly, ZF is executed to the following iCFO estimation and channel ambiguity elimination to remove the ICI and ISI.

iCFO Estimation

The core idea of iCFO estimation is to minimise the signal power on the null subcarriers in the designed subsymbol. Given that iCFO is absent ($\phi_{\mathrm{I}} = 0$), the signal power of $(\mathbf{A}^{t})^{\dagger}\hat{\mathbf{r}}_{\mathrm{F},0}^{t}$ on the specific null subcarriers should be zero. However, this is not true if iCFO exists ($\phi_{\mathrm{I}} \neq 0$).

Given a largest iCFO search range $[-K/2, K/2)$ and an iCFO trial value $\tilde{\phi}_{\mathrm{I}}$, an iCFO compensated $\hat{\mathbf{r}}_{\mathrm{F},0}^{t}$ is obtained as $\boldsymbol{\kappa}_{\mathrm{I}}^{t}(\tilde{\phi}_{\mathrm{I}}) = \mathbf{E}_{\mathrm{N}}^{t}(-\tilde{\phi}_{\mathrm{I}})\hat{\mathbf{r}}_{\mathrm{F},0}^{t}$. ZF algorithm is then implemented, obtaining $\tilde{\boldsymbol{\kappa}}_{\mathrm{I}}^{t,\tilde{\phi}_{\mathrm{I}}} = \mathbf{A}_{t}^{\dagger}\boldsymbol{\kappa}_{\mathrm{I}}^{t}(\tilde{\phi}_{\mathrm{I}})$. Therefore, iCFO is determined by

$$\hat{\phi}_{\mathrm{I}} = \arg \min_{\tilde{\phi}_{\mathrm{I}} \in [-\frac{K}{2}, \frac{K}{2})} \sum\nolimits_{t=0}^{L_{\mathrm{cp}}} \sum\nolimits_{k \in \mathbb{P}_{\mathrm{pil,cfo}}} \parallel \tilde{\boldsymbol{\kappa}}_{\mathrm{I}}^{t,\tilde{\phi}_{\mathrm{I}}}(k) \parallel_{\mathrm{F}}^{2} . \tag{6.18}$$

iCFO is then compensated, yielding $\hat{\mathbf{r}}_{\mathrm{I},0}^{t} = \mathbf{E}_{\mathrm{N}}^{t}(-\hat{\phi}_{\mathrm{I}})\hat{\mathbf{r}}_{\mathrm{F},0}^{t}$. The integral CFO is estimated by $\hat{\phi} = \hat{\phi}_{\mathrm{I}} + \hat{\phi}_{\mathrm{F}}$.

6.3.4 Channel Ambiguity Elimination

After performing ZF algorithm, $\hat{\mathbf{d}}_0^t = (\mathbf{A}^t)^\dagger \hat{\mathbf{r}}_{\mathrm{I},0}^t$ is obtained. With a small number of pilots in a single subsymbol, the complex channel ambiguity is computed by

$$\hat{c} = \frac{1}{P_{\mathrm{pil,cha}}(L_{\mathrm{cp}}+1)} \sum_{t=0}^{L_{\mathrm{cp}}} \sum_{k \in \mathbb{P}_{\mathrm{pil,cha}}} \frac{\hat{\mathbf{d}}_0^t(k)}{\mathbf{d}_0(k)}. \tag{6.19}$$

The CFO-included channel is then estimated as $\hat{\mathbf{h}} = \hat{c}\hat{\mathbf{h}}_0$. Hence, the channel ambiguity due to blind estimation has been eliminated.

According to (6.15), the transmitted signal is easily detected by ZF algorithm

$$\hat{\mathbf{d}}_i^t = (\mathbf{A}^t \hat{\mathbf{C}})^\dagger \mathbf{E}_{\mathrm{N}}^t(-\hat{\phi}) \mathbf{r}_i^t, \tag{6.20}$$

where $\hat{\mathbf{C}} = \mathrm{diag}\{[\hat{c}, \cdots, \hat{c}]\}$. Then, the averaged signal estimate is $\hat{\mathbf{d}}_i = \frac{1}{L_{\mathrm{cp}}+1} \sum_{t=0}^{L_{\mathrm{cp}}} \hat{\mathbf{d}}_i^t$.

It is worth noticing that ZF algorithm has been performed on the received signal in the above estimations, which is able to eliminate the ICI and ISI introduced by the nonorthogonal filters [2] for both CFO estimation and channel ambiguity elimination. Meanwhile, the blind channel estimate is regardless of the nonorthogonal filters and is not affected by its introduced ICI and ISI as discussed previously. Hence, the proposed scheme with semi-blind estimation of both channel and CFO are more robust against the ICI and ISI caused by the nonorthogonal filters than the existing methods [3, 9, 11].

Table 6.1: Analytical computational complexity (K: Number of subcarriers per GFDM subsymbol, M: Number of subsymbols per GFDM symbol, N_{s}: Number of symbols in a frame, L: Channel length, N_{r}: Number of receive antennas, N: $N = KM$, $P_{\mathrm{pil,cfo}}$: Number of subcarriers used for CFO estimation, $P_{\mathrm{pil,cha}}$: Number of subcarriers used for channel scalar ambiguity estimation, L_{cp}: CP length and δ: fCFO search step size.)

Item	RSCCE scheme
Blind channel estimation	$2(N-L+1)^2 N_{\mathrm{r}}^2 N_{\mathrm{s}}(L_{\mathrm{cp}}+1) - N_{\mathrm{r}}^2 L^2 N^2$ $+N_{\mathrm{r}}^3 L^2 N(N-L+1) + (N-L+1)^3 N_{\mathrm{r}}^3$
fCFO estimation	$(4N^2(L_{\mathrm{cp}}+1) + N^3 + 2P_{\mathrm{pil,cfo}})(\frac{1}{\delta}+1)$
iCFO estimation	$2(N^2 + P_{\mathrm{pil,cfo}})(L_{\mathrm{cp}}+1)(K+1)$
Channel ambiguity elimination	$P_{\mathrm{pil,cha}}(L_{\mathrm{cp}}+1)$

6.4 Complexity Analysis

In Table 6.1, the computational complexity of the proposed RSCCE scheme is presented, in terms of the number of complex additions and multiplications. They are summarised into four aspects, namely blind channel estimation, fCFO estimation, iCFO estimation and channel ambiguity elimination. Regarding channel estimation, the proposed subspace-based blind channel estimation dominates the whole complexity, resulting from the computations of the auto-correlation matrix of the received signal, EVD and etc. The complexity for channel ambiguity elimination can be negligible. Both fCFO and iCFO estimation may suffer high complexity due to the exhaustive fCFO and iCFO searches. For instance, the complexity of fCFO estimation is inversely proportional to fCFO search step size δ. Moreover, iCFO estimation is likely to have a lower complexity than fCFO estimation, since iCFO has a search step size of 1.

6.5 Simulation Results

Simulation results are used to demonstrate the performance of the proposed RSCCE scheme for GFDM systems. System parameters are set as follows. Each GFDM symbol contains $M = 3$ subsymbols each with $K = 16$ subcarriers. The number of receive antennas is $N_{\mathrm{r}} = 4$. The CP length is $L_{\mathrm{cp}} = 4$. The channel model follows an exponential profile with channel length $L = 3$. $N_{\mathrm{s}} = 30$ received symbols are used for semi-blind estimation, except for Fig. 6.6. The CFO value is randomly generated in $[-K/2, K/2)$. The first subsymbol of the first GFDM symbol is used for training where $P_{\mathrm{pil,cfo}} = 12$ and $p_{\mathrm{Pil,cha}} = 4$ are exploited for CFO estimation and channel ambiguity elimination, respectively, except for Fig. 6.7. The fCFO search step size is $\delta = 0.001$; root raised cosine prototype filter with roll-off coefficient 0.5 is utilised for GFDM except for Fig. 6.5. QPSK scheme is used. The MSEs of channel and fCFO estimation are defined as

$$\mathrm{MSE}_{\mathrm{channel}} = \frac{1}{N_{\mathrm{r}}L}\mathbb{E}\{||\hat{\mathbf{h}} - \mathbf{h}||_{\mathrm{F}}^{2}\}, \tag{6.21}$$

and

$$\mathrm{MSE}_{\mathrm{fCFO}} = \mathbb{E}\{(\hat{\phi} - \phi)^2\}. \tag{6.22}$$

It is noteworthy that the CRLBs on semi-blind channel and CFO estimation for GFDM can be derived easily in a similar manner to that for FD OFDM in Chapter 5. Since the key contribution of this work lies in the high-robustness estimation of channel and CFO in GFDM systems, the following simulation results are mainly utilised to verify the superiority of the proposed RSCCE scheme in terms of the robustness against ICI and ISI, and the corresponding CRLBs are not included yet. As a complement, the BER performance in the ideal case with the perfect estimation of channel and CFO is adopted as a benchmark for the overall system performance.

Fig. 6.3 illustrates the BER performance of the proposed RSCCE scheme in comparison to the methods in [3, 9, 10] and [11]. Due to the lack of iCFO estimation approach for general GFDM systems in the literature, for fair comparison, the iCFO estimation approach in the proposed RSCCE scheme is performed with the existing methods for general GFDM systems including fCFO estimation in [3] and [11], channel estimation in [9] and ZF based signal detection in [10]. They are arranged into three groups, namely g1: CP [3]+LS [9]+ZF [10], g2: PN [3,11]+LS [9]+ZF [10] and g3: ZF [10] with perfect CFO and channel estimations. Note that g1 and g2 have 1 and 3 subsymbols in total for training, while the proposed RSCCE scheme needs a single subsymbol only. The proposed RSCCE scheme has a much superior BER performance to the existing methods g1 and g2, and its BER also approaches the ideal case with perfect CFO and channel estimations at receiver as SNR increases. Due to the biased fCFO and channel estimation resulting from ICI and ISI as will be seen in Figs. 6.4 and 6.5, the existing methods g1 and g2 suffer error floors as well in BER.

Fig. 6.4 shows the MSE performance of fCFO estimation by the proposed scheme, in comparison to the methods in [3] and [11]. The existing CP [3] and PN [3, 11] based algorithms are selected. The fCFO estimation range of CP based algorithm is $[-0.5/M, 0.5/M)$. When $M = 3$, its possible fCFO estimation range is $[-0.17, 0.17)$.

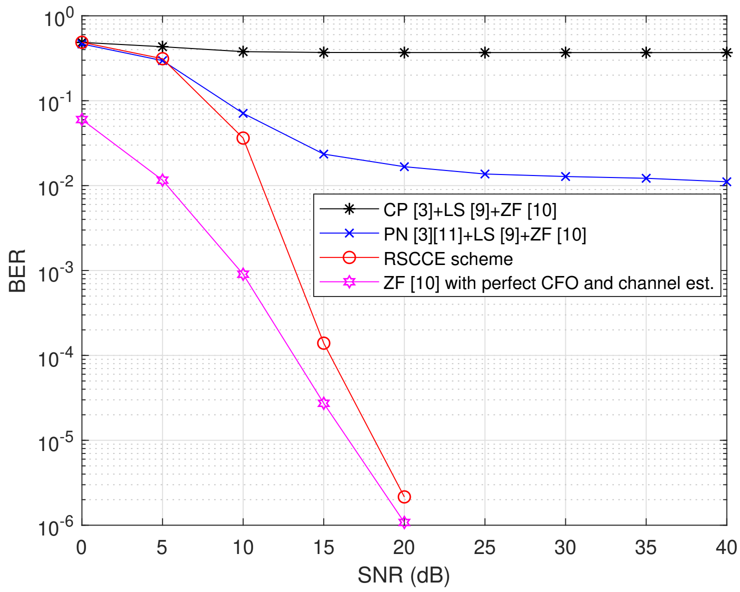

Figure 6.3: BER performance of the proposed RSCCE scheme and the existing methods [3, 9–11] (est.: estimation).

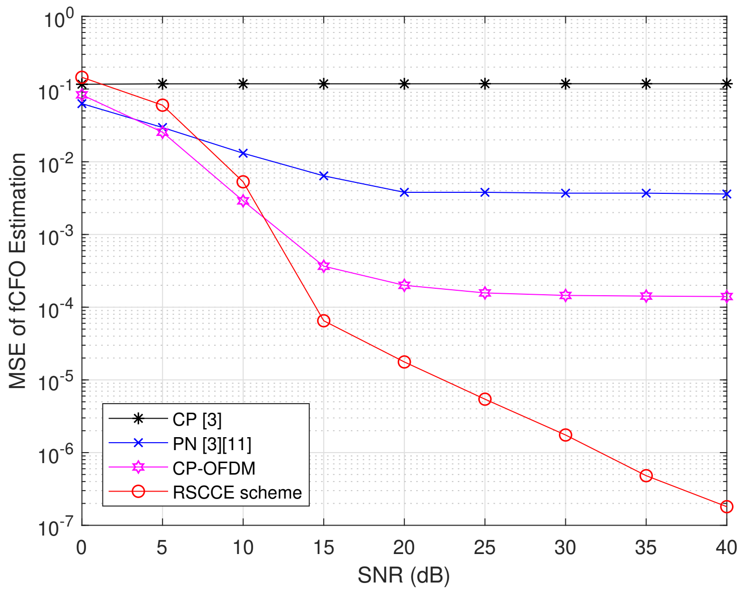

Figure 6.4: MSE performance of fCFO estimation of the proposed RSCCE scheme and the existing CP and PN based methods [3, 11].

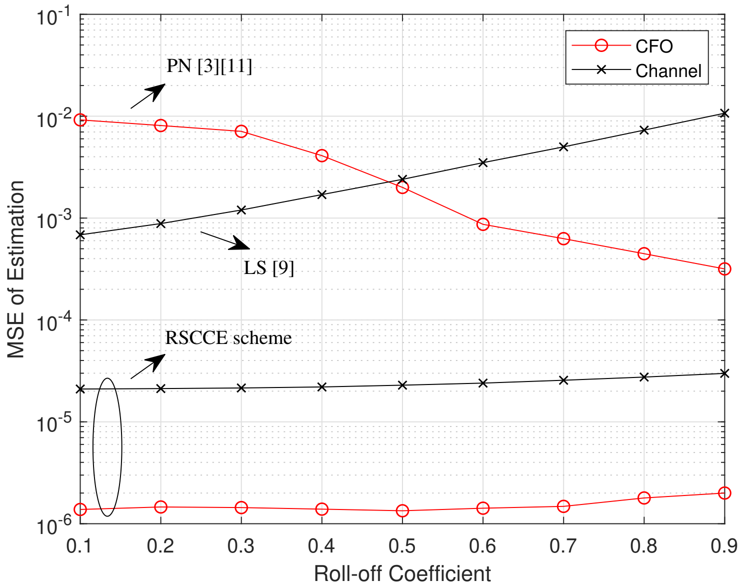

Figure 6.5: MSE performance of fCFO and channel estimation of the proposed RSCCE scheme and the existing PN and LS based methods [3,9,11] versus the roll-off coefficient at SNR=30 dB.

Thus, its performance is the worst and an error floor is formed for GFDM systems with $M = 3$ and fCFO of $[-0.5, 0.5)$ in Fig. 6.4. Instead, the CP based algorithm has a good performance for OFDM systems and however also biased at high SNRs due to the multi-path fading. Regarding PN based method [3, 11], the first two identical subsymbols are utilised as pilots to determine the fCFO by exploring their phase shift relationship. Nevertheless, owing to the ICI and ISI from the nonorthogonal filter, its performance with about two-fold training overhead over the proposed scheme is poor as well. The proposed RSCCE scheme outperforms the existing methods [3, 11] significantly especially from medium to high SNRs and do not suffer any error floors induced by the ICI and ISI.

Fig. 6.5 investigates the impact of the roll-off coefficient of the nonorthogonal filter on the MSE performances of fCFO and channel estimation of the proposed scheme and the existing methods [3,9,11] at SNR=30 dB. To avoid the impact from CFO estimation when studying channel estimation, it is assumed that CFO has been compensated perfectly. A single subsymbol of the first GFDM block is considered as pilots for channel estimation in LS based method [9], while the proposed scheme only utilises its quarter for channel estimation. By utilising the subspace method in the initial blind channel estimation and considering interference mitigation in the following CFO estimation and channel ambiguity elimination, the proposed scheme is shown to be more robust against the roll-off coefficient than the existing methods [3, 9, 11] in terms of both fCFO and channel estimation. The existing methods [3, 9, 11] suffer ICI and ISI and their performances are susceptible to the nonorthogonal filter matrix $\mathbf{A}$ which changes with the roll-off coefficient. The existing fCFO estimator [3, 11] has a decreasing MSE as the roll-off coefficient increases, because a larger roll-off coefficient could reduce the power difference between the received two identical subsymbols. In contrast, the LS channel estimator [9] tends to perform worse at a larger roll-off coefficient, owing to the noise enhancement. For a trade-off between channel and fCFO estimation for the existing methods [3, 9, 11], the roll-off coefficient is specified as 0.5 in Figs. 6.3, 6.4, 6.6 and 6.7.

Fig. 6.6 shows the MSE of channel estimation of the proposed RSCCE scheme and the existing method in OFDM [12] versus the number of received symbols N_{s} at SNR=15 dB and SNR=20 dB, respectively. To the best of the author's knowledge, there is no semi-blind channel estimation method for GFDM systems in the literature. The existing semi-blind joint channels and CFOs estimator [12] for OFDM described in Subsection 3.3.2, referred to as SB-OFDM here, is chosen for comparison with the proposed scheme. It is observed that $N_{\mathrm{s}} = 30$ symbols are sufficient to output a good performance for the proposed scheme, thanks to the increased number of signal samples per received symbol to compute the auto-correlation matrix of the received signal as discussed in Subsection 6.3.1. In contrast, more than 200 symbols are required for the SB-OFDM method in OFDM systems [12].

Fig. 6.7 demonstrates the probability of correct iCFO estimation of the proposed RSCCE scheme and the existing method in [7]. Since full-range iCFO estimation technique for general GFDM systems is lacking in the literature, the existing ML based iCFO estimator for OFDM [7] described in Subsection 3.3.2 is chosen for comparison,

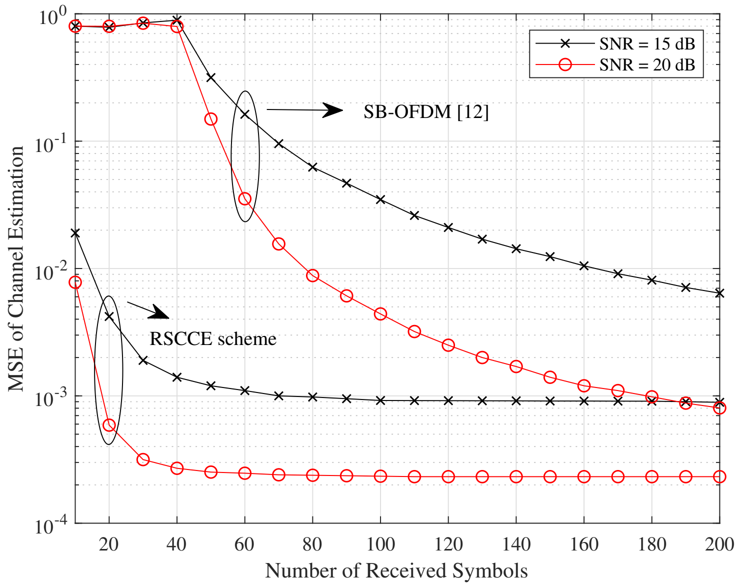

Figure 6.6: MSE performance of channel estimation of the proposed RSCCE scheme and the existing SB-OFDM method [12] versus the number of received symbols N_s at SNR=15 dB and SNR=20 dB.

referred to as iCFO-OFDM. The proposed scheme with $P_{\text{pil,cfo}} = 14$ is shown to have a higher iCFO detection probability than a symbol aided iCFO estimator [7] in OFDM systems which do not suffer from ICI and ISI introduced in GFDM systems. For example, at SNR=8 dB, the iCFO detection probability of the existing method [7] is enhanced approximately 17% by the proposed RSCCE scheme.

6.6 Summary

A semi-blind integral solution to channel and CFO estimation has been proposed for a wide range of GFDM systems, which enables high-accuracy channel estimation based on the second order statistics of tens of the received symbols and high-accuracy estimation of iCFO and fCFO in the full range, with a small number of subcarriers within a single subsymbol for training. Table 6.2 compares the proposed RSCCE scheme with the previous approaches [3,9–12]. With much higher spectrum efficiency, the proposed semi-

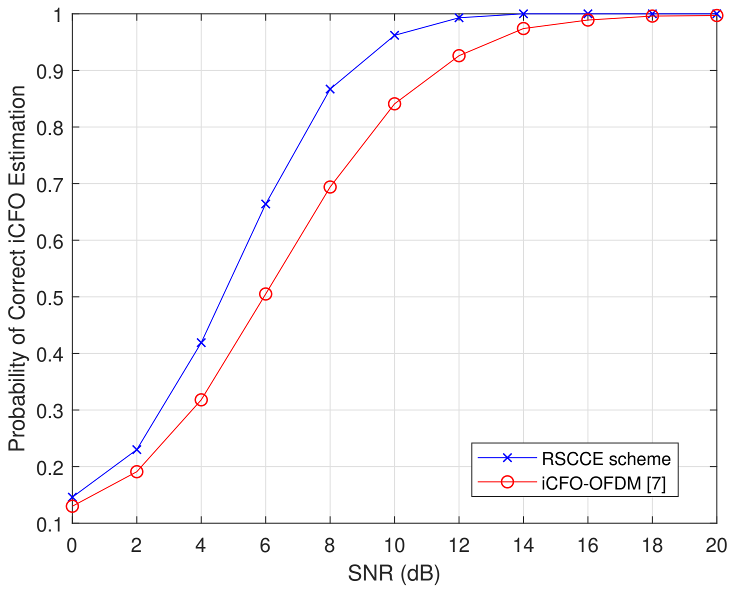

Figure 6.7: Probability of correct iCFO estimation of the proposed RSCCE scheme and the pilot aided approach for OFDM [7].

blind scheme not only outperforms the existing methods [3,9–11] in terms of both CFO and channel estimation performance, but also achieves a BER performance close to the ideal case with perfect CFO and channel estimations at receiver especially at medium and high SNRs. It is more robust against ICI and ISI resulted from the nonorthogonal filters than the previous methods [3, 9, 11].

However, the proposed RSCCE scheme suffers high computational complexity, due to the blind channel estimation as well as the exhaustive search for fCFO and iCFO, respectively. The closed-form solution similarly to that in [8] is hard to provide for the semi-blind CFO estimation in GFDM, since its cost function has multiple minimums. A possible attempt to reduce the computational complexity of the proposed RSCCE scheme is to estimate the fractional part of CFO with two stages: coarse fCFO estimation and fine fCFO estimation. For instance in [142], a large fCFO search step size was utilised to offer an initial fCFO estimate first to approach the global minimum of the cost function. Then, a refined fCFO estimate is obtained by searching in a small range with a small search step size. Similarly to Chapter 5, multiple receive antennas are also required for the proposed RSCCE scheme.

Table 6.2: Comparison of the proposed RSCCE scheme and the existing approaches.

Item	RSCCE	CP [3]	PN [3, 11]	iCFO-OFDM [7]	LS [9]	SB-OFDM [12]
iCFO estimation	✓	✗	✗	✓	✗	✓
fCFO estimation	✓	✓	✓	✗	✗	✓
Channel estimation	✓	✗	✗	✗	✓	✓
Training overhead	Low	Low	High	High	High	Low
Robustness against ICI and ISI	High	High	Low	N/A	Low	N/A
Number of symbols for semi-blind estimation	Tens	N/A	N/A	N/A	N/A	Hundreds
Complexity	High	Low	Low	Medium	Low	High
Receive antennas	Multiple	Single	Single	Multiple	Single	Multiple

Chapter 7

Semi-Blind Estimation of Channels, CFOs and IQ Imbalance for GFDMA Systems with Generalised CAS

CFO estimation has been investigated for OFDM systems and single-user GFDM systems in the previous chapters. However, these work cannot be extended to GFDMA systems with multiple users. GFDMA, as a combination of GFDM and FDMA, has become a promising multi-user technique. In this chapter, an open topic of a practical GFDMA system in the presence of CFOs and IQ imbalance is investigated. A semi-blind joint estimation scheme of multiple channels, multiple CFOs and IQ imbalance is proposed. By utilising the subspace approach, CFOs and channels corresponding to U users are first separated into U groups. For each individual user, the CFO is extracted by minimising the smallest eigenvalue whose corresponding eigenvector is utilised to estimate the channel in a blind manner. IQ imbalance parameters are estimated jointly with channel ambiguities by very few pilots. The proposed scheme is feasible for a wider range of receive antennas number and has no constraints on carrier assignment scheme, modulation type, cyclic prefix length and symmetry of IQ imbalance. Simulation results show that the proposed semi-blind scheme significantly outperforms the existing methods in terms of BER, outage probability, MSEs of CFO estimation, channel and IQ imbalance estimation, while at much higher spectrum efficiency. The CRLB is derived to verify the effectiveness of the proposed scheme, which is shown to be close to simulation results.

7.1 Introduction

GFDM [2], a generalised form of OFDM, has been regarded as a potential waveform for B5G networks. GFDMA, as a combination of GFDM and FDMA, has become a promising solution for multi-user communications [58, 143–145].

Signal detection of GFDMA encounters several critical challenges. First, it is difficult to estimate multiple channels from the received GFDMA signal, due to the inherent ICI and ISI in the mixture of signals from multiple users caused by its nonorthogonal prototype filters. Second, GFDMA is sensitive to RF impairments, such as CFOs and IQ imbalance. CFO worsens the ICI and ISI in GFDMA [143]. IQ imbalance is likely to incur an additional image interference in GFDMA and lead to biased signal estimates. Third, it is much challenging to investigate GFDMA systems with generalised CAS where subcarriers may be arranged arbitrarily and randomly for each user, and the properties of periodic subcarriers arrangement in the subband and interleaved CAS do not hold any more. Thus, the aforementioned issues of the estimation of multiple channels, multiple CFOs and IQ imbalance are critical for GFDMA with generalised CAS, which however is still an open area in the literature.

The research on GFDMA systems is limited in the literature. Lim *et al.* [143] investigated the impact of CFOs on the system performance of GFDMA, and proposed two multi-user interference cancellation schemes by optimising the weight and filter coefficient to mitigate the impact of CFOs. A low-complexity ZF receiver was developed to avoid the huge computation caused by the inverse of a large dimensional channel matrix for GFDMA in [58], while a precoding technique was proposed for PAPR reduction in [144]. However, none of the work in [58, 143, 144] considered the estimation of CFOs and channels. With a pilot containing two similar Zadoff-Chu training sequences, multiple CFOs and multiple channels were estimated jointly based on ML criterion for GFDMA in [145]. However, it demands long training sequences to suppress ICI and ISI, and thereby leading to low spectrum efficiency; it assumed a only specific frequency spreading GFDM transmitter structure in [50]. Meanwhile, all the aforementioned work in [58, 143–145] is for GFDMA with subband CAS only, and does not take into account IQ imbalance.

Section 6.1 has reviewed a number of approaches for channel estimation and CFO estimation in GFDM systems [3, 9, 11, 109, 133–136, 140, 141], which however ignore the presence of IQ imbalance. IQ imbalance was addressed in [15, 146, 147] for GFDM systems. Nevertheless, its estimation in [15] and [147] is assisted by a whole GFDM symbol, leading to high training overhead. Besides, the approaches in [15] and [146] are applicable to asymmetric IQ imbalance only, which however does not hold for symmetric IQ imbalance. In summary, the aforementioned work on GFDM [3, 9, 11, 15, 109, 133–136, 140, 141, 146, 147] have two key shortcomings namely: a) they dealt with only one of the issues of channel estimation [9, 133–136, 140], CFO estimation [3, 11, 109, 141] and IQ imbalance estimation [15, 146, 147] without considering their impacts on one another; b) they were for a single-user system, and cannot be easily extended to GFDMA systems with multiple users.

The existing work on OFDMA with RF impairments has considered either CFOs or IQ imbalance. A number of CFO estimation approaches were developed for OFDMA in [14, 148–151]. However, the systems in [148] and [149] were based on interleaved CAS only. The blind CFO estimation approach in [150] was applicable for generalised CAS, which however works only under the assumptions of constant modulus constellation and short CP; and requires prohibitively high complexity for exhaustive search. In [14] and [151], joint estimation of multiple CFOs and multiple channels was studied for OFDMA with generalised CAS. However, the rank-reduction criterion based approach in [14] described in Chapter 3 demands a multitude of receive antennas as well as vast computations to search for CFOs, and the p ilot-assisted scheme developed by Kalman and particle filtering in [151] reduces the spectral efficiency and significantly underperforms its derived CRLB especially at medium to high SNR. By utilising the space alternating generalised expectation maximisation approach, IQ imbalance was solved in [152] and [153] for OFDMA systems with two-path successive relaying and bit-interleaved coded modulation, respectively. However, the approaches in [152, 153] are computationally inefficient due to the iterative implementation and the method in [153] is applicable to interleaved OFDMA only. Both CFO and IQ imbalance were considered and estimated for OFDM systems in [154–156]. However, the aforementioned work for OFDMA [14, 148–153] and OFDM [154–156] is not applicable to GFDMA, owing to the inherently nonorthogonal prototype filters of GFDMA.

In summary, there is limited research on GFDMA in the presence of RF impairments, *e.g.*, only CFO, not IQ imbalance, was considered in [145]; the approaches developed for single-user GFDM [3, 9, 11, 15, 109, 133–136, 140, 141, 146, 147] cannot be easily extended to GFDMA with mutiple users; the approaches proposed for OFDMA [14, 148–153] and OFDM [154–156] are also not applicable to GFDMA due to the intrinsic ICI and ISI caused by the nonorthogonal filters of GFDMA. Furthermore, the existing work on GFDMA [58, 143–145] can work effectively only for specific GFDMA systems, *e.g.*, subband GFDMA [58, 143–145] and specific frequency spreading GFDMA [145].

Motivated by the above open issues, an uplink GFDMA system of U users with arbitrary CAS in the presence of CFOs and IQ imbalance is investigated, and a semi-blind joint multi-CFO, multi-channel and IQ imbalance estimation (JCCIQE) scheme is proposed for it. First, U CFOs and U channels are separated into U groups by user, assisted by a subspace approach. For each individual user, the CFO is extracted by minimising the smallest eigenvalue whose corresponding eigenvector is utilised to estimate the channel in a blind manner. Finally, the IQ imbalance parameters are estimated jointly with the channel ambiguities by very few pilots. The contributions of this work are as follows.

- To the best of the author's knowledge, this is the first work to investigate the estimation of channels and multiple RF impairments (CFOs and IQ imbalance) at the same time for a practical GFDMA system with generalised CAS, where the prior work on GFDMA [58,143–145], GFDM [3,9,11,15,109,133–136,140,141,146, 147], OFDMA [14,148–153] and OFDM [154–156] is not applicable, as summarised earlier. The proposed JCCIQE scheme for GFDMA significantly outperforms the existing methods for OFDMA [14] and for single-user GFDM [3, 9, 15] in terms of BER, outage probability, MSEs of CFO estimation and equivalent channel estimation. The CRLB on MSE of CFO estimation is derived for the first time for GFDMA systems with generalised CAS, which is close to simulation results and therefore verify the effectiveness of the proposed JCCIQE scheme. While CRLB analysis was not presented in [58, 143–145].

- The proposed JCCIQE scheme requires very low training overhead. Channels and CFOs are first estimated blindly, and joint elimination of channel ambiguities and IQ imbalance is conducted in a semi-blind manner, assisted by very few pilots serving two purposes at the same time. The resulting training overhead is 12-fold lower than that of [3, 9] and [15] which demand a large number of separate pilots for CFO estimation, channel estimation and IQ imbalance elimination. The multi-CFO compensation implemented at receiver side avoids the signalling overhead to feed CFOs back to the respective transmitters, unlike [157].

- The proposed JCCIQE scheme is feasible for a wide range of GFDMA systems. It has no constrains on CAS, modulation type, CP length and symmetry of IQ imbalance, while the existing approaches for GFDMA [58,143–145] and GFDM [3, 9, 15] work only under certain system specifications. Extensive simulation results show that JCCIQE is more robust against ICI and ISI in GFDMA systems than the pilots assisted approaches [3,9] for GFDM without an error floor. It is resilient to various CASs and also allows a wider range of the number of receive antennas than the rank-reduction criterion based approach for OFDMA in [14].

- The proposed JCCIQE scheme demands low complexity. U CFOs, U channels and two IQ imbalance parameters are separated and estimated individually, decomposing a complex $(2U+2)$-dimensional problem into $(2U+2)$ low-complexity one-dimensional problems. It achieves a tens-fold complexity reduction over the approach for OFDMA in [14].

The rest of this chapter is organised as follows. Section 7.2 presents the system model. The proposed semi-blind JCCIQE scheme is described in Section 7.3. Performance and complexity analysis are given in Section 7.4. Simulation results are demonstrated in Section 7.5. Section 7.6 draws the conclusion.

7.2 System Model

An uplink SIMO GFDMA system of U users with generalised CAS in the presence of CFOs and IQ imbalance is considered, where each user and BS are equipped with a single transmit antenna and N_r receive antennas, respectively. Each GFDMA symbol is divided into M subsymbols each with K subcarriers, and define $N = MK$. P arbitrary subcarriers are assigned to each user with $P = K/U$. The set of P arbitrary subcarriers assigned to user u $(u = 0, \cdots, U-1)$ is denoted as $\mathbf{K}_u$, where $\bigcup_{u=0}^{U-1} \mathbf{K}_u = \{0, 1, \cdots, K-1\}$ and $\mathbf{K}_u \bigcap \mathbf{K}_v = \varnothing$, $\forall u \neq v$. $\mathbf{K}_u(p)$ denotes the p-th to the smallest subcarrier index in $\mathbf{K}_u$.

Define $\mathbf{d}_{i,u} = [d_{i,u,0,0}, \cdots, d_{i,u,0,P-1}, \cdots, d_{i,u,M-1,0}, \cdots, d_{i,u,M-1,P-1}]^T$, where $d_{i,u,m,p}$ is the data of user u in the m-th $(m = 0, \cdots, M-1)$ subsymbol of i-th $(i = 0, \cdots, N_\mathrm{s}-1)$ symbol on the $\mathbf{K}_u(p)$-th $(p = 0, \cdots, P-1)$ subcarrier, and N_s is the number of symbols in a frame. Each $d_{i,u,m,p}$ is transmitted with the corresponding pulse shape [58, 143]

$$g_{m,k}[n] = g[(n - mK) \bmod N] \cdot \exp(-j2\pi kn/K). \tag{7.1}$$

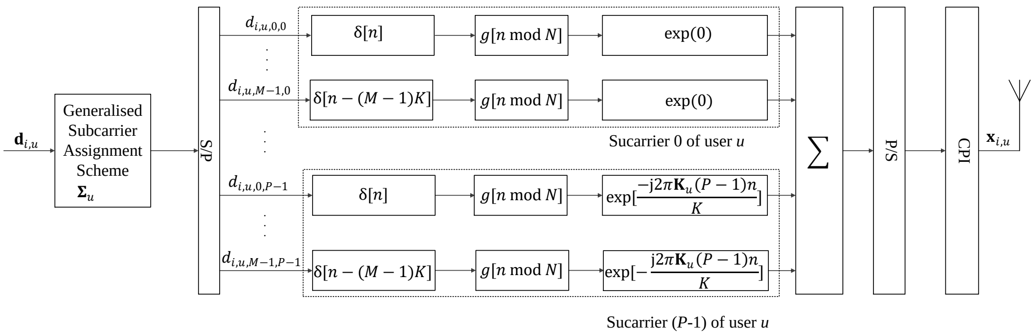

Figure 7.1: Transmitter of user u in an uplink SIMO GFDMA system with generalised CAS.

After pulse shaping, the transmit signal $\epsilon_{i,u}[n]$ is given by

$$\epsilon_{i,u}[n] = \sum\nolimits_{p=0}^{P-1} \sum\nolimits_{m=0}^{M-1} g_{m,\mathbf{K}_u(p)}[n] d_{i,u,m,p}. \tag{7.2}$$

Denote $\boldsymbol{\epsilon}_{i,u} = [\epsilon_{i,u}[0], \epsilon_{i,u}[1], \cdots, \epsilon_{i,u}[N-1]]^T$ as the transmit signal vector of user u in the i-th symbol, which can be expressed as

$$\boldsymbol{\epsilon}_{i,u} = \mathbf{A}\boldsymbol{\Sigma}_u \mathbf{d}_{i,u}, \tag{7.3}$$

where $\mathbf{A} = [\mathbf{g}_{0,0}, \cdots, \mathbf{g}_{0,K-1}, \cdots, \mathbf{g}_{M-1,0}, \cdots, \mathbf{g}_{M-1,K-1}]$ is an $N \times N$ pulse shaping filter matrix with $\mathbf{g}_{m,k} = [g_{m,k}[0], \cdots, g_{m,k}[N-1]]^T$, and $\boldsymbol{\Sigma}_u = \mathbf{I}_M \otimes \boldsymbol{\sigma}_u$ is the subcarrier assignment matrix with $\boldsymbol{\sigma}_u$ denoting a $K \times P$ matrix whose p-th column vector corresponds to the $\mathbf{K}_u(p)$-th column of the identity matrix $\mathbf{I}_K$. A CP of length $L_{\rm cp}$ is pre-pended to the symbol $\boldsymbol{\epsilon}_{i,u}$, yielding a signal vector $\mathbf{x}_{i,u}$ of length $G = N + L_{\rm cp}$, which is given by

$$\mathbf{x}_{i,u} = \boldsymbol{\Psi}_u \mathbf{d}_{i,u}, \tag{7.4}$$

where $\boldsymbol{\Psi}_u = \mathbf{A}_{\rm cp}\boldsymbol{\Sigma}_{\boldsymbol{u}}$ and $\mathbf{A}_{\rm cp} = [\mathbf{A}^T(N - L_{\rm cp} : N-1, 1:N), \mathbf{A}^T]^T$. Fig. 7.1 illustrates the transmitter of user u in an uplink SIMO GFDMA system with generalised CAS.

CIR is assumed to exhibit quasi-static fading and remains constant over a frame. Denote $\boldsymbol{\hbar}_{u,n_{\rm r}} = [\hbar_{u,n_{\rm r}}[0], \cdots, \hbar_{u,n_{\rm r}}[L-1]]^T$ as the CIR vector for the $n_{\rm r}$-th receive antenna of user u, with L being the length of CIR. ϕ_u is defined as the CFO between user u and BS. By incorporating CFO into the channel of each user as in Chapters 5 and 6, the time-domain received signal in the i-th symbol at the n_r-th receive antenna can be written as

$$y_{i,n_\mathrm{r}}[g] = \sum\nolimits_{u=0}^{U-1} \sum\nolimits_{l=0}^{L-1} h_{u,n_\mathrm{r}}[l] e^{\jmath 2\pi\phi_u(g-l)/K} x_{i,u}[g-l] + w_{i,n_\mathrm{r}}[g], \tag{7.5}$$

where $h_{u,n_\mathrm{r}}[l] = e^{\jmath 2\pi\phi_u l/K} \hbar_{u,n_\mathrm{r}}[l]$ is the CFO-included channel and $w_{i,n_\mathrm{r}}[g]$ ($g = 0, \cdots, G-1$) is the additive white Gaussian noise with zero mean and variance σ^2. Similar to Chapters 5 and 6, the first $(L-1)$ signal samples, $y_{i,n_\mathrm{r}}[0]$ to $y_{i,n_\mathrm{r}}[L-2]$, which suffer from ISI caused by multi-path fading, are discarded and are not utilised for estimation. The received signal samples $y_{i,n_\mathrm{r}}[L-1]$ to $y_{i,n_\mathrm{r}}[G-1]$ from N_r received antennas are collected into a vector, yielding $\mathbf{y}_i = [y_{i,0}[L-1], \cdots, y_{i,N_\mathrm{r}-1}[L-1], \cdots, y_{i,0}[G-1], \cdots, y_{i,N_\mathrm{r}-1}[G-1]]^T$ of size $N_\mathrm{r}(G-L+1)$, which can be expressed as

$$\mathbf{y}_i = \sum\nolimits_{u=0}^{U-1} \underbrace{\mathbf{H}_u \mathbf{E}_\mathrm{G}(\phi_u) \mathbf{\Psi}_u}_{\mathbf{G}_u} \mathbf{d}_{i,u} + \mathbf{w}_i, \tag{7.6}$$

where $\mathbf{E}_\mathrm{G}(\phi_u) = \mathrm{diag}\{[1, e^{\jmath 2\pi\phi_u/K}, \cdots, e^{\jmath 2\pi\phi_u(G-1)/K}]\}$ is the CFO matrix of user u, $\mathbf{H}_u$ is the channel circulant matrix defined as

$$\mathbf{H}_u = \begin{bmatrix} \mathbf{h}_u(L-1) & \cdots & \mathbf{h}_u(0) & \cdots & \cdots & \mathbf{0}_{N_\mathrm{r}\times 1} \\ \vdots & \ddots & \ddots & \ddots & \ddots & \vdots \\ \mathbf{0}_{N_\mathrm{r}\times 1} & \cdots & \cdots & \mathbf{h}_u(L-1) & \cdots & \mathbf{h}_u(0) \end{bmatrix}, \tag{7.7}$$

with $\mathbf{h}_u(l) = [h_{u,0}[l], \cdots, h_{u,N_\mathrm{r}-1}[l]]^T$, and similarly $\mathbf{w}_i = [w_{i,0}[L-1], \cdots, w_{i,N_\mathrm{r}-1}[L-1], \cdots, w_{i,0}[G-1], \cdots, w_{i,N_\mathrm{r}-1}[G-1]]^T$.

IQ imbalance can be modelled in two ways, being either symmetric or asymmetric, as demonstrated in Subsection 3.4.1. According to Subsection 3.4.1, the symmetric IQ imbalance parameters α and β are defined in (3.45) and (3.46), while the counterparts for asymmetric IQ imbalance are in (3.47) and (3.48). Note that the asymmetric IQ imbalance model has a property of $\alpha + \beta^* = 1$ [15, 112]. To reduce the hardware cost and power consumption, it is assumed that there is only one RF chain at receiver. In other words, multiple receive antennas share the same RF chain and thus share the same IQ imbalance [158, 159]. The received signal in the i-th symbol with IQ imbalance is expressed as

$$\tilde{\mathbf{y}}_i = \alpha \mathbf{y}_i + \beta \mathbf{y}_i^*. \tag{7.8}$$

According to (7.6) and (7.8), $\tilde{\mathbf{y}}_i$ can be further expressed as

$$\tilde{\mathbf{y}}_i = \alpha \sum\nolimits_{u=0}^{U-1} \underbrace{\mathbf{H}_u \mathbf{E}_{\mathrm{G}}(\phi_u) \mathbf{\Psi}_u}_{\mathbf{G}_u} \mathbf{d}_{i,u} + \beta \sum\nolimits_{u=0}^{U-1} \underbrace{\mathbf{H}_u^* \mathbf{E}_{\mathrm{G}}(-\phi_u) \mathbf{\Psi}_u^*}_{\mathbf{G}_u^*} \mathbf{d}_{i,u}^* + \underbrace{\alpha \mathbf{w}_i + \beta \mathbf{w}_i^*}_{\tilde{\mathbf{w}}_i}. \tag{7.9}$$

7.3 Semi-Blind JCCIQE Scheme

The purpose of this work is to determine U CFOs, U channels and two IQ imbalance parameters from (7.9), which is a complex problem of $(2U+2)$ dimensions. A semi-blind JCCIQE scheme is proposed for SIMO GFDMA systems with generalised CAS in the section. Thanks to the orthogonality between noise subspace and each signal subspace of U users, CFOs and channels are first separated into U groups corresponding to U users. Second, for each user, CFO is first extracted by minimising the smallest eigenvalue to satisfy the orthogonality, while the channel is determined by the corresponding eigenvector. Third, the estimation of two IQ imbalance parameters and channel ambiguities elimination are conducted jointly by very few pilots. Thereby, a $(2U + 2)$-dimensional estimation problem is decomposed into $(2U + 2)$ one-dimensional problems and solved with low complexity. Fig. 7.2 illustrates the block diagram of the proposed JCCIQE scheme for GFDMA systems.

7.3.1 Joint Multi-CFO and Multi-Channel Separation

To separate U channels and U CFOs into U groups by user, the eigenvectors corresponding to the noise subspace should be obtained. By exploiting N_{r} receive antennas, the frame of N_{s} received symbols is used to compute the auto-correlation matrix of the

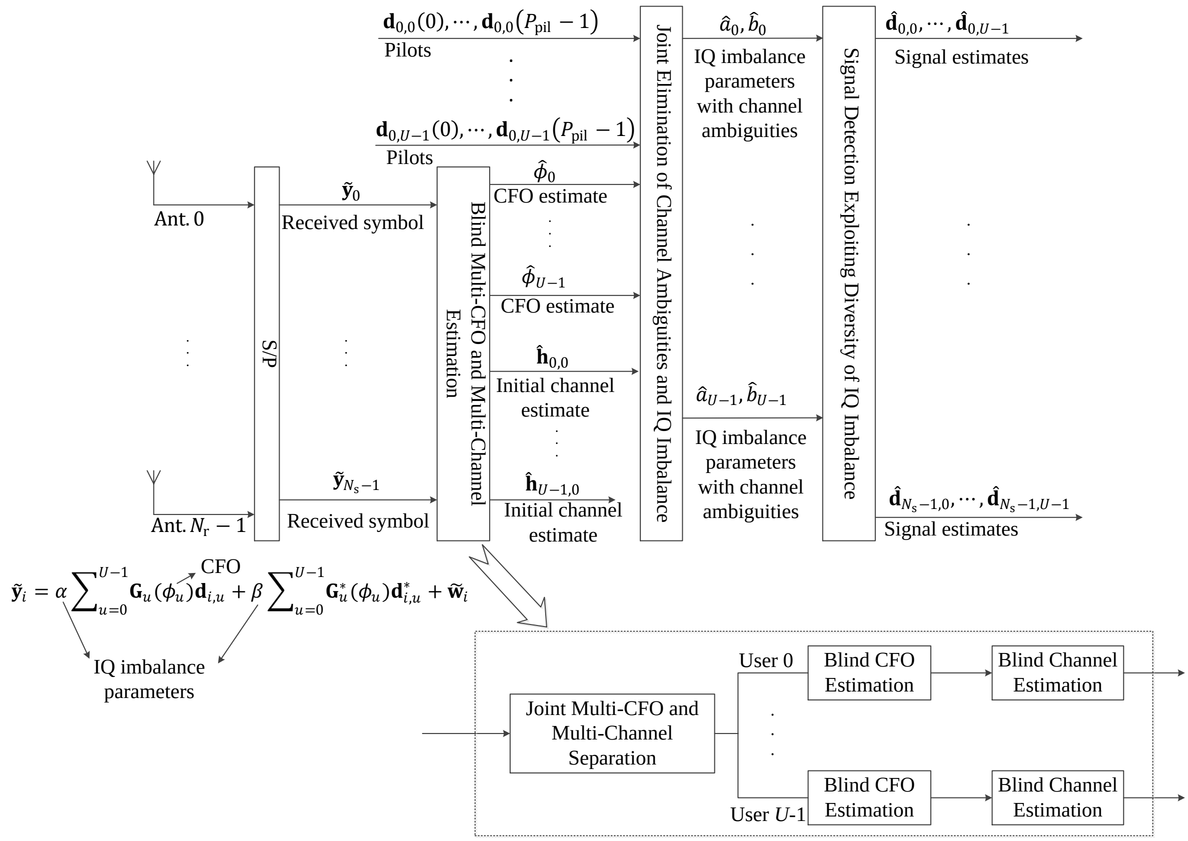

Figure 7.2: Block diagram of the proposed JCCIQE scheme for GFDMA systems with generalised CAS.

received signal, yielding $\mathbf{R}_{\mathrm{yy}}$ given by

$$\mathbf{R}_{\mathrm{yy}} = \frac{1}{N_{\mathrm{s}}} \sum_{i=0}^{N_{\mathrm{s}}-1} \tilde{\mathbf{y}}_i \tilde{\mathbf{y}}_i^H. \tag{7.10}$$

By performing EVD on $\mathbf{R}_{\mathrm{yy}}$, the noise eigenvectors can be determined, which correspond to the Q ($Q = N_{\mathrm{r}}(G-L+1)-2N$) smallest eigenvalues of $\mathbf{R}_{\mathrm{yy}}$. Hence, the number of receive antennas should satisfy $N_{\mathrm{r}}(G-L+1) > 2N$. It is noteworthy that the signal subspace has a dimension of $2N$, where the multiple of 2 results from the image signal induced by IQ imbalance. Note that given a special case without IQ imbalance, the number of noise eigenvectors should be $Q = N_{\mathrm{r}}(G-L+1)-N$. The q-th ($q = 0, \cdots, Q-1$)

noise eigenvector is expressed as $\boldsymbol{\gamma}_q = [\boldsymbol{\gamma}_q^T(0), \boldsymbol{\gamma}_q^T(1), \cdots, \boldsymbol{\gamma}_q^T(G-L)]^T$, where $\boldsymbol{\gamma}_q(g)$ is a column vector of length N_r. Due to orthogonality between the noise subspace and each signal subspace, the columns of $\mathbf{G}_u$ and $\mathbf{G}_u^*$ are orthogonal to each noise eigenvector, *i.e.*, $\boldsymbol{\gamma}_q^H \mathbf{G}_u = \mathbf{0}_{1\times MP}$ and $\boldsymbol{\gamma}_q^H \mathbf{G}_u^* = \mathbf{0}_{1\times MP}$. Since each user occupies exclusive subcarriers, $\mathbf{G}_u$ an $\mathbf{G}_u^*$ differ between different users. Define $\mathbf{h}_u = [\mathbf{h}_u^T(L-1), \mathbf{h}_u^T(L-2), \cdots, \mathbf{h}_u^T(0)]^T$ as the CFO-included CIR of user u. The CFO and the CFO-included CIR of user u can be estimated by

$$[\hat{\phi}_u, \hat{\mathbf{h}}_u] = \arg \min_{\phi_u, \mathbf{h}_u} \sum\nolimits_{q=0}^{Q-1} (\| \boldsymbol{\gamma}_q^H \mathbf{G}_u \mathbf{G}_u^H \boldsymbol{\gamma}_q \|_\mathrm{F}^2 + \| \boldsymbol{\gamma}_q^H \mathbf{G}_u^* \mathbf{G}_u^T \boldsymbol{\gamma}_q \|_\mathrm{F}^2). \tag{7.11}$$

Note that $\mathbf{G}_u^*$ and $\mathbf{G}_u^T$ originate from the image signal of user u which usually has lower power and thus lower SNR than the source signal [156]. As a result, the term $\| \boldsymbol{\gamma}_q^H \mathbf{G}_u^* \mathbf{G}_u^T \boldsymbol{\gamma}_q \|_\mathrm{F}^2$ in (7.11) is likely to deteriorate the estimation performance, and can be removed from (7.11), resulting in the following problem formulation:

$$[\hat{\phi}_u, \hat{\mathbf{h}}_u] = \arg \min_{\phi_u, \mathbf{h}_u} \sum\nolimits_{q=0}^{Q-1} \| \boldsymbol{\gamma}_q^H \mathbf{G}_u \mathbf{G}_u^H \boldsymbol{\gamma}_q \|_\mathrm{F}^2 . \tag{7.12}$$

Therefore, by utilising the orthogonality property, the CFOs and channels can be separated by user. It is noteworthy that the proposed JCCIQE scheme has a looser requirement on the CP length and the number of receive antennas. The CP length takes any value, while it is limited to $L_\mathrm{cp} < \frac{P-1}{2}$ in [150], where P is the number of subcarriers per user. The proposed JCCIQE scheme requires a minimum number of receive antennas to satisfy $N_\mathrm{r} > \frac{2KM}{(KM+L_\mathrm{cp}-L+1)}$ which is smaller than that required in [14], where the number of receive antennas should satisfy $N_\mathrm{r} \geq UL$. With $K = 16$, $M = 2$, $L = 3$, $L_\mathrm{cp} = 4$ and $U = 4$, the minimum number of receive antennas required by the proposed JCCIQE scheme and the approach in [14] is $N_\mathrm{r} = 2$ and $N_\mathrm{r} = 12$, respectively.

7.3.2 Blind Estimation of CFO and Channel for Each User

After the separation of CFOs and channels by user, each CFO is first extracted to satisfy the orthogonality between noise subspace and each signal subspace by minimising the smallest eigenvalue, whose corresponding eigenvector is exploited to determine the CFO-included CIR in a blind manner.

Define $\mathbf{R}_u(\tilde{\phi}_u) = \parallel \boldsymbol{\gamma}_q^H \mathbf{G}_u(\tilde{\phi}_u)\mathbf{G}_u^H(\tilde{\phi}_u)\boldsymbol{\gamma}_q \parallel_{\mathrm{F}}^2$, where $\mathbf{G}_u(\tilde{\phi}_u) = \mathbf{H}_u\mathbf{E}_{\mathrm{G}}(\tilde{\phi}_u)\boldsymbol{\Psi}_u$, with $\tilde{\phi}_u$ denoting as the CFO trial value of user u. $\mathbf{R}_u(\tilde{\phi}_u)$ can be written as

$$\mathbf{R}_u(\tilde{\phi}_u) = \boldsymbol{\gamma}_q^H \mathbf{H}_u \mathbf{E}_{\mathrm{G}}(\tilde{\phi}_u)\boldsymbol{\Psi}_u\boldsymbol{\Psi}_u^H\mathbf{E}_{\mathrm{G}}^H(\tilde{\phi}_u)\mathbf{H}_u^H\boldsymbol{\gamma}_q. \tag{7.13}$$

According to [160], $\mathbf{H}_u$, as a Toeplitz matrix, has a property of $\boldsymbol{\gamma}_q^H\mathbf{H}_u = \mathbf{h}_u^T\boldsymbol{\Upsilon}_q$, where $\boldsymbol{\Upsilon}_q$ is an $N_{\mathrm{r}}L \times G$ matrix given by

$$\boldsymbol{\Upsilon}_q = \begin{bmatrix} \boldsymbol{\gamma}_q^*(0) & \cdots & \boldsymbol{\gamma}_q^*(G-L) & \cdots & \cdots & \mathbf{0}_{N_{\mathrm{r}}\times 1} \\ \vdots & \ddots & \ddots & \ddots & \ddots & \vdots \\ \mathbf{0}_{N_{\mathrm{r}}\times 1} & \cdots & \cdots & \boldsymbol{\gamma}_q^*(0) & \cdots & \boldsymbol{\gamma}_q^*(G-L) \end{bmatrix}. \tag{7.14}$$

Therefore, (7.13) can be rewritten as

$$\mathbf{R}_u(\tilde{\phi}_u) = \mathbf{h}_u^T \underbrace{\boldsymbol{\Upsilon}_q\mathbf{E}_{\mathrm{G}}(\tilde{\phi}_u)\boldsymbol{\Psi}_u}_{\mathbf{P}_{u,q}(\tilde{\phi}_u)} \underbrace{\boldsymbol{\Psi}_u^H\mathbf{E}_{\mathrm{G}}^H(\tilde{\phi}_u)\boldsymbol{\Upsilon}_q^H}_{\mathbf{P}_{u,q}^H(\tilde{\phi}_u)} \mathbf{h}_u^*. \tag{7.15}$$

Define $\mathbf{P}_u(\tilde{\phi}_u) = [\mathbf{P}_{u,0}(\tilde{\phi}_u), \mathbf{P}_{u,1}(\tilde{\phi}_u), \cdots, \mathbf{P}_{u,Q-1}(\tilde{\phi}_u)]$ of size $N_{\mathrm{r}}L \times MPQ$. The CFO and CFO-included CIR of user u can be estimated by

$$[\hat{\phi}_u, \hat{\mathbf{h}}_u] = \arg \min_{\tilde{\phi}_u, \mathbf{h}_u} \parallel \mathbf{h}_u^T\mathbf{P}_u(\tilde{\phi}_u)\mathbf{P}_u^H(\tilde{\phi}_u)\mathbf{h}_u^* \parallel_{\mathrm{F}}^2 . \tag{7.16}$$

In the following, they are estimated in two steps:

Step 1: The auto-correlation matrix of $\mathbf{P}_u(\tilde{\phi}_u)$ is calculated by

$$\mathbf{R}_u^{\mathbf{PP}}(\tilde{\phi}_u) = \mathbf{P}_u(\tilde{\phi}_u)\mathbf{P}_u^H(\tilde{\phi}_u). \tag{7.17}$$

If $\tilde{\phi}_u$ is the true CFO ($\tilde{\phi}_u = \phi_u$), the rank of $\mathbf{R}_u^{\mathbf{PP}}$ is $(N_\mathrm{r}L - 1)$, otherwise the rank is $N_\mathrm{r}L$. Hence, the CFO of user u can be extracted by minimising the smallest eigenvalue of $\mathbf{R}_u^{\mathbf{PP}}(\tilde{\phi}_u)$. It is equivalent to minimise the determinant of $\mathbf{R}_u^{\mathbf{PP}}(\tilde{\phi}_u)$, *i.e.*,

$$\hat{\phi}_u = \arg \min_{\tilde{\phi}_u \in [-0.5, 0.5)} \det\,(\mathbf{R}_u^{\mathbf{PP}}(\tilde{\phi}_u)). \tag{7.18}$$

Note that estimating CFO by (7.18) requires a relatively small search step size for a high accuracy performance, which however demands high computational complexity. Inspired by [142], the CFO estimation problem in (7.18) can be solved with a reduced computational complexity by the following two steps:

Step 1.1 - Coarse Estimation: The CFO of user u is extracted as $\hat{\phi}_{u,0}$ by (7.18) with a relatively large search step size δ to obtain an initial value to approach the global minimum of $\det(\mathbf{R}_u^{\mathbf{PP}}(\tilde{\phi}_u))$;

Step 1.2 - Fine Estimation: A refined CFO is estimated by searching in the range of $(\hat{\phi}_{u,0} - \delta/2, \hat{\phi}_{u,0} + \delta/2)$ by the golden section search and parabolic interpolation algorithms.

Step 2: With the CFO estimate $\hat{\phi}_u$, the CFO-included CIR of user u is determined as the conjugate of the eigenvector corresponding to its smallest eigenvalue of $\mathbf{R}_u^{\mathbf{PP}}(\hat{\phi}_u)$, and is denoted as $\hat{\mathbf{h}}_{u,0}$.

It is noteworthy that CFO and CFO-included channel of each user are estimated blindly, which do not suffer the ICI and ISI from data symbols, unlike the existing pilot assisted approaches [3, 9, 11]. The orthogonality between the signal and noise subspaces is independent of the value of M, which allows CFO estimation in the range of $[-0.5, 0.5)$, unlike $[-0.5/M, 0.5/M)$ in the CP [3] and ML [109] based approaches. As U channels and U CFOs are estimated individually, signalling overhead due to feedback of multiple CFO estimates to transmitters for multi-CFO compensation can be avoided, unlike [157]. It is worth noticing that a complex channel scaling ambiguity c_u exists between the CFO-included CIR estimate $\hat{\mathbf{h}}_{u,0}$ and its true CFO-included CIR $\mathbf{h}_u$, which can be eliminated jointly with IQ imbalance parameters by very few pilots as described in Subsection 7.3.3.

In addition, CFO estimation of the proposed JCCIQE scheme is based on rank-reduction criterion as well, which however needs a much smaller number of receive antennas than rank-reduction criterion based CFO estimator for OFDMA in [17] as discussed in Subsection 7.3.1. The proposed CFO estimation demonstrates much lower computational complexity than the work [17] for OFDMA as will be seen in Subsection 7.4.2. Besides, the work [17] for OFDMA did not consider the presence of IQ imbalance, and suffers an error floor as will be shown in Section 7.5.

7.3.3 Joint Elimination of Channel Ambiguities and IQ Imbalance for Each User

With the blind estimates of CFO and CFO-included CIR namely $\hat{\phi}$ and $\hat{\mathbf{h}}_{u,0}$ in Subsection 7.3.2, the estimate of matrix $\mathbf{G}_u$ in (7.9) can be denoted as $\hat{\mathbf{G}}_u$. The received signal $\tilde{\mathbf{y}}_i$ in (7.9) can be rewritten as

$$\tilde{\mathbf{y}}_i = \sum\nolimits_{u=0}^{U-1} \hat{\mathbf{G}}_u \mathbf{d}_{i,u} \underbrace{c_u\alpha}_{a_u} + \sum\nolimits_{u=0}^{U-1} \hat{\mathbf{G}}_u^* \mathbf{d}_{i,u}^* \underbrace{c_u^*\beta}_{b_u} + \tilde{\mathbf{w}}_i, \tag{7.19}$$

where $a_u = c_u\alpha$ and $b_u = c_u^*\beta$ correspond to the IQ imbalance parameters by taking into account channel ambiguities c_u and c_u^*.

Define $\hat{\mathbf{G}} = [\hat{\mathbf{G}}_0, \hat{\mathbf{G}}_0^*, \cdots, \hat{\mathbf{G}}_{U-1}, \hat{\mathbf{G}}_{U-1}^*]$ of size $N_{\mathrm{r}}(G-L+1)\times 2N$. Assume that P_{pil} pilots in the first GFDMA symbol are utilised for joint elimination of channel ambiguities and IQ imbalance. By ZF detection, the received signal vector $\tilde{\mathbf{y}}_0$ is multiplied with the pseudoinverse of $\hat{\mathbf{G}}$, obtaining $\mathbf{r} = \hat{\mathbf{G}}^{\dagger}\tilde{\mathbf{y}}_0$. Define $\mathbf{r} = [\mathbf{r}_{0,0}^T, \mathbf{r}_{1,0}^T, \cdots, \mathbf{r}_{0,U-1}^T, \mathbf{r}_{1,U-1}^T]^T$, where $\mathbf{r}_{0,u}$ and $\mathbf{r}_{1,u}$ are respectively given by

$$\mathbf{r}_{0,u} = \mathbf{d}_{0,u}a_u + \tilde{\mathbf{w}}_{0,u}, \tag{7.20}$$

and

$$\mathbf{r}_{1,u} = \mathbf{d}_{0,u}^{*} b_u + \tilde{\mathbf{w}}_{1,u}, \tag{7.21}$$

with $\tilde{\mathbf{w}}_{0,u}$ and $\tilde{\mathbf{w}}_{1,u}$ being the noise vectors. It is noteworthy that the ICI and ISI from the nonorthogonal filters are eliminated thanks to the ZF algorithm, assuming the filter matrix $\mathbf{A}$ is well-conditioned and its inverse exists [2]. Hence, the following estimation of channel ambiguities and IQ imbalance parameters is more robust against ICI and ISI. By utilising P_{pil} pilots in the first GFDMA symbol, the estimates of a_u and b_u in (7.19) are given by

$$\hat{a}_u = \frac{1}{P_{\text{pil}}} \sum\nolimits_{p=0}^{P_{\text{pil}}-1} \frac{\mathbf{r}_{0,u}(p)}{\mathbf{d}_{0,u}(p)}, \tag{7.22}$$

and

$$\hat{b}_u = \frac{1}{P_{\text{pil}}} \sum\nolimits_{p=0}^{P_{\text{pil}}-1} \frac{\mathbf{r}_{1,u}(p)}{\mathbf{d}_{0,u}^{*}(p)}. \tag{7.23}$$

Define $\mathbf{h}_{\text{I},u}$ and $\mathbf{h}_{\text{Q},u}$ as the equivalent CIRs of user u by taking into account IQ imbalance, which are expressed as $\mathbf{h}_{\text{I},u} = \mathbf{h}_u \alpha$ and $\mathbf{h}_{\text{Q},u} = \mathbf{h}_u^{*} \beta$, respectively. The estimates of $\mathbf{h}_{\text{I},u}$ and $\mathbf{h}_{\text{Q},u}$ are given by $\hat{\mathbf{h}}_{\text{I},u} = \hat{\mathbf{h}}_{u,0} \hat{a}_u$ and $\hat{\mathbf{h}}_{\text{Q},u} = \hat{\mathbf{h}}_{u,0}^{*} \hat{b}_u$, where $\hat{\mathbf{h}}_{u,0}$ is the initial blind channel estimate obtained in Subsection 7.3.2. It is noteworthy that the property of $\alpha + \beta^{*} = 1$ with asymmetric IQ imbalance was exploited for IQ imbalance estimation in [15], while the proposed JCCIQE scheme is feasible for both symmetric and asymmetric IQ imbalances.

7.3.4 Signal Detection Exploiting Diversity of IQ Imbalance

Thanks to the diversity provided by IQ imbalance, signal can be detected with an enhanced accuracy in the following. Defining $\mathbf{D}_{1,u} = \hat{\mathbf{G}}_u \hat{a}_u$ and $\mathbf{D}_{2,u} = \hat{\mathbf{G}}_u^{*} \hat{b}_u$, $\tilde{\mathbf{y}}_i$ in (7.9) can be rewritten as

$$\tilde{\mathbf{y}}_i = \sum\nolimits_{u=0}^{U-1} \mathbf{D}_{1,u} \mathbf{d}_{i,u} + \sum\nolimits_{u=0}^{U-1} \mathbf{D}_{2,u} \mathbf{d}_{i,u}^{*} + \tilde{\mathbf{w}}_i. \tag{7.24}$$

By concatenating $\tilde{\mathbf{y}}_i$ and its conjugate $\tilde{\mathbf{y}}_i^*$,

$$\begin{bmatrix} \tilde{\mathbf{y}}_i \\ \tilde{\mathbf{y}}_i^* \end{bmatrix} = \begin{bmatrix} \mathbf{D}_1 & \mathbf{D}_2 \\ \mathbf{D}_2^* & \mathbf{D}_1^* \end{bmatrix} \begin{bmatrix} \mathbf{d}_i \\ \mathbf{d}_i^* \end{bmatrix} + \begin{bmatrix} \tilde{\mathbf{w}}_i \\ \tilde{\mathbf{w}}_i^* \end{bmatrix} \tag{7.25}$$

is obtained, where $\mathbf{D}_1 = [\mathbf{D}_{1,0}, \cdots, \mathbf{D}_{1,U-1}]$ of size $(G-L+1)N_\mathrm{r} \times N$, $\mathbf{D}_2 = [\mathbf{D}_{2,0}, \cdots, \mathbf{D}_{2,U-1}]$ of size $(G-L+1)N_\mathrm{r} \times N$ and $\mathbf{d}_i = [\mathbf{d}_{i,0}^T, \cdots, \mathbf{d}_{i,U-1}^T]^T$ of size $N \times 1$.

Denote $\tilde{\mathbf{d}}_{\mathrm{I},i}$ and $\tilde{\mathbf{d}}_{\mathrm{Q},i}$ as the respective estimates of the source signal $\mathbf{d}_i$ and its image signal $\mathbf{d}_i^*$, which can be obtained as

$$\begin{bmatrix} \tilde{\mathbf{d}}_{\mathrm{I},i} \\ \tilde{\mathbf{d}}_{\mathrm{Q},i} \end{bmatrix} = \begin{bmatrix} \mathbf{D}_1 & \mathbf{D}_2 \\ \mathbf{D}_2^* & \mathbf{D}_1^* \end{bmatrix}^\dagger \begin{bmatrix} \tilde{\mathbf{y}}_i \\ \tilde{\mathbf{y}}_i^* \end{bmatrix}. \tag{7.26}$$

Since the source signal estimate $\mathbf{d}_{\mathrm{I},i}$ is the conjugate of the image signal estimate $\mathbf{d}_{\mathrm{Q},i}$, *i.e.*, $\mathbf{d}_{\mathrm{Q},i} = \mathbf{d}_{\mathrm{I},i}^*$, the estimate of source signal $\mathbf{d}_i$ can be obtained as $\hat{\mathbf{d}}_i = (\tilde{\mathbf{d}}_{\mathrm{I},i} + \tilde{\mathbf{d}}_{\mathrm{Q},i}^*)/2$, by exploiting the diversity resulting from IQ imbalance. Note that the proposed JCCIQE scheme is independent of the modulation type, while the method in [150] for OFDMA works only with a constant modulus constellation.

7.4 Performance and Complexity Analysis

7.4.1 CRLB Analysis

The CRLB for blind multi-CFO, multi-channel and IQ imbalance estimation is derived in this subsection, which provides an analytical benchmark for the proposed JCCIQE scheme. CRLB is determined by taking a derivative of the received signal vector with respect to the unknown variables vector. Generally, the received signal samples from all the received antennas within a frame should be collected as a column vector. However, the dimension of this column vector is likely to be extremely large, and the inverse of such a huge matrix is computationally prohibitive. To simplify the computation, an approximate CRLB is derived in the following, inspired by [128].

By incorporating IQ imbalance parameters α and β into the original circulant channel matrix $\mathbf{H}_u$ and the image circulant channel matrix $\mathbf{H}_u^*$, the equivalent circulant channel matrices are obtained as $\mathbf{H}_{\mathrm{I},u} = \alpha\mathbf{H}_u$ and $\mathbf{H}_{\mathrm{Q},u} = \beta\mathbf{H}_u^*$. $\mathbf{H}_{\mathrm{I},u}$ and $\mathbf{H}_{\mathrm{Q},u}$ are same as $\mathbf{H}_u$ in (7.7), except that $\mathbf{h}_u$ in (7.7) is replaced by $\mathbf{h}_{\mathrm{I},u}$ and $\mathbf{h}_{\mathrm{Q},u}$, respectively. Thus, a system model equivalent to that given by (7.9) is obtained, where the received signal vector in the i-th symbol can be rewritten as

$$\tilde{\mathbf{y}}_i = \sum\nolimits_{u=0}^{U-1} \mathbf{H}_{\mathrm{I},u}\mathbf{E}_{\mathrm{G}}(\phi_u)\boldsymbol{\Psi}_u\mathbf{d}_{i,u} + \sum\nolimits_{u=0}^{U-1} \mathbf{H}_{\mathrm{Q},u}\mathbf{E}_{\mathrm{G}}(-\phi_u)\boldsymbol{\Psi}_u^*\mathbf{d}_{i,u}^* + \tilde{\mathbf{w}}_i. \tag{7.27}$$

Since the signal vectors $\mathbf{d}_{i,u}$ and $\mathbf{d}_{i,u}^*$ are unknown to the receiver, the equivalent CIR vectors $\mathbf{h}_{\mathrm{I},u}$ and $\mathbf{h}_{\mathrm{Q},u}$ are estimated with a scaling ambiguity [161]. Similar to [161], the last elements of the equivalent CIR vectors of user u are assumed to be known at the receiver, which suggests that the channel ambiguities along with IQ imbalance are eliminated perfectly. Thus, the unknown variables are the CFO vector $\boldsymbol{\phi} = [\phi_0, \cdots, \phi_{U-1}]^T$, the equivalent CIR vectors $\mathbf{h}_{\mathrm{I}} = [\mathbf{h}_{\mathrm{I},0}(0 : N_{\mathrm{r}}L-2)^T, \cdots, \mathbf{h}_{\mathrm{I},U-1}(0 : N_{\mathrm{r}}L-2)^T]^T$ and $\mathbf{h}_{\mathrm{Q}} = [\mathbf{h}_{\mathrm{Q},0}(0 : N_{\mathrm{r}}L-2)^T, \cdots, \mathbf{h}_{\mathrm{Q},U-1}(0 : N_{\mathrm{r}}L-2)^T]^T$, and the unknown data vector $\mathbf{d}_i$. All the unknown variables are collected in a column vector, *i.e.*, $\boldsymbol{\Theta} = [\boldsymbol{\phi}^T, \mathrm{Re}\{\mathbf{h}_{\mathrm{I}}^T\}, \mathrm{Im}\{\mathbf{h}_{\mathrm{I}}^T\}, \mathrm{Re}\{\mathbf{h}_{\mathrm{Q}}^T\}, \mathrm{Im}\{\mathbf{h}_{\mathrm{Q}}^T\}, \mathrm{Re}\{\mathbf{d}_i^T]^T\}, \mathrm{Im}\{\mathbf{d}_i^T]^T\}$. Define $\mathbf{U}_i = \sum_{u=0}^{U-1} \mathbf{H}_{\mathrm{I},u}\mathbf{E}_{\mathrm{G}}(\phi_u)\boldsymbol{\Psi}_u\mathbf{d}_{i,u} + \sum_{u=0}^{U-1} \mathbf{H}_{\mathrm{Q},u}\mathbf{E}_{\mathrm{G}}(-\phi_u)\boldsymbol{\Psi}_u^*\mathbf{d}_{i,u}^*$. The FIM can be expressed as

$$\boldsymbol{\Pi}_i = \frac{2}{\sigma^2}\mathrm{Re}\Big[\frac{\partial\mathbf{U}_i^H}{\partial\boldsymbol{\Theta}}\frac{\partial\mathbf{U}_i}{\partial\boldsymbol{\Theta}^T}\Big]. \tag{7.28}$$

The derivative of $\mathbf{U}_i$ with respect to CFO of user u ϕ_u is denoted as $\mathbf{q}_{\phi,i,u}$, which is given by $\mathbf{q}_{\phi,i,u} = \frac{2\pi}{K}(\mathbf{H}_{\mathrm{I},u}\mathbf{L}\mathbf{E}_{\mathrm{G}}(\phi_u)\boldsymbol{\Psi}_u\mathbf{d}_{i,u} - \mathbf{H}_{\mathrm{Q},u}\mathbf{L}\mathbf{E}_{\mathrm{G}}(-\phi_u)\boldsymbol{\Psi}_u^*\mathbf{d}_{i,u}^*)$, with $\mathbf{L} = \mathrm{diag}\{0, \cdots, G-1\}$. Define $\mathrm{Re}\{h_{\mathrm{I},u}^{n_{\mathrm{r}}}(l)\}$ as the real part of the equivalent CIR response of user u $\mathbf{h}_{\mathrm{I},u}$ corresponding to its l-th path and n_{r}-th receive antenna. By taking the derivative of $\mathbf{U}_i$ with respect to $\mathrm{Re}\{h_{\mathrm{I},u}^{n_{\mathrm{r}}}(l)\}$, $\mathbf{q}_{\mathbf{h}_{\mathrm{I}},i,u,n_{\mathrm{r}},l} = \mathrm{circshift}(\mathbf{q}_l^1, n_{\mathrm{r}}, 1)\mathbf{E}(\phi_u)\boldsymbol{\Psi}_u\mathbf{d}_{i,u}$ yields, where $\mathbf{q}_l^1 = \mathrm{circshift}(\mathbf{q}^1, l, 2)$, and $\mathbf{q}^1$ is the same as $\mathbf{H}_u$ in (7.7), except that the elements with $h_u^0(L-1)$ in (7.7) are replaced by ones and all the other elements are by zeros. Thus, the derivative of $\mathbf{U}_i$ with respect to the real part of the u-

th equivalent CIR vector $\mathrm{Re}\{\mathbf{h}_{\mathrm{I},u}^T\}$ is obtained as $\mathbf{q}_{\mathbf{h}_{\mathrm{I}},i,u} = \left[\mathbf{q}_{\mathbf{h}_{\mathrm{I}},i,u,0}, \cdots, \mathbf{q}_{\mathbf{h}_{\mathrm{I}},i,u,N_{\mathrm{r}}-1}\right]$, where $\mathbf{q}_{\mathbf{h}_{\mathrm{I}},i,u,n_{\mathrm{r}}} = [\mathbf{q}_{\mathbf{h}_{\mathrm{I}},i,u,n_{\mathrm{r}},0}, \cdots, \mathbf{q}_{\mathbf{h}_{\mathrm{I}},i,u,n_{\mathrm{r}},L-1}]$ for $n_{\mathrm{r}} = 0, \cdots, N_{\mathrm{r}} - 2$ and $\mathbf{q}_{\mathbf{h}_{\mathrm{I}},i,u,n_{\mathrm{r}}} = [\mathbf{q}_{\mathbf{h}_{\mathrm{I}},i,u,N_{\mathrm{r}}-1,0}, \cdots, \mathbf{q}_{\mathbf{h}_{\mathrm{I}},i,u,N_{\mathrm{r}}-1,L-2}]$ for $n_{\mathrm{r}} = N_{\mathrm{r}} - 1$. Define $\mathbf{q}_{\mathbf{d}_{\mathrm{I}},i,u} = \mathbf{H}_{\mathrm{I},u}\mathbf{E}_{\mathrm{G}}(\phi_u)\mathbf{\Psi}_u + \mathbf{H}_{\mathrm{Q},u}\mathbf{E}_{\mathrm{G}}(-\phi_u)\mathbf{\Psi}_u^*$ and $\mathbf{q}_{\mathbf{d}_{\mathrm{Q}},i,u} = \mathbf{H}_{\mathrm{I},u}\mathbf{E}_{\mathrm{G}}(\phi_u)\mathbf{\Psi}_u - \mathbf{H}_{\mathrm{Q},u}\mathbf{E}_{\mathrm{G}}(-\phi_u)\mathbf{\Psi}_u^*$ as the derivative of $\mathbf{U}_i$ with respect to the real and imaginary parts of $\mathbf{d}_{i,u}$, respectively. Hence,

$$\frac{\partial \mathbf{U}_i^H}{\partial \mathbf{\Theta}} = [\jmath\mathbf{Q}_{\phi,i}, \mathbf{Q}_{\mathbf{h}_{\mathrm{I}},i}, \jmath\mathbf{Q}_{\mathbf{h}_{\mathrm{I}},i}, \mathbf{Q}_{\mathbf{h}_{\mathrm{Q}},i}, \jmath\mathbf{Q}_{\mathbf{h}_{\mathrm{Q}},i}, \mathbf{Q}_{\mathbf{d}_{\mathrm{I}},i}, \jmath\mathbf{Q}_{\mathbf{d}_{\mathrm{Q}},i}]^H \tag{7.29}$$

and

$$\frac{\partial \mathbf{U}_i}{\partial \mathbf{\Theta}^T} = [\jmath\mathbf{Q}_{\phi,i}, \mathbf{Q}_{\mathbf{h}_{\mathrm{I}},i}, \jmath\mathbf{Q}_{\mathbf{h}_{\mathrm{I}},i}, \mathbf{Q}_{\mathbf{h}_{\mathrm{Q}},i}, \jmath\mathbf{Q}_{\mathbf{h}_{\mathrm{Q}},i}, \mathbf{Q}_{\mathbf{d}_{\mathrm{I}},i}, \jmath\mathbf{Q}_{\mathbf{d}_{\mathrm{Q}},i}] \tag{7.30}$$

are obtained, where $\mathbf{Q}_{\phi,i} = [\mathbf{q}_{\phi,i,0}, \mathbf{q}_{\phi,i,1}, \cdots, \mathbf{q}_{\phi,i,U-1}]$; $\mathbf{Q}_{\mathbf{h}_{\mathrm{I}},i} = [\mathbf{q}_{\mathbf{h}_{\mathrm{I}},i,0}, \cdots, \mathbf{q}_{\mathbf{h}_{\mathrm{I}},i,U-1}]$; $\mathbf{Q}_{\mathbf{h}_{\mathrm{Q}},i}$ is obtained in a similar way to $\mathbf{Q}_{\mathbf{h}_{\mathrm{I}},i}$ but $\mathbf{q}_{\mathbf{h}_{\mathrm{I}},i,u,n_{\mathrm{r}},l} = \mathrm{circshift}(\mathbf{q}_l^1, n_{\mathrm{r}}, 1)\mathbf{E}_{\mathrm{G}}(\phi_u)\mathbf{\Psi}_u\mathbf{d}_{i,u}$ is replaced by $\mathbf{q}_{\mathbf{h}_{\mathrm{I}},i,u,n_{\mathrm{r}},l} = \mathrm{circshift}(\mathbf{q}_l^1, n_{\mathrm{r}}, 1)\mathbf{E}_{\mathrm{G}}(-\phi_u)\mathbf{\Psi}_u^*\mathbf{d}_{i,u}^*$; $\mathbf{Q}_{\mathbf{d}_{\mathrm{I}},i} = [\mathbf{q}_{\mathbf{d}_{\mathrm{I}},i,0}, \mathbf{q}_{\mathbf{d}_{\mathrm{I}},i,1}, \cdots, \mathbf{q}_{\mathbf{d}_{\mathrm{I}},i,U-1}]$; and $\mathbf{Q}_{\mathbf{d}_{\mathrm{Q}},i} = [\mathbf{q}_{\mathbf{d}_{\mathrm{Q}},i,0}, \mathbf{q}_{\mathbf{d}_{\mathrm{Q}},i,1}, \cdots, \mathbf{q}_{\mathbf{d}_{\mathrm{Q}},i,U-1}]$.

According to [128], the approximate FIM is computed by $\mathbf{\Pi}_{\mathrm{appro}} = \sum_{i=0}^{N_{\mathrm{s}}-1}\mathbf{\Pi}_i$. Thus, the CRLB for blind estimation of multiple CFOs and equivalent channels can be obtained as the diagonal elements of $\boldsymbol{\chi}_{\mathrm{appro}}$, where $\boldsymbol{\chi}_{\mathrm{appro}} = \mathbf{\Pi}_{\mathrm{appro}}^{-1}$. Since the CRLB on MSE of the equivalent channel estimation is derived assuming perfect elimination of channel ambiguities and IQ imbalance, it is unfair to compare it with the proposed JCCIQE scheme without perfect ambiguities and IQ imbalance elimination. Hence, similar to [161], the CRLB on MSE of CFO estimation is mainly investigated, which is given by

$$\mathrm{CRLB}_{\mathrm{CFO}} = \frac{1}{U}\sum_{v=0}^{U-1}\boldsymbol{\chi}_{\mathrm{appro}}(v, v). \tag{7.31}$$

7.4.2 Complexity Analysis

The complexity of the proposed JCCIQE scheme is analysed, in comparison to rank-reduction criterion based scheme [14] in Subsection 3.3.2 for multi-CFO and multi-channel estimation in OFDMA systems with generalised CAS, as there lacks work on

Table 7.1: Complexity analysis (K: Number of subcarriers per GFDMA subsymbol/OFDMA symbol, M: Number of subsymbols per GFDMA symbol, U: Number of users, L: Channel length, P_{pil}: Number of pilots, N_{r}: Number of receive antennas, N_{s}: Number of symbols in a frame, δ: Search step size in the coarse CFO estimation, ξ: Number of cost function evaluations in the fine CFO estimation, Δ: CFO search step size in [14], N/A: Not available).

<table>
<tr><th>Item</th><th>JCCIQE for GFDMA</th><th>Rank-reduction criterion [14] based scheme for OFDMA</th></tr>
<tr><td>Blind multi-CFO and multi-channel estimation</td><td>$2K^2M^2N_{\mathrm{r}}^2N_{\mathrm{s}} + K^3M^3N_{\mathrm{r}}^3 + K^2M^2(2K^2M^2 + 2KMN_{\mathrm{r}}L + 2N_{\mathrm{r}}^2L^2)(N_{\mathrm{r}} - 2)(\xi + 1/\delta)$</td><td>$U/\Delta(N_{\mathrm{s}}N_{\mathrm{r}}K(2K + \log_2 K) + 2N_{\mathrm{r}}N_{\mathrm{s}}(K - K/U)(K + N_{\mathrm{r}}) + N_{\mathrm{r}}^3) + U(2KN_{\mathrm{s}}N_{\mathrm{r}} + (N_{\mathrm{r}} - (U-1)L)^2)(N_{\mathrm{r}} - (U-1)L)$</td></tr>
<tr><td>Channel ambiguities elimination</td><td rowspan="2">$K^2M^2N_{\mathrm{r}}(2KMU + 18KM + 4) + 8K^3M^3 + 2P_{\mathrm{pil}}$</td><td>$(2L+6)(N_{\mathrm{r}} - (U-1)L)UP_{\mathrm{pil}}$</td></tr>
<tr><td>IQ imbalance elimination</td><td>N/A</td></tr>
<tr><td>Signal detection</td><td>$K^2M^2N_{\mathrm{r}}(32KM + 8N_{\mathrm{s}} + 4) + 8K^3M^3$</td><td>$(N_{\mathrm{r}} - (U-1)L)(2L+6)KN_{\mathrm{s}}$</td></tr>
</table>

estimation of CFOs, channels or IQ imbalance for GFDMA with generalised CAS. Their symbolic computational complexities are demonstrated in Table 7.1, in terms of the number of complex additions and multiplications. They are compared in four aspects, namely blind mutli-CFO and multi-channel estimation, channel ambiguities elimination, IQ imbalance elimination and signal detection. The complexity of blind multi-CFO and multi-channel estimation depends on the CFO search step size, which is denoted by δ for JCCIQE and Δ for rank-reduction criterion based scheme [14], respectively. Meanwhile, the proposed JCCIQE scheme computes the second-order statistics of the received signal and implements EVD for only once, while U/Δ times of such calculation and implementation are demanded for rank-reduction criterion based scheme [14]. Usually, there is a trade-off for the choice of the CFO search step size between the estimation accuracy and computational complexity. For example, a smaller step size contributes to a higher CFO estimation accuracy, while at the expense of a large number of computations. Thanks to the two-step CFO search of the proposed JCCIQE scheme, the coarse CFO search step size δ of JCCIQE can be chosen to be much larger than the CFO search step size Δ of rank-reduction criterion based scheme [14]. Regarding the fine CFO search of the proposed JCCIQE scheme, the number of cost function evaluations ξ is counted when implementing the golden section search and parabolic interpolation algorithms, which is shown to be less than 10 by simulation, making its complexity negligible compared to that of coarse CFO search. It is also noteworthy that the proposed JCCIQE scheme is capable of eliminating channel ambiguities and IQ imbalance jointly, while rank-reduction criterion based scheme [14] does not take into account IQ imbalance elimination.

Table 7.2: Normalised numerical complexity ($K = 16$, $U = 2$, $L = 3$, $P_{\text{pil}} = 8$, $N_{\text{r}} = 4$, $N_{\text{s}} = 200$, $\delta = 0.01$, $\xi = 6$, $\Delta = 0.001$, N/A: Not available).

Item	JCCIQE for OFDMA ($M = 1$)	JCCIQE for GFDMA ($M = 2$)	Rank-reduction criterion based scheme [14] for OFDMA
Blind multi-CFO and multi-channel estimation	2×10^5	1.3×10^6	7.5×10^6
Channel ambiguities elimination	2.1×10^3	1.7×10^4	1
IQ imbalance elimination			N/A
Signal detection	1.1×10^4	5.7×10^4	2×10^2
Total	2.1×10^5	1.4×10^6	7.5×10^6

The normalised numerical complexity analysis is provided in Table 7.2, by setting the number of subcarriers for each of $M = 2$ GFDMA subsymbol and each of OFDMA symbol to $K = 16$, the number of users to $U = 2$, the channel length to $L = 3$, the number of pilots to $P_{\text{pil}} = 8$, the number of receive antennas to $N_{\text{r}} = 4$, the frame length to $N_{\text{s}} = 200$, the search step size in coarse CFO estimation of the JCCIQE scheme to $\delta = 0.01$, the number of cost function evaluations to $\xi = 6$, and the CFO search step size for rank-reduction criterion based scheme [14] to $\Delta = 0.001$. The numerical complexity of the proposed JCCIQE scheme for OFDMA systems by setting $M = 1$ is also included for comparison. It can be seen that multi-CFO and multi-channel estimation dominates the overall complexity of both JCCIQE and rank-reduction criterion based [14] schemes.

In OFDMA systems, the proposed JCCIQE scheme has much higher computational efficiency than rank-reduction criterion based scheme [14], with up to 36-fold complexity reduction, which shows the superiority and generality of JCCIQE. The complexity of JCCIQE for GFDMA systems is approximately 5-fold lower than that of rank-reduction criterion based scheme [14] for OFDMA systems.

7.5 Simulation Results

7.5.1 Simulation Setup

Monte Carlo simulations have been carried out to demonstrate the performance of the proposed JCCIQE scheme for SIMO GFDMA systems with generalised CAS in the presence of CFOs and IQ imbalance. Since there lacks research on estimation of CFOs, channels and IQ imbalance for GFDMA with generalised CAS, the rank-reduction criterion based CFO estimation scheme for OFDMA [14] described in Subsection 3.3.2 is adopted as a benchmark. Also, a single-user GFDM system is simulated for comparison, which conducts the PN sequence based CFO estimation approach in [3], and the low-complexity IQ imbalance estimation in [15] and the LS channel estimation in [9] consecutively. Note that LS channel estimation [9] and PN sequence based CFO estimation approach [3] for GFDM are respectively a variant of LS channel estimator and Moose's CFO estimator for OFDM in Subsections 3.2.1 and 3.3.2, whereas a brief description of low-complexity IQ imbalance estimation approach [15] for GFDM refers to Subsection 3.4.2. The CRLB on multi-CFO estimation derived in Subsection 7.4.1 is also exploited as a benchmark in Figs. 7.5, 7.6 and 7.7.

System parameters are specified as follows. Each GFDMA subsymbol includes $K = 16$ subcarriers. Each GFDMA symbol contains $M = 2$ subsymbols, except for Figs. 7.8 and 7.10. The number of users is $U = 2$, except for Fig. 7.4. The receiver is equipped with $N_{\mathrm{r}} = 4$ antennas. The channel follows an exponential delay profile with channel length of $L = 3$ and the normalised root mean square delay spread of 1.5. The CP length is $L_{\mathrm{cp}} = 4$. Each frame has a length of $N_{\mathrm{s}} = 200$ symbols, except for Fig. 7.10.

Generalised CAS is adopted, except for Fig. 7.7. The CFOs are randomly generated in the range of $[-0.4, 0.4)$ [14]. Root raised cosine prototype filter with roll-off coefficient of 0.4 [109] is utilised for GFDMA. The symmetric IQ imbalance model is adopted, except for Figs. 7.5 and 7.9, with its amplitude and phase mismatches set to $\upsilon = 0.2$ and $\theta = 10°$, respectively. $\delta = 0.01$ is chosen for the coarse CFO estimation of the proposed JCCIQE scheme [142]. QPSK modulation is utilised.

The number of pilots for joint elimination of channel ambiguities and IQ imbalance is set to $P_{\text{pil}} = 8$, contributing to the training overhead of 0.125%, except for Fig. 7.11. Rank-reduction criterion based scheme [14] for OFDMA adopts the same number of pilots as that of the proposed JCCIQE scheme. Regarding the single-user GFDM system [3, 9, 15], two identical subsymbols are exploited to estimate CFO first, and one GFDM symbol is utilised to estimate IQ imbalance and channel, respectively, unless otherwise specified. The total number of pilots in the single-user GFDM system [3,9,15] is 96 pilots, which is 12-fold more than that of the proposed JCCIQE scheme.

The MSE of CFO estimation, and the MSE of the equivalent channel estimation with IQ imbalance included are respectively defined as

$$\text{MSE}_{\text{CFO}} = \frac{1}{U} \sum\nolimits_{u=0}^{U-1} \mathbb{E}\{(\hat{\phi}_u - \phi_u)^2\} \tag{7.32}$$

and

$$\text{MSE}_{\text{Channel,IQ}} = \frac{1}{2UN_{\text{r}}L} \sum\nolimits_{u=0}^{U-1} \mathbb{E}\{(\| \hat{\mathbf{h}}_{\text{I},u} - \mathbf{h}_{\text{I},u} \|_{\text{F}}^2 + \| \hat{\mathbf{h}}_{\text{Q},u} - \mathbf{h}_{\text{Q},u} \|_{\text{F}}^2)\}. \tag{7.33}$$

7.5.2 BER Performance

Fig. 7.3 demonstrates the BER performance of the proposed JCCIQE scheme for GFDMA, in comparison to rank-reduction criterion based scheme for OFDMA [14] and the single-user GFDM system with the approaches in [3, 9] and [15]. The proposed JC-CIQE scheme for GFDMA significantly outperforms the existing approaches [3,9,14,15]. Its performance is close to that of the ideal case with perfect estimation of CFOs, chan-

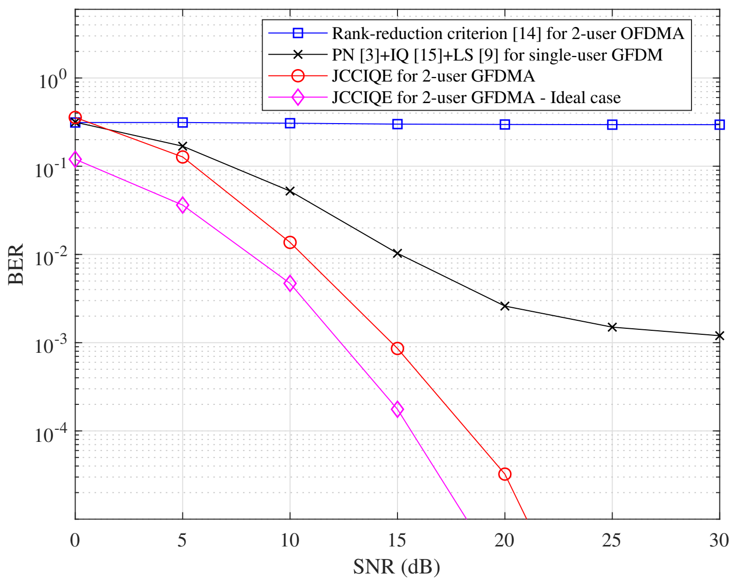

Figure 7.3: BER with $N_\mathrm{s} = 200$ GFDMA symbols each with $M = 2$ subsymbols, $N_\mathrm{r} = 4$ receive antennas, symmetric IQ imbalance and generalised CAS;
Ideal case: perfect estimation of CFOs, channels and IQ imbalance.

nels and IQ imbalance. For instance, at a BER of 10^{-3}, the proposed JCCIQE scheme achieves an SNR gain of approximately 15 dB over the single-user GFDM system. Since the single-user GFDM system estimates the CFO, IQ imbalance and channel separately, without considering their impacts on one another, it suffers an error floor at medium to high SNR. Rank-reduction criterion based scheme [14] demonstrates the worst performance at all SNRs. This is because rank-reduction criterion based scheme [14] requires at least $N_\mathrm{r} = 6$ receive antennas to work effectively with $U = 2$ and $L = 3$, while the proposed scheme only requires the number of receive antennas to be larger than or equal to $N_\mathrm{r} = 2$, which is independent of the number of users, as discussed in Subsection 7.3.1.

Fig. 7.4 shows the outage probabilities of the proposed JCCIQE scheme and rank-reduction criterion based scheme [14] with $U = 4$ users and $N_\mathrm{r} = 4$ receive antennas, at SNR=12 dB, 15 dB and 18 dB. The outage probability is defined as the probability of the system BER being larger than a threshold λ. The proposed JCCIQE scheme demonstrates a much lower outage probability than that of rank-reduction criterion

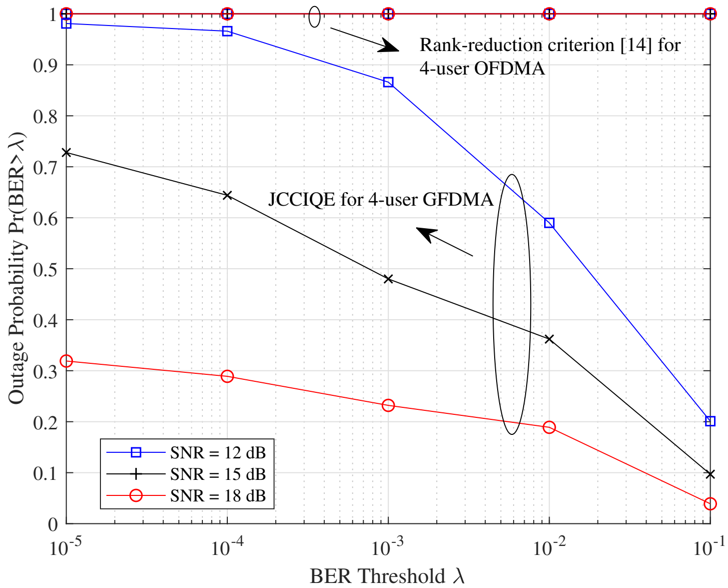

Figure 7.4: Outage probability with $U = 4$ users, $N_\mathrm{r} = 4$ receive antennas, $N_\mathrm{s} = 200$ GFDMA symbols each with $M = 2$ subsymbols, symmetric IQ imbalance and generalised CAS.

based scheme [14], which has an outage probability of one regardless of the values of SNR and BER threshold. This is because rank-reduction criterion based scheme [14] demands at least $N_\mathrm{r} = 12$ receive antennas with $U = 4$ and $L = 3$, while the proposed scheme only requires the number of receive antennas to be no less than $N_\mathrm{r} = 2$, same as that in Fig. 7.3.

7.5.3 MSE of CFO Estimation

Fig. 7.5 shows the MSE of CFO estimation of the proposed JCCIQE scheme in the absence of IQ imbalance, in comparison to rank-reduction criterion based scheme [14] for OFDMA and PN sequence based approach [3] for single-user GFDM, neither of which considered IQ imbalance in their system models. The proposed JCCIQE scheme demonstrates a substantially lower MSE performance than the approaches in [3] and [14]. For example, at an MSE of 10^{-6}, the proposed JCCIQE scheme achieves an SNR gain of approximately 10 dB and 15 dB over PN sequence based approach [3] and rank-

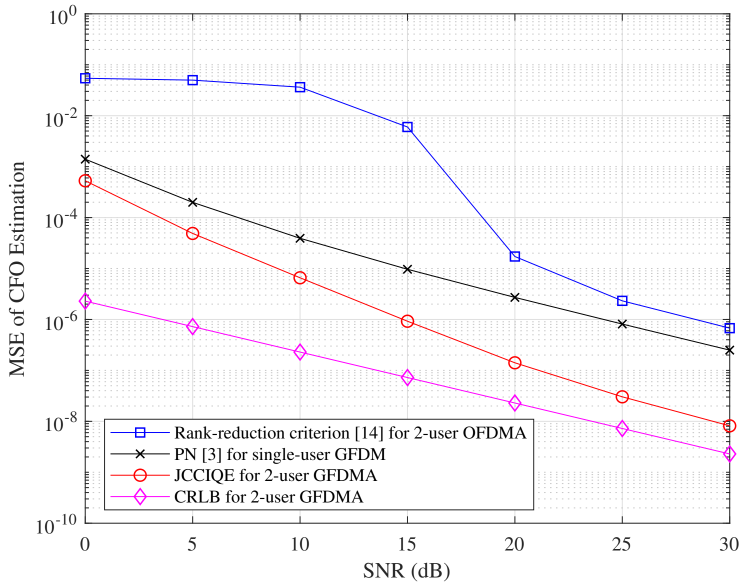

Figure 7.5: MSE of CFO estimation in the absence of IQ imbalance, with $N_{\mathrm{s}} = 200$ GFDMA symbols each with $M = 2$ subsymbols, $N_{\mathrm{r}} = 4$ receive antennas, and generalised CAS.

reduction criterion based scheme [14], respectively. Its MSE performance is close to the CRLB especially at high SNR.

Fig. 7.6 exhibits the MSE of CFO estimation of the proposed JCCIQE scheme with symmetric IQ imbalance, rank-reduction criterion based scheme [14] and PN sequence based approach [3]. The proposed JCCIQE scheme has a performance closer to the CRLB at low SNR, compared to Fig. 7.5. This is because a smaller number of low-accuracy noise eigenvectors are utilised for blind multi-CFO estimation with IQ imbalance than that without IQ imbalance, which could mitigate the impact of noise. The proposed scheme presents a much larger performance gain over rank-reduction criterion based scheme [14] and PN sequence based approach [3] with IQ imbalance than without IQ imbalance, compared to Fig. 7.5, while the latter two approaches [3, 14] with IQ imbalance suffer an error floor at medium to high SNR.

Fig. 7.7 shows the impact of various CASs on MSE of CFO estimation of the proposed JCCIQE scheme and rank-reduction criterion based scheme [14]. The proposed

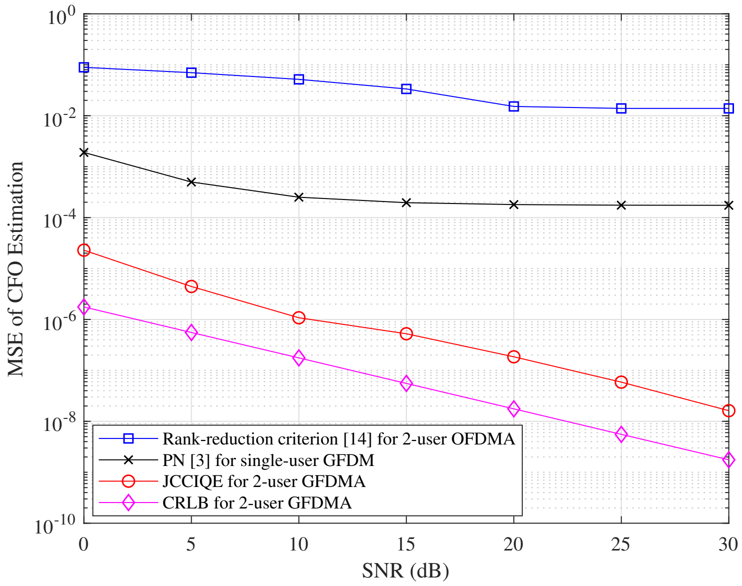

Figure 7.6: MSE of CFO estimation, with symmetric IQ imbalance, $N_{\mathrm{s}} = 200$ GFDMA symbols each with $M = 2$ subsymbols, $N_{\mathrm{r}} = 4$ receive antennas, and generalised CAS.

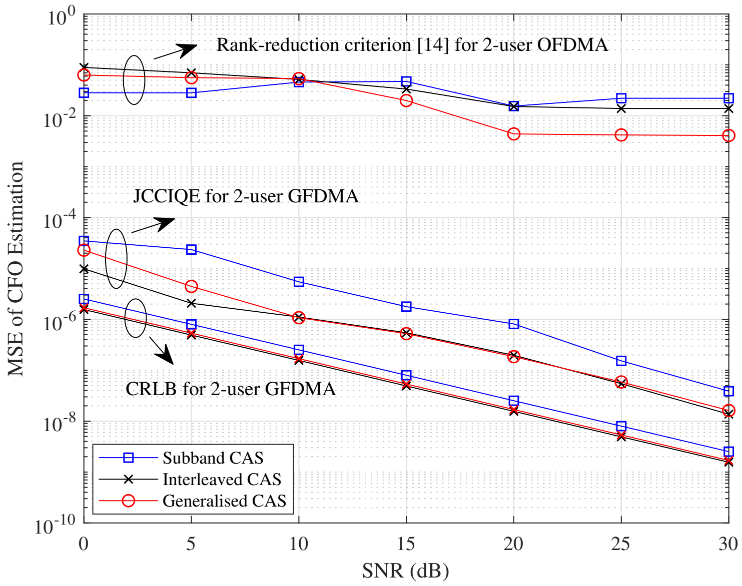

Figure 7.7: Impact of CAS on MSE of CFO estimation, with $N_{\mathrm{s}} = 200$ GFDMA symbols each with $M = 2$ subsymbols, $N_{\mathrm{r}} = 4$ receive antennas, and symmetric IQ imbalance.

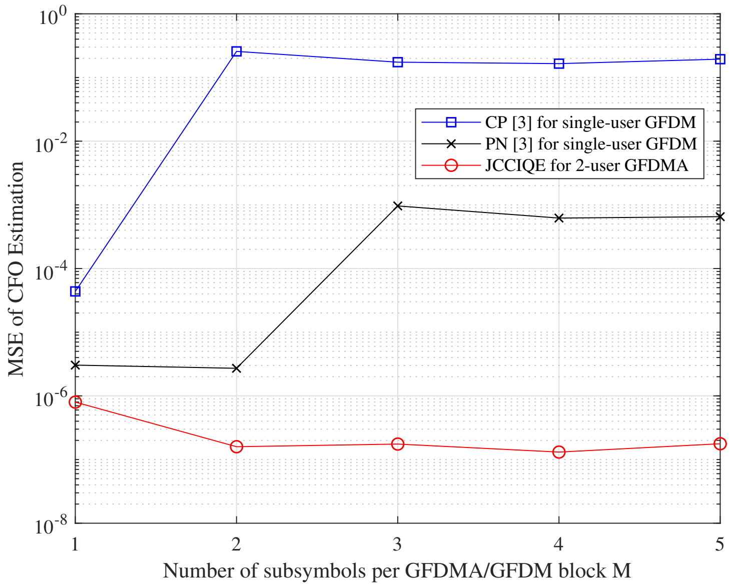

Figure 7.8: Impact of the number of subsymbols per GFDMA/GFDM symbol on MSE of CFO estimation at SNR=20 dB, with $N_\mathrm{r} = 4$ receive antennas, $N_\mathrm{s} = 200$ symbols and symmetric IQ imbalance.

JCCIQE scheme is robust against various CASs. Its performance is slightly worse with subband CAS, due to deep fade caused by frequency selective fading [55]. Its MSEs achieved are also close to the CRLBs with different CASs. The performance of JCCIQE scheme is much better than that of rank-reduction criterion based scheme [14] for all types of CAS.

Fig. 7.8 demonstrates the impact of the number of subsymbols per GFDMA/GFDM symbol on MSE of CFO estimation of the proposed JCCIQE scheme, in comparison to PN sequence [3] and CP [3] based approaches at SNR=20 dB. The proposed JCCIQE scheme is robust against the number of subsymbols M, since its blind CFO estimation is independent of ISI and CFO estimation range, as discussed in Subsection 7.3.2. In contrast, the CP and PN sequence based approaches in [3] demonstrate poor performance when $M \geq 2$ and $M \geq 3$, respectively. This is because CFO estimation range of CP based approach [3] is $[-0.5/M, 0.5/M)$, and PN sequence approach with two identical subsymbols [3] is likely to suffer severe ISI when $M \geq 3$, as mentioned in Subsection

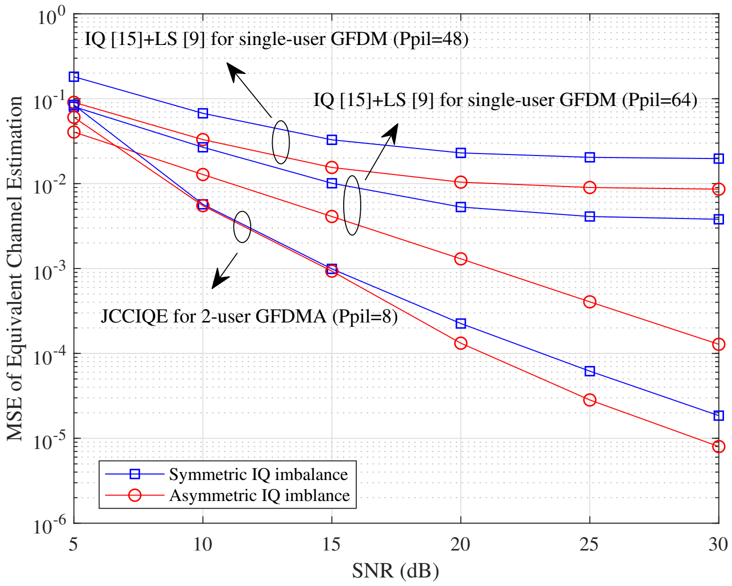

Figure 7.9: MSE of equivalent channel estimation in the presence of the symmetric and asymmetric IQ imbalances, with $N_{\mathrm{s}} = 200$ GFDMA symbols each with $M = 2$ subsymbols, $N_{\mathrm{r}} = 4$ receive antennas, and generalised CAS.

3.3.2.

7.5.4 MSE of Equivalent Channel Estimation

Fig. 7.9 shows the MSE of equivalent channel estimation of the proposed JCCIQE scheme with symmetric and asymmetric IQ imbalances and pilot length of $P_{\mathrm{pil}} = 8$, in comparison to the single-user GFDM system [15] [9] with $P_{\mathrm{pil}} = 48$ and $P_{\mathrm{pil}} = 64$. To avoid an error propagation from CFO estimation, perfect frequency synchronisation is assumed for both systems. The single-user GFDM system [15] [9] requires at least one symbol to estimate IQ imbalance and thus cannot work with $P_{\mathrm{pil}} = 8$. As mentioned in Section 7.5.1, one symbol is exploited to estimate IQ imbalance [15] and channel [9], respectively, giving rise to the pilot length of $P_{\mathrm{pil}} = 64$ for the single-user GFDM system. Thanks to the ICI and ISI mitigation by utilising two symbols as pilots, the single-user GFDM system with the asymmetric IQ imbalance and $P_{\mathrm{pil}} = 64$ does not suffer an error floor caused by ICI and ISI. Regarding the single-user GFDM system with $P_{\mathrm{pil}} = 48$, IQ

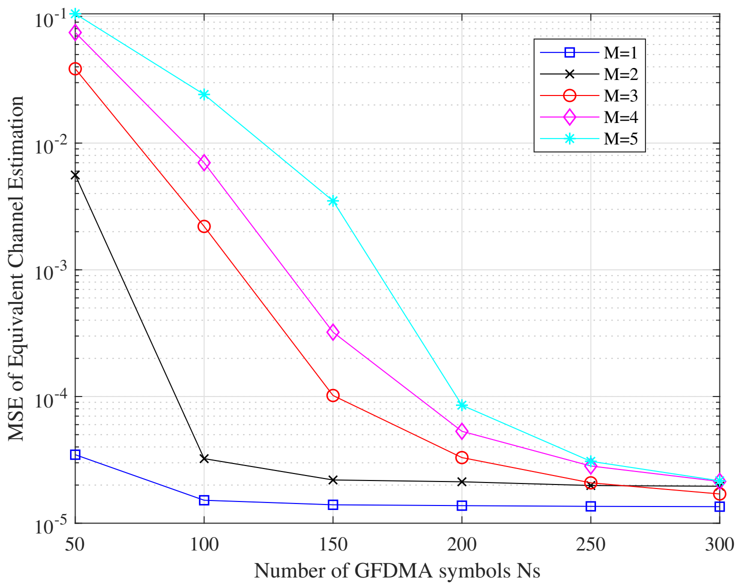

Figure 7.10: Impacts of the number of subsymbols per GFDMA symbol and the number of GFDMA symbols on MSE of equivalent channel estimation at SNR=30 dB, with $U = 2$ users, $N_\mathrm{r} = 4$ receive antennas, symmetric IQ imbalance and generalised CAS.

imbalance and channel are estimated by one symbol (32 pilots) and one subsymbol (16 pilots), respectively, which suffers an error floor due to the severe ICI and ISI from the data subsymbol. The single-user GFDM system has a biased MSE performance with symmetric IQ imbalance regardless of the value of P_pil, since the approach in [15] works effectively for asymmetric IQ imbalance only. In contrast, the proposed JCCIQE scheme with up to 8-fold training overhead reduction over the single-user GFDM system [9, 15] achieves a comparable MSE performance between the symmetric and asymmetric IQ imbalances.

Fig. 7.10 exhibits the impacts of the number of subsymbols per GFDMA symbol and the number of GFDMA symbols on MSE of equivalent channel estimation of the proposed JCCIQE scheme, at SNR=30 dB. For all values of M, utilising more GFDMA symbols lowers the MSE of channel estimation substantially. Given the number of GFDMA symbols, the performance of the proposed JCCIQE scheme deteriorates as the value of M increases. This is because the size of GFDMA symbol increases with M,

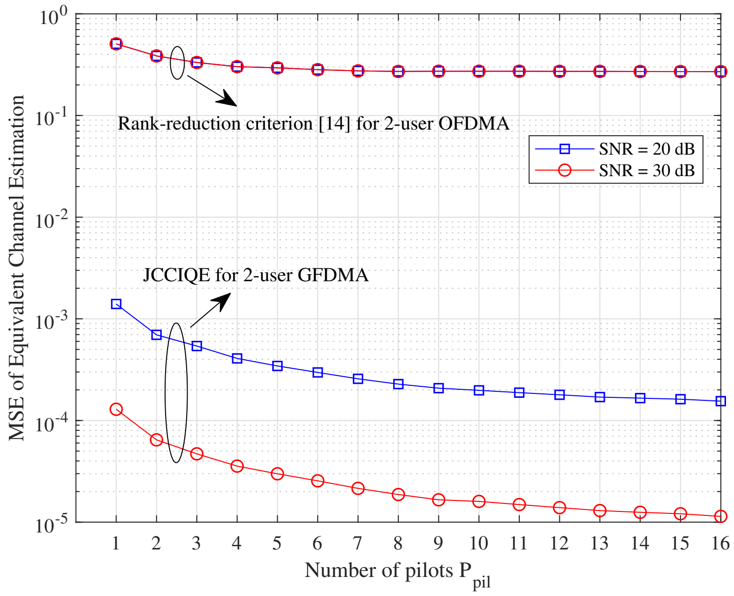

Figure 7.11: Impact of the number of pilots on MSE of equivalent channel estimation at SNR=20 dB and 30 dB, with $U = 2$ users, $N_\mathrm{s} = 200$ GFDMA symbols each with $M = 2$ subsymbols, $N_\mathrm{r} = 4$ receive antennas, symmetric IQ imbalance and generalised CAS.

which in turn requires more GFDMA symbols to achieve a good second-order statistics of the received signal for blind CFO and channel estimation.

Fig. 7.11 demonstrates the impact of the number of pilots on MSE of equivalent channel estimation of the proposed JCCIQE scheme, in comparison to rank-reduction criterion based scheme [14] for OFDMA, at SNR=20 dB and 30 dB. JCCIQE significantly outperforms rank-reduction criterion based scheme [14] with loose limitation on the number of receive antennas. Its performance improves with pilot length and reaches a steady state at $P_\mathrm{pil} = 8$ pilots.

7.6 Summary

A semi-blind estimation scheme has been proposed for GFDMA systems, taking into account multiple performance limiting factors at the same time, namely, CAS, CFO, IQ imbalance, channel estimation, training overhead, ICI and ISI, as summarised in

Table 7.3: Comparison of the proposed JCCIQE scheme and the existing approaches [3, 9, 14, 15].

Item	JCCIQE	Rank-reduction criterion [14]	PN [3]	CP [3]	LS [9]	IQ [15]
System	GFDMA	OFDMA	Single-user GFDM	Single-user GFDM	Single-user GFDM	Single-user GFDM
CAS	Generalised	Generalised	N/A	N/A	N/A	N/A
fCFO estimation	✓	✓	✓	✓	✗	✗
Symmetric IQ imbalance	✓	✗	✗	✗	✗	✗
Asymmetric IQ imbalance	✓	✗	✗	✗	✗	✓
Channel estimation	✓	✓	✗	✗	✓	✗
Training overhead	Low	Low	High	Low	High	High
Robustness against ICI and ISI	High	N/A	Low	High	Low	Low
Complexity	Medium	High	Low	Low	Low	Low
Receive antennas	Multiple	Massive	Single	Single	Single	Single
Number of symbols for blind estimation	Hundreds	Tens	N/A	N/A	N/A	N/A

Table 7.3 against other approaches [3, 9, 14, 15]. The proposed JCCIQE scheme has much lower training overhead of 0.125% with the frame length of 200 symbols, which is approximately 12-fold lower than that of the existing pilot assisted approaches [3,9,15]. Besides, no signalling feedback is demanded thanks to multi-CFO compensation performed at receive side, unlike [157]. JCCIQE demonstrates much superior performances in terms of BER, outage probability, MSE of CFO estimation and MSE of equivalent channel estimation than the existing methods [3,9,14,15]. The performance of JCCIQE approaches that of its counterpart with perfect estimation of all parameters as well as the CRLB on MSE of CFO estimation. In addition, it is robust against CAS and does not suffer any error floors caused by the ICI and ISI encountered in the previous pilot assisted approaches [3,9]. It achieves a comparable performance between the asymmetric and symmetric IQ imbalance unlike the approach in [15] which works for asymmetric IQ imbalance only.

Owing to the semi-blind implementation, the proposed JCCIQE scheme is less computationally efficient than the existing pilot assisted approaches [3, 9, 15]. However, it has a complexity reduction of tens of times over the semi-bind rank-reduction criterion based scheme in [14], thanks to the initial coarse CFO estimation and the following fine CFO estimation. Similar to Chapters 5 and 6, the proposed JCCIQE scheme also requires multiple antennas at the receiver, whose number however is much smaller than that demanded in [14]. In addition, the number of received symbols for blind channel estimation should be reduced to make the JCCIQE scheme feasible for the short-frame communications systems. Future work should take into account the integer CFO estimation as well.

Chapter 8

Conclusions and Future Work

8.1 Conclusions

Multi-carrier techniques are of great importance for 5G and B5G wireless communication systems, since they are capable of offering high data rate as well as high robustness against frequency selective fading. An overview of wireless communications is given in Chapter 2. Herein, OFDM has been adopted as the 5G waveform, thanks to its high spectral efficiency and low-complexity equaliser design, while GFDM is considered as a potential waveform for B5G network as it is flexible to cater for the diverse service requirements in B5G. Chapter 3 first gives an introduction and background of RF channel and impairments, and then reviews the existing estimation approaches for them. The estimation of RF impairments and channels is an indispensable stage for multi-carrier communication systems to guarantee their effectiveness. As a result, a comprehensive study on the estimation of RF impairments and channels has been carried out in this thesis for multi-carrier 5G and B5G, including OFDM based systems in Chapters 4 and 5 as well as GFDM based systems in Chapters 6 and 7. Table 8.1 summarises and compares the four proposals in many aspects.

In Chapter 4, a pilot assisted joint multi-TOA and multi-CFO estimation scheme is proposed for multi-user OFDM systems. It enjoys low computational complexity, where the complex multi-dimensional estimation problem can be decomposed into a number of low-complexity one-dimensional estimation problems, by means of the carefully designed pilot with Hadamard matrix. Besides, each TOA and each CFO can be estimated independently of each other and in closed-form by the ESPRIT algorithm. The CFO estimation performance can be further enhanced by the proposed NS-CFO estimator to approach the derived CRLB. However, this work has a serious issue of high training overhead, whose pilot length increases with the number of users. For the sake of high spectral efficiency, the semi-blind subspace-based estimation approach is proposed for the estimation of RF impairments and channels in Chapters 5, 6 and 7, respectively.

In Chapter 5, an iterative semi-blind scheme is proposed for the estimation of channels and CFO in short-frame FD OFDM systems. By deriving an equivalent system model with CFO included implicitly, the estimation of channels and CFO are conducted with two stages. First, the subspace-based blind channel estimation is performed by a short frame with tens of received symbols, after which the CFO and channel ambiguities can be estimated with a single symbol by the PM based channel estimation approach. Then, both channel and CFO estimates are refined iteratively by making use of the detected data symbols, and attain convergence within 3 iterations. Meanwhile, closed-form solutions are provided for both channel and CFO at each iteration. The proposed iterative semi-blind scheme exhibits a close performance to the CRLB, while at the expense of medium complexity owing to the iterative and semi-blind implementation. Unlike the proposal in Chapter 4, the subspace-based proposals in Chapters 5, 6 and 7 can work with multiple receive antennas only.

In Chapter 6, a robust semi-blind estimation scheme of channel and CFO has been proposed for single-user GFDM systems. Similarly to Chapter 5, by deriving an equivalent system model with CFO included implicitly, channel is first estimated blindly with tens of received symbols by subspace. After that, the fractional and integer parts of CFO are estimated in series with the help of a small number of nulls, while channel ambiguity is eliminated by very few pilots. The proposed scheme exhibits high robustness against ICI and ISI caused by the GFDM nonorthogonal filters. Albeit of high spectral efficiency, the proposed scheme suffers high computational complexity, due to the exhaustive search for iCFO and fCFO, respectively.

Unlike the work in Chapters 4, 5 and 6 includes channel and CFO only, IQ imbalance either in symmetric or asymmetric is taken into account in Chapter 7. Considering multiple users, a semi-blind joint estimation scheme of multiple channels, multiple CFOs and IQ imbalance is proposed for GFDMA systems with generalised CAS in Chapter 7. Thanks to the subspace approach, multiple CFOs and multiple channels are separated by users first. Then, for each individual user, CFO is estimated by minimising the smallest eigenvalue whose corresponding eigenvector is exploited to blindly determine the channel. Finally, IQ imbalance parameters and channel ambiguities are estimated jointly by very few pilots. The proposed scheme has a close performance to its counterpart with perfect estimation of all parameters as well as CRLB on MSE of CFO estimation. The resulted training overhead is approximately 12-fold lower than that of the previous pilot assisted approaches. Similarly to Chapter 6, it is also more robust against the ICI and ISI due to the GFDM nonorthogonal filters. Unlike Chapter 6, CFO here is estimated in two stages with a coarse CFO search first and then a fine CFO search to reduce the complexity. In contrast to the work in Chapters 5 and 6, hundreds of received symbols are demanded for semi-blind estimation in Chapter 7.

To summarise, the estimation of RF impairments and channels is investigated for four multi-carrier 5G and B5G systems in this thesis, considering two multi-carrier techniques with OFDM and GFDM, two duplex modes with HD and FD, and serving both single user and multiple users. The proposed estimation approaches are either assisted by pilot with low complexity or semi-blind with high spectral efficiency. The proposed CFO estimators are either computationally efficient with closed-form solutions or aided by a direct search with high accuracy. Hence, this thesis has provided a thorough investigation on the estimation of RF impairments and channels for multi-carrier 5G and B5G systems, which would have profound significance in promoting the future development of this topic.

Table 8.1: Comparison of four proposals in this thesis.

<table>
<tr><td colspan="2">Proposals</td><td>Chapter 4</td><td>Chapter 5</td><td>Chapter 6</td><td>Chapter 7</td></tr>
<tr><td colspan="2">Multi-carrier technique</td><td>OFDM</td><td>OFDM</td><td>GFDM</td><td>GFDM</td></tr>
<tr><td colspan="2">Duplex mode</td><td>HD</td><td>FD</td><td>HD</td><td>HD</td></tr>
<tr><td colspan="2">Users</td><td>Multiple</td><td>Single</td><td>Single</td><td>Multiple</td></tr>
<tr><td colspan="2">Receive Antennas</td><td>Single/Multiple</td><td>Multiple</td><td>Multiple</td><td>Multiple</td></tr>
<tr><td rowspan="2">Channel estimation</td><td>TOA</td><td>✓</td><td rowspan="2">✓</td><td rowspan="2">✓</td><td rowspan="2">✓</td></tr>
<tr><td>Other parameters</td><td>✗</td></tr>
<tr><td rowspan="2">CFO estimation</td><td>iCFO</td><td>✓</td><td>✓</td><td>✓</td><td>✗</td></tr>
<tr><td>fCFO</td><td>✓</td><td>✓</td><td>✓</td><td>✓</td></tr>
<tr><td colspan="2">IQ imbalance estimation</td><td>✗</td><td>✗</td><td>✗</td><td>✓</td></tr>
<tr><td colspan="2">Estimation approach</td><td>Pilot</td><td colspan="3">Semi-blind by subspace</td></tr>
<tr><td colspan="2">Training overhead</td><td>High</td><td>Low</td><td>Low</td><td>Low</td></tr>
<tr><td colspan="2">Complexity</td><td>Low</td><td>Medium</td><td>High</td><td>Medium</td></tr>
<tr><td colspan="2">Number of received symbols for semi-blind estimation</td><td>N/A</td><td>Tens</td><td>Tens</td><td>Hundreds</td></tr>
</table>

8.2 Future Work

A number of possible continuations of the work in this thesis are listed in the following:

- A single user is considered for GFDM in Chapter 6. B5G network is anticipated to support a massive number of users especially for IoT applications. It is of big significance to extend the work in Chapter 6 to multi-user GFDM systems, where multiple users share frequency resources simultaneously.

- The proposed multi-CFO, multi-channel and IQ imbalance estimation scheme for GFDMA systems in Chapter 7 demands a large number of received symbols, which makes it unsuitable for short-frame communications. Short-frame communications are a key enabler to support URLLC and eURLLC in 5G and B5G networks. It is considerable to extend the proposed work in Chapter 7 to short-frame communications, which is left for future work. The integer CFO should be included as well.

- This thesis focuses on estimation of time-invariant frequency selective fading channel, where channel maintains constant over a frame. With the expeditious development of high-speed railways and V2X communications, the research for high-mobility wireless communications, where channel changes rapidly within a symbol, has gained overwhelming interest in both academia and industry. The estimation of time-varying channel(s) and/or RF impairment(s) is confronted with numerous new challenges. For instance, the number of pilots is likely to increase due to the increased number of channel parameters to be estimated. Basis expansion model is exploited to model time-varying channel, in order to reduce the number of channel parameters to be estimated. Based on this model, expectation maximisation has been developed as an effective approach to estimate time-varying channel and/or RF impairment(s), which however not only suffers high training overhead but also is computationally inefficient due to the exhaustive iterative search. Thus, it is worth investigating the low-complexity semi-blind estimation for channel(s) and/or RF impairment(s) in the future. It is also considerable to study the new modulation technique orthogonal time frequency space, which is able to convert the time-varying channel in time-frequency domain into time-invariant channel in the delay-Doppler domain.

- Machine learning has been successfully applied to numerous fields, such as image recognition, computer vision, automatic control, and so forth. Recently, it is regarded as an important technology to spearhead the emergence of B5G networks. The proposed solutions in this thesis are based on either pilots or semi-blind subspace-based approach utilising the second-order statistics of the received signal. Signal detection is performed after the estimates of channel(s) and RF impairment(s) are obtained consecutively. The implementation is trivial. By utilising machine learning technique, signal detection problem for wireless communication systems in the presence of RF impairments can be solved without requiring explicit estimation of channel and RF impairments. Since learning phase can be performed offline, the training overhead is expected to be reduced greatly, especially for IoT applications with massive number of devices and complex channel conditions. Thereby, it is an interesting topic to investigate and explore in the future.

Bibliography

[1] Y. S. Cho, J. Kim, W. Y. Yang, and C. G. Kang, *MIMO-OFDM wireless communications with MATLAB.* John Wiley & Sons, 2010.

[2] N. Michailow, M. Matthé, I. S. Gaspar, A. N. Caldevilla, L. L. Mendes, A. Festag, and G. Fettweis, "Generalized frequency division multiplexing for 5th generation cellular networks," *IEEE Transactions on Communications*, vol. 62, no. 9, pp. 3045–3061, Sep. 2014.

[3] Z. Na, M. Zhang, M. Xiong, J. Xia, X. Liu, and W. Lu, "Pseudo-noise sequence based synchronization for generalized frequency division multiplexing in 5G communication system," *IEEE Access*, vol. 6, pp. 14 812–14 819, 2018.

[4] G. Durisi, T. Koch, and P. Popovski, "Toward massive, ultrareliable, and low-latency wireless communication with short packets," *Proceedings of the IEEE*, vol. 104, no. 9, pp. 1711–1726, Sep. 2016.

[5] R. Heath and A. Lozano, *Foundations of MIMO Communication.* Cambridge University Press, 2018. [Online]. Available: https://books.google.com.sg/books?id=3o92DwAAQBAJ

[6] V. U. Prabhu and D. Jalihal, "An improved ESPRIT based time-of-arrival estimation algorithm for vehicular OFDM systems," in *Proc. IEEE VTC-Spring*, Barcelona, Spain, Apr. 2009, pp. 1–4.

[7] Y. Jiang, H. Minn, X. Gao, X. You, and Y. Li, "Frequency offset estimation and training sequence design for MIMO OFDM," *IEEE Transactions on Wireless Communications*, vol. 7, no. 4, pp. 1244–1254, Apr. 2008.

[8] W. Zhang, Q. Yin, and W. Wang, "Blind closed-form carrier frequency offset estimation for OFDM with multi-antenna receiver," *IEEE Transactions on Vehicular Technology*, vol. 64, no. 8, pp. 3850–3856, Aug. 2015.

[9] S. Ehsanfar, M. Matthe, D. Zhang, and G. Fettweis, "Theoretical analysis and CRLB evaluation for pilot-aided channel estimation in GFDM," in *Proc. IEEE GLOBECOM 2016*, Washington, DC, USA, Dec. 2016, pp. 1–7.

[10] A. Farhang, N. Marchetti, and L. E. Doyle, "Low-complexity modem design for GFDM," *IEEE Transactions on Signal Processing*, vol. 64, no. 6, pp. 1507–1518, Mar. 2016.

[11] I. S. Gaspar, L. L. Mendes, N. Michailow, and G. Fettweis, "A synchronization technique for generalized frequency division multiplexing," *EURASIP Journal on Advances in Signal Processing*, vol. 2014, no. 1, p. 67, May 2014.

[12] Y. Zeng, A. R. Leyman, and T. Ng, "Joint semiblind frequency offset and channel estimation for multiuser MIMO-OFDM uplink," *IEEE Transactions on Communications*, vol. 55, no. 12, pp. 2270–2278, Dec. 2007.

[13] J. Hampton, *Introduction to MIMO Communications.* Cambridge University Press, 2014. [Online]. Available: https://books.google.com.sg/books?id=Ee_CAQAAQBAJ

[14] W. Zhang and F. Gao, "Blind frequency synchronization for multiuser OFDM uplink with large number of receive antennas," *IEEE Transactions on Signal Processing*, vol. 64, no. 9, pp. 2255–2268, May 2016.

[15] N. Tang, S. He, C. Xue, Y. Huang, and L. Yang, "IQ imbalance compensation for generalized frequency division multiplexing systems," *IEEE Wireless Communications Letters*, vol. 6, no. 4, pp. 422–425, Aug. 2017.

[16] T. Singal, *Wireless Communications.* McGraw-Hill Education (India) Pvt Limited, 2010. [Online]. Available: https://books.google.com.hk/books?id=cQJJzA8CCUUC

[17] I. B. F. de Almeida, L. L. Mendes, J. J. P. C. Rodrigues, and M. A. A. da Cruz, "5G waveforms for IoT applications," *IEEE Communications Surveys and Tutorials*, vol. 21, no. 3, pp. 2554–2567, Third quarter 2019.

[18] S. J. Nawaz, S. K. Sharma, S. Wyne, M. N. Patwary, and M. Asaduzzaman, "Quantum machine learning for 6G communication networks: State-of-the-art and vision for the future," *IEEE Access*, vol. 7, pp. 46 317–46 350, 2019.

[19] L. Zhang, Y. Liang, and D. Niyato, "6G visions: Mobile ultra-broadband, super Internet-of-things, and artificial intelligence," *China Communications*, vol. 16, no. 8, pp. 1–14, Aug. 2019.

[20] Z. Zhang, Y. Xiao, Z. Ma, M. Xiao, Z. Ding, X. Lei, G. K. Karagiannidis, and P. Fan, "6G wireless networks: Vision, requirements, architecture, and key technologies," *IEEE Vehicular Technology Magazine*, vol. 14, no. 3, pp. 28–41, Sep. 2019.

[21] Q. Bi, "Ten trends in the cellular industry and an outlook on 6G," *IEEE Communications Magazine*, vol. 57, no. 12, pp. 31–36, Dec. 2019.

[22] H. Holma, A. Toskala, and T. Nakamura, *5G Technology: 3GPP New Radio.* John Wiley & Sons, 2020.

[23] L. Song, R. Wichman, Y. Li, and Z. Han, *Full-duplex communications and networks.* Cambridge University Press, 2017.

[24] T. Schenk, *RF Imperfections in High-rate Wireless Systems: Impact and Digital Compensation.* Springer Netherlands, 2008. [Online]. Available: https://books.google.co.uk/books?id=nLzk11P15IAC

[25] A. Mohammadi and F. Ghannouchi, *RF Transceiver Design for MIMO Wireless Communications*, ser. Lecture Notes in Electrical Engineering. Springer Berlin Heidelberg, 2012. [Online]. Available: https://books.google.com.sg/books?id=03k1ZYhXSr4C

[26] M. Vaezi, Z. Ding, and H. Poor, *Multiple Access Techniques for 5G Wireless Networks and Beyond.* Springer International Publishing, 2018. [Online]. Available: https://books.google.co.jp/books?id=3pNqDwAAQBAJ

[27] W. Xiang, K. Zheng, and X. Shen, *5G Mobile Communications.* Springer International Publishing, 2016. [Online]. Available: https://books.google.co.jp/books?id=tHRCDQAAQBAJ

[28] Y. Tao, L. Liu, S. Liu, and Z. Zhang, "A survey: Several technologies of non-orthogonal transmission for 5G," *China Communications*, vol. 12, no. 10, pp. 1–15, Oct. 2015.

[29] X. Li and K. Pahlavan, "Super-resolution TOA estimation with diversity for indoor geolocation," *IEEE Transactions on Wireless Communications*, vol. 3, no. 1, pp. 224–234, Jan. 2004.

[30] A. Gaber and A. Omar, "A study of wireless indoor positioning based on joint TDOA and DOA estimation using 2-D matrix pencil algorithms and IEEE 802.11ac," *IEEE Transactions on Wireless Communications*, vol. 14, no. 5, pp. 2440–2454, May 2015.

[31] D. Kim, H. Lee, and D. Hong, "A survey of in-band full-duplex transmission: From the perspective of PHY and MAC layers," *IEEE Communications Surveys and Tutorials*, vol. 17, no. 4, pp. 2017–2046, Fourth quarter 2015.

[32] T. Le-Ngoc and A. Masmoudi, *Full-Duplex Wireless Communications Systems: Self-Interference Cancellation*, ser. Wireless Networks. Springer International Publishing, 2017. [Online]. Available: https://books.google.com.hk/books?id=10rpAQAACAAJ

[33] G. Pocovi, H. Shariatmadari, G. Berardinelli, K. Pedersen, J. Steiner, and Z. Li, "Achieving ultra-reliable low-latency communications: Challenges and envisioned system enhancements," *IEEE Network*, vol. 32, no. 2, pp. 8–15, Mar. 2018.

[34] B. Lee, S. Park, D. J. Love, H. Ji, and B. Shim, "Packet structure and receiver design for low latency wireless communications with ultra-short packets," *IEEE Transactions on Communications*, vol. 66, no. 2, pp. 796–807, Feb. 2018.

[35] O. L. A. Lopez, E. M. G. Fernández, R. D. Souza, and H. Alves, "Ultra-reliable cooperative short-packet communications with wireless energy transfer," *IEEE Sensors Journal*, vol. 18, no. 5, pp. 2161–2177, Mar. 2018.

[36] M. H. Alsharif and R. Nordin, "Evolution towards fifth generation (5G) wireless networks: Current trends and challenges in the deployment of millimetre wave, massive MIMO, and small cells," *Telecommunication Systems*, vol. 64, no. 4, pp. 617–637, 2017.

[37] O. Elijah, C. Y. Leow, T. A. Rahman, S. Nunoo, and S. Z. Iliya, "A comprehensive survey of pilot contamination in massive MIMO—5G system," *IEEE Communications Surveys and Tutorials*, vol. 18, no. 2, pp. 905–923, Second quarter 2016.

[38] S. A. Busari, K. M. S. Huq, S. Mumtaz, L. Dai, and J. Rodriguez, "Millimeter-wave massive MIMO communication for future wireless systems: A survey," *IEEE Communications Surveys and Tutorials*, vol. 20, no. 2, pp. 836–869, Second quarter 2018.

[39] A. Osseiran, J. Monserrat, and P. Marsch, *5G Mobile and Wireless Communications Technology.* Cambridge University Press, 2016. [Online]. Available: https://books.google.com.sg/books?id=qnMjDAAAQBAJ

[40] J. Wang, C. Jiang, H. Zhang, Y. Ren, K. Chen, and L. Hanzo, "Thirty years of machine learning: The road to pareto-optimal wireless networks," *IEEE Communications Surveys and Tutorials*, pp. 1–1, (Early access) 2020.

[41] X. Gao, L. Dai, Y. Zhang, T. Xie, X. Dai, and Z. Wang, "Fast channel tracking for terahertz beamspace massive MIMO systems," *IEEE Transactions on Vehicular Technology*, vol. 66, no. 7, pp. 5689–5696, Jul. 2017.

[42] Z. Chen, X. Ma, B. Zhang, Y. Zhang, Z. Niu, N. Kuang, W. Chen, L. Li, and S. Li, "A survey on terahertz communications," *China Communications*, vol. 16, no. 2, pp. 1–35, Feb. 2019.

[43] M. Jung, W. Saad, Y. Jang, G. Kong, and S. Choi, "Performance analysis of large intelligent surfaces (LISs): Asymptotic data rate and channel hardening effects," *IEEE Transactions on Wireless Communications*, pp. 1–1, (Early access) 2020.

[44] V. Savaux and Y. Louët, "LMMSE channel estimation in OFDM context: a review," *IET Signal Processing*, vol. 11, no. 2, pp. 123–134, 2016.

[45] F. Sandoval, G. Poitau, and F. Gagnon, "Hybrid peak-to-average power ratio reduction techniques: Review and performance comparison," *IEEE Access*, vol. 5, pp. 27 145–27 161, 2017.

[46] O. O. Oyerinde and S. H. Mneney, "Review of channel estimation for wireless communication systems," *IETE Technical review*, vol. 29, no. 4, pp. 282–298, 2012.

[47] T. Hwang, C. Yang, G. Wu, S. Li, and G. Y. Li, "OFDM and its wireless applications: A survey," *IEEE Transactions on Vehicular Technology*, vol. 58, no. 4, pp. 1673–1694, 2008.

[48] M. K. Ozdemir and H. Arslan, "Channel estimation for wireless OFDM systems," *IEEE Communications Surveys and Tutorials*, vol. 9, no. 2, pp. 18–48, Second quarter 2007.

[49] Y. Liu, Z. Tan, H. Hu, L. J. Cimini, and G. Y. Li, "Channel estimation for OFDM," *IEEE Communications Surveys and Tutorials*, vol. 16, no. 4, pp. 1891–1908, Fourth quarter 2014.

[50] B. Farhang-Boroujeny and H. Moradi, "OFDM inspired waveforms for 5G," *IEEE Communications Survey and Tutorial*, vol. 18, no. 4, pp. 2474–2492, Fourth quarter 2016.

[51] A. F. Demir, M. Elkourdi, M. Ibrahim, and H. Arslan, "Waveform design for 5G and beyond," *arXiv preprint arXiv:1902.05999*, 2019.

[52] A. Goldsmith, *Wireless communications.* Cambridge university press, 2005.

[53] Y. Jiang, X. Zhu, E. Lim, Y. Huang, and H. Lin, *Semi-Blind Carrier Frequency Offset Estimation and Channel Equalization*, ser. Springer Briefs in Electrical and Computer Engineering. Springer International Publishing, 2015. [Online]. Available: https://books.google.com.hk/books?id=M2oiCwAAQBAJ

[54] T. Chiueh, P. Tsai, and I. Lai, *Baseband Receiver Design for Wireless MIMO-OFDM Communications*, ser. Wiley - IEEE. Wiley, 2012. [Online]. Available: https://books.google.com.sg/books?id=zfX0Ow6x2tkC

[55] M. Morelli, C. C. J. Kuo, and M. Pun, "Synchronization techniques for orthogonal frequency division multiple access (OFDMA): A tutorial review," *Proceedings of the IEEE*, vol. 95, no. 7, pp. 1394–1427, Jul. 2007.

[56] G. Fettweis, M. Krondorf, and S. Bittner, "GFDM - generalized frequency division multiplexing," in *IEEE 2009 VTC Spring*, Barcelona, Spain, Apr. 2009, pp. 1–4.

[57] M. Towliat, S. M. J. A. Tabatabaee, and M. Rajabzadeh, "A simple ML detection for coded generalized frequency division multiplexing in MIMO channels," *IEEE Transactions on Signal Processing*, vol. 67, no. 3, pp. 798–807, 2019.

[58] H. Wang and R. Song, "Low complexity ZF receiver design for multi-user GFDMA uplink systems," *IEEE Access*, vol. 6, pp. 28 661–28 667, May 2018.

[59] M. Matthé, D. Zhang, and G. Fettweis, "Low-complexity iterative MMSE-PIC detection for MIMO-GFDM," *IEEE Transactions on Communications*, vol. 66, no. 4, pp. 1467–1480, 2018.

[60] S. Tiwari and S. S. Das, "Low-complexity joint-MMSE GFDM receiver," *IEEE Transactions on Communications*, vol. 66, no. 4, pp. 1661–1674, 2018.

[61] P. Chen, B. Su, and Y. Huang, "Matrix characterization for GFDM: Low complexity MMSE receivers and optimal filters," *IEEE Transactions on Signal Processing*, vol. 65, no. 18, pp. 4940–4955, 2017.

[62] F. Hu, *Opportunities in 5G Networks: A Research and Development Perspective.* CRC Press, 2016. [Online]. Available: https://books.google.co.jp/books?id=UcL1CwAAQBAJ

[63] R. Vannithamby and S. Talwar, *Towards 5G: Applications, Requirements and Candidate Technologies.* Wiley, 2017. [Online]. Available: https://books.google.co.jp/books?id=xy1FDQAAQBAJ

[64] A. Saljoghei, A. Farhang, C. Browning, P. Perry, N. Marchetti, L. E. Doyle, and L. P. Barry, "Comparison of OFDMA and GFDMA for next-generation pons," *IEEE/OSA Journal of Optical Communications and Networking*, vol. 9, no. 12, pp. 1064–1073, Dec 2017.

[65] I. Parvez, A. Rahmati, I. Guvenc, A. I. Sarwat, and H. Dai, "A survey on low latency towards 5G: RAN, core network and caching solutions," *IEEE Communications Surveys and Tutorials*, vol. 20, no. 4, pp. 3098–3130, Fourth quarter 2018.

[66] G. J. Sutton, J. Zeng, R. P. Liu, W. Ni, D. N. Nguyen, B. A. Jayawickrama, X. Huang, M. Abolhasan, and Z. Zhang, "Enabling ultra-reliable and low-latency communications through unlicensed spectrum," *IEEE Network*, vol. 32, no. 2, pp. 70–77, Mar. 2018.

[67] J. Sachs, G. Wikstrom, T. Dudda, R. Baldemair, and K. Kittichokechai, "5G radio network design for ultra-reliable low-latency communication," *IEEE Network*, vol. 32, no. 2, pp. 24–31, Mar. 2018.

[68] H. Chen, R. Abbas, P. Cheng, M. Shirvanimoghaddam, W. Hardjawana, W. Bao, Y. Li, and B. Vucetic, "Ultra-reliable low-latency cellular networks: Use cases, challenges and approaches," *arXiv preprint arXiv:1709.00560*, 2017.

[69] M. Sybis, K. Wesolowski, K. Jayasinghe, V. Venkatasubramanian, and V. Vukadinovic, "Channel coding for ultra-reliable low-latency communication in 5G systems," in *Proc. IEEE VTC-Fall 2016*, Montreal, QC, Canada, Sep. 2016, pp. 1–5.

[70] M. Matthé, L. L. Mendes, N. Michailow, D. Zhang, and G. Fettweis, "Widely linear estimation for space-time-coded GFDM in low-latency applications," *IEEE Transactions on Communications*, vol. 63, no. 11, pp. 4501–4509, Nov. 2015.

[71] F. Schaich, T. Wild, and Y. Chen, "Waveform contenders for 5G - suitability for short packet and low latency transmissions," in *Proc. IEEE VTC Spring 2014*, Seoul, South Korea, May 2014, pp. 1–5.

[72] X. Sun, S. Yan, N. Yang, Z. Ding, C. Shen, and Z. Zhong, "Short-packet downlink transmission with non-orthogonal multiple access," *IEEE Transactions on Wireless Communications*, pp. 1–1, 2018.

[73] Y. Yu, H. Chen, Y. Li, Z. Ding, and B. Vucetic, "On the performance of non-orthogonal multiple access in short-packet communications," *IEEE Communications Letters*, vol. 22, no. 3, pp. 590–593, Mar. 2018.

[74] A. Azari, P. Popovski, G. Miao, and C. Stefanovic, "Grant-free radio access for short-packet communications over 5G networks," in *Proc. IEEE GLOBECOM 2017*, Singapore, Dec. 2017, pp. 1–7.

[75] Y. Gu, H. Chen, Y. Li, and B. Vucetic, "Ultra-reliable short-packet communications: Half-duplex or full-duplex relaying?" *IEEE Wireless Communications Letters*, pp. 1–1, 2017.

[76] F. E. Airod, H. Chafnaji, and H. Yanikomeroglu, "Performance analysis of low latency multiple full-duplex selective decode and forward relays," *arXiv preprint arXiv:1802.04076*, 2018.

[77] S. S. Ullah, G. Liva, and S. C. Liew, "Short packet physical-layer network coding with mismatched channel state information," in *Proc. IEEE WCNC 2018*, Barcelona, Spain, Apr. 2018, pp. 1–5.

[78] M. Mousaei and B. Smida, "Optimizing pilot overhead for ultra-reliable short-packet transmission," in *Proc. IEEE ICC 2017*, Paris, France, May 2017, pp. 1–5.

[79] G. Liu, F. R. Yu, H. Ji, V. C. M. Leung, and X. Li, "In-band full-duplex relaying: A survey, research issues and challenges," *IEEE Communications Surveys and Tutorials*, vol. 17, no. 2, pp. 500–524, Second quarter 2015.

[80] M. Duarte, C. Dick, and A. Sabharwal, "Experiment-driven characterization of full-duplex wireless systems," *IEEE Transactions on Wireless Communications*, vol. 11, no. 12, pp. 4296–4307, Dec. 2012.

[81] E. Everett, A. Sahai, and A. Sabharwal, "Passive self-interference suppression for full-duplex infrastructure nodes," *IEEE Transactions on Wireless Communications*, vol. 13, no. 2, pp. 680–694, Feb. 2014.

[82] J. Lee, "Self-interference cancelation using phase rotation in full-duplex wireless," *IEEE Transactions on Vehicular Technology*, vol. 62, no. 9, pp. 4421–4429, Nov. 2013.

[83] H. Duan, X. Zhu, Y. Jiang, Z. Wei, and S. Sun, "An adaptive self-interference cancelation/ utilization and ICA assisted semi-blind full-duplex relay system for LLHR IoT," *IEEE Internet of Things Journal*, pp. 1–1, 2019.

[84] A. Molisch, *Wireless Communications*, ser. Wiley - IEEE. Wiley, 2012. [Online]. Available: https://books.google.com/books?id=877tFGeQo5oC

[85] E. Biglieri, R. Calderbank, A. Constantinides, A. Goldsmith, A. Paulraj, and H. Poor, *MIMO Wireless Communications.* Cambridge University Press, 2007. [Online]. Available: https://books.google.com.sg/books?id=TuP4P_j__soC

[86] B. Clerckx and C. Oestges, *MIMO Wireless Networks: Channels, Techniques and Standards for Multi-Antenna, Multi-User and Multi-Cell Systems.* Elsevier Science, 2013. [Online]. Available: https://books.google.com.sg/books?id=drEX1J7jHUIC

[87] A. Sibille, C. Oestges, and A. Zanella, *MIMO: From Theory to Implementation.* Elsevier Science, 2010. [Online]. Available: https://books.google.com.sg/books?id=fIiu8XMNjiAC

[88] K. Zhang, *Wireless Communications: Principles, Theory and Methodology.* Wiley, 2015. [Online]. Available: https://books.google.com/books?id=GGXKCQAAQBAJ

[89] J. Mietzner, R. Schober, L. Lampe, W. H. Gerstacker, and P. A. Hoeher, "Multiple-antenna techniques for wireless communications - a comprehensive literature survey," *IEEE Communications Surveys and Tutorials*, vol. 11, no. 2, pp. 87–105, Second quarter 2009.

[90] S. Yang and L. Hanzo, "Fifty years of MIMO detection: The road to large-scale MIMOs," *IEEE Communications Surveys and Tutorials*, vol. 17, no. 4, pp. 1941–1988, Fourth quarter 2015.

[91] K. Zheng, L. Zhao, J. Mei, B. Shao, W. Xiang, and L. Hanzo, "Survey of large-scale MIMO systems," *IEEE Communications Surveys and Tutorials*, vol. 17, no. 3, pp. 1738–1760, Third quarter 2015.

[92] M. A. Albreem, M. Juntti, and S. Shahabuddin, “Massive MIMO detection techniques: A survey,” *IEEE Communications Surveys and Tutorials*, vol. 21, no. 4, pp. 3109–3132, Fourth quarter 2019.

[93] Y. Li, *In-Phase and Quadrature Imbalance: Modeling, Estimation, and Compensation*, ser. SpringerBriefs in Electrical and Computer Engineering. Springer New York, 2013. [Online]. Available: https://books.google.co.uk/books?id=day8BAAAQBAJ

[94] F. Ling, *Synchronization in Digital Communication Systems.* Cambridge University Press, 2017. [Online]. Available: https://books.google.com.hk/books?id=xBniDgAAQBAJ

[95] D. Tse and P. Viswanath, *Fundamentals of Wireless Communication*, ser. Wiley series in telecommunications. Cambridge University Press, 2005. [Online]. Available: https://books.google.com/books?id=66XBb5tZX6EC

[96] J. Wu and P. Fan, “A survey on high mobility wireless communications: Challenges, opportunities and solutions,” *IEEE Access*, vol. 4, pp. 450–476, 2016.

[97] P. Fan, J. Zhao, and C. I., “5G high mobility wireless communications: Challenges and solutions,” *China Communications*, vol. 13, no. Supplement2, pp. 1–13, N 2016.

[98] I. Guvenc and C. Chong, “A survey on TOA based wireless localization and NLOS mitigation techniques,” *IEEE Communications Surveys and Tutorials*, vol. 11, no. 3, pp. 107–124, Third quarter 2009.

[99] Z. Gao, L. Dai, Z. Lu, C. Yuen, and Z. Wang, “Super-resolution sparse MIMO-OFDM channel estimation based on spatial and temporal correlations,” *IEEE Communications Letters*, vol. 18, no. 7, pp. 1266–1269, Jul. 2014.

[100] M. Duarte, C. Dick, and A. Sabharwal, "Experiment-driven characterization of full-duplex wireless systems," *IEEE Transactions on Wireless Communications*, vol. 11, no. 12, pp. 4296–4307, Dec. 2012.

[101] S. Li and R. D. Murch, "An investigation into baseband techniques for single-channel full-duplex wireless communication systems," *IEEE Transactions on Wireless Communications*, vol. 13, no. 9, pp. 4794–4806, Sep. 2014.

[102] Z. Gao, L. Dai, W. Dai, B. Shim, and Z. Wang, "Structured compressive sensing-based spatio-temporal joint channel estimation for FDD massive MIMO," *IEEE Transactions on Communications*, vol. 64, no. 2, pp. 601–617, Feb. 2016.

[103] R. Roy and T. Kailath, "Esprit-estimation of signal parameters via rotational invariance techniques," *IEEE Transactions on Acoustics, Speech, and Signal Processing*, vol. 37, no. 7, pp. 984–995, Jul. 1989.

[104] A. Masmoudi and T. Le-Ngoc, "A maximum-likelihood channel estimator for self-interference cancelation in full-duplex systems," *IEEE Transactions on Vehicular Technology*, vol. 65, no. 7, pp. 5122–5132, Jul. 2016.

[105] A. A. Nasir, S. Durrani, H. Mehrpouyan, S. D. Blostein, and R. A. Kennedy, "Timing and carrier synchronization in wireless communication systems: a survey and classification of research in the last 5 years," *EURASIP Journal on Wireless Communications and Networking*, vol. 2016, no. 1, p. 180, 2016.

[106] A. Narasimhamurthy, C. Tepedelenlioglu, and M. Banavar, *OFDM Systems for Wireless Communications*, ser. Synthesis lectures on algorithms and software in engineering. Morgan & Claypool Publishers, 2010. [Online]. Available: https://books.google.com.hk/books?id=ZrJQe4hjQzYC

[107] P. H. Moose, "A technique for orthogonal frequency division multiplexing frequency offset correction," *IEEE Transactions on Communications*, vol. 42, no. 10, pp. 2908–2914, Oct. 1994.

[108] Byungjoon Park, Hyunsoo Cheon, Eunseok Ko, Changeon Kang, and Daesik Hong, "A blind OFDM synchronization algorithm based on cyclic correlation," *IEEE Signal Processing Letters*, vol. 11, no. 2, pp. 83–85, Feb. 2004.

[109] P. Wang and D. W. Lin, "Maximum-likelihood blind synchronization for GFDM systems," *IEEE Signal Processing Letters*, vol. 23, no. 6, pp. 790–794, Jun. 2016.

[110] A. Masmoudi and T. Le-Ngoc, "Channel estimation and self-interference cancelation in full-duplex communication systems," *IEEE Transactions on Vehicular Technology*, vol. 66, no. 1, pp. 321–334, Jan. 2017.

[111] M. Windisch, *Estimation and Compensation of IQ Imbalance in Broadband Communications Receivers*, ser. Beiträge aus der Informationstechnik. Vogt, 2007. [Online]. Available: https://books.google.co.uk/books?id=krfd2NPRyjQC

[112] A. Schoonen, "IQ imbalance in OFDM wireless LAN systems," *Master's thesis, Eindhoven University of Technology*, vol. 64, no. 7, pp. 3039–3051, Jan. 2006.

[113] D. Oh, S. Kim, S. H. Yoon, and J. W. Chong, "Two-Dimensional ESPRIT-Like shift-invariant TOA estimation algorithm using multi-band chirp signals robust to carrier frequency offset," *IEEE Transactions on Wireless Communications*, vol. 12, no. 7, pp. 3130–3139, Jul. 2013.

[114] T. H. Pham, S. A. Fahmy, and I. V. McLoughlin, "Efficient integer frequency offset estimation architecture for enhanced OFDM synchronization," *IEEE Transactions on Very Large Scale Integration Systems*, vol. 24, no. 4, pp. 1412–1420, Apr. 2016.

[115] Y. Jiang, X. Zhu, E. Lim, Y. Huang, and H. Lin, "Low-complexity semiblind multi-CFO estimation and ICA-based equalization for CoMP OFDM systems," *IEEE Transactions on Vehicular Technology*, vol. 63, no. 4, pp. 1928–1934, May 2014.

[116] A. A. D'Amico, L. Taponecco, and U. Mengali, "Ultra-wideband TOA estimation in the presence of clock frequency offset," *IEEE Transactions on Wireless Communications*, vol. 12, no. 4, pp. 1606–1616, Apr. 2013.

[117] Y. Jiang, X. Zhu, E. G. Lim, Y. Huang, Z. Wei, and H. Lin, "Semi-blind precoding aided ML CFO estimation for ICA based MIMO OFDM systems," in *Proc. IEEE ICC*, Kuala Lumpur, Malaysia, May 2016, pp. 1–5.

[118] D. Oh, Y. Ju, and J. Lee, "An improved MVDR-like TOA estimation without EVD for high-resolution ranging system," *IEEE Communications Letters*, vol. 18, no. 5, pp. 753–756, May 2014.

[119] W. Zhang, F. Gao, H. Minn, and H. Wang, "Scattered pilots-based frequency synchronization for multiuser OFDM systems with large number of receive antennas," *IEEE Transactions on Communications*, vol. 65, no. 4, pp. 1733–1745, 2017.

[120] T. A. Khan, R. W. Heath, and P. Popovski, "Wirelessly powered communication networks with short packets," *IEEE Transactions on Communications*, vol. 65, no. 12, pp. 5529–5543, Dec. 2017.

[121] M. G. Sarret, G. Berardinelli, N. H. Mahmood, and P. Mogensen, "Can full duplex boost throughput and delay of 5G ultra-dense small cell networks?" in *Proc. IEEE VTC Spring 2016*, Nanjing, China, May 2016, pp. 1–5.

[122] Z. Wei, X. Zhu, S. Sun, Y. Huang, L. Dong, and Y. Jiang, "Full-duplex versus half-duplex amplify-and-forward relaying: Which is more energy efficient in 60-GHz dual-hop indoor wireless systems?" *IEEE Journal on Selected Areas in Communications*, vol. 33, no. 12, pp. 2936–2947, Dec. 2015.

[123] A. Koohian, H. Mehrpouyan, A. A. Nasir, S. Durrani, and S. D. Blostein, "Residual self-interference cancellation and data detection in full-duplex communication systems," in *Proc. IEEE ICC 2017*, Paris, France, May 2017, pp. 1–6.

[124] F. Shu, J. Wang, J. Li, R. Chen, and W. Chen, "Pilot optimization, channel estimation, and optimal detection for full-duplex OFDM systems with IQ imbalances," *IEEE Transactions on Vehicular Technology*, vol. 66, no. 8, pp. 6993–7009, Aug. 2017.

[125] D. Korpi, L. Anttila, V. Syrjälä, and M. Valkama, "Widely linear digital self-interference cancellation in direct-conversion full-duplex transceiver," *IEEE Journal on Selected Areas in Communications*, vol. 32, no. 9, pp. 1674–1687, Sep. 2014.

[126] S. Shaboyan, E. Ahmed, A. S. Behbahani, W. Younis, and A. M. Eltawil, "Frequency and timing synchronization for in-band full-duplex OFDM system," in *Porc. IEEE GLOBECOM 2017*, Singapore, Dec. 2017, pp. 1–7.

[127] H. Lee, J. Choi, D. Kim, and D. Hong, "Impact of time and frequency misalignments in OFDM based in-band full-duplex systems," in *Proc. IEEE WCNC 2017*, San Francisco, CA, USA, Mar. 2017, pp. 1–6.

[128] F. Gao, Y. Zeng, A. Nallanathan, and T. S. Ng, "Robust subspace blind channel estimation for cyclic prefixed MIMO ODFM systems: algorithm, identifiability and performance analysis," *IEEE Journal on Selected Areas in Communications*, vol. 26, no. 2, pp. 378–388, Feb. 2008.

[129] C. Shin, R. W. Heath, and E. J. Powers, "Blind channel estimation for MIMO-OFDM systems," *IEEE Transactions on Vehicular Technology*, vol. 56, no. 2, pp. 670–685, Mar. 2007.

[130] C. Wei and D. W. Lin, "A decision-directed channel estimator for OFDM-based bursty vehicular communication," *IEEE Transactions on Vehicular Technology*, vol. 66, no. 6, pp. 4938–4953, Jun. 2017.

[131] J. Chen, Y. Wu, S. Ma, and T. Ng, "Joint CFO and channel estimation for multiuser MIMO-OFDM systems with optimal training sequences," *IEEE Transactions on Signal Processing*, vol. 56, no. 8, pp. 4008–4019, Aug. 2008.

[132] J. M. Cioffi, G. P. Dudevoir, M. V. Eyuboglu, and G. D. Forney, “MMSE decision-feedback equalizers and coding. I. Equalization results,” *IEEE Transactions on Communications*, vol. 43, no. 10, pp. 2582–2594, Oct. 1995.

[133] U. Vilaipornsawai and M. Jia, “Scattered-pilot channel estimation for GFDM,” in *Proc. IEEE WCNC 2014*, Istanbul, Turkey, Apr. 2014, pp. 1053–1058.

[134] S. Ehsanfar, M. Matthe, D. Zhang, and G. Fettweis, “Interference-free pilots insertion for MIMO-GFDM channel estimation,” in *Proc. IEEE WCNC 2017*, San Francisco, CA, USA, Mar. 2017, pp. 1–6.

[135] J. Jeong, Y. Park, S. Weon, J. Kim, S. Choi, and D. Hong, “Eigendecomposition-based GFDM for interference-free data transmission and pilot insertion for channel estimation,” *IEEE Transactions on Wireless Communications*, vol. 17, no. 10, pp. 6931–6943, Oct. 2018.

[136] Z. Na, Z. Pan, M. Xiong, J. Xia, and W. Lu, “Soft decision control iterative channel estimation for the Internet of things in 5G networks,” *IEEE Internet of Things Journal*, vol. 6, no. 4, pp. 5990–5998, Aug. 2019.

[137] B. Lim and Y. Ko, “SIR analysis of OFDM and GFDM waveforms with timing offset, CFO, and phase noise,” *IEEE Transactions on Wireless Communications*, vol. 16, no. 10, pp. 6979–6990, Oct. 2017.

[138] T. Kadur, I. Gaspar, N. Michailow, and G. Fettweis, “Non-data aided frequency synchronization exploiting ICI in non-orthogonal systems,” in *Proc. IEEE VTC 2014-Fall*, Vancouver, BC, Canada, Sep. 2014, pp. 1–5.

[139] D. Zhang, A. Festag, and G. P. Fettweis, “Performance of generalized frequency division multiplexing based physical layer in vehicular communications,” *IEEE Transactions on Vehicular Technology*, vol. 66, no. 11, pp. 9809–9824, Nov. 2017.

[140] S. Ehsanfar, M. Matthé, M. Chafii, and G. P. Fettweis, "Pilot- and CP-aided channel estimation in MIMO non-orthogonal multi-carriers," *IEEE Transactions on Wireless Communications*, vol. 18, no. 1, pp. 650–664, Jan. 2019.

[141] H. Shayanfar, H. Saeedi-Sourck, and A. Farhang, "Low-complexity search method for CFO estimation in GFDM," *Electronics Letters*, vol. 55, no. 6, pp. 355–357, Mar. 2019.

[142] L. B. Thiagarajan, S. Attallah, K. Abed-Meraim, Y. Liang, and H. Fu, "Non-data-aided joint carrier frequency offset and channel estimator for uplink MC-CDMA systems," *IEEE Transactions on Signal Processing*, vol. 56, no. 9, pp. 4398–4408, Sep. 2008.

[143] B. Lim and Y. Ko, "Multiuser interference cancellation for GFDM with timing and frequency offsets," *IEEE Transactions on Communications*, vol. 67, no. 6, pp. 4337–4349, Jun. 2019.

[144] Z. Sharifian, M. J. Omidi, H. Saeedi-Sourck, and A. Farhang, "Linear precoding for PAPR reduction of GFDMA," *IEEE Wireless Communications Letters*, vol. 5, no. 5, pp. 520–523, Oct. 2016.

[145] H. Shayanfar, H. Saeedi-Sourck, A. Farhang, and L. E. Doyle, "Maximum-likelihood synchronization and channel estimation with multiuser detection in GFDMA," *Transactions on Emerging Telecommunications Technology*, vol. 29, no. 6, p. e3424, 2018.

[146] H. Cheng, Y. Xia, Y. Huang, L. Yang, and D. P. Mandic, "A normalized complex LMS based blind I/Q imbalance compensator for GFDM receivers and its full second-order performance analysis," *IEEE Transactions on Signal Processing*, vol. 66, no. 17, pp. 4701–4712, Sep. 2018.

[147] ——, "Joint channel estimation and Tx/Rx I/Q imbalance compensation for GFDM systems," *IEEE Transactions on Wireless Communications*, vol. 18, no. 2, pp. 1304–1317, Feb. 2019.

[148] M. Huang, L. Huang, C. Guo, P. Zhang, J. Zhang, and L. Yang, "Carrier frequency offset estimation in uplink OFDMA systems: an approach relying on sparse recovery," *IEEE Transactions on Vehicular Technology*, vol. 66, no. 10, pp. 9592–9597, Oct. 2017.

[149] P. Cheng, Z. Chen, F. de Hoog, and C. K. Sung, "Sparse blind carrier-frequency offset estimation for OFDMA uplink," *IEEE Transactions on Communications*, vol. 64, no. 12, pp. 5254–5265, Dec. 2016.

[150] Y. Wang and S. Phoong, "Blind CFO estimation in OFDMA uplink transmission with general carrier assignment scheme," *IEEE Communications Letters*, vol. 22, no. 5, pp. 1014–1017, May 2018.

[151] H. Abdzadeh-Ziabari, W. Zhu, and M. N. S. Swamy, "Joint carrier frequency offset and doubly selective channel estimation for MIMO-OFDMA uplink with Kalman and particle filtering," *IEEE Transactions on Signal Processing*, vol. 66, no. 15, pp. 4001–4012, Aug. 2018.

[152] M. Marey, "Solving IQ mismatch problem for two-path successive relaying OFDMA uplink systems with direct conversion transceivers," *IEEE Wireless Commununications Letters*, vol. 8, no. 1, pp. 33–36, Feb. 2019.

[153] M. Marey and H. Steendam, "Novel data detection and channel estimation algorithms for BICM-OFDMA uplink asynchronous systems in the presence of IQ imbalance," *IEEE Transactions on Wireless Communications*, vol. 13, no. 5, pp. 2706–2716, May 2014.

[154] F. Horlin, A. Bourdoux, and L. Van Der Perre, "Low-complexity EM-based joint acquisition of the carrier frequency offset and IQ imbalance," *IEEE Transactions on Wireless Communications*, vol. 7, no. 6, pp. 2212–2220, Jun. 2008.

[155] M. A. Ali, M. Arif, and W. Kumar, "Joint CIR, CFO, DCO and FI/FS Rx IQ imbalance estimation," *IET Communications*, vol. 10, no. 15, pp. 2025–2033, 2016.

[156] Y. Meng, W. Zhang, and W. Wang, "Blind frequency synchronization for OFDM systems with I/Q imbalance," *IEEE Transactions on Vehicular Technology*, vol. 66, no. 9, pp. 7862–7876, Sep. 2017.

[157] M. Morelli, "Timing and frequency synchronization for the uplink of an OFDMA system," *IEEE Transactions on Communications*, vol. 52, no. 2, pp. 296–306, Feb. 2004.

[158] J. Qi and S. Aissa, "Analysis and compensation of I/Q imbalance in MIMO transmit-receive diversity systems," *IEEE Transactions on Communications*, vol. 58, no. 5, pp. 1546–1556, May 2010.

[159] S. Javed, O. Amin, S. S. Ikki, and M. Alouini, "Multiple antenna systems with hardware impairments: New performance limits," *IEEE Transactions on Vehicular Technology*, vol. 68, no. 2, pp. 1593–1606, Feb. 2019.

[160] C. Li and S. Roy, "Subspace-based blind channel estimation for OFDM by exploiting virtual carriers," *IEEE Transactions on Wireless Communications*, vol. 2, no. 1, pp. 141–150, Jan. 2003.

[161] W. Zhang and Q. Yin, "Blind maximum likelihood carrier frequency offset estimation for OFDM with multi-antenna receiver," *IEEE Transactions on Signal Processing*, vol. 61, no. 9, pp. 2295–2307, May 2013.